

LINEAR AND NONLINEAR FLUCTUATIONS IN MULTICOMPONENT PLASMAS APPLIED TO MAGNETOSPHERIC ENVIRONMENTS

by

Mugemana Aaron

*Submitted in fulfillment of the requirements for the degree of Doctor of Philosophy in the
School of Chemistry and Physics, University of KwaZulu-Natal, Durban*

December, 2015.

As the candidate's Supervisor I have/have not approved this thesis for submission.

Supervisor : Dr S Moolla

Abstract

In this thesis, we discussed the linear and nonlinear effects in multicomponent plasmas. By multicomponent, we refer to electron-positron-ion and electron-positron-dust type plasmas. The linear electrostatic waves in magnetized three-component electron-positron-ion plasmas consisting of cool ions, and hot Boltzmann electrons and positrons have been investigated in the low-frequency limit. By using the continuity and momentum equations with the Poisson equation, the dispersion relation is derived. Two stable modes of the waves are investigated in different cases, viz parallel and perpendicular propagation. The effects of the density and the temperature ratio on the wave structures are investigated. We also studied the behavior of the nonlinear electrostatic waves: first, we consider the electrons and positrons as having Boltzmann density distributions and the ions being governed by the fluid equations, and second we extend our model by assuming that all species are governed by the fluid equations. The set of nonlinear differential equations is obtained and this set is numerically solved for the electric field. The numerical solutions exhibit the range of period varying from sinusoidal to sawtooth to spiky waveforms. The effects of the driving electric field, temperature, concentration, drift velocity, Mach number and propagation angle on the wave structures are investigated. Finally, the study ends by investigating solitary waves in an electron-positron-dust plasma. The arbitrary amplitude dust acoustic solitary waves has been studied by using Sagdeev pseudopotential approach in a plasma consisting of hot electrons and positrons, and cold dust grains. The conditions of the existence of solitons are found assuming constant dust charge.

PREFACE

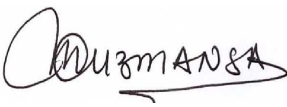
The work presented in this thesis was carried out in the School of Chemistry and Physics, University of KwaZulu–Natal, Westville Campus from August 2012 to November 2015, under the supervision of Dr Suleman Moolla and Dr Ian Joseph Lazarus.

These studies represent original work by the author and have not otherwise been submitted in any form for any degree or diploma to any tertiary institution. Where use has been made of the work of others it is duly acknowledged in the text.

DECLARATION 1 - PLAGIARISM

I, Aaron Mugemana, declare that this thesis titled '*Linear and nonlinear fluctuations in multicomponent plasmas applied to magnetospheric environments*' and the work presented in it are my own. I confirm that:

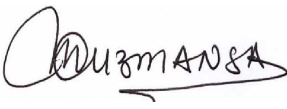
1. The research reported in this thesis, except where otherwise indicated, is my original research.
2. This thesis has not been submitted for any degree or examination at any other university.
3. This thesis does not contain other persons' data, graphs, pictures or other information, unless specifically acknowledged as being sourced from other persons.
4. This thesis does not contain other persons' writing, unless specifically acknowledged as being sourced from other researchers. Where other written sources have been quoted, then:
 - (a) Their words have been re-written but the general information attributed to them has been referenced.
 - (b) Where their exact words have been used, then their writing has been placed inside quotation marks, and referenced.
5. This thesis does not contain text, graphics copied and pasted from the Internet, unless specifically acknowledged, and the source being detailed in the thesis and in the References sections.

Signed: 

DECLARATION 2 - PUBLICATIONS

This work is based on the following papers:

1. **Mugemana, A.; Lazarus, I. J.; Moolla, S. (2014)** '*Linear electrostatic waves in a three-component electron-positron-ion plasma*' *Physics of Plasmas*, 21, 122119; doi: 10.1063/1.4905067.
2. **Mugemana, A.; Moolla, S; Lazarus, I. J,** '*Nonlinear waves in electron - positron - ion plasmas including charge separation*' *Pramana* (Submitted).
3. **Mugemana, A.; Moolla, S; Lazarus, I. J,** '*Nonlinear waves in electron - positron - ion plasmas including full dynamics for all species*' (Manuscript).
4. **Mugemana, A.; Moolla, S; Lazarus, I. J,** '*Solitary waves in three-component electron - positron - dust plasmas*' (Manuscript).

Signed: 

ACKNOWLEDGEMENT

I am thankful to a few people who have made this work both possible and pleasurable: my supervisors, Dr Suleman Moolla and Dr Ian Joseph Lazarus, for their guidance, stimulation and support throughout this study and especially for their very encouraging remarks.

Contents

1	Introduction	1
2	Linear electrostatic waves in electron-positron-ion plasmas	7
2.1	Literature Review	7
2.2	Fluid Theory Approach	9
2.2.1	The model of fluid equations	9
2.3	Numerical results and Discussion	16
3	Nonlinear waves in electron-positron- ion plasmas	24
3.1	Literature Review	24
3.2	Basic theory and Model of fluid equations governing the plasma dynamics . .	26
3.2.1	Linear Analysis	27
3.2.2	Nonlinear Analysis	29
3.2.3	Calculation of Initial Conditions	30
3.3	The numerical results and Discussion	32
4	Nonlinear waves in electron - positron - ion plasmas including the full dynamics for all species	63
4.1	Literature Review	63
4.2	Basic theory and Model of fluid equations governing the plasma dynamics . .	64
4.2.1	Nonlinear Analysis	65
4.2.2	Calculation of Initial Conditions	67

4.3	Numerical Results and Discussion	70
5	Solitary waves in three-component electron - positron - dust plasmas	108
5.1	Literature Review	108
5.2	Basic theory and Model of fluid equations governing the plasma dynamics . .	110
5.3	Arbitrary Amplitude solitary waves in an electron-positron-dust plasma . . .	113
5.3.1	Sagdeev pseudopotential Approach	115
5.4	Numerical results and Discussion	117
6	Summary	125
A	CODES	128

2.6	Normalized real frequency as a function of the normalized wavenumber. The fixed parameters are $T_i/T_h = 0.01$, $n_{i0}/n_{e0} = 0.11$ and $R = 0.333$. The curves present the cyclotron branch for different values of angles propagation $\theta = 0^0$ (dashddot=black), 9^0 (dashdot=blue), 22.5^0 (broken=green), 45^0 (dotted=red).	23
3.1	Numerical solution of normalized parallel electric field for an electron-positron-ion plasma for the parameters $M = 2.5$, $\delta_i = 0.0$, $n_{i0}/n_{e0} = 0.5$, $T_i/T_h = 0.0$, $R = 3.0$, $\theta = 2^0$ and $E_0 = 0.01$. The period of the wave is $T_w = 1.06\tau_{ci}$ (frequency $f_w = 0.94f_{ci}$).	33
3.2	Numerical solution of normalized parallel electric field for an electron-positron-ion plasma for the parameters $M = 2.5$, $\delta_i = 0.0$, $n_{i0}/n_{e0} = 0.5$, $T_i/T_h = 0.0$, $R = 3.0$, $\theta = 2^0$ and $E_0 = 0.1$. The period of the wave is $T_w = 1.31\tau_{ci}$ (frequency $f_w = 0.76f_{ci}$).	34
3.3	Numerical solution of normalized parallel electric field for an electron-positron-ion plasma for the parameters $M = 2.5$, $\delta_i = 0.0$, $n_{i0}/n_{e0} = 0.5$, $T_i/T_h = 0.0$, $R = 3.0$, $\theta = 2^0$ and $E_0 = 0.2$. The period of the wave is $T_w = 2.06\tau_{ci}$ (frequency $f_w = 0.48f_{ci}$).	35
3.4	Numerical solution of normalized parallel electric field for an electron-positron-ion plasma for the parameters $M = 2.5$, $\delta_i = 0.0$, $n_{i0}/n_{e0} = 0.5$, $T_i/T_h = 0.0$, $R = 3.0$, $\theta = 2^0$ and $E_0 = 0.3$. The period of the wave is $T_w = 3.44\tau_{ci}$ (frequency $f_w = 0.29f_{ci}$).	36
3.5	Numerical solution of normalized parallel electric field for the parameters $E_0 = 0.3$, $M = 2.5$, $R = 3.0$, $\delta_i = 0.0$, $n_{i0}/n_{e0} = 0.5$, $\theta = 2^0$ and $T_i/T_h = 0.0$. The period of the wave is $T_w = 3.44\tau_{ci}$ (frequency $f_w = 0.290f_{ci}$).	38
3.6	Numerical solution of normalized parallel electric field for the parameters $E_0 = 0.3$, $M = 2.5$, $R = 3.0$, $\delta_i = 0.0$, $n_{i0}/n_{e0} = 0.5$, $\theta = 2^0$ and $T_i/T_h = 0.05$. The period of the wave is $T_w = 3.51\tau_{ci}$ (frequency $f_w = 0.284f_{ci}$).	39

3.7	Numerical solution of normalized parallel electric field for the parameters $E_0 = 0.3$, $M = 2.5$, $R = 3.0$, $\delta_i = 0.0$, $n_{i0}/n_{e0} = 0.5$, $\theta = 2^0$ and $T_i/T_h = 0.15$. The period of the wave is $T_w = 3.56\tau_{ci}$ (frequency $f_w = 0.280f_{ci}$).	40
3.8	Numerical solution of normalized parallel electric field for the parameters $E_0 = 0.3$, $M = 2.5$, $R = 3.0$, $\delta_i = 0.0$, $n_{i0}/n_{e0} = 0.5$, $\theta = 2^0$ and $T_i/T_h = 0.2$. The period of the wave is $T_w = 3.62\tau_{ci}$ (frequency $f_w = 0.273f_{ci}$).	41
3.9	Numerical solution of normalized parallel electric field for the parameters $E_0 = 0.3$, $M = 2.5$, $R = 3.0$, $\delta_i = 0.0$, $\theta = 2^0$, $T_i/T_h = 0.0$ and $n_{p0}/n_{e0} = 0.3$. The period of the wave is $T_w = 1.94\tau_{ci}$ (frequency $f_w = 0.515f_{ci}$).	43
3.10	Numerical solution of normalized parallel electric field for the parameters $E_0 = 0.3$, $M = 2.5$, $R = 3.0$, $\delta_i = 0.0$, $\theta = 2^0$, $T_i/T_h = 0.0$ and $n_{p0}/n_{e0} = 0.35$. The period of the wave is $T_w = 2.20\tau_{ci}$ (frequency $f_w = 0.454f_{ci}$).	44
3.11	Numerical solution of normalized parallel electric field for the parameters $E_0 = 0.3$, $M = 2.5$, $R = 3.0$, $\delta_i = 0.0$, $\theta = 2^0$, $T_i/T_h = 0.0$ and $n_{p0}/n_{e0} = 0.4$. The period of the wave is $T_w = 2.43\tau_{ci}$ (frequency $f_w = 0.411f_{ci}$).	45
3.12	Numerical solution of normalized parallel electric field for the parameters $E_0 = 0.3$, $M = 2.5$, $R = 3.0$, $\delta_i = 0.0$, $\theta = 2^0$, $T_i/T_h = 0.0$ and $n_{p0}/n_{e0} = 0.5$. The period of the wave is $T_w = 2.83\tau_{ci}$ (frequency $f_w = 0.353f_{ci}$).	46
3.13	Numerical solution of normalized parallel electric field for the parameters $E_0 = 0.3$, $M = 2.5$, $R = 3.0$, $\theta = 2^0$, $T_i/T_h = 0.0$, $n_{i0}/n_{e0} = 0.5$ and $\delta_i = -0.20$. The period of the wave is $T_w = 4.12\tau_{ci}$ (frequency $f_w = 0.242f_{ci}$).	48
3.14	Numerical solution of normalized parallel electric field for the parameters $E_0 = 0.3$, $M = 2.5$, $R = 3.0$, $\theta = 2^0$, $T_i/T_h = 0.0$, $n_{i0}/n_{e0} = 0.5$ and $\delta_i = -0.10$. The period of the wave is $T_w = 3.83\tau_{ci}$ (frequency $f_w = 0.261f_{ci}$).	49
3.15	Numerical solution of normalized parallel electric field for the parameters $E_0 = 0.3$, $M = 2.5$, $R = 3.0$, $\theta = 2^0$, $T_i/T_h = 0.0$, $n_{i0}/n_{e0} = 0.5$ and $\delta_i = 0.0$. The period of the wave is $T_w = 3.46\tau_{ci}$ (frequency $f_w = 0.289f_{ci}$).	50

3.16	Numerical solution of normalized parallel electric field for the parameters $E_0 = 0.3$, $M = 2.5$, $R = 3.0$, $\theta = 2^0$, $T_i/T_h = 0.0$, $n_{i0}/n_{e0} = 0.5$ and $\delta_i = 0.10$. The period of the wave is $T_w = 3.08\tau_{ci}$ (frequency $f_w = 0.324f_{ci}$).	51
3.17	Numerical solution of normalized parallel electric field for the parameters $E_0 = 0.3$, $M = 2.5$, $R = 3.0$, $\theta = 2^0$, $T_i/T_h = 0.0$, $n_{i0}/n_{e0} = 0.5$ and $\delta_i = 0.20$. The period of the wave is $T_w = 2.81\tau_{ci}$ (frequency $f_w = 0.355f_{ci}$).	52
3.18	Numerical solution of normalized parallel electric field for the parameters $M = 2.5$, $\delta_i = 0.0$, $n_{i0}/n_{e0} = 0.5$, $T_i/T_h = 0.0$, $R = 3.0$, $E_0 = 0.3$ and $\theta = 2^0$	54
3.19	Numerical solution of normalized parallel electric field for the parameters $M = 2.5$, $\delta_i = 0.0$, $n_{i0}/n_{e0} = 0.5$, $T_i/T_h = 0.0$, $R = 3.0$, $E_0 = 0.3$ and $\theta = 25^0$	55
3.20	Numerical solution of normalized parallel electric field for the parameters $M = 2.5$, $\delta_i = 0.0$, $n_{i0}/n_{e0} = 0.5$, $T_i/T_h = 0.0$, $R = 3.0$, $E_0 = 0.3$ and $\theta = 50^0$	56
3.21	Numerical solution of normalized parallel electric field for the parameters $M = 2.5$, $\delta_i = 0.0$, $n_{i0}/n_{e0} = 0.5$, $T_i/T_h = 0.0$, $R = 3.0$, $E_0 = 0.3$ and $\theta = 80^0$	57
3.22	Numerical solution of normalized parallel electric field for the parameters $E_0 = 0.3$, $R = 3.0$, $\delta_i = \delta_e = \delta_p = 0.0$, $\theta = 2^0$, $T_i/T_h = 0.0$, $n_{p0}/n_{e0} = n_{i0}/n_{e0} = 0.5$ and $M = 2.2$	59
3.23	Numerical solution of normalized parallel electric field for the parameters $E_0 = 0.3$, $R = 3.0$, $\delta_i = \delta_e = \delta_p = 0.0$, $\theta = 2^0$, $T_i/T_h = 0.0$, $n_{p0}/n_{e0} = n_{i0}/n_{e0} = 0.5$ and $M = 2.3$	60
3.24	Numerical solution of normalized parallel electric field for the parameters $E_0 = 0.3$, $R = 3.0$, $\delta_i = \delta_e = \delta_p = 0.0$, $\theta = 2^0$, $T_i/T_h = 0.0$, $n_{p0}/n_{e0} = n_{i0}/n_{e0} = 0.5$ and $M = 2.4$	61
3.25	Numerical solution of normalized parallel electric field for the parameters $E_0 = 0.3$, $R = 3.0$, $\delta_i = \delta_e = \delta_p = 0.0$, $\theta = 2^0$, $T_i/T_h = 0.0$, $n_{p0}/n_{e0} = n_{i0}/n_{e0} = 0.5$ and $M = 2.5$	62

4.1	Numerical solution of normalized parallel electric field for the parameters $M = 3.5$, $R = 5.0$, $\delta_i = \delta_e = \delta_p = 0.0$, $n_{i0}/n_{e0} = 0.5$, $n_{p0}/n_{e0} = 0.5$, $T_i/T_h = 0.0$, $\theta = 2^0$ and $E_0 = 0.35$	71
4.2	Numerical solution of normalized parallel electric field for the parameters $M = 3.5$, $R = 5.0$, $\delta_i = \delta_e = \delta_p = 0.0$, $n_{i0}/n_{e0} = 0.5$, $n_{p0}/n_{e0} = 0.5$, $T_i/T_h = 0.0$, $\theta = 2^0$ and $E_0 = 0.5$	72
4.3	Numerical solution of normalized parallel electric field for the parameters $M = 3.5$, $R = 5.0$, $\delta_i = \delta_e = \delta_p = 0.0$, $n_{i0}/n_{e0} = 0.5$, $n_{p0}/n_{e0} = 0.5$, $T_i/T_h = 0.0$, $\theta = 2^0$ and $E_0 = 1.5$	73
4.4	Numerical solution of normalized parallel electric field for the parameters $M = 3.5$, $R = 5.0$, $\delta_i = \delta_e = \delta_p = 0.0$, $n_{i0}/n_{e0} = 0.5$, $n_{p0}/n_{e0} = 0.5$, $T_i/T_h = 0.0$, $\theta = 2^0$ and $E_0 = 2.5$	74
4.5	Numerical solution of normalized parallel electric field for the parameters $E_0 = 2.5$, $M = 3.5$, $R = 5.0$, $\delta_i = \delta_e = \delta_p = 0.0$, $n_{i0}/n_{e0} = 0.5$, $\theta = 2^0$ and $T_i/T_h = 0.0$	76
4.6	Numerical solution of normalized parallel electric field for the parameters $E_0 = 2.5$, $M = 3.5$, $R = 5.0$, $\delta_i = \delta_e = \delta_p = 0.0$, $n_{i0}/n_{e0} = 0.5$, $\theta = 2^0$ and $T_i/T_h = 0.05$	77
4.7	Numerical solution of normalized parallel electric field for the parameters $E_0 = 2.5$, $M = 3.5$, $R = 5.0$, $\delta_i = \delta_e = \delta_p = 0.0$, $n_{i0}/n_{e0} = 0.5$, $\theta = 2^0$ and $T_i/T_h = 0.15$	78
4.8	Numerical solution of normalized parallel electric field for the parameters $E_0 = 2.5$, $M = 3.5$, $R = 5.0$, $\delta_i = \delta_e = \delta_p = 0.0$, $n_{i0}/n_{e0} = 0.5$, $\theta = 2^0$ and $T_i/T_h = 0.2$	79
4.9	Numerical solution of normalized parallel electric field for the parameters $E_0 = 2.5$, $M = 3.5$, $R = 5.0$, $\delta_i = \delta_e = \delta_p = 0.0$, $n_{i0}/n_{e0} = 0.5$ and $\theta = 2^0$. The curves present the effects of the temperature for different values of ratio $T_i/T_h = 0.0$ (dashddot=red), 0.05 (dashdot=blue), 0.15 (broken=green), 0.2 (dotted=black).	80

4.10	Numerical solution of normalized parallel electric field for the parameters $E_0 = 2.5$, $M = 3.5$, $R = 5.0$, $\delta_i = \delta_e = \delta_p = 0.0$, $\theta = 2^0$, $T_i/T_h = 0.0$ and $n_{i0}/n_{e0} = 0.7$.	82
4.11	Numerical solution of normalized parallel electric field for the parameters $E_0 = 2.5$, $M = 3.5$, $R = 5.0$, $\delta_i = \delta_e = \delta_p = 0.0$, $\theta = 2^0$, $T_i/T_h = 0.0$ and $n_{i0}/n_{e0} = 0.65$.	83
4.12	Numerical solution of normalized parallel electric field for the parameters $E_0 = 2.5$, $M = 3.5$, $R = 5.0$, $\delta_i = \delta_e = \delta_p = 0.0$, $\theta = 2^0$, $T_i/T_h = 0.0$ and $n_{i0}/n_{e0} = 0.6$.	84
4.13	Numerical solution of normalized parallel electric field for the parameters $E_0 = 2.5$, $M = 3.5$, $R = 5.0$, $\delta_i = \delta_e = \delta_p = 0.0$, $\theta = 2^0$, $T_i/T_h = 0.0$ and $n_{i0}/n_{e0} = 0.5$.	85
4.14	Numerical solution of normalized parallel electric field for the parameters $E_0 = 2.5$, $R = 5.0$, $\delta_i = \delta_e = \delta_p = 0.0$, $\theta = 2^0$, $T_i/T_h = 0.0$, $n_{p0}/n_{e0} = n_{i0}/n_{e0} = 0.5$ and $M = 3.5$.	87
4.15	Numerical solution of normalized parallel electric field for the parameters $E_0 = 2.5$, $R = 5.0$, $\delta_i = \delta_e = \delta_p = 0.0$, $\theta = 2^0$, $T_i/T_h = 0.0$, $n_{p0}/n_{e0} = n_{i0}/n_{e0} = 0.5$ and $M = 3.7$.	88
4.16	Numerical solution of normalized parallel electric field for the parameters $E_0 = 2.5$, $R = 5.0$, $\delta_i = \delta_e = \delta_p = 0.0$, $\theta = 2^0$, $T_i/T_h = 0.0$, $n_{p0}/n_{e0} = n_{i0}/n_{e0} = 0.5$ and $M = 3.8$.	89
4.17	Numerical solution of normalized parallel electric field for the parameters $E_0 = 2.5$, $R = 5.0$, $\delta_i = \delta_e = \delta_p = 0.0$, $\theta = 2^0$, $T_i/T_h = 0.0$, $n_{p0}/n_{e0} = n_{i0}/n_{e0} = 0.5$ and $M = 4.0$.	90
4.18	Numerical solution of normalized parallel electric field for the parameters $E_0 = 2.5$, $M = 3.5$, $R = 5.0$, $\delta_i = \delta_e = \delta_p = 0.0$, $T_i/T_h = 0.0$, $n_{p0}/n_{e0} = n_{i0}/n_{e0} = 0.5$ and $\theta = 2^0$.	92
4.19	Numerical solution of normalized parallel electric field for the parameters $E_0 = 2.5$, $M = 3.5$, $R = 5.0$, $\delta_i = \delta_e = \delta_p = 0.0$, $T_i/T_h = 0.0$, $n_{p0}/n_{e0} = n_{i0}/n_{e0} = 0.5$ and $\theta = 6^0$.	93

4.20	Numerical solution of normalized parallel electric field for the parameters $E_0 = 2.5$, $M = 3.5$, $R = 5.0$, $\delta_i = \delta_e = \delta_p = 0.0$, $T_i/T_h = 0.0$, $n_{p0}/n_{e0} = n_{i0}/n_{e0} = 0.5$ and $\theta = 10^0$	94
4.21	Numerical solution of normalized parallel electric field for the parameters $E_0 = 2.5$, $M = 3.5$, $R = 5.0$, $\delta_i = \delta_e = \delta_p = 0.0$, $T_i/T_h = 0.0$, $n_{p0}/n_{e0} = n_{i0}/n_{e0} = 0.5$ and $\theta = 15^0$	95
4.22	Numerical solution of normalized parallel electric field for the parameters $E_0 = 2.5$, $M = 3.5$, $R = 5.0$, $\delta_i = \delta_p = 0.0$, $\theta = 2^0$, $T_i/T_h = 0.5$, $n_{p0}/n_{e0} = n_{i0}/n_{e0} = 0.5$ and $\delta_e = -0.10$	97
4.23	Numerical solution of normalized parallel electric field for the parameters $E_0 = 2.5$, $M = 3.5$, $R = 5.0$, $\delta_i = \delta_p = 0.0$, $\theta = 2^0$, $T_i/T_h = 0.5$, $n_{p0}/n_{e0} = n_{i0}/n_{e0} = 0.5$ and $\delta_e = 0.0$	98
4.24	Numerical solution of normalized parallel electric field for the parameters $E_0 = 2.5$, $M = 3.5$, $R = 5.0$, $\delta_i = \delta_p = 0.0$, $\theta = 2^0$, $T_i/T_h = 0.5$, $n_{p0}/n_{e0} = n_{i0}/n_{e0} = 0.5$ and $\delta_e = 0.10$	99
4.25	Numerical solution of normalized parallel electric field for the parameters $E_0 = 2.5$, $M = 3.5$, $R = 5.0$, $\delta_e = \delta_p = 0.0$, $\theta = 2^0$, $T_i/T_h = 0.5$, $n_{p0}/n_{e0} = n_{i0}/n_{e0} = 0.5$ and $\delta_i = -0.10$	101
4.26	Numerical solution of normalized parallel electric field for the parameters $E_0 = 2.5$, $M = 3.5$, $R = 5.0$, $\delta_e = \delta_p = 0.0$, $\theta = 2^0$, $T_i/T_h = 0.5$, $n_{p0}/n_{e0} = n_{i0}/n_{e0} = 0.5$ and $\delta_i = 0.0$	102
4.27	Numerical solution of normalized parallel electric field for the parameters $E_0 = 2.5$, $M = 3.5$, $R = 5.0$, $\delta_e = \delta_p = 0.0$, $\theta = 2^0$, $T_i/T_h = 0.5$, $n_{p0}/n_{e0} = n_{i0}/n_{e0} = 0.5$ and $\delta_i = 0.1$	103
4.28	Numerical solution of normalized parallel electric field for the parameters $E_0 = 2.5$, $M = 3.5$, $R = 5.0$, $\delta_i = \delta_e = 0.0$, $\theta = 2^0$, $T_i/T_h = 0.5$, $n_{p0}/n_{e0} = n_{i0}/n_{e0} = 0.5$ and $\delta_p = -0.10$	105

4.29	Numerical solution of normalized parallel electric field for the parameters $E_0 = 2.5$, $M = 3.5$, $R = 5.0$, $\delta_i = \delta_e = 0.0$, $\theta = 2^0$, $T_i/T_h = 0.5$, $n_{p0}/n_{e0} = n_{i0}/n_{e0} = 0.5$ and $\delta_p = 0.0$	106
4.30	Numerical solution of normalized parallel electric field for the parameters $E_0 = 2.5$, $M = 3.5$, $R = 5.0$, $\delta_i = \delta_e = 0.0$, $\theta = 2^0$, $T_i/T_h = 0.5$, $n_{p0}/n_{e0} = n_{i0}/n_{e0} = 0.5$ and $\delta_p = 0.1$	107
5.1	Plot of the Sagdeev potential $V(\psi)$ against the potential ψ for the the fixed parameters $Z_d = 1000$, $m/m_d = 10^{-7}$, $\sigma_{ep} = 0.5$ and $\alpha = 0.5$	119
5.2	Plot of the Sagdeev potential $V(\psi)$ for the parameters $Z_d = 1000$, $m/m_d = 10^{-7}$, $\sigma_{ep} = 0.5$ and $M = 0.01$	120
5.3	Plot of the Sagdeev potential $V(\psi)$ for the parameters $Z_d = 1000$, $m/m_d = 10^{-7}$, $\alpha = 0.5$, and $M = 0.01$	121
5.4	Soliton profile $\psi(S)$ for selected curves from Fig. 5.1 with the dotted(solid) curves corresponding to $M = 0.009$ (0.011) for the fixed parameters $Z_d = 1000$, $m/m_d = 10^{-7}$, $\sigma_{ep} = 0.5$ and $\alpha = 0.5$	122
5.5	Soliton profile $\psi(S)$ for selected curves from Fig.5.2 with the solid (dotted) curves corresponding to $\alpha = 0.45$ (0.5) for the fixed parameters $M = 0.011$, $Z_d = 1000$, $m/m_d = 10^{-7}$ and $\sigma_{ep} = 0.5$	123
5.6	Soliton profile $\psi(S)$ for selected curves from Fig. 5.3, with the dotted (solid) curves corresponding to $\sigma_{ep} = 0.2$ (0.8) for the fixed parameters $M = 0.011$, $Z_d = 1000$, $m/m_d = 10^{-7}$, $T_e/T_p = 0.5$ and $\alpha = 0.5$	124

Chapter 1

Introduction

Magnetosphere is defined as the region of space surrounding the Earth where its magnetic influences control the behavior of the ionized gas (plasma). The shape of the Earth's magnetosphere resulting from the interaction between the solar wind and the geomagnetic field, and the pressure of the solar wind on Earth's magnetic field compresses the field on the dayside of Earth and stretches the field into a long tail on the nightside. This interaction in the magnetosphere is answerable for many miraculous natural phenomena such as the aurora and whistler waves.

The dynamics of the terrestrial magnetosphere is controlled by the Earth's magnetic field so that the magnetosphere can be categorized into several regions, e.g. Magnetopause, Magnetosheath, Magnetotail, Bow Shocks, which are generated by the topology of this magnetic field. In the interior of the magnetosphere, the plasma is not distributed uniformly but is grouped into different regions with different temperatures and densities. These plasmas can be termed as dusty plasmas as almost all space and astrophysical plasmas are now found to carry massive dust particles [Temerin et al., 1982; Meuris and Verheest, 1996; Pickett et al., 2004]. The variability of plasmas in the magnetosphere arises from fluctuations in the solar wind flow, and provides several processes like reconnection, collisionless shocks, particle acceleration and turbulence.

The study of astrophysical environments revealed the existence of electron-positron (e-p)

pairs which are assumed to be the most important constituents of the plasma originating in pulsars and in the inner region of the accretion disks surrounding the central black holes in active galactic nuclei [Goldreich and Julian, 1969; Michel, 1982; Begelman et al., 1984]. They may be developed in the magnetospheres of pulsars by the pair-production cascade breeding process [Ruderman and Sutherland, 1975]. On the other hand, the presence of ions in such plasmas has been confirmed by different authors and their behaviours have been discussed by Hoshino and Arons [1991] and Jammalamadaka et al. [1996]. They reported that the presence of ions in e-p plasmas leads to several new linear and nonlinear modes. Therefore, the study of three component electron-positron-ion (e-p-i) plasmas can furnish further information in an understanding of the behaviour in both astrophysical and laboratory plasmas, and the magnetosphere may be an admirable natural laboratory where the different processes occurred in plasmas can be investigated on a variety of spatial scales.

The existence of electron-positron-ion triplets in various astrophysical environments remains a great topic of research due to their potential relevance to space plasmas [Michel, 1982; Miller and Witta, 1987; Kozlovsky et al., 2004; Lee and Ruiz, 2005]. The study of both linear and nonlinear wave propagation in e-p-i plasmas plays a vital role in understanding different types of collective processes in space plasmas. Such plasmas are found in the early universe [Miller and Witta, 1987], in solar atmospheres [Kozlovsky et al., 2004], active galactic nuclei (AGN) [Miller and Witta, 1987], near the polar cusp regions of pulsars, neutron star atmospheres [Michel, 1982] and in the inner region of the accretion disks surrounding the central black holes [Lee and Ruiz, 2005]. The ions presented in most of these astrophysical plasmas originate from some interior source, for example, as a result of evaporation or seismic processes on the surface of a star in the process of accretion [Zeba et al., 2012]. Moreover, the propagation of intense short laser pulses in matter can be accompanied by the formation of e-p-i plasma due to photo production during photon scattering by nuclei [Berezhiani and Mahajan, 1994]. In fact, such three component plasmas have been seen in laboratory experiments when positrons are used to probe particle transport in tokamaks, due to their sufficient lifetime, two-component electron-ion (e-i) plasmas evolves to a three-

component e-p-i plasma [Surko and Murphy, 1990]. In many astrophysical environments there exists a small number of ions along with the electrons and positrons, therefore, it is pertinent to study observationally, experimentally and theoretically behavior of linear and nonlinear wave motions in an e-p-i plasma.

Earliest observations of the plasmas in the dayside polar magnetosphere were obtained with the earth-satellite Imp 5 during July-August 1969. Frank [1971] revealed the existence of the bands which have the shape of the geomagnetic cavity formed by the interaction of the solar wind with the geomagnetic field across the dayside high-latitude magnetopause (one band in the northern hemisphere and a second in the southern hemisphere). These two bands/ regions of the magnetopause through which the magnetosheath plasma has direct access to the magnetosphere, and the corresponding extension of these bands from magnetopause to auroral altitudes have been identified as the polar cusps.

Gurnett et al. [1976] reported a space observation of a new type of plasma wave emissions by the IMP-8 satellite in the plasma sheet boundary layer of the Earth's magnetotail. The emission was purely electrostatic, and it had a broadband spectrum from ion plasma and lower hybrid frequencies up to and higher than the electron plasma and cyclotron frequencies. The emissions were named as broadband electrostatic noise (BEN).

Several linear theories based on electron-acoustic instabilities [Tokar and Gary, 1984; Gary and Tokar, 1985; Bharuthram, 1991; Dubouloz et al., 1991] have been devoted in order to explain the higher frequency part of BEN spectrum. However, there is still no satisfactory explanations for the low-frequency part of BEN: BEN does not consist of continuous waves, but impulsive ones [Anderson et al., 1982; Nishida et al., 1985].

Tokar and Gary [1984] analyzed the full electromagnetic Vlasov dispersion equation and studied the stability of the electrostatic and electromagnetic waves for the case of upward moving electron beams observed in the polar cusp region. Their numerical simulations showed electron-acoustic waves (EAWs) to be unstable and these results were confirmed by Schriver and Ashour-Abdalla [1987]. Theoretical studies of electrostatic waves driven by ion beam instabilities in relation to BEN in three-component plasmas (hot ions, hot elec-

trons and cold electrons) was successfully conducted by Omidi [1985] after different authors [Grabbe and Eastman, 1984; Dusenbery and Lyons, 1985] showed that higher angles of wave propagation (with respect to the background magnetic field) can have much larger growth rates at lower frequencies. In an extension of the work [Omidi, 1985] by Akimoto and Omidi [1986], it was revealed that two different instabilities can be excited by an ion beam and the propagation angle determines which is excited.

Further nonlinear investigations were conducted in theoretical and numerical studies and laboratory experiments to understand the nature of the BEN emissions. Dubouloz et al. [1991] showed that the nonlinear effects can play a significant role in the generation of BEN in the dayside auroral zone. Recent high time-resolution measurements by the fast auroral snapshot (FAST) satellites have confirmed the presence of coherent nonlinear phenomena and the BEN found had waveforms of solitary bipolar electric field pulses which are named Electrostatic Solitary Waves (ESWs)[Matsumoto et al., 1994]. These solitary waves are electrostatic in most cases, because the polarizations of the bipolar pulses are mostly along the static magnetic field without any transverse magnetic field components. Mach

The fast solitary waves have been observed not only in the mid-altitude auroral zone [Ergun et al., 1998], but also in the high altitude polar magnetosphere, between 2 and 8.5 times the radius of the Earth [Dombeck et al., 2001] and they evolve in heating and accelerating charged particles in these environments. The observations from different spacecrafts [Wu et al., 1996; Pickett et al., 2008] have revealed the nature of the electrostatic solitary waves (ESWs) in different regions in near-earth plasmas. The results of these observations have pointed out the existence of super-thermal components of various plasma species. The electric field structures found are exclusively in regions of BEN and contributing to its spectral features at high frequencies. Similar fast moving solitary waves have been found in the high altitude polar cusp region by Cattell et al. [1999].

It is therefore important to theoretically explain certain satellite observations of nonlinear electrostatic fluctuations in different regions of the Earth's magnetosphere. By inspection of

these observations, we model the space plasmas and our theoretical results are compared to the experimental findings.

This thesis is structured as follows: The background information related to our topic is presented and the scope of this work is outlined in Chapter One.

In Chapter Two, we discuss the linear electrostatic waves in a magnetized, three-component e-p-i plasma to model the pulsar magnetosphere, with hot electrons and positrons and cool ions. The cool ions are governed by the fluid equations while the hot electron and positron densities are assumed to be Boltzmann distributed. With Poisson's equation, we examine the behavior of the electrostatic waves in such plasmas in the low frequency limit, taking into account the mass of the ions. The effects of the density, temperature ratio and propagation angle on the wave structures are investigated in two limiting cases: parallel and perpendicular propagation.

In Chapter Three, we study nonlinear electrostatic fluctuations in magnetospheric environments. We attempt to provide an explanation of nonlinear low frequency waves observed by spacecraft missions in the auroral regions by using a theoretical model formed by a magnetized, three-component e-p-i plasma including charge separation. By using the continuity and momentum equations with Poisson's equation, the three component plasma consisting of cool ions, and hot Boltzmann electrons and positrons are investigated and the effect of the electric field, temperature, density, ion drift, *Mach* number and propagation angle on the wave structures are discussed.

In Chapter Four, we extend the theoretical model of nonlinear electrostatic waves in magnetospheric environments discussed in Chapter 3, hereby all species are described by fluid equations. In this chapter, the additional information on the effect of the electron and positron density and their corresponding drift velocity are also examined.

Chapter Five describes solitary structures in an unmagnetized three component electron-positron-dust plasma. We investigate nonlinear electrostatic structures in the magnetosphere by using the Sagdeev pseudo-potential technique. The study is inspired by results of different spacecraft observations of electrostatic solitary waves (ESW) in the near-earth and

magnetospheric plasmas, and recent experimental realization of existence of superthermal electron component in various space plasmas.

Finally, we shall summarize our work in Chapter Six.

Chapter 2

Linear electrostatic waves in electron-positron-ion plasmas

2.1 Literature Review

Linear wave propagation in electron-positron (e-p) plasmas is different by comparison with the ordinary electron-ion (e-i) plasmas. A particularly interesting feature of (e-p) plasmas by comparison with the usual (e-i) plasmas is that both electron and positron species have the same mass and equal magnitude of charge. The behavior of the wave motion in e-p-i plasmas are different from those in two component electron-positron (e-p) and electron-ion (e-i) plasmas [Popel et al., 1995; Tiwari et al., 2007]. The presence of ions leads to the existence of several low -frequency waves which otherwise do not propagate in e-p plasmas [Pakzad, 2009; Tarsem et al., 2007].

Linear electron-positron plasmas have been studied by various researchers [Bulanov, 2004; Zank and Greaves, 1995; Kluger et al., 1991; Greaves et al., 1994]. It was shown that the e-p plasma symmetry is broken in the presence of ions, and both fast and slow time scales can occur in the dynamics of e-p-i plasmas [Zeba et al., 2012].

Linear electrostatic waves have been investigated in an unmagnetized three-component e-p-i plasma [Popel et al., 1995; Alinejad and Mamun, 2011; Jilani et al., 2013]. Several

authors have studied theoretically and experimentally linear and nonlinear wave propagation in magnetized e-p-i plasmas using different models [Nejoh, 1996; Hasegawa et al., 2002; Nejoh, 1997; Kakati and Goswami, 1998, 2000; Haque et al., 2002; Salahuddin et al., 2002]. Tiwari et al. [2007] and Tiwari [2008] investigated the effects of the density and temperature on ion-acoustic waves in a three-component plasma and found that the amplitude of the structures in an e-p-i plasma decreases with increasing positron concentration or temperature ratio.

Recently, theoretical studies on linear waves has been investigated by Lazarus et al. [2012] to explain the behavior of electrostatic waves in a four component, two-temperature electron-positron plasma. By assuming that the temperatures of the cool electrons and cool positrons are equal and that the temperatures of hot electrons and hot positrons are equal and obey the Boltzmann density distributions, the different modes of wave propagation were analyzed.

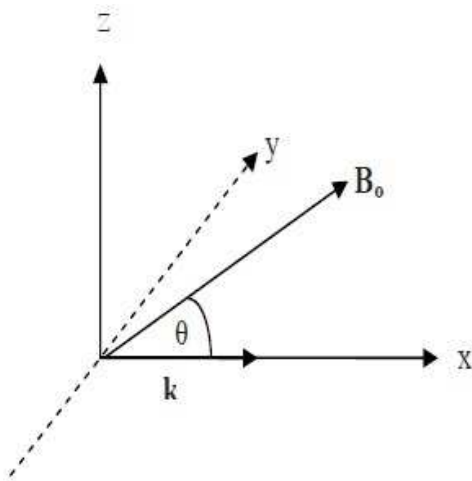
At present, several theoretical studies of linear as well as nonlinear wave phenomena in both unmagnetized and magnetized e-p-i plasmas have been of interest [Popel et al., 1995; Alinejad and Mamun, 2011; Jilani et al., 2013; Nejoh, 1996; Hasegawa et al., 2002]. Abdelsalam et al. [2008] and Rasheed et al. [2010] investigated ion-acoustic waves in e-p-i plasmas by using different forms of distributions for electrons and positrons, such as the Thomas-Fermi approximation and nonrelativistic electron/positron equation of state and observed that the ion-acoustic speed in the degenerate pair-ion plasma depends both on the electron temperature and ion mass as well as the concentration of the positron and ions in the plasma. Alinejad and Mamun [2011] studied linear and nonlinear propagation of ion-acoustic waves subjected to an external magnetic field in an e-p-i plasma and found that when the positron concentration is increased, the frequencies of both the slow and fast modes decreased. They investigated the effects of obliqueness, magnetic field, densities and the temperature ratio on such plasmas. For most of these investigations, the general dispersion relation for multicomponent plasmas had been obtained without considering the mass of the ions. It is thus of interest to investigate the effects of the ion mass on the structure of the waves propagating in an e-p-i plasma.

In this chapter, we pay particular attention to a magnetized, three-component, e-p-i plasma to model the pulsar magnetosphere with a hot species of electrons, positrons and cool ions and two different approaches will be adopted. The cool ions are governed by the fluid equations and the hot electron and positron densities are assumed to be Boltzmann distributed. Our studies will focus on the behavior of the electrostatic waves in such plasmas in the low frequency limit, taking into account the mass of the ions. By using the fluid theory approach, the effects of the density and the temperature ratio on the wave structures will be investigated at two limiting cases: parallel and perpendicular propagation. It is worth noting that recombination and annihilation of electron-positron pairs are neglected throughout this thesis.

2.2 Fluid Theory Approach

2.2.1 The model of fluid equations

We consider a collisionless, magnetized three-component plasma having cold ions (i) and hot positron (p) and hot electron species (e) in the presence of an external magnetic field B_0 . Wave propagation is in the x -direction at an angle θ to the ambient magnetic field B_0 , which is assumed to be in the $x - z$ plane.



The hot electrons and hot positrons are assumed to obey the Boltzmann distribution

with equal temperatures T_h . At equilibrium the densities of the electrons and positrons are different and denoted n_{e0} and n_{p0} respectively. The basic equations, governing the dynamics of the positive ions are the equations of continuity and momentum:

$$\frac{\partial n_i}{\partial t} + \frac{\partial n_i v_{ix}}{\partial x} = 0, \quad (2.1)$$

$$\frac{\partial v_{ix}}{\partial t} + v_{ix} \frac{\partial v_{ix}}{\partial x} + \frac{1}{n_i m_i} \frac{\partial p_i}{\partial x} = -\frac{e}{m_i} \frac{\partial \varphi}{\partial x} + \Omega_i v_{iy} \sin \theta, \quad (2.2)$$

$$\frac{\partial v_{iy}}{\partial t} + v_{ix} \frac{\partial v_{iy}}{\partial x} = \Omega_i v_{iz} \cos \theta - \Omega_i v_{ix} \sin \theta, \quad (2.3)$$

$$\frac{\partial v_{iz}}{\partial t} + v_{ix} \frac{\partial v_{iz}}{\partial x} = -\Omega_i v_{iy} \cos \theta, \quad (2.4)$$

$$\frac{\partial p_i}{\partial t} + v_{ix} \frac{\partial p_i}{\partial x} + 3p_i \frac{\partial v_{ix}}{\partial x} = 0. \quad (2.5)$$

The electrons and positrons in the electrostatic potential perturbation are assumed to follow the Boltzmann distributions, respectively, as

$$n_e = n_{e0} \exp\left(\frac{e\varphi}{T_h}\right) \quad (2.6)$$

$$n_p = n_{p0} \exp\left(-\frac{e\varphi}{T_h}\right). \quad (2.7)$$

Equations (2.1) - (2.7) are closed with the Poisson equation

$$\varepsilon_0 \frac{\partial^2 \varphi}{\partial x^2} = -e(n_p - n_e + n_i) \quad (2.8)$$

where $\Omega_i = eB_0/m_i$ is the ion cyclotron frequency, n_i is the ion density, $n_e(n_p)$ is the density of hot electrons (positrons), v_{ix}, v_{iy} and v_{iz} are the components of the ion velocity along the x, y and z directions, p_i is the ion pressure, φ is the electrostatic potential and m_i is the ion mass.

Assuming that the above equations have harmonic solutions, such that all variables are of

the form $\exp(i(kx - \omega t))$, $\partial/\partial x$ is replaced with ik and $\partial/\partial t$ is replaced with $-i\omega$. Linearizing by neglecting the higher order perturbations, the continuity equation becomes

$$-n_i i\omega + ikv_{ix}n_{i0} = 0 \quad (2.9)$$

for which

$$n_i = \frac{kn_{i0}}{\omega}v_{ix}. \quad (2.10)$$

Linearizing the momentum equations, we obtain the velocity components for the cool ions as follows

$$v_{ix} = \frac{3k}{\omega}v_{ti}^2 \left(\frac{n_i}{n_{i0}} \right) + \frac{ke}{\omega m_i} \phi + i \frac{\Omega_i}{\omega} v_{iy} \sin \theta, \quad (2.11)$$

$$v_{iy} = \frac{i\Omega_i}{\omega} (v_{iz} \cos \theta - v_{ix} \sin \theta), \quad (2.12)$$

$$v_{iz} = -\frac{i\Omega_i}{\omega} v_{iy} \cos \theta, \quad (2.13)$$

where $v_{ti} = (T_i/m_i)^{1/2}$ is the thermal speed for the ions (the Boltzmann constant is omitted i.e. set to 1).

Substituting for v_{iz} from equation (2.13) into equation (2.12) and using equation (2.11), v_{ix} becomes

$$v_{ix} = \frac{(\omega^2 - \Omega_i^2 \cos^2 \theta)(3kv_{ti}^2 m_i (n_i/n_{i0}) + ke\phi)}{\omega m_i (\omega^2 - \Omega_i^2)}. \quad (2.14)$$

Substituting the above equation into equation (2.10), the perturbed density of the ions is expressed as follows:

$$n_i = \frac{k^2 n_{i0} e \phi}{m_i} \frac{(\omega^2 - \Omega_i^2 \cos^2 \theta)}{\omega^2 (\omega^2 - \Omega_i^2) - 3k^2 v_{ti}^2 (\omega^2 - \Omega_i^2 \cos^2 \theta)}. \quad (2.15)$$

Linearizing equations (2.6) and (2.7), we have dropped the second and higher order terms in a Taylor series expansion of the exponential and the perturbed densities of hot species

such that

$$n_e = n_{e0} \frac{e\varphi}{T_h} \quad (2.16)$$

$$n_p = -n_{p0} \frac{e\varphi}{T_h}. \quad (2.17)$$

Substituting equations (2.15), (2.16) and (2.17) into the Poisson equation (2.8), the general dispersion relation for multicomponent plasma consisting of hot electrons and positrons and cold ions is

$$\omega^4 - \omega^2 (\Omega_i^2 + 3k^2 v_{ti}^2) + 3k^2 v_{ti}^2 \Omega_i^2 \cos^2 \theta = k^2 v_{ia}^2 \frac{(\omega^2 - \Omega_i^2 \cos^2 \theta)}{k^2 \lambda_{Dh}^2 + \frac{n_{p0}}{n_{e0}} + 1}. \quad (2.18)$$

Rearranging terms, the above equation becomes

$$\omega^4 - \omega^2 \left(\Omega_i^2 + 3k^2 v_{ti}^2 + \frac{k^2 v_{ia}^2}{k^2 \lambda_{Dh}^2 + \frac{n_{p0}}{n_{e0}} + 1} \right) + \Omega_i^2 \cos^2 \theta \left(3k^2 v_{ti}^2 + \frac{k^2 v_{ia}^2}{k^2 \lambda_{Dh}^2 + \frac{n_{p0}}{n_{e0}} + 1} \right) = 0 \quad (2.19)$$

where $v_{ia} = (n_{0i}m/n_{e0}m_i)^{1/2}v_{th}$ is the ion acoustic speed, $v_{th} = (T_h/m)^{1/2}$ is electron thermal speed and $\lambda_{Dh} = (\varepsilon_0 T_h/n_0 e^2)^{1/2}$ is electron Debye length.

The above equation can be rewritten as following

$$\omega^4 - \omega^2 \Omega_i^2 - 3k^2 v_{ti}^2 \omega^2 - \frac{k^2 v_{ia}^2}{k^2 \lambda_{Dh}^2 + \frac{n_{p0}}{n_{e0}} + 1} \omega^2 + 3k^2 v_{ti}^2 \Omega_i^2 \cos^2 \theta + \frac{k^2 v_{ia}^2}{k^2 \lambda_{Dh}^2 + \frac{n_{p0}}{n_{e0}} + 1} \Omega_i^2 \cos^2 \theta = 0, \quad (2.20)$$

Rearranging terms of the equation (2.20), we get

$$\omega^2 (\omega^2 - \Omega_i^2) - 3k^2 v_{ti}^2 (\omega^2 - \Omega_i^2 \cos^2 \theta) - \frac{k^2 v_{ia}^2}{k^2 \lambda_{Dh}^2 + \frac{n_{p0}}{n_{e0}} + 1} (\omega^2 - \Omega_i^2 \cos^2 \theta) = 0. \quad (2.21)$$

In the limit $\omega \ll \Omega_i \cos \theta$, i.e for wave frequencies much lower than the gyrofrequency, equation (2.21) reduces to

$$\omega^2 \Omega_i^2 - 3k^2 v_{ti}^2 \Omega_i^2 \cos^2 \theta - \frac{k^2 v_{ia}^2}{k^2 \lambda_{Dh}^2 + \frac{n_{p0}}{n_{e0}} + 1} \Omega_i^2 \cos^2 \theta = 0. \quad (2.22)$$

Solving equation (2.22), one obtains for the associated acoustic mode

$$\omega^2 = \left(3k^2 v_{ti}^2 + \frac{k^2 v_{ia}^2}{k^2 \lambda_{Dh}^2 + \frac{n_{p0}}{n_{e0}} + 1} \right) \cos^2 \theta. \quad (2.23)$$

Considering the short wavelength limit where $k^2 \lambda_{Dh}^2 \gg 1$, the general dispersion relation (2.19) reduces to

$$\omega^4 - \omega^2 \left(\Omega_i^2 + 3k^2 v_{ti}^2 + \frac{v_{ia}^2}{\lambda_{Dh}^2} \right) + \Omega_i^2 \cos^2 \theta \left(3k^2 v_{ti}^2 + \frac{v_{ia}^2}{\lambda_{Dh}^2} \right) = 0. \quad (2.24)$$

The above equation can take the following form

$$\omega^4 - \omega^2 (\Omega_i^2 + 3k^2 v_{ti}^2 + \omega_{pi}^2) + \Omega_i^2 \cos^2 \theta (3k^2 v_{ti}^2 + \omega_{pi}^2) = 0, \quad (2.25)$$

where $\omega_{pi}^2 = v_{ia}^2 / \lambda_{Dh}^2$ is the ion plasma frequency.

Equation (2.25) may be rewritten as

$$\omega^4 - \omega^2 (3k^2 v_{ti}^2 + \omega_{UH}^2) + \Omega_i^2 \cos^2 \theta (3k^2 v_{ti}^2 + \omega_{pi}^2) = 0, \quad (2.26)$$

where

$$\omega_{UH}^2 = \Omega_i^2 + \omega_{pi}^2. \quad (2.27)$$

The expression (2.27) is known as the upper hybrid frequency.

In solving equation (2.26), we assume that

$$(3k^2 v_{ti}^2 + \omega_{UH}^2)^2 \gg 4\Omega_i^2 \cos^2 \theta (3k^2 v_{ti}^2 + \omega_{pi}^2) \quad (2.28)$$

and we obtain two roots; the positive (+) root

$$\omega_+^2 = 3k^2 v_{ti}^2 + \omega_{UH}^2 - \frac{\Omega_i^2 \cos^2 \theta (3k^2 v_{ti}^2 + \omega_{pi}^2)}{(3k^2 v_{ti}^2 + \omega_{UH}^2)} \quad (2.29)$$

and the negative (-) root

$$\omega_-^2 = \frac{\Omega_i^2 \cos^2 \theta (3k^2 v_{ti}^2 + \omega_{pi}^2)}{(3k^2 v_{ti}^2 + \omega_{UH}^2)}. \quad (2.30)$$

The results obtained for an electron-positron-ion plasma have the similar characteristics as the electron cyclotron and electron acoustic waves investigated by Lazarus et al. [2012] for four-component, two-temperature electron-positron plasma.

For analyzing equation (2.21), we focus on two extreme limits viz, parallel and perpendicular propagation which will be discussed below.

A) Parallel propagation

Considering parallel propagation ($\theta = 0^0$), the general dispersion relation (2.21) reduces to

$$\omega^2(\omega^2 - \Omega_i^2) - \left(3k^2 v_{ti}^2 + \frac{k^2 v_{ia}^2}{k^2 \lambda_{Dh}^2 + \frac{n_{p0}}{n_{e0}} + 1} \right) (\omega^2 - \Omega_i^2) = 0. \quad (2.31)$$

Solving equation (2.31), we obtain two solutions,

the first

$$\omega_+^2 = \Omega_i^2, \quad (2.32)$$

which is a constant frequency, non-propagating ion cyclotron mode

and the second

$$\omega_-^2 = 3k^2 v_{ti}^2 + \frac{k^2 v_{ia}^2}{k^2 \lambda_{Dh}^2 + \frac{n_{p0}}{n_{e0}} + 1} \quad (2.33)$$

is the ion-acoustic mode. The above equation is similar to results found in Lazarus et al. [2012].

Now: $v_{ia}^2 = v_{th}^2 \frac{n_{i0}}{n_{e0}} \frac{m}{m_i} = \frac{T_h}{m} \frac{n_{i0}}{n_{e0}} \frac{m}{m_i} = \frac{T_h}{m_i} \frac{n_{i0}}{n_{e0}}$

In the limit $k^2 \lambda_{Dh}^2 \ll 1$, equation (2.33) reduces to

$$\omega_-^2 = k^2 v_{ia}^2 \left(3 \frac{T_i n_{e0}}{T_h n_{i0}} + 1 / \left(\frac{n_{p0}}{n_{e0}} + 1 \right) \right). \quad (2.34)$$

Equation (2.34) is the ion acoustic mode which arises from the motion of the cool ions.

In the limit $k^2 \lambda_{Dh}^2 \gg 1$, we obtain the following expression

$$\omega_-^2 = 3k^2v_{ti}^2 + \omega_{pi}^2. \quad (2.35)$$

which corresponds to the dispersion relation for Langmuir waves in an electron-positron plasma [Zank and Greaves, 1995; Lazarus et al., 2012].

B) Perpendicular propagation

Considering perpendicular propagation ($\theta = 90^\circ$), equation (2.21) may be rewritten as

$$\omega^4 - \omega^2 \left(\Omega_i^2 + 3k^2v_{ti}^2 + \frac{k^2v_{ia}^2}{k^2\lambda_{Dh}^2 + \frac{n_{p0}}{n_{e0}} + 1} \right) = 0. \quad (2.36)$$

Solving the above equation, we obtain the normal mode frequencies

$$\omega = 0, \quad (2.37)$$

which is a non-propagating mode and

$$\omega^2 = \Omega_i^2 + 3k^2v_{ti}^2 + \frac{k^2v_{ia}^2}{k^2\lambda_{Dh}^2 + \frac{n_{p0}}{n_{e0}} + 1}, \quad (2.38)$$

is the ion cyclotron mode which arises from both the cool and hot species.

In the limit $k^2\lambda_{Dh}^2 \gg 1$, i.e in the short wavelength limit, equation (2.38) becomes

$$\omega^2 = \Omega_i^2 + 3k^2v_{ti}^2 + \frac{v_{ia}^2}{\lambda_{Dh}^2}, \quad (2.39)$$

which may be rewritten in the following form

$$\omega^2 = \omega_{UH}^2 + 3k^2v_{ti}^2. \quad (2.40)$$

The expression (2.40) is the upper hybrid mode, which depends on the cooler species (ions) and is similar to results obtained by Zank and Greaves [1995] and Lazarus et al. [2012].

By taking $k^2 \lambda_{Dh}^2 \ll 1$, i.e the long wavelength limit, the dispersion relation for perpendicular propagation equation (2.38) reduces to

$$\omega^2 = \Omega_i^2 + 3k^2 v_{ti}^2 + \frac{k^2 v_{ia}^2}{\left(\frac{n_{p0}}{n_{e0}} + 1\right)}, \quad (2.41)$$

and may rewritten as

$$\omega^2 = \Omega_i^2 + k^2 v_{ia}^2 \left(3 \frac{T_i n_{e0}}{T_h n_{i0}} + 1 / \left(\frac{n_{p0}}{n_{e0}} + 1 \right) \right). \quad (2.42)$$

The above expression is the cyclotron mode for electron-positron-ion plasmas with contributions from the hot and cooler species.

2.3 Numerical results and Discussion

In this section, we focus on the effects of the density and temperature for parallel ($\theta = 0^\circ$) and perpendicular ($\theta = 90^\circ$) propagation. Normalizing the temperature with T_h , the fluid speed by the thermal velocity $v_{th} = (T_h/m)^{1/2}$, the spatial length by $\lambda_D = (\varepsilon_0 T_h / n_{e0} e^2)^{1/2}$, the particle density by the total equilibrium plasma density $n_{e0} = n_{i0} + n_{p0}$ and time by $\omega_{pi}^{-1} = (n_{e0} e^2 / \varepsilon_0 m_i)^{-1/2}$ in equation (2.19), we obtain the normalized general dispersion relation,

$$\tilde{\omega}^4 - \tilde{\omega}^2 \left(\frac{1}{R^2} + 3\tilde{k}^2 \frac{T_i}{T_h} \frac{m}{m_i} + \frac{\tilde{k}^2 \tilde{n}_{0c} \frac{m}{m_i}}{\tilde{k}^2 + \tilde{n}_{0h} + 1} \right) + \frac{\cos^2 \theta}{R^2} \left(3\tilde{k}^2 \frac{T_i}{T_h} \frac{m}{m_i} + \frac{\tilde{k}^2 \tilde{n}_{0c} \frac{m}{m_i}}{\tilde{k}^2 + \tilde{n}_{0h} + 1} \right) = 0 \quad (2.43)$$

where $\tilde{\omega} = \omega / \omega_p$, $\tilde{k} = k \lambda_D$, $\tilde{n}_{0c} = n_{0i} / n_{e0}$, $\tilde{n}_{0h} = n_{p0} / n_{e0}$, $R = \omega_{pi} / \Omega_i$.

This relation is similar to Lazarus et al. [2012] with an additional mass ratio $\frac{m}{m_i}$.

Equation (2.43) can be solved numerically. The parameter R in equation (2.43) characterizes the strength of the magnetic field for a fixed total plasma density and $R \ll 1$ corresponds

to a strongly magnetized plasma and $R \gg 1$ corresponds to a weakly magnetized plasma. We choose $R = 0.333$ for an easy comparison with the findings of [Zank and Greaves, 1995; Lazarus et al., 2012].

For fixed parameters $R = 0.333$, and $\frac{T_i}{T_h} = 0.01$, the variation of the normalized frequency with normalized wavenumber is plotted. The effects of different values of n_{i0}/n_{e0} for parallel propagation ($\theta = 0^\circ$) are represented in Fig. 2.1. Equation (2.43) shows the electron-to-ion mass ratio $\frac{m}{m_i}$ which is not present in an e-p plasma. This ratio reduces the frequency significantly compared to results obtained by Lazarus et al. [2012].

This figure shows that the frequency of the mode increases with an increasing density ratio and can also be deduced from equation (2.33). The dispersion curves obtained is identified as ion-acoustic mode.

Figure 2.2 shows the curves representing the variation of the normalized frequency for different values of $\frac{T_i}{T_h}$ for the following fixed parameters: $R = 0.333, n_{i0}/n_{e0} = 0.11$ and $\theta = 0^\circ$ (parallel propagation). The frequency of the wave increases with an increase in $\frac{T_i}{T_h}$.

The curves representing the different values of the density ratio for the following fixed parameters $R = 0.333, \frac{T_i}{T_h} = 0.01$ and $\theta = 90^\circ$ (perpendicular propagation) are shown in Fig. 2.3. The frequency increases with an increase in n_{i0}/n_{e0} . The ion cyclotron mode (2.38) arises from the cool and hot species. For small proportions of the hot species, the mode approaches the upper hybrid frequency (2.40). Figure 2.4 represents the different values of the temperature ratio for the fixed parameters $R = 0.333, n_{i0}/n_{e0} = 0.11$ and $\theta = 90^\circ$ (perpendicular propagation). This is the ion-cyclotron mode and the frequency increases with an increase in T_i/T_h .

Figures 2.5 and 2.6 show the ion-acoustic and cyclotron branches for different angles of propagation, respectively. The ion-acoustic mode decreases with increase in the propagation angle and disappears at $\theta = 90^\circ$. The curves represented in Fig. 2.6 are identified as the cyclotron mode and the frequency of this mode increases with increase in the propagation angle.

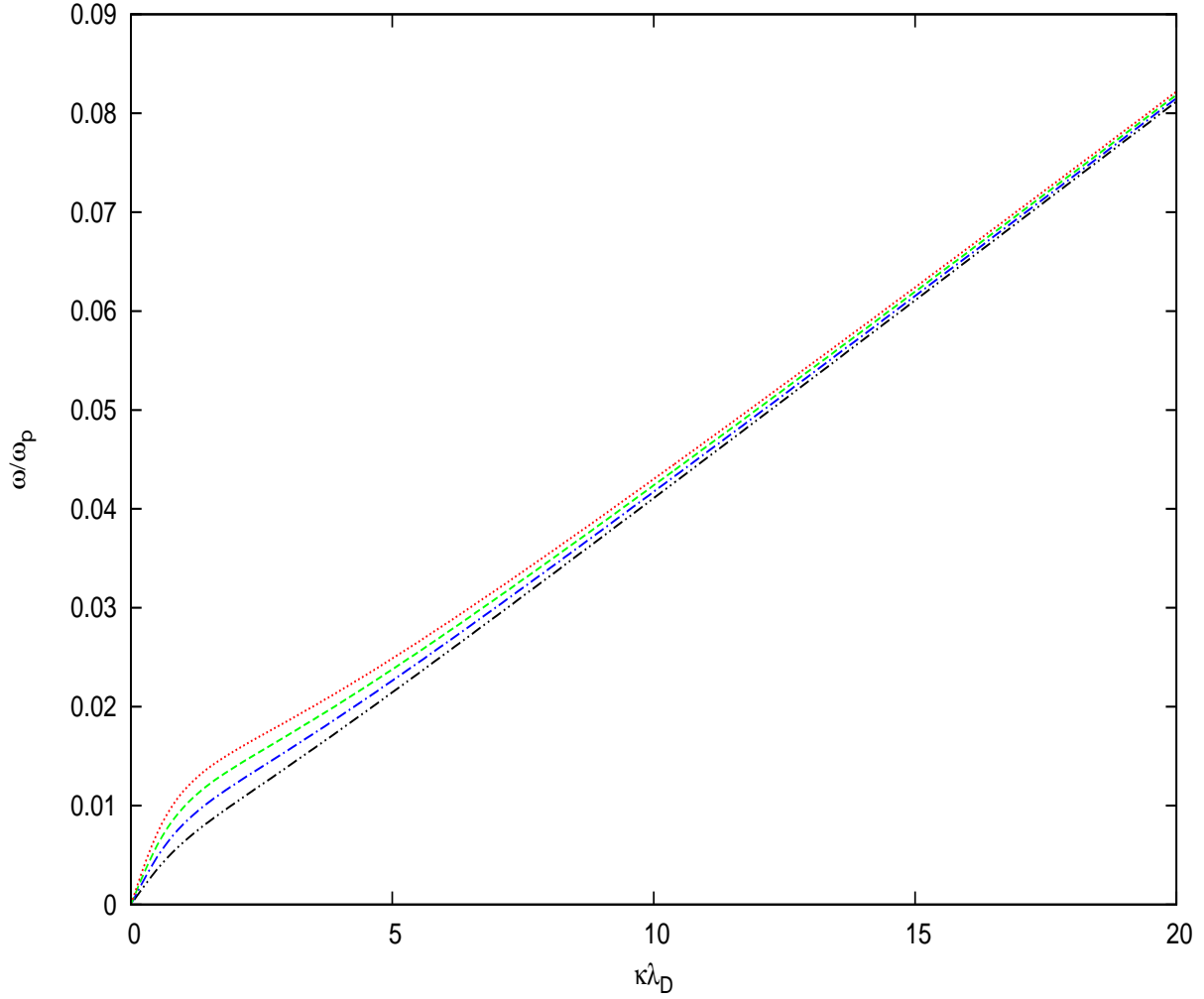


Figure 2.1: Normalized real frequency as a function of the normalized wavenumber. The fixed parameters are $\theta = 0^\circ$, $T_i/T_h = 0.01$ and $R = 0.333$. The curves present different values of the equilibrium density ratio $n_{i0}/n_{e0} = 0.11$ (dashddot=black), 0.25 (dashdot=blue), 0.43 (broken=green), 0.66 (dotted=red).

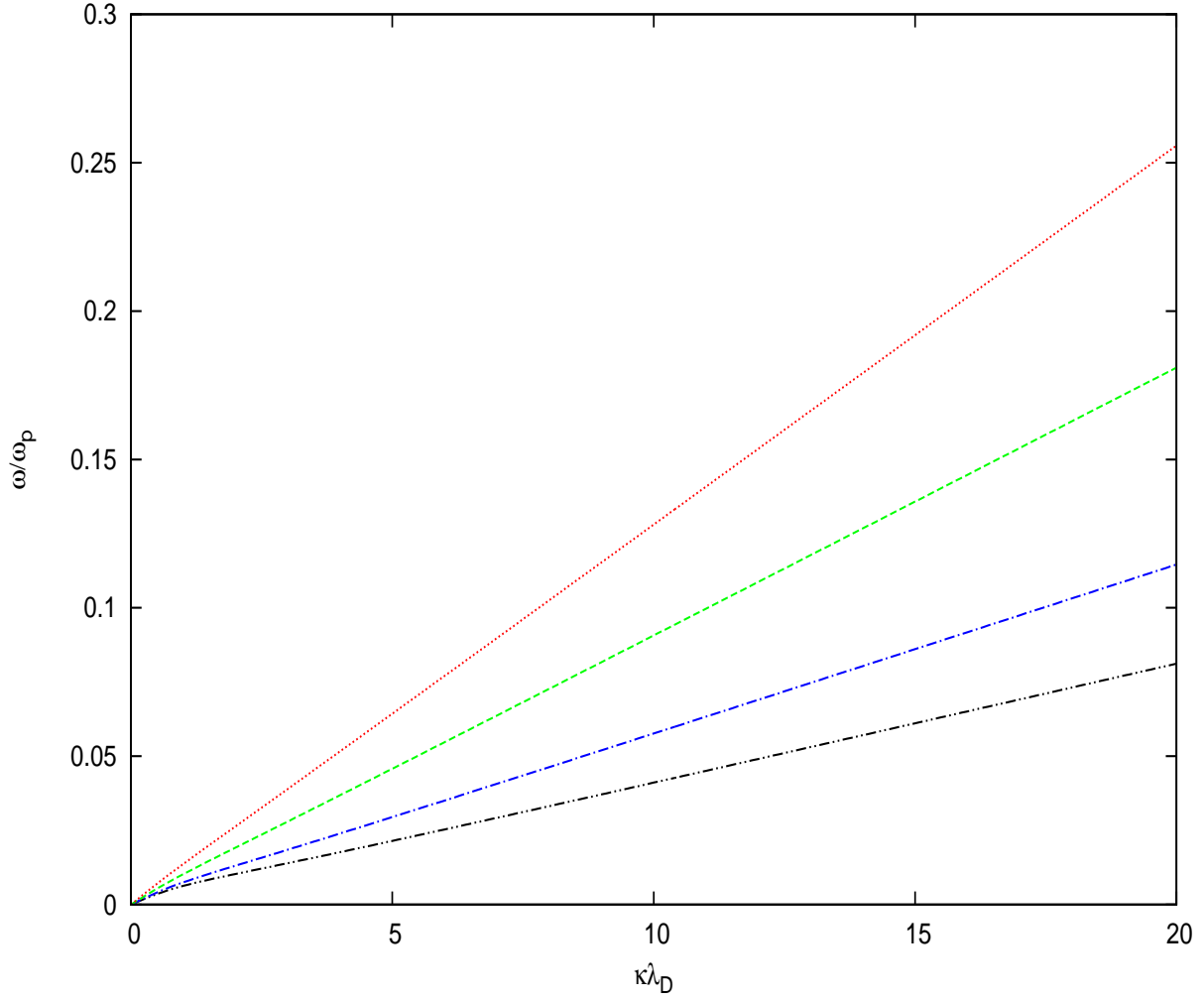


Figure 2.2: Normalized real frequency as a function of the normalized wavenumber. The fixed parameters are $\theta = 0^0$, $n_{i0}/n_{e0} = 0.11$ and $R = 0.333$. The curves present different values of the equilibrium density ratio $T_i/T_h = 0.01$ (dashddot=black), 0.02 (dashdot=blue), 0.05 (broken=green), 0.1 (dotted=red).

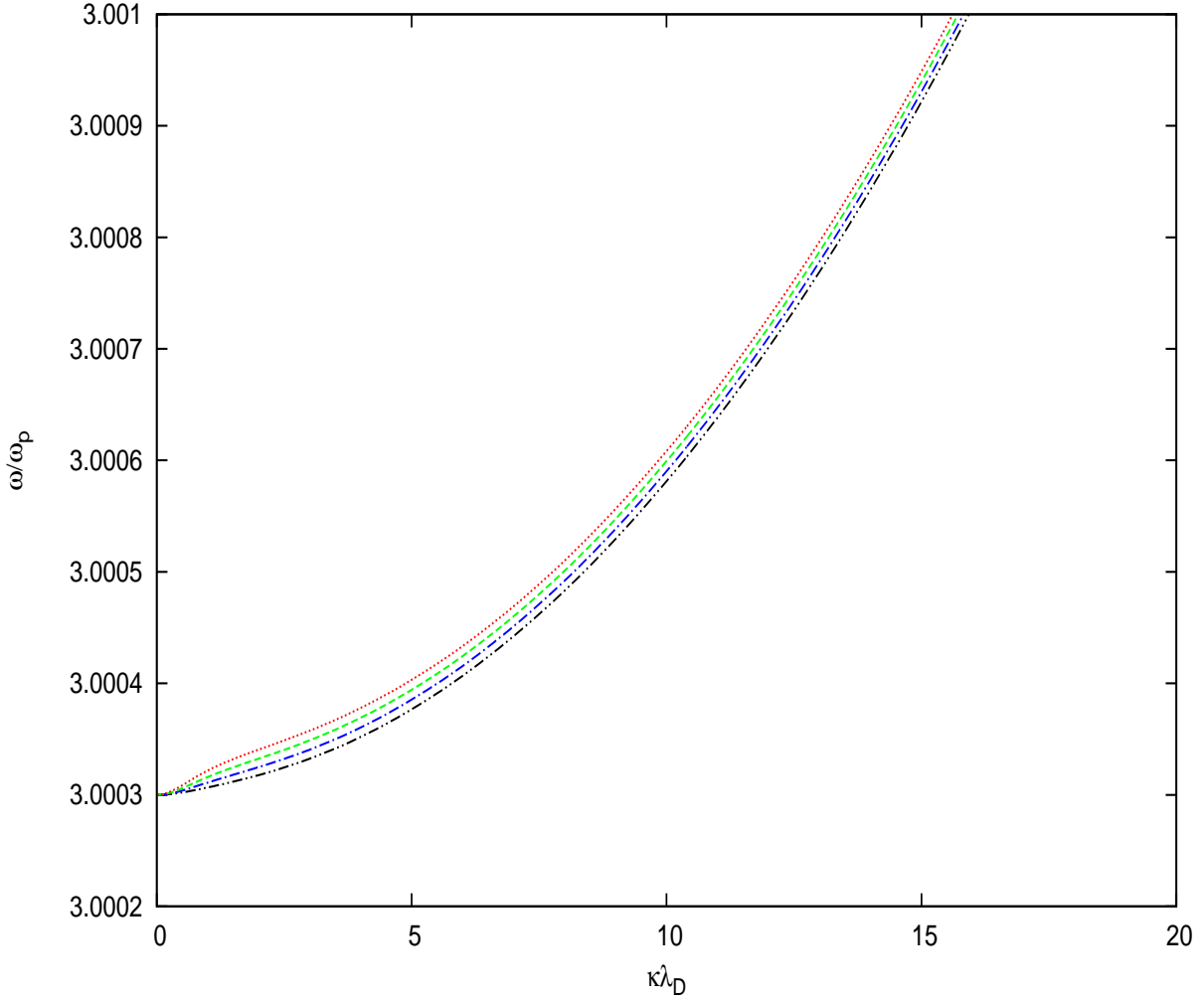


Figure 2.3: Normalized real frequency as a function of the normalized wavenumber. The fixed parameters are $\theta = 90^\circ$, $T_i/T_h = 0.01$ and $R = 0.333$. The curves present different values of the equilibrium density ratio $n_{i0}/n_{e0} = 0.11$ (dashddot=black), 0.25 (dashdot=blue), 0.43 (broken=green), 0.66 (dotted=red).

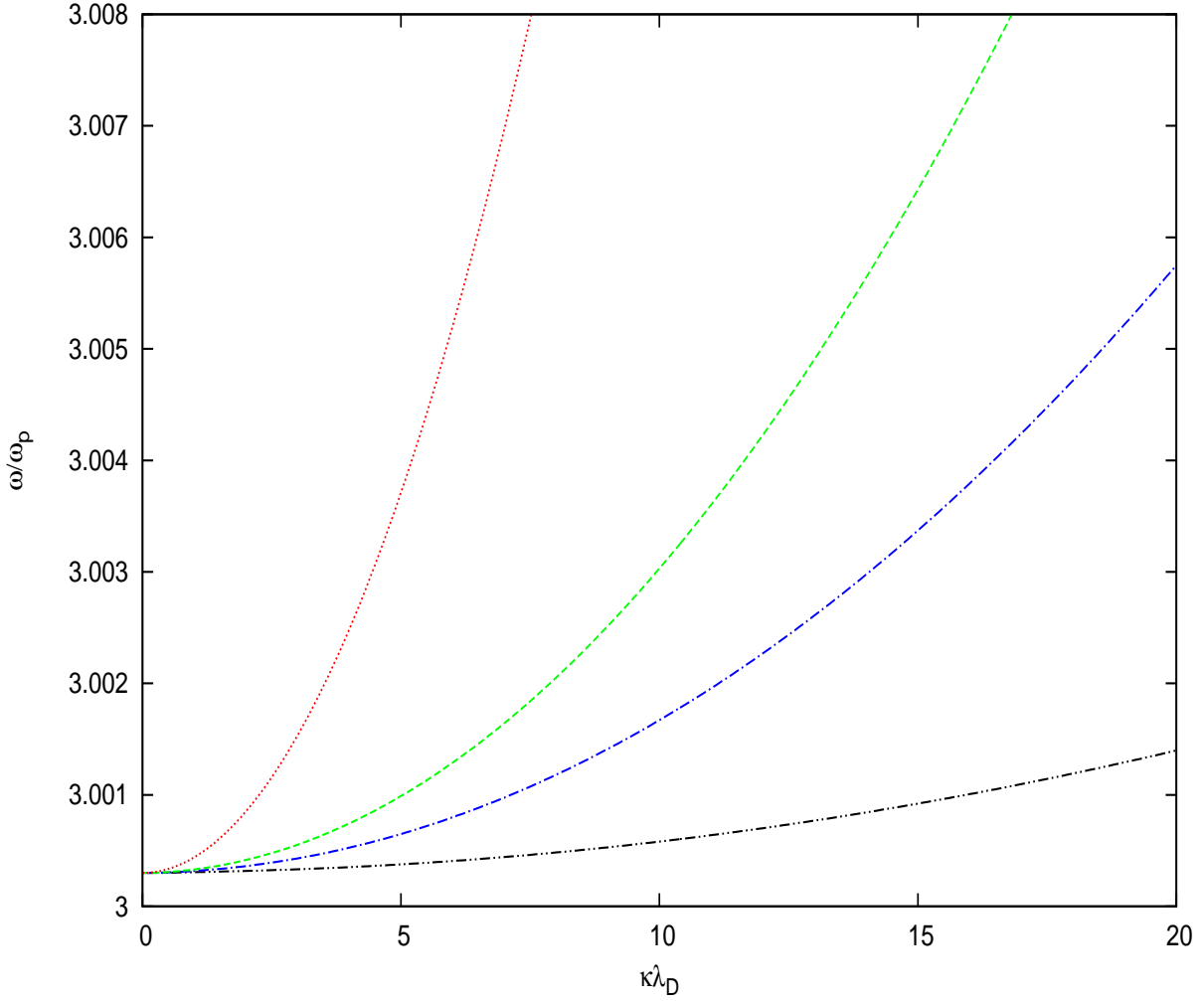


Figure 2.4: Normalized real frequency as a function of the normalized wavenumber. The fixed parameters are $\theta = 90^\circ$, $n_{i0}/n_{e0} = 0.11$ and $R = 0.333$. The curves present different values of the equilibrium density ratio $T_i/T_h = 0.01$ (dashddot=black), 0.05 (dashdot=blue), 0.1 (broken=green), 0.5 (dotted=red).

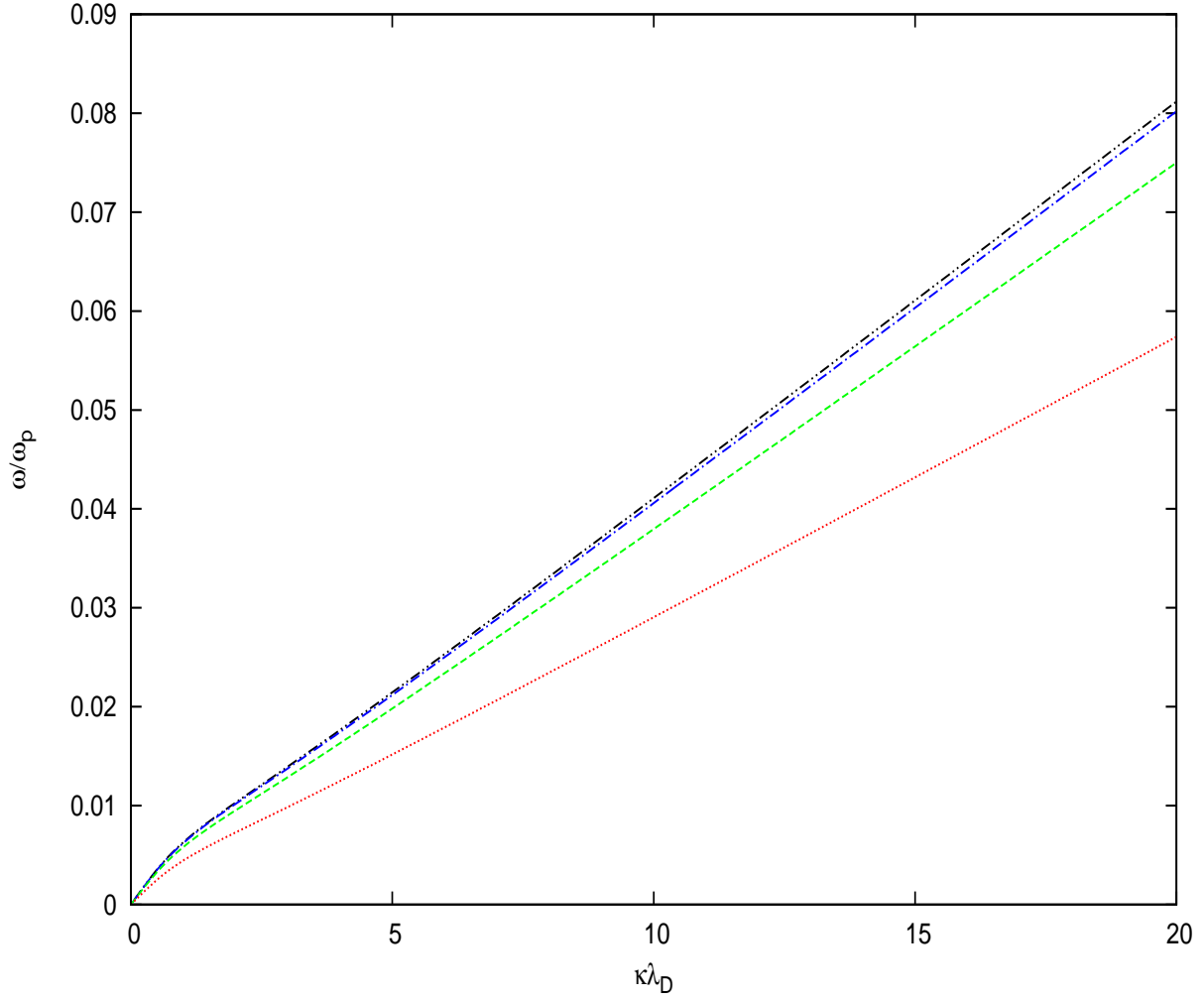


Figure 2.5: Normalized real frequency as a function of the normalized wavenumber. The fixed parameters are $T_i/T_h = 0.01$, $n_{i0}/n_{e0} = 0.11$ and $R = 0.333$. The curves present the ion-acoustic branch for different values of angles propagation $\theta = 0^\circ$ (dashdot=black), 9° (dashdot=blue), 22.5° (broken=green), 45° (dotted=red).

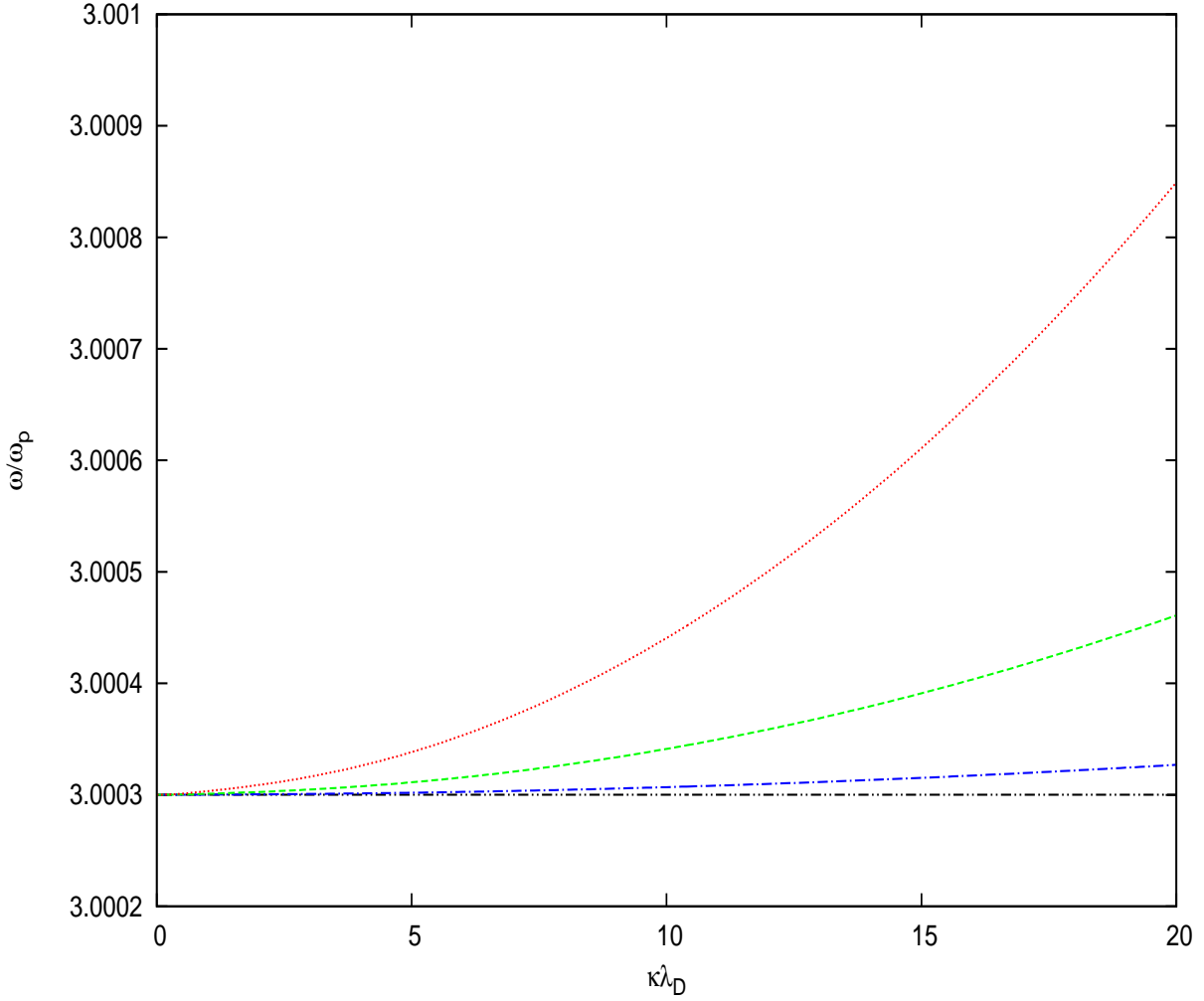


Figure 2.6: Normalized real frequency as a function of the normalized wavenumber. The fixed parameters are $T_i/T_h = 0.01$, $n_{i0}/n_{e0} = 0.11$ and $R = 0.333$. The curves present the cyclotron branch for different values of angles propagation $\theta = 0^\circ$ (dashdot=black), 9° (dashdot=blue), 22.5° (broken=green), 45° (dotted=red).

Chapter 3

Nonlinear waves in electron-positron-ion plasmas

3.1 Literature Review

Nonlinear propagation of intense electrostatic waves in electron-positron (e-p) plasmas has received a large amount of theoretical interest mainly because such plasmas are naturally produced under certain astrophysical conditions. In fact, most astrophysical plasmas usually consist of ions, in addition to electrons and positrons. The properties of wave motion in the presence of heavy ions are significantly different from those in electron-positron (e-p) plasmas [Rizzato, 1988; Popel et al., 1995]. Since electron-positron-ion (e-p-i) plasmas are thought to have been present in the early Universe, plasma processes are expected to be key in understanding the evolution of the Universe. The existence of low-frequency waves in such plasmas are evident [Hamid, 2009].

Recently, it has been suggested that the nonlinear study of wave propagation can be helpful in understanding nonlinear structures similar to broadband electrostatic noise (BEN) observed by numerous satellites (spacecrafts) in the Earth's Magnetosphere such as Viking [Boström et al., 1988], Geotail [Matsumoto et al., 1994], FAST [Ergun et al., 1998], Polar [Mozer et al., 1997] and Cluster [Pickett et al., 2003]. The waveform observations with

the high time resolution confirm that one of the common features of these waves is the burstiness, i.e amplitudes or frequencies rapidly change in the order of a few milliseconds to a few hundreds of milliseconds [Matsumoto et al., 1994].

Further, the observations show that the electrostatic waves (ESW) identified are the parallel propagating waves relative to the ambient magnetic field and exhibit large amplitude, spiky behaviour. It was shown that the nonlinear coupling between the ion cyclotron and ion acoustic modes lead to the generation of parallel electric fields with the periods of the waves varying from ion cyclotron range to the ion acoustic range [Temerin et al., 1982; Reddy et al., 2002]. The investigation of ion-acoustic solitons in e-p-i plasmas under different regimes and models has been studied by different researchers. Kourakis et al. [2007, 2009] have shown the existence of envelope structures of solitons and holes in e-p-i plasmas. Dubinov and Sazonkin [2009] investigated the nonlinear theory of ion-acoustic waves in plasmas with cold ions and inertialess isothermal electrons and positrons and reported that the propagation velocity of a solitary wave is always higher than the linear ion sound velocity. Mahmood et al. [2003] and Mahmood and Akhtar [2008] studied arbitrary amplitude solitons propagating obliquely with respect to an external magnetic field in a homogeneous magnetized electron-positron-ion plasma and found that the amplitude of solitary structures increase with increasing presence of positrons. Nejoh [1996] investigated the effect of ion temperature on the large-amplitude ion-acoustic waves in e-p-i plasmas and observed that the ion temperature decreased the amplitude and increased the maximum *Mach* number of the ion-acoustic waves. On the other hand, space plasma observations clearly indicate the presence of ion and electron populations that are far away from their thermodynamic equilibrium [Shukla et al., 1986; Ghosh and Bharuthram, 2008; Pakzad, 2009].

Using fluid theory, Reddy et al. [2002] and Bharuthram et al. [2002] studied nonlinear low frequency waves in an e-i plasma and revealed that the nonlinear coupling between the ion acoustic mode and ion cyclotron oscillations lead to the generation of the spiky structures of the electric fields. Moolla et al. [2003] studied high-frequency nonlinear waves in the Earth's magnetosphere and showed that a nonlinear coupling between large-amplitude

electron cyclotron and electron acoustic waves can account for the high-frequency component of the field aligned bipolar electric field pulses observed within the broadband electrostatic noise in the auroral, polar and magnetotail regions of the Earth's magnetosphere. The sawtooth and spiky waveforms found were in agreement with the observations of Ergun et al. [1998].

Moolla et al. [2010] studied nonlinear low-frequency structures in the auroral plasma in the presence of an oxygen beam including charge separation. The inclusion of charge separation effects tends to, in most cases, increase the frequency of oscillation of the nonlinear structures. It was shown that, for a weakly magnetized plasma, the amplitude of the oscillations are found to be constant while they are modulated in strongly magnetized plasmas.

Later, Moolla et al. [2012] studied nonlinear low-frequency structures in an electron-positron-ion plasma. The nonlinear electric field structures found were based on the quasineutrality approximation. Bharuthram et al. [2014] studied the evolution of nonlinear waves in different plasmas and showed that the nonlinear waves evolve in a consistent fashion irrespective of the plasma composition.

In this chapter, we focus our studies on nonlinear waves in electron-positron-ion plasmas, allowing for the charge separation effect. The hot electrons and positrons are assumed to have a Boltzmann density distribution and the cold ions are governed by the fluid equations. Finally the system of equations is closed with the Poisson equation.

3.2 Basic theory and Model of fluid equations governing the plasma dynamics

We consider a collisionless, magnetized three-component plasma having warm ions (i) and hot positron (p) and hot electron species (e). The ions species are drifting along the magnetic field with speed v_0 and the wave propagation is taken to be in the x direction at an angle θ to the magnetic field B_0 , which is assumed to be in the $x - z$ plane. The hot electrons and hot positrons are assumed to obey the Boltzmann distribution with equal temperatures T_h ,

and different equilibrium densities n_{e0} and n_{p0} respectively. The continuity and momentum equations for the positive ions are expressed as follows:

$$\frac{\partial n_i}{\partial t} + \frac{\partial n_i v_{ix}}{\partial x} = 0, \quad (3.1)$$

$$\frac{\partial v_{ix}}{\partial t} + v_{ix} \frac{\partial v_{ix}}{\partial x} + \frac{1}{n_i m_i} \frac{\partial p_i}{\partial x} = -\frac{e}{m_i} \frac{\partial \varphi}{\partial x} + \Omega_i v_{iy} \sin \theta, \quad (3.2)$$

$$\frac{\partial v_{iy}}{\partial t} + v_{ix} \frac{\partial v_{iy}}{\partial x} = \Omega_i v_{iz} \cos \theta - \Omega_i v_{ix} \sin \theta, \quad (3.3)$$

$$\frac{\partial v_{iz}}{\partial t} + v_{ix} \frac{\partial v_{iz}}{\partial x} = -\Omega_i v_{iy} \cos \theta, \quad (3.4)$$

$$\frac{\partial p_i}{\partial t} + v_{ix} \frac{\partial p_i}{\partial x} + 3p_i \frac{\partial v_{ix}}{\partial x} = 0. \quad (3.5)$$

The electrons and positrons are assumed to follow the Boltzmann distribution, and are given respectively, as

$$n_e = n_{e0} \exp\left(\frac{e\varphi}{T_h}\right), \quad (3.6)$$

$$n_p = n_{p0} \exp\left(-\frac{e\varphi}{T_h}\right). \quad (3.7)$$

Equations (3.1) - (3.7) are closed with the Poisson's equation

$$\varepsilon_0 \frac{\partial^2 \varphi}{\partial x^2} = -e(n_{ph} - n_{eh} + n_i). \quad (3.8)$$

In equations (3.1) - (3.8), $\Omega_i = eB_0/m_i$ is ion cyclotron frequency, n_i is the ion density, v_{ix}, v_{iy} and v_{iz} are the components of the ion velocity along the x, y and z directions respectively, p_i is the ion pressure, φ is the electrostatic potential and m_i is the ion mass.

3.2.1 Linear Analysis

Before proceeding with the evolution of nonlinear waves, we discuss the linear modes of the system. In the limit, the set of equations (3.1)-(3.8) give rise to the following dispersion

relation.

$$\omega^2 = \frac{1}{2} \left(\Omega_i^2 + 3k^2 v_{ti}^2 + \frac{k^2 v_{ia}^2}{k^2 \lambda_{Dh}^2 + \frac{n_{p0}}{n_{e0}} + 1} \right) \left[1 \pm \left(1 - \frac{4\Omega_i^2 \cos^2 \theta \left(3k^2 v_{ti}^2 + \frac{k^2 v_{ia}^2}{k^2 \lambda_{Dh}^2 + \frac{n_{p0}}{n_{e0}} + 1} \right)}{\left(\Omega_i^2 + 3k^2 v_{ti}^2 + \frac{k^2 v_{ia}^2}{k^2 \lambda_{Dh}^2 + \frac{n_{p0}}{n_{e0}} + 1} \right)^2} \right)^{1/2} \right] \quad (3.9)$$

where $v_{ti} = (T_i/m_i)^{1/2}$ is the thermal speed for the ions, $v_{ia} = (n_{i0}m/n_{e0}m_i)^{1/2}v_{th}$ is the ion acoustic speed and $\lambda_{Dh} = (\varepsilon_0 T_h/n_{e0}e^2)^{1/2}$ is electron Debye length.

In the limit

$$\left(\Omega_i^2 + 3k^2 v_{ti}^2 + \frac{k^2 v_{ia}^2}{k^2 \lambda_{Dh}^2 + \frac{n_{p0}}{n_{e0}} + 1} \right)^2 \gg 4\Omega_i^2 \cos^2 \theta \left(3k^2 v_{ti}^2 + \frac{k^2 v_{ia}^2}{k^2 \lambda_{Dh}^2 + \frac{n_{p0}}{n_{e0}} + 1} \right), \quad (3.10)$$

we obtain two modes from equation (3.9).

The first mode is the ion cyclotron mode given as

$$\omega_+^2 = \Omega_i^2 + 3k^2 v_{ti}^2 + \frac{k^2 v_{ia}^2}{k^2 \lambda_{Dh}^2 + \frac{n_{p0}}{n_{e0}} + 1} - \frac{\Omega_i^2 \cos^2 \theta \left(3k^2 v_{ti}^2 + \frac{k^2 v_{ia}^2}{k^2 \lambda_{Dh}^2 + \frac{n_{p0}}{n_{e0}} + 1} \right)}{\Omega_i^2 + 3k^2 v_{ti}^2 + \frac{k^2 v_{ia}^2}{k^2 \lambda_{Dh}^2 + \frac{n_{p0}}{n_{e0}} + 1}} \quad (3.11)$$

and the second mode is the ion acoustic mode given as

$$\omega_-^2 = \frac{\Omega_i^2 \cos^2 \theta \left(3k^2 v_{ti}^2 + \frac{k^2 v_{ia}^2}{k^2 \lambda_{Dh}^2 + \frac{n_{p0}}{n_{e0}} + 1} \right)}{\Omega_i^2 + 3k^2 v_{ti}^2 + \frac{k^2 v_{ia}^2}{k^2 \lambda_{Dh}^2 + \frac{n_{p0}}{n_{e0}} + 1}}. \quad (3.12)$$

The two modes obtained for electron-positron-ion plasmas have similar characteristics as the electron cyclotron and electron acoustic waves investigated by Lazarus et al. [2012] for a four-component, two-temperature electron-positron plasma.

The linear dispersion relation (3.9) merely predicts the modes of the system in terms of the frequency range. In next section, we can thus identify these modes by measuring the periods of electric field structures.

3.2.2 Nonlinear Analysis

In the nonlinear regime, we transform equations (3.1)-(3.5) and (3.8) to a stationary frame $s = (x - vt)/(v/\Omega_i)$ and normalize velocities with respect to the ion thermal velocity $C_s = \sqrt{T_i/m_i}$, densities with respect to the total unperturbed electron density n_{e0} , pressures with respect to $n_{e0}T_h$ and potential with respect to T_h/e . We replace $\frac{\partial}{\partial t}$ by $-\Omega_i\frac{\partial}{\partial s}$ and $\frac{\partial}{\partial x}$ by $(\Omega_i/v)\frac{\partial}{\partial s}$ in equations (3.1)-(3.8) and define the normalized electric potential $\psi = e\varphi/T_h$ and the electric field $E = -\frac{\partial\psi}{\partial s}$. We use the following initial conditions: $\psi = 0$, $\partial\psi/\partial s = E_0$, $\partial^2\psi/\partial s^2 = 0$, $n_i = n_{i0}$ and $V_x = v_0\cos\theta$ at $s = 0$. In addition, we assume point quasineutrality, that is, $n_{i0} + n_{p0} = n_{e0}$ at equilibrium.

After introducing the above definitions, the set of differential equations in the stationary frame can be expressed as follows

$$\frac{\partial\psi}{\partial s} = -E \quad (3.13)$$

$$\frac{\partial E}{\partial s} = M^2 R^2 \frac{n_{e0}}{n_{i0}} \left(\frac{n_{p0}}{n_{e0}} e^{-\psi} - e^{\psi} + \tilde{n}_i \right) \quad (3.14)$$

$$\frac{\partial\tilde{n}_i}{\partial s} = \frac{\tilde{n}_i^3 [-E - Mv_{iy}\sin\theta]}{(\frac{n_{i0}}{n_{e0}})^2 (M - \delta_i)^2 - 3\tilde{n}_i\tilde{P}_i} \quad (3.15)$$

$$\frac{\partial\tilde{P}_i}{\partial s} = \frac{3\tilde{P}_i\tilde{n}_i^2 [-E - M\tilde{v}_{iy}\sin\theta]}{(\frac{n_{i0}}{n_{e0}})^2 (M - \delta_i)^2 - 3\tilde{n}_i\tilde{P}_i} \quad (3.16)$$

$$\frac{\partial\tilde{v}_{iy}}{\partial s} = \left(\frac{n_{e0}}{n_{i0}}\right) \frac{\tilde{n}_i M}{(M - \delta_i)} \left[\sin\theta \left(M - \left(\frac{n_{i0}}{n_{e0}}\right) \frac{(M - \delta_i)}{\tilde{n}_i} \right) - \tilde{v}_{iz} \cos\theta \right] \quad (3.17)$$

$$\frac{\partial\tilde{v}_{iz}}{\partial s} = \frac{\tilde{n}_i M \tilde{v}_{iy} \cos\theta}{\frac{n_{i0}}{n_{e0}} (M - \delta_i)} \quad (3.18)$$

where $\delta_i = v_0/C_s$ is the ion drift, $M = v/C_s$ is the *Mach* number and $R = \omega_{pi}/\Omega_i$ represents the strength of the magnetic field for a plasma with a fixed total density. The additional superscript ' \sim ' introduced in equations (3.14) - (3.18) indicates normalized quantities.

3.2.3 Calculation of Initial Conditions

The initial values for most plasma parameters were prescribed, but \tilde{v}_{iy0} and \tilde{v}_{iz0} are calculated self consistently as follows:

At equilibrium, we use the quasineutrality condition which is expressed below

$$\tilde{n}_i = \tilde{n}_e - \tilde{n}_p, \quad (3.19)$$

where \tilde{n}_i , \tilde{n}_e and \tilde{n}_p are the normalized densities for ions, electrons and positrons respectively.

Differentiating the above equation we get

$$\frac{\partial \tilde{n}_i}{\partial s} = \frac{\partial \tilde{n}_e}{\partial s} - \frac{\partial \tilde{n}_p}{\partial s}. \quad (3.20)$$

Normalizing equations (3.6) and (3.7), we obtain

$$\tilde{n}_e = \exp(\varphi) \quad (3.21)$$

$$\tilde{n}_p = \frac{n_{p0}}{n_{e0}} \exp(-\varphi). \quad (3.22)$$

Substituting equations (3.15), (3.21) and (3.22) into equation (3.20), we obtain the initial value of \tilde{v}_{iy} as

$$\tilde{v}_{iy0} = \frac{E_0 \left[\left(\frac{(\frac{n_{i0}}{n_{e0}})^2 (M - \delta_i)^2 - 3\tilde{n}_i \tilde{P}_i}{\tilde{n}_i^3} \right) \left(1 + \frac{n_{p0}}{n_{e0}} \right) - 1 \right]}{M \sin \theta} \quad (3.23)$$

where $E = E_0$ at $\psi = 0$.

Now, the value of \tilde{v}_{iz} is determined by differentiating the quasineutrality condition (3.19) twice

$$\frac{\partial^2 \tilde{n}_i}{\partial s^2} = \frac{\partial^2 \tilde{n}_e}{\partial s^2} - \frac{\partial^2 \tilde{n}_p}{\partial s^2}. \quad (3.24)$$

To simplify the calculations, we introduce the following definitions:

$$F_1 = \tilde{n}_i^3 \quad (3.25)$$

$$F_2 = \left(\frac{n_{0i}}{n_{0e}}\right)^2 (M - \delta_i)^2 - 3\tilde{n}_i \tilde{P}_i \quad (3.26)$$

$$A = \frac{n_{p0}}{n_{e0}} - 1 \quad (3.27)$$

Using the above definitions, equation (3.24) reduces to

$$\frac{\partial}{\partial s} \left[\left(\frac{F_1}{F_2} \right) (-E - M\tilde{v}_{iy} \sin \theta) \right] = -AE_0^2 \quad (3.28)$$

which can be rewritten as

$$(-E - M\tilde{v}_{iy} \sin \theta) \frac{\partial}{\partial s} \left(\frac{F_1}{F_2} \right) + \left(\frac{F_1}{F_2} \right) \left(M \sin \theta \frac{\partial \tilde{v}_{iy}}{\partial s} \right) = -AE_0^2. \quad (3.29)$$

Solving the above equation and using equation (3.27), we finally get the initial value of \tilde{v}_{iz} as

$$\tilde{v}_{iz0} = \left[M - \frac{(M - \delta_i)}{\tilde{n}_i} \left(\frac{n_{i0}}{n_{p0}} \right) \right] \frac{\sin \theta}{\cos \theta} - \left[\left(\frac{F_2}{F_1} \right) \frac{(M - \delta_i)}{M^2 \tilde{n}_i \sin \theta \cos \theta} \left(\frac{n_{i0}}{n_{e0}} \right) \right] \left[AE_0^2 + (-E - M\tilde{v}_{iy} \sin \theta) \frac{\partial}{\partial s} \left(\frac{F_1}{F_2} \right) \right], \quad (3.30)$$

where

$$\frac{\partial}{\partial s} \left(\frac{F_1}{F_2} \right) = \frac{3\tilde{n}_i^5 (-E - M\tilde{v}_{iy} \sin \theta)}{\left(\frac{n_{i0}}{n_{e0}} \right)^2 (M - \delta_i)^2 - 3\tilde{n}_i \tilde{P}_i} + \frac{12\tilde{n}_i^6 \tilde{P}_i (-E - M\tilde{v}_{iy} \sin \theta)}{\left(\frac{n_{i0}}{n_{e0}} \right)^2 (M - \delta_i)^2 - 3\tilde{n}_i \tilde{P}_i}^3. \quad (3.31)$$

3.3 The numerical results and Discussion

Using the Runge-Kutta method, the set of nonlinear differential equations (3.13)-(3.18) is solved numerically. At $t = 0$, the following initial conditions at $s = 0$; $\psi = 0$, $E = E_0$, $\tilde{n}_i = n_{i0}/n_{e0}$, $\tilde{P}_i = n_{i0}T_i/n_{e0}T_h$ are given, but the initial values \tilde{v}_{iy0} and \tilde{v}_{iz0} are calculated self consistently in Section 3.2. The parameter R in equation (3.14) characterizes the strength of the magnetic field for fixed total plasma density. The plasma is strongly magnetized for $R \ll 1$ and weakly magnetized for $R \gg 1$. Our model of study showed that the electrostatic waves were possible for $R = 3$. The parameter regime considered here is relevant for the case of magnetospheric plasmas. The results are presented below.

Effect of the driving amplitude, E_0 on the driving electric field

Our investigation is an extension of the work of Moolla et al. [2012] by including the Poisson equation, thereby allowing for the charge separation effect. For fixed parameters $M = 2.5$, $\delta_i = 0.0$, $\frac{n_{i0}}{n_{e0}} = 0.5$, $\frac{T_i}{T_h} = 0.0$, $R = 3.0$ and $\theta = 2^0$, we vary the driving electric field. The results are shown in Figures 3.1-3.4. By increasing the driver strengths E_0 , the period of oscillations increases from $1.06\tau_{ci}$ to $3.44\tau_{ci}$, where $\tau_{ci} = 2\pi/\Omega_i$ is the ion cyclotron period. As E_0 increases, we observe the transition from ion-cyclotron waves to ion-acoustic waves and the electric field structure evolves from a sinusoidal waveform to a sawtooth structure. Bharuthram et al. [2002] and Moolla et al. [2012] found that the driving field strength for the onset of spikes was 1.1 and 0.3 respectively while in our study this value is 0.01. The introduction of the Poisson's equation increases the *Mach* number to generate the waveforms, but for a slightly lower driving amplitude to obtain spikes.

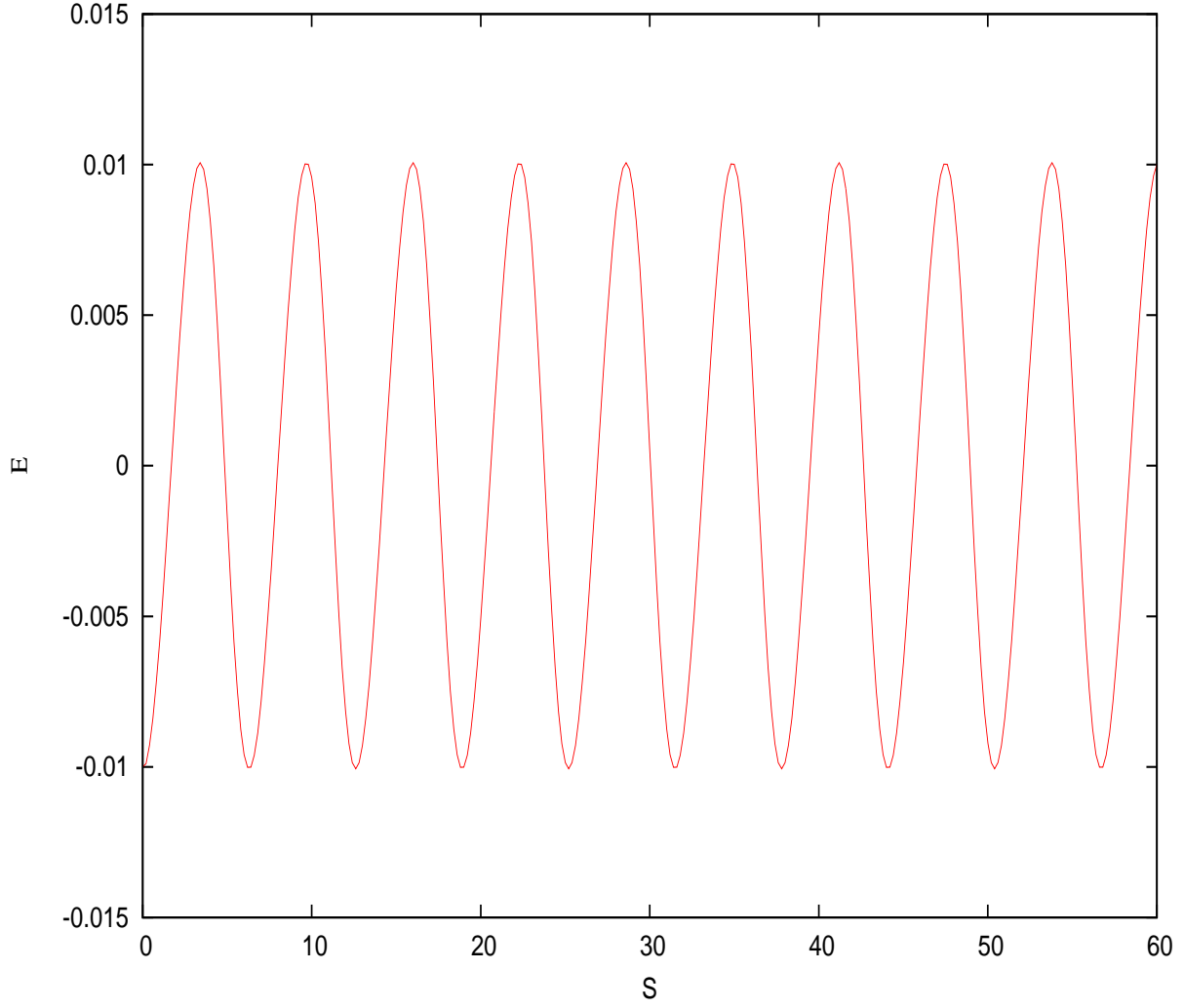


Figure 3.1: Numerical solution of normalized parallel electric field for an electron-positron-ion plasma for the parameters $M = 2.5$, $\delta_i = 0.0$, $n_{i0}/n_{e0} = 0.5$, $T_i/T_h = 0.0$, $R = 3.0$, $\theta = 2^\circ$ and $E_0 = 0.01$. The period of the wave is $T_w = 1.06\tau_{ci}$ (frequency $f_w = 0.94f_{ci}$).

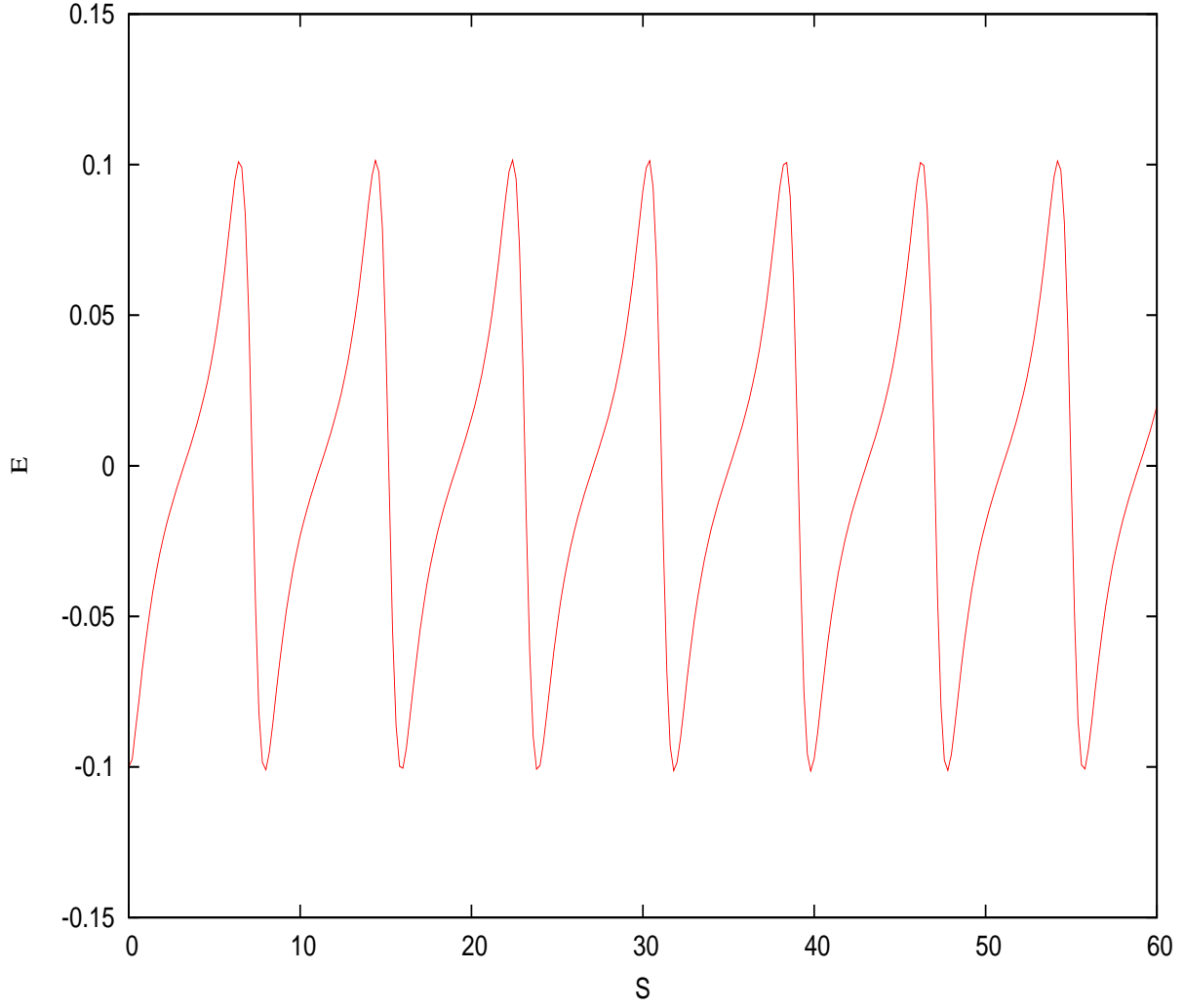


Figure 3.2: Numerical solution of normalized parallel electric field for an electron-positron-ion plasma for the parameters $M = 2.5$, $\delta_i = 0.0$, $n_{i0}n_{e0} = 0.5$, $T_iT_h = 0.0$, $R = 3.0$, $\theta = 2^0$ and $E_0 = 0.1$. The period of the wave is $T_w = 1.31\tau_{ci}$ (frequency $f_w = 0.76f_{ci}$).

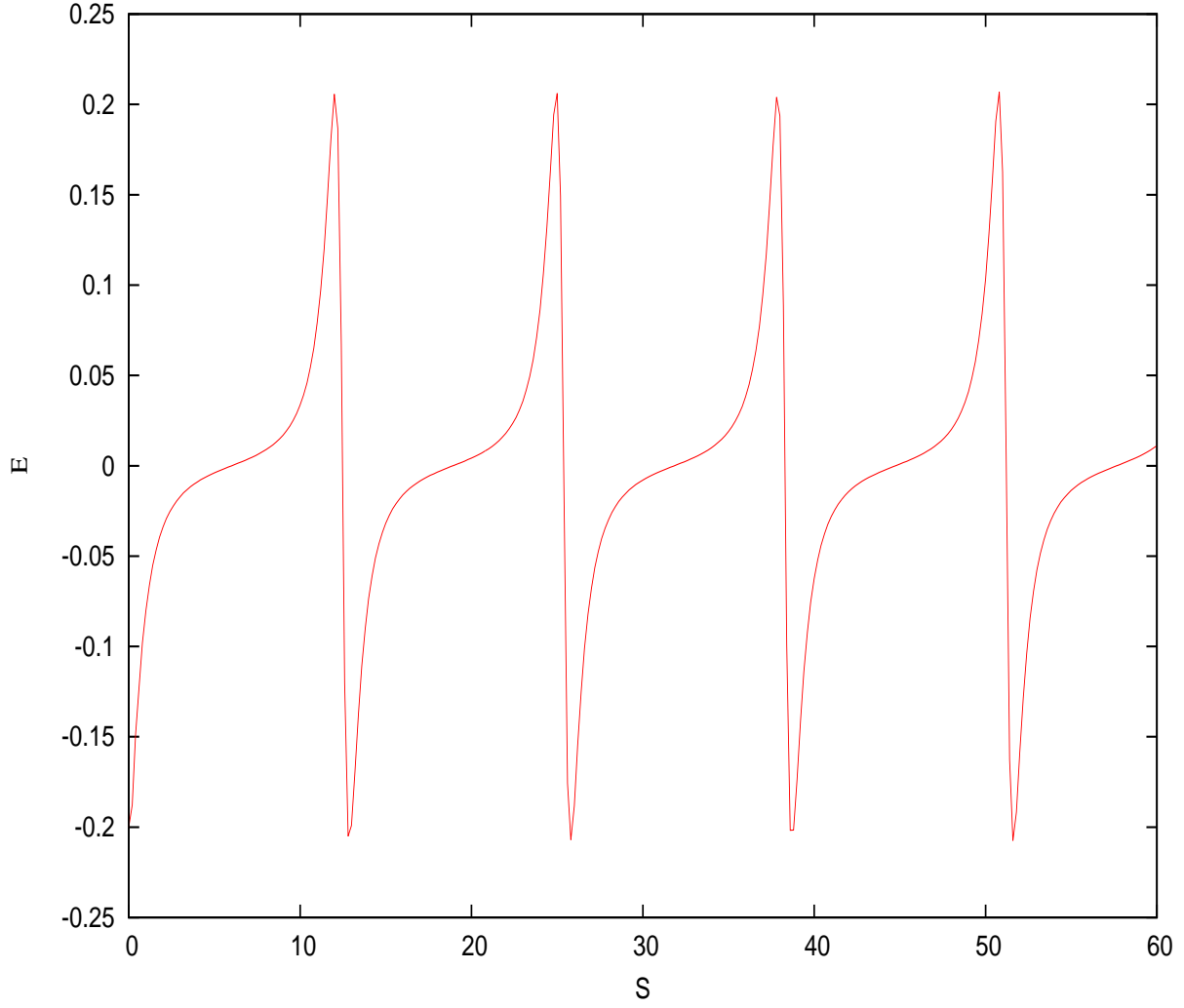


Figure 3.3: Numerical solution of normalized parallel electric field for an electron-positron-ion plasma for the parameters $M = 2.5$, $\delta_i = 0.0$, $n_{i0}/n_{e0} = 0.5$, $T_i/T_h = 0.0$, $R = 3.0$, $\theta = 2^\circ$ and $E_0 = 0.2$. The period of the wave is $T_w = 2.06\tau_{ci}$ (frequency $f_w = 0.48f_{ci}$).

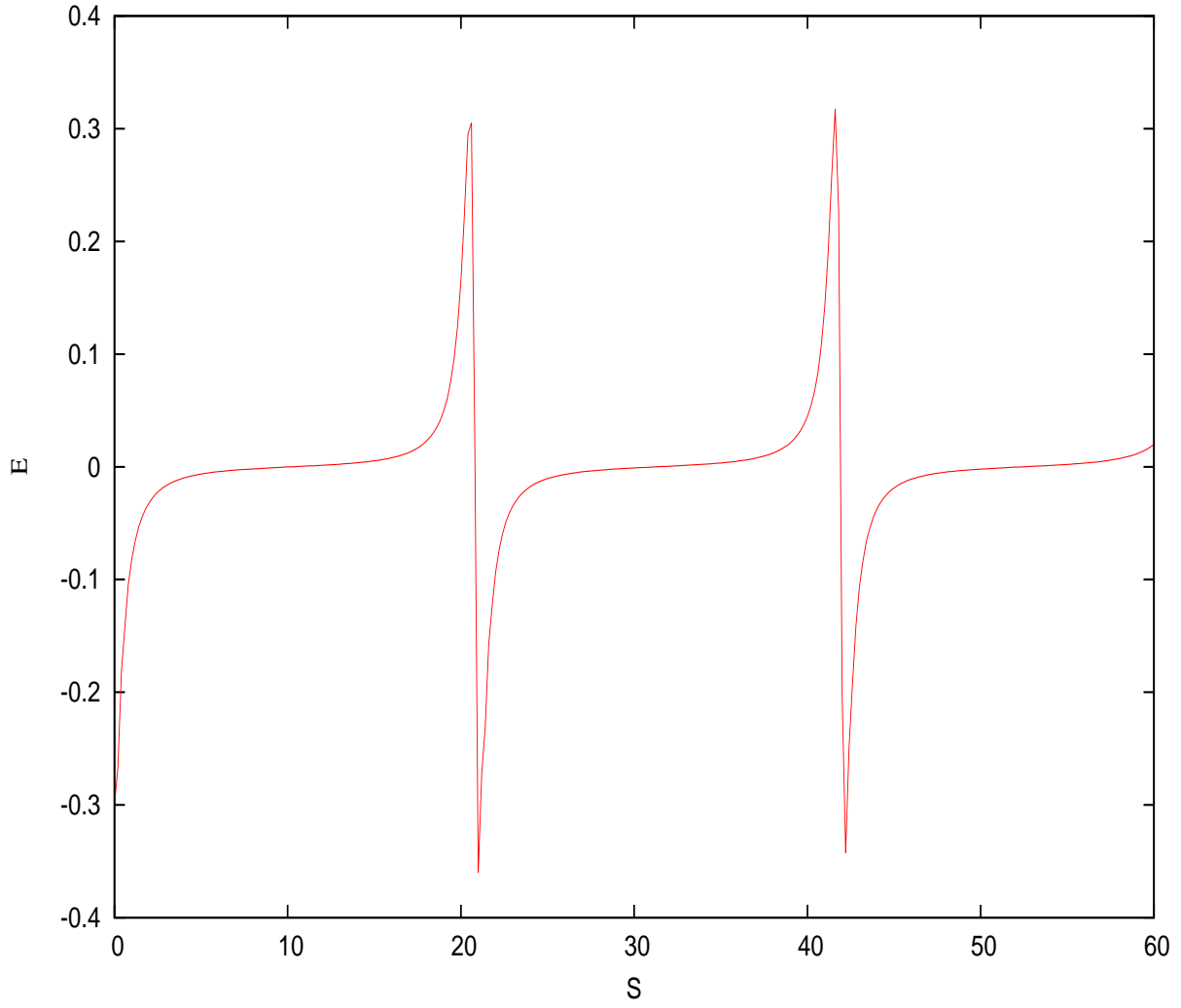


Figure 3.4: Numerical solution of normalized parallel electric field for an electron-positron-ion plasma for the parameters $M = 2.5$, $\delta_i = 0.0$, $n_{i0}/n_{e0} = 0.5$, $T_i/T_h = 0.0$, $R = 3.0$, $\theta = 2^0$ and $E_0 = 0.3$. The period of the wave is $T_w = 3.44\tau_{ci}$ (frequency $f_w = 0.29f_{ci}$).

Effect of ion temperature

The effect of the ion-electron temperature ratio T_i/T_h on the parallel electric field structures for the following fixed parameters $M = 2.50$, $E_0 = 0.3$, $\delta_i = 0.0$, $n_{i0}/n_{e0} = 0.5$, $R = 3.0$ and $\theta = 2^0$ is represented in Figures 3.5 - 3.8. Increasing this ratio from 0.0 to 0.2 results in the period of the waves increasing from $3.44\tau_{ci}$ to $3.62\tau_{ci}$. This behavior is predicted by equation (3.12) showing that the frequency decreases with an increase in T_i/T_h .

The graphs represented in Figures 3.5 - 3.8 show that the increase in cold ion temperature does not affect the nonlinearity of the waves [Moolla et al., 2012].

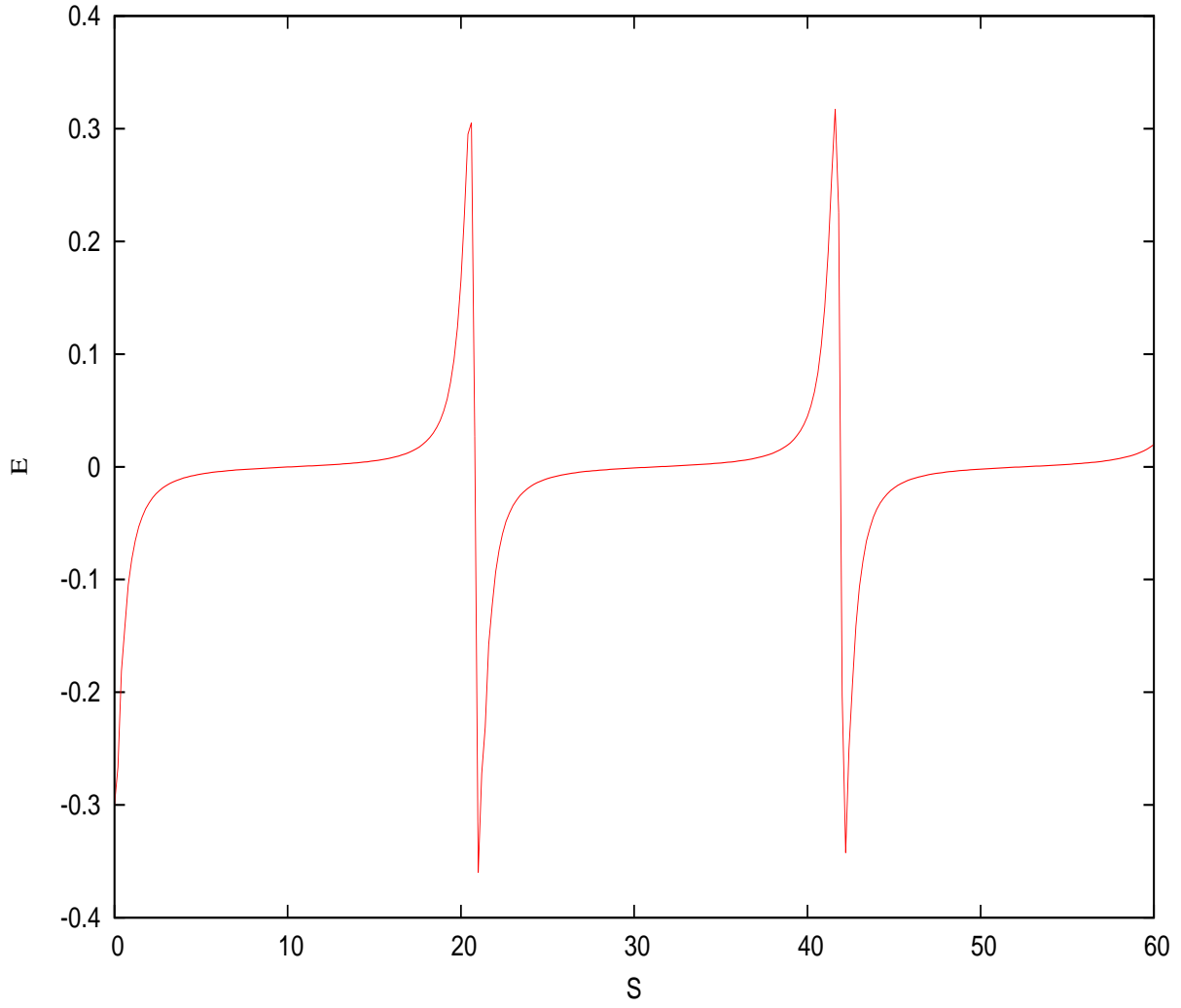


Figure 3.5: Numerical solution of normalized parallel electric field for the parameters $E_0 = 0.3$, $M = 2.5$, $R = 3.0$, $\delta_i = 0.0$, $n_{i0}/n_{e0} = 0.5$, $\theta = 2^\circ$ and $T_i/T_h = 0.0$. The period of the wave is $T_w = 3.44\tau_{ci}$ (frequency $f_w = 0.290f_{ci}$).

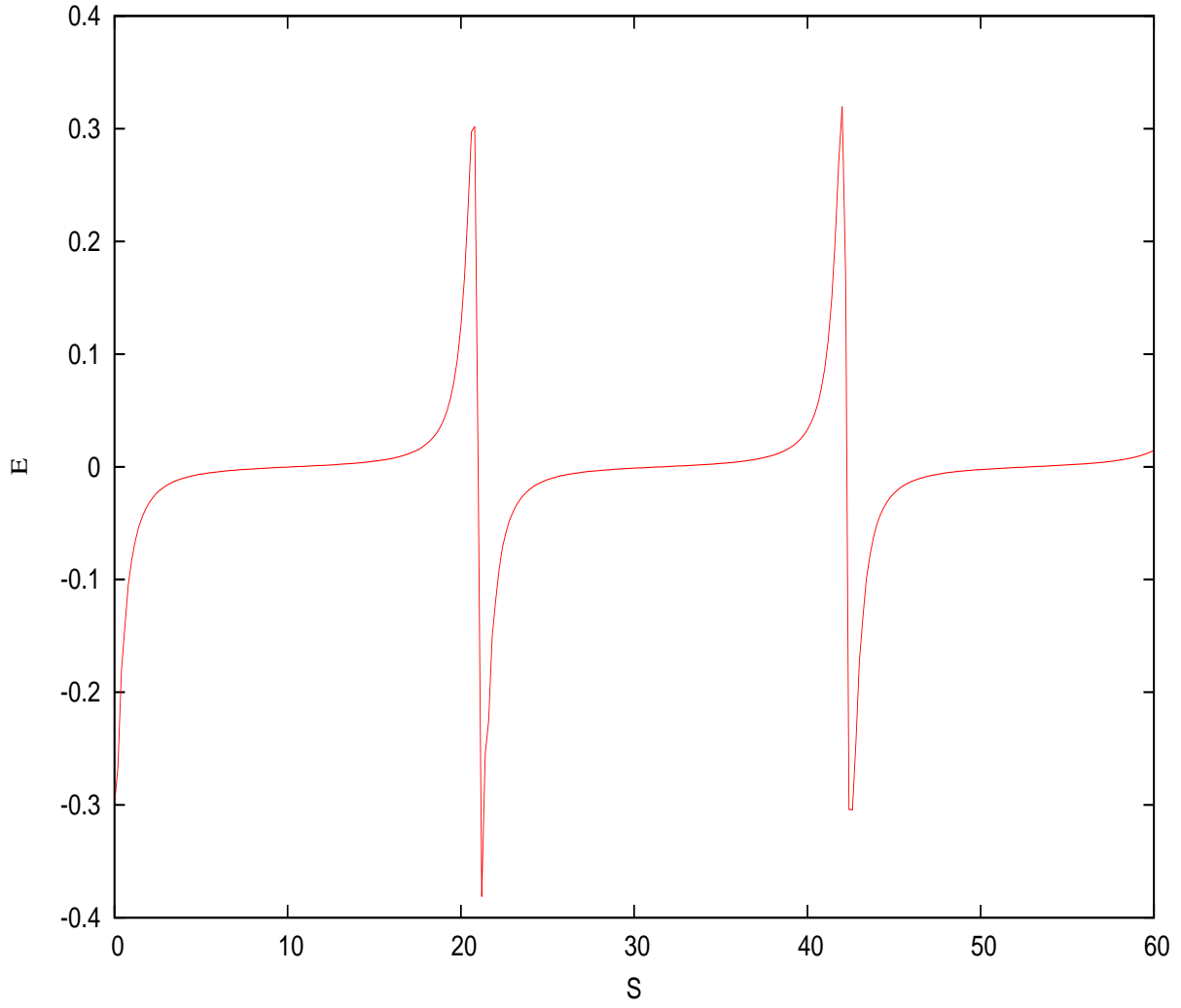


Figure 3.6: Numerical solution of normalized parallel electric field for the parameters $E_0 = 0.3$, $M = 2.5$, $R = 3.0$, $\delta_i = 0.0$, $n_{i0}/n_{e0} = 0.5$, $\theta = 2^0$ and $T_i/T_h = 0.05$. The period of the wave is $T_w = 3.51\tau_{ci}$ (frequency $f_w = 0.284f_{ci}$).

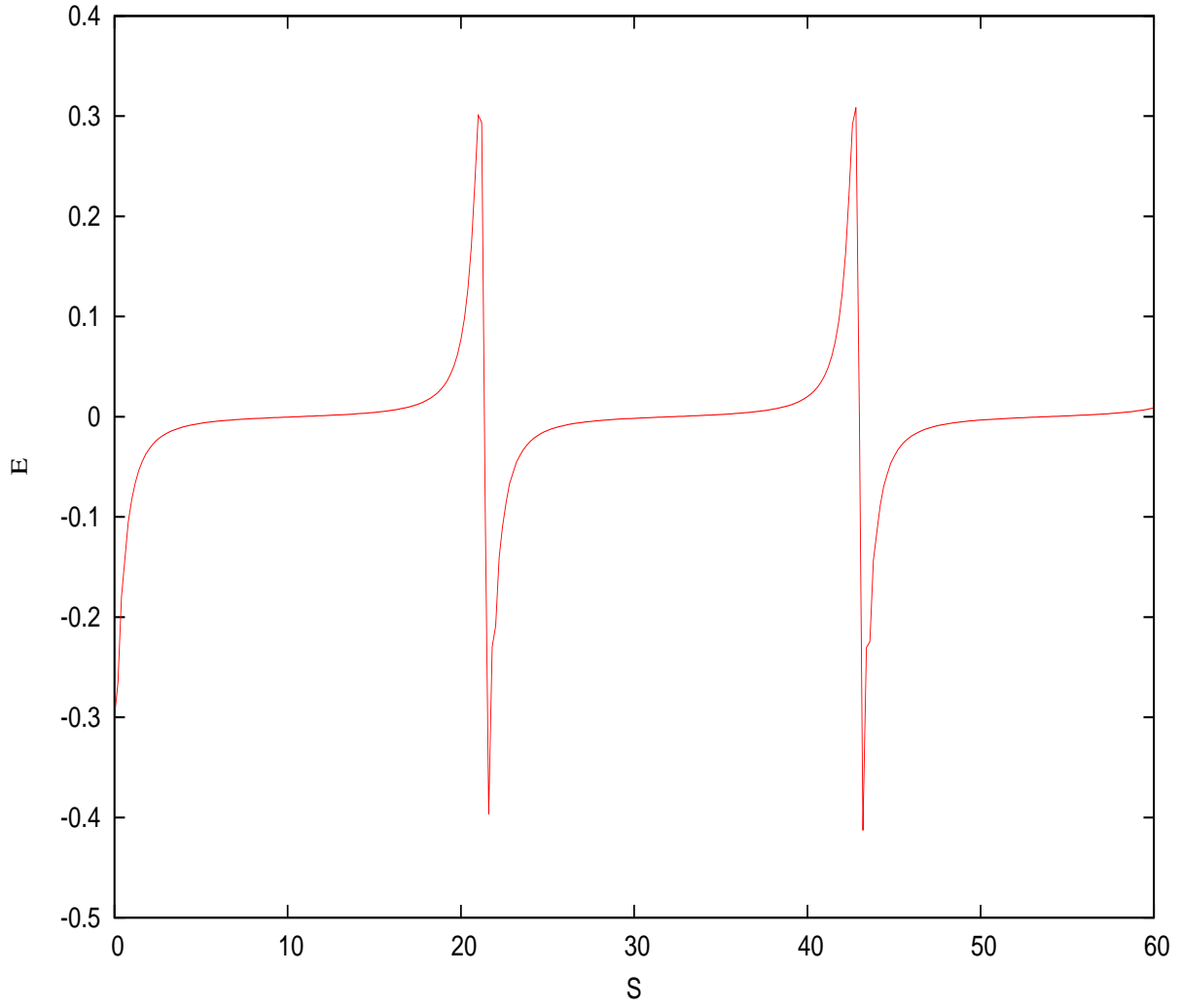


Figure 3.7: Numerical solution of normalized parallel electric field for the parameters $E_0 = 0.3$, $M = 2.5$, $R = 3.0$, $\delta_i = 0.0$, $n_{i0}/n_{e0} = 0.5$, $\theta = 2^\circ$ and $T_i/T_h = 0.15$. The period of the wave is $T_w = 3.56\tau_{ci}$ (frequency $f_w = 0.280f_{ci}$).

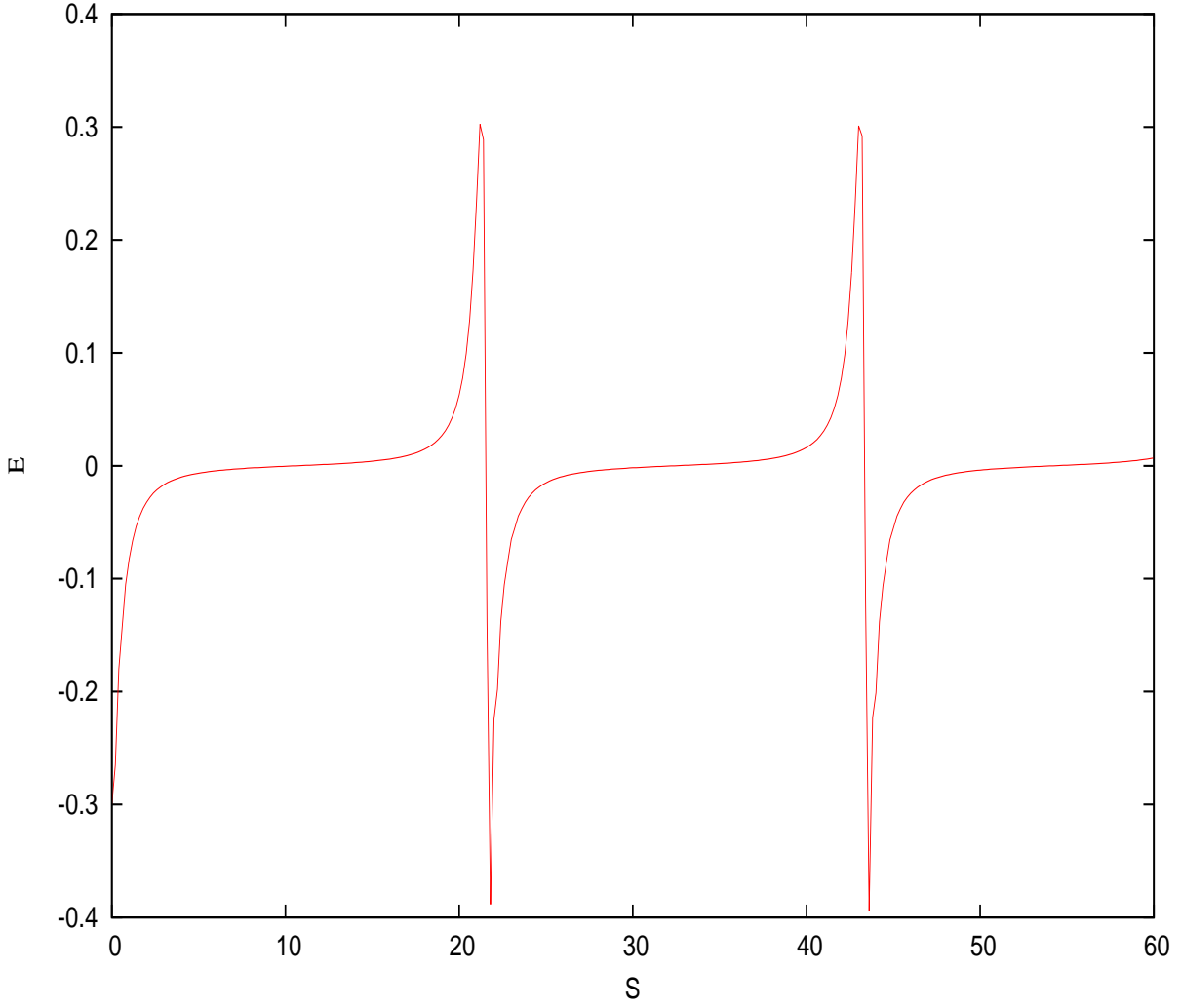


Figure 3.8: Numerical solution of normalized parallel electric field for the parameters $E_0 = 0.3$, $M = 2.5$, $R = 3.0$, $\delta_i = 0.0$, $n_{i0}/n_{e0} = 0.5$, $\theta = 2^\circ$ and $T_i/T_h = 0.2$. The period of the wave is $T_w = 3.62\tau_{ci}$ (frequency $f_w = 0.273f_{ci}$).

Effect of positron density

We next investigate the effect of the positron density on the electric field structures. The positron density is calculated from quasineutrality condition ($n_{p0}/n_{e0} = 1 - n_{i0}/n_{e0}$ at $s = 0$). It is seen from Figures 3.9 - 3.12 that as the positron density increases from 0.3 to 0.5, the waveforms become more nonlinear and the period of these waveforms increases from $1.94\tau_{ci}$ to $2.83\tau_{ci}$. These results are similar to those of Moolla et al. [2012]. Thus, for both a quasineutral and charge separated plasma of this type, an increase in positron densities enhances nonlinearity making spiky structures easier to generate.

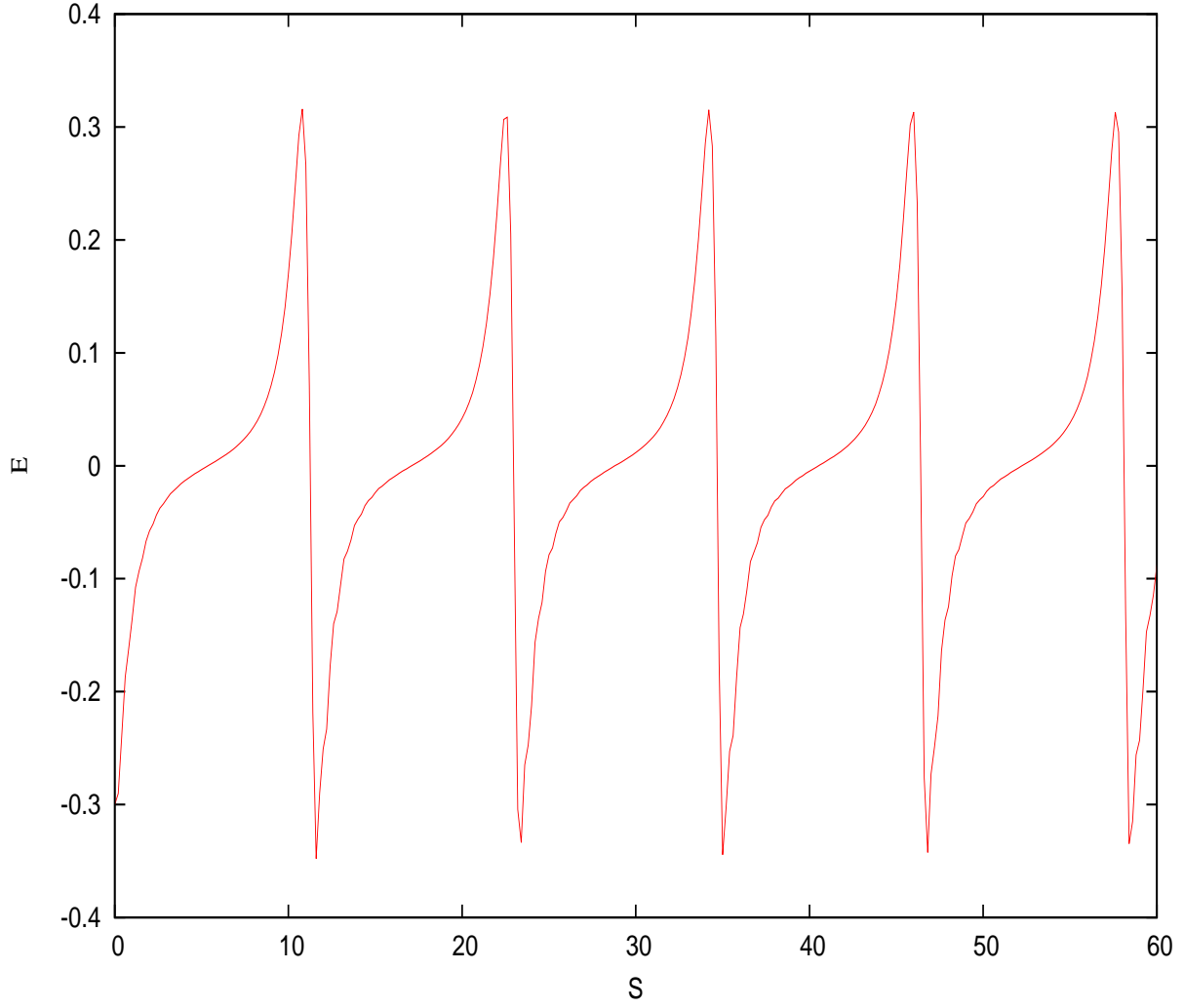


Figure 3.9: Numerical solution of normalized parallel electric field for the parameters $E_0 = 0.3$, $M = 2.5$, $R = 3.0$, $\delta_i = 0.0$, $\theta = 2^\circ$, $T_i/T_h = 0.0$ and $n_{p0}/n_{e0} = 0.3$. The period of the wave is $T_w = 1.94\tau_{ci}$ (frequency $f_w = 0.515f_{ci}$).

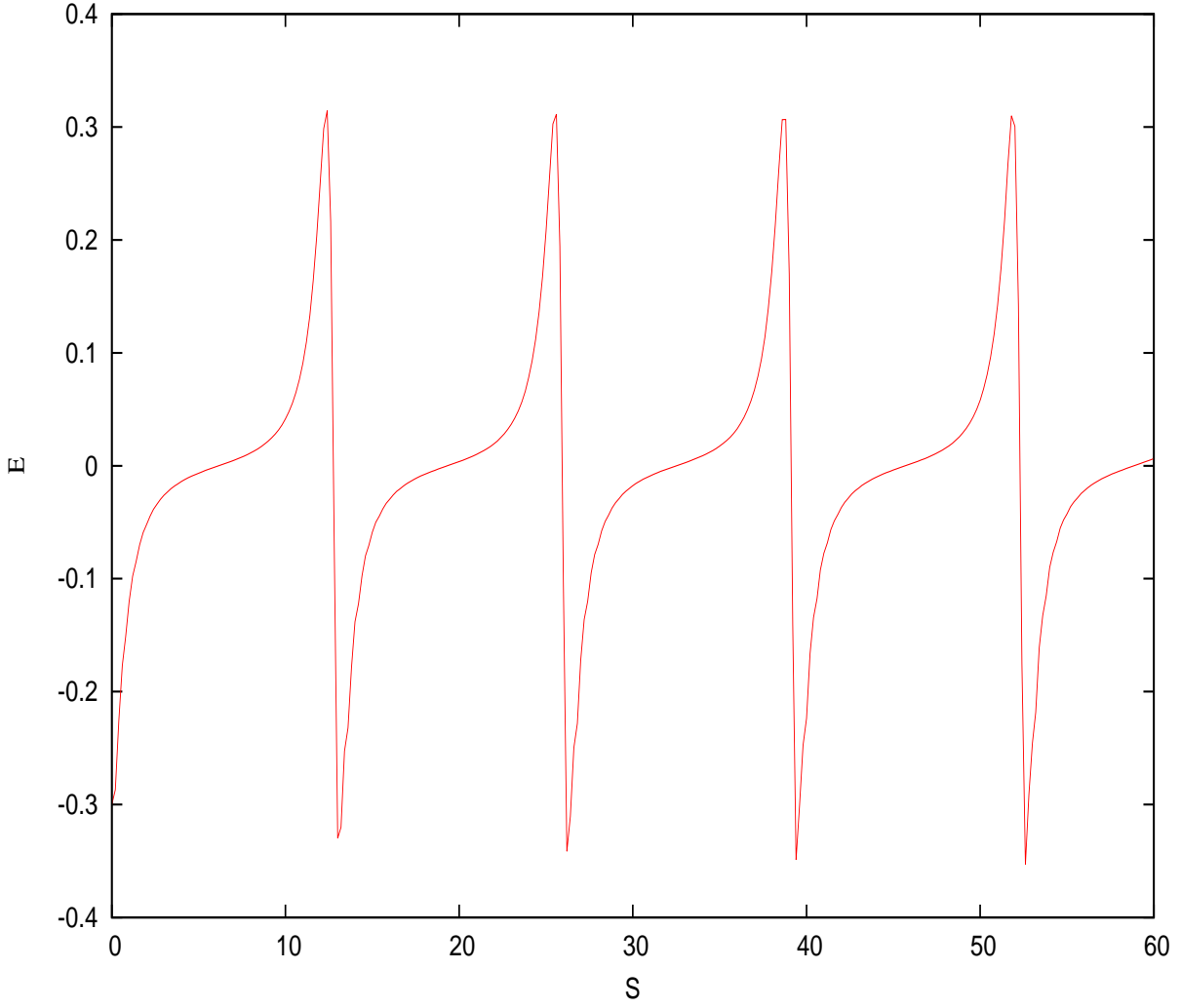


Figure 3.10: Numerical solution of normalized parallel electric field for the parameters $E_0 = 0.3$, $M = 2.5$, $R = 3.0$, $\delta_i = 0.0$, $\theta = 2^\circ$, $T_i/T_h = 0.0$ and $n_{p0}/n_{e0} = 0.35$. The period of the wave is $T_w = 2.20\tau_{ci}$ (frequency $f_w = 0.454f_{ci}$).

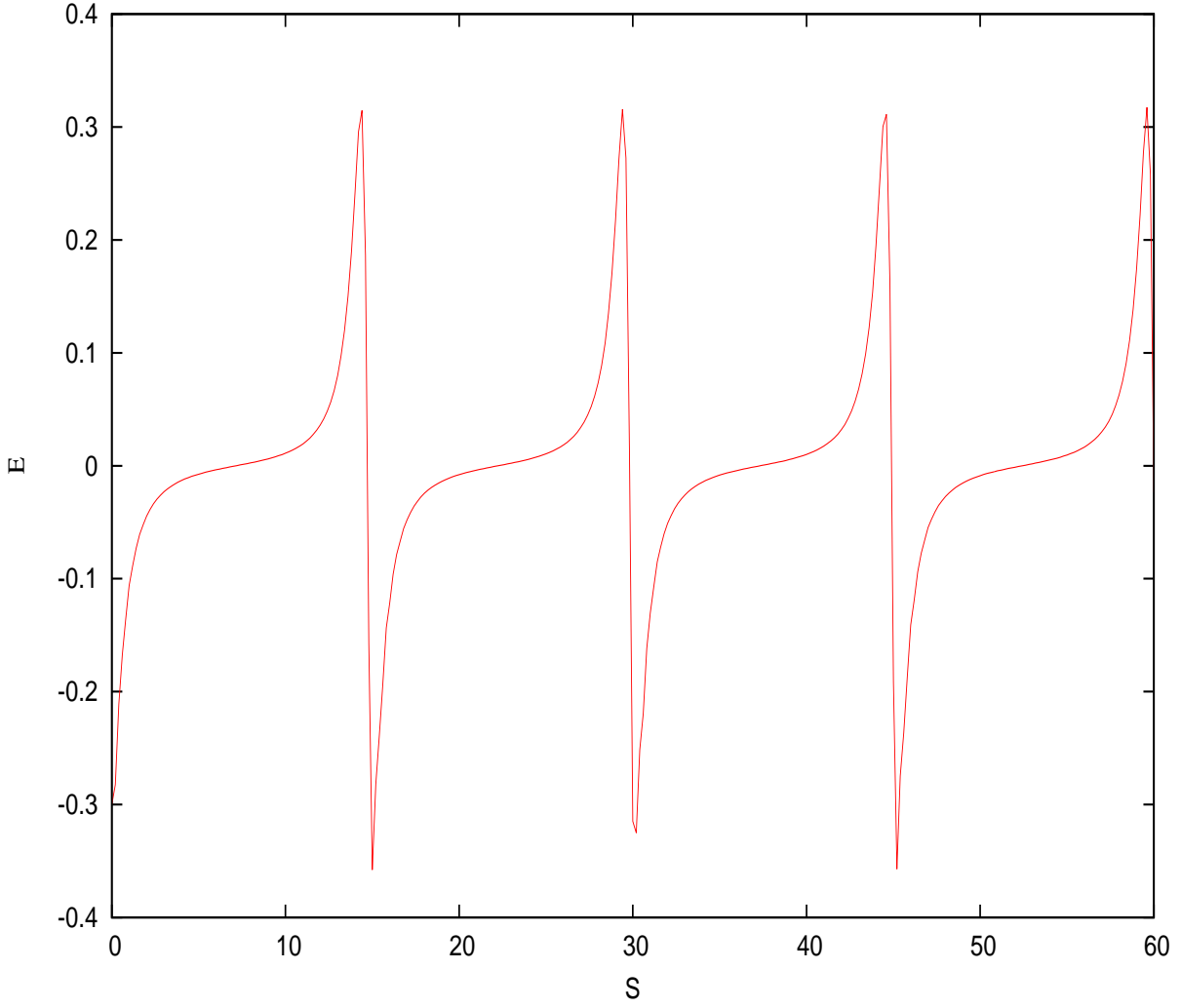


Figure 3.11: Numerical solution of normalized parallel electric field for the parameters $E_0 = 0.3$, $M = 2.5$, $R = 3.0$, $\delta_i = 0.0$, $\theta = 2^\circ$, $T_i/T_h = 0.0$ and $n_{p0}/n_{e0} = 0.4$. The period of the wave is $T_w = 2.43\tau_{ci}$ (frequency $f_w = 0.411f_{ci}$).

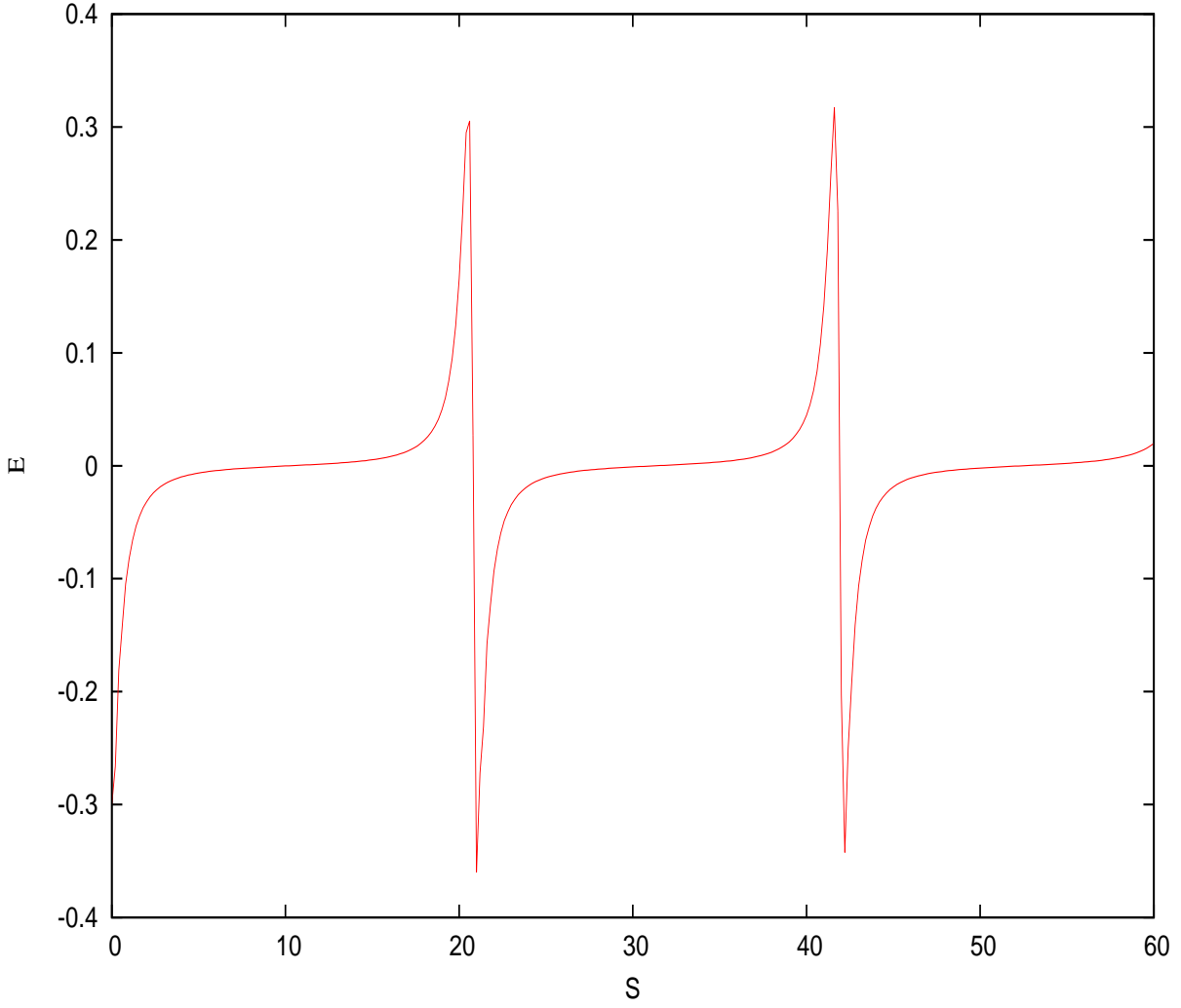


Figure 3.12: Numerical solution of normalized parallel electric field for the parameters $E_0 = 0.3$, $M = 2.5$, $R = 3.0$, $\delta_i = 0.0$, $\theta = 2^\circ$, $T_i/T_h = 0.0$ and $n_{p0}/n_{e0} = 0.5$. The period of the wave is $T_w = 2.83\tau_{ci}$ (frequency $f_w = 0.353f_{ci}$).

Effect of ion drift

We now investigate the effect of the ion drift velocity on the electric field structures as shown in Figures 3.13 - 3.17 for the fixed the parameters $E_0 = 0.3$, $M = 2.5$, $R = 3.0$, $\theta = 2^\circ$, $T_i/T_h = 0.0$ and $n_{i0}/n_{e0} = 0.5$. It is seen that for antiparallel ion drift ($\delta_i < 0$), the periods of the waves are significantly higher compared to parallel drift ($\delta_i > 0$). From anti-parallel to parallel drifts, the period of the spikes decrease from $4.12\tau_{ci}$ for $\delta_i = -0.20$ to $2.81\tau_{ci}$ for $\delta_i = 0.20$. However, the nonlinearity is unaffected and all waveforms are spiky in nature. These results are similar to those of Moolla et al. [2012] confirming satellite observations. Noting that, these observations show that the period of the spiky structures varies rapidly [Kojima et al., 1994], and this could be due to the drifting particles being accelerated in bursts [Moolla et al., 2003].

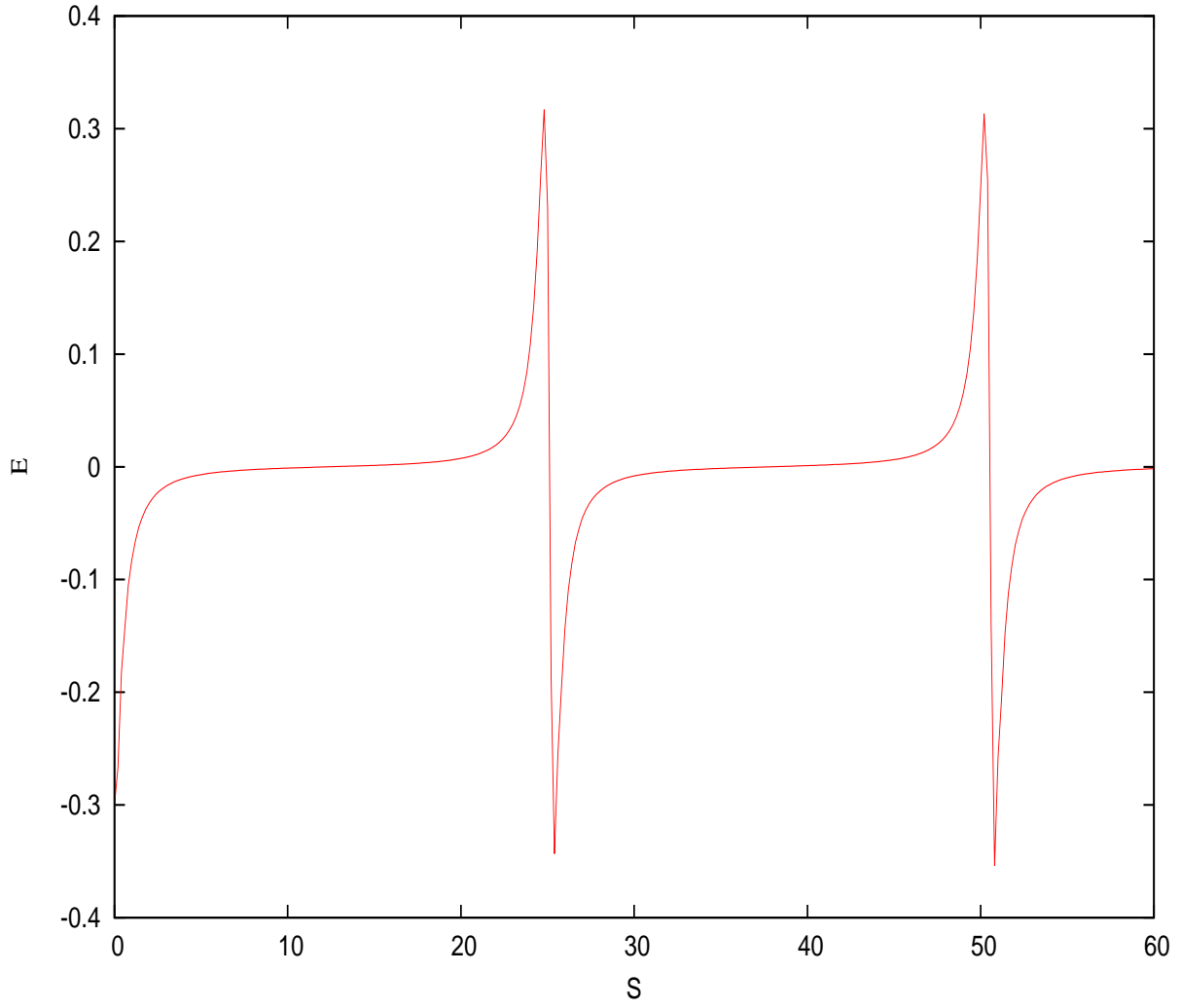


Figure 3.13: Numerical solution of normalized parallel electric field for the parameters $E_0 = 0.3$, $M = 2.5$, $R = 3.0$, $\theta = 2^\circ$, $T_i/T_h = 0.0$, $n_{i0}/n_{e0} = 0.5$ and $\delta_i = -0.20$. The period of the wave is $T_w = 4.12\tau_{ci}$ (frequency $f_w = 0.242f_{ci}$).

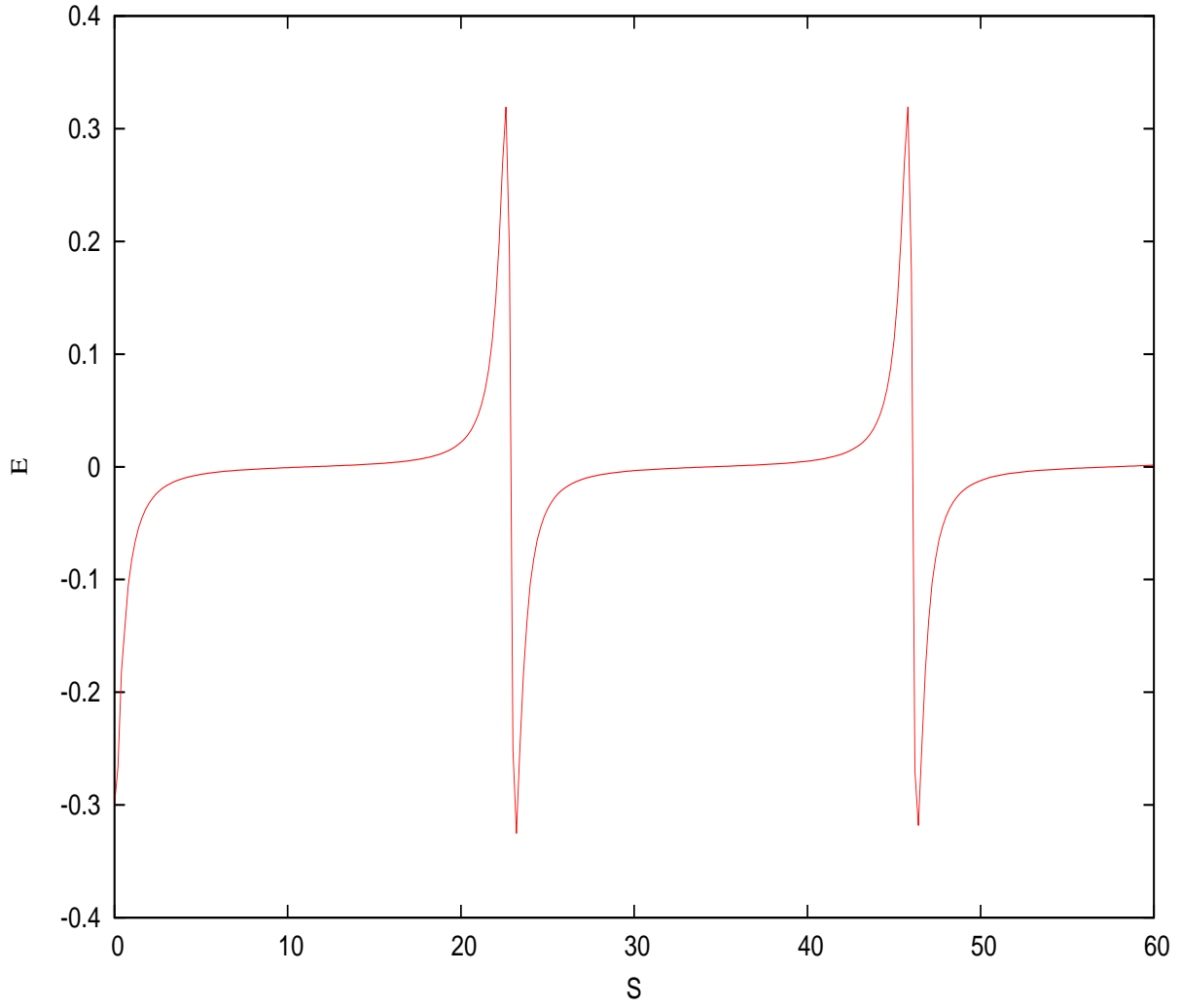


Figure 3.14: Numerical solution of normalized parallel electric field for the parameters $E_0 = 0.3$, $M = 2.5$, $R = 3.0$, $\theta = 2^\circ$, $T_i/T_h = 0.0$, $n_{i0}/n_{e0} = 0.5$ and $\delta_i = -0.10$. The period of the wave is $T_w = 3.83\tau_{ci}$ (frequency $f_w = 0.261f_{ci}$).

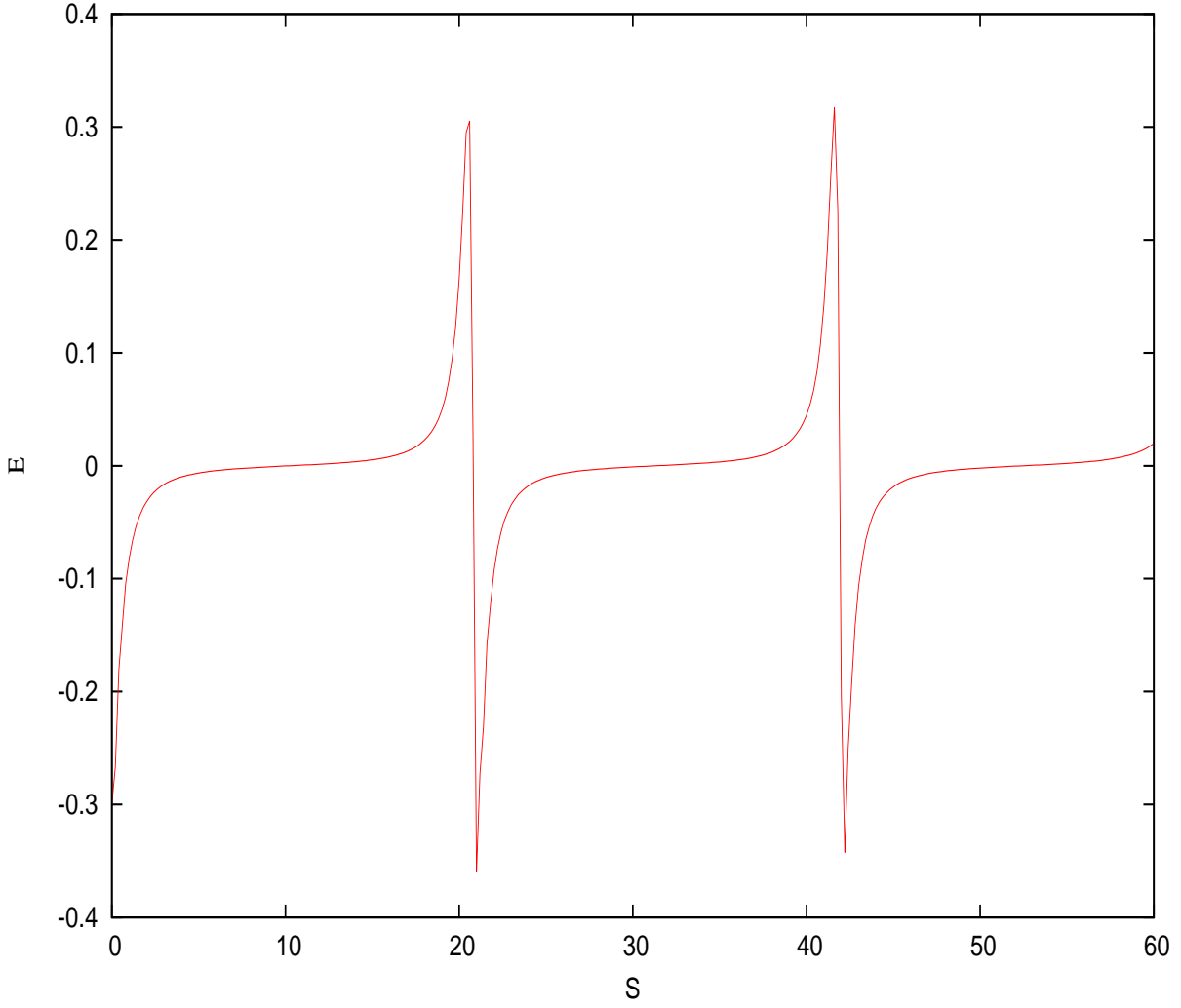


Figure 3.15: Numerical solution of normalized parallel electric field for the parameters $E_0 = 0.3$, $M = 2.5$, $R = 3.0$, $\theta = 2^\circ$, $T_i/T_h = 0.0$, $n_{i0}/n_{e0} = 0.5$ and $\delta_i = 0.0$. The period of the wave is $T_w = 3.46\tau_{ci}$ (frequency $f_w = 0.289f_{ci}$).

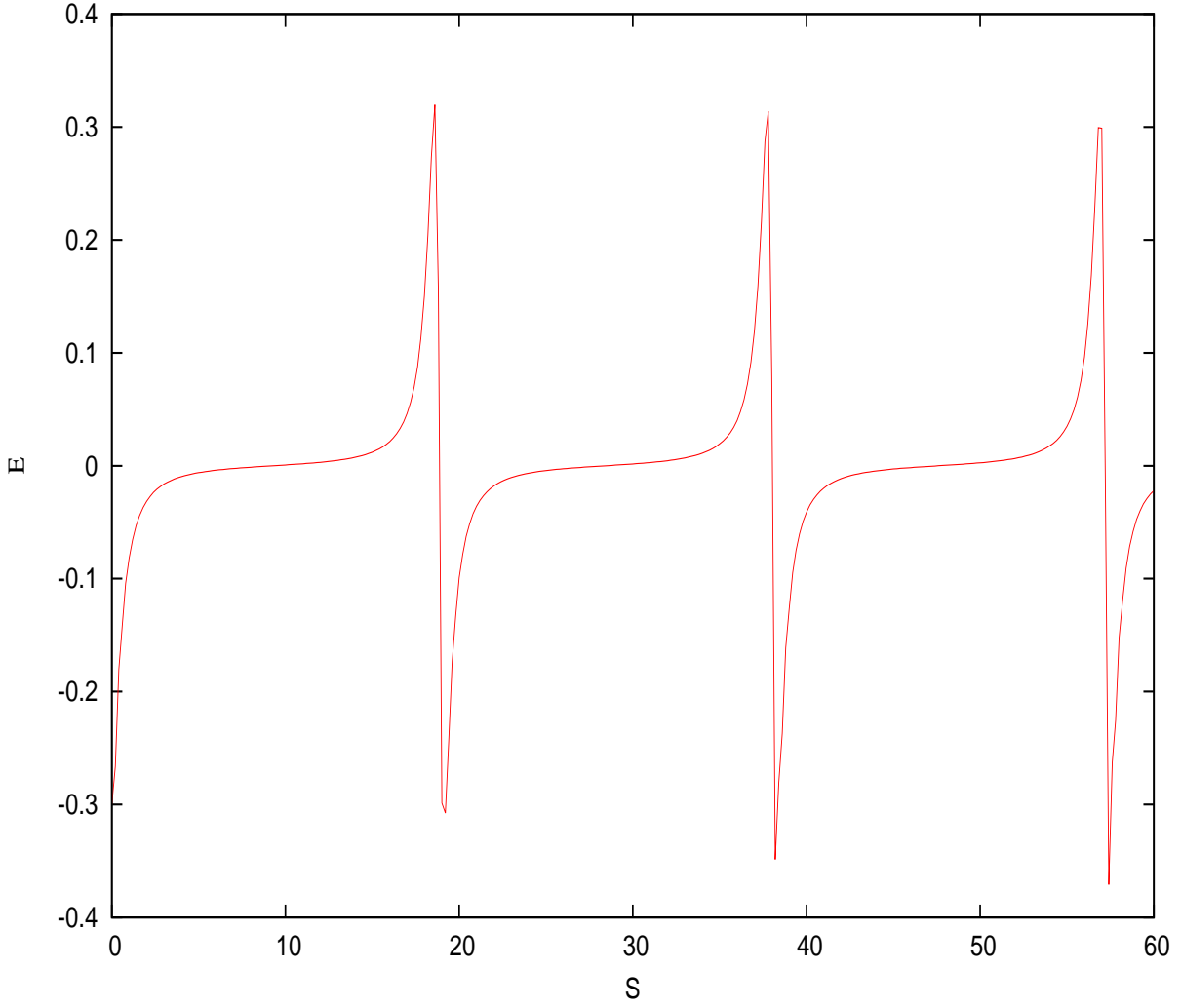


Figure 3.16: Numerical solution of normalized parallel electric field for the parameters $E_0 = 0.3$, $M = 2.5$, $R = 3.0$, $\theta = 2^\circ$, $T_i/T_h = 0.0$, $n_{i0}/n_{e0} = 0.5$ and $\delta_i = 0.10$. The period of the wave is $T_w = 3.08\tau_{ci}$ (frequency $f_w = 0.324f_{ci}$).

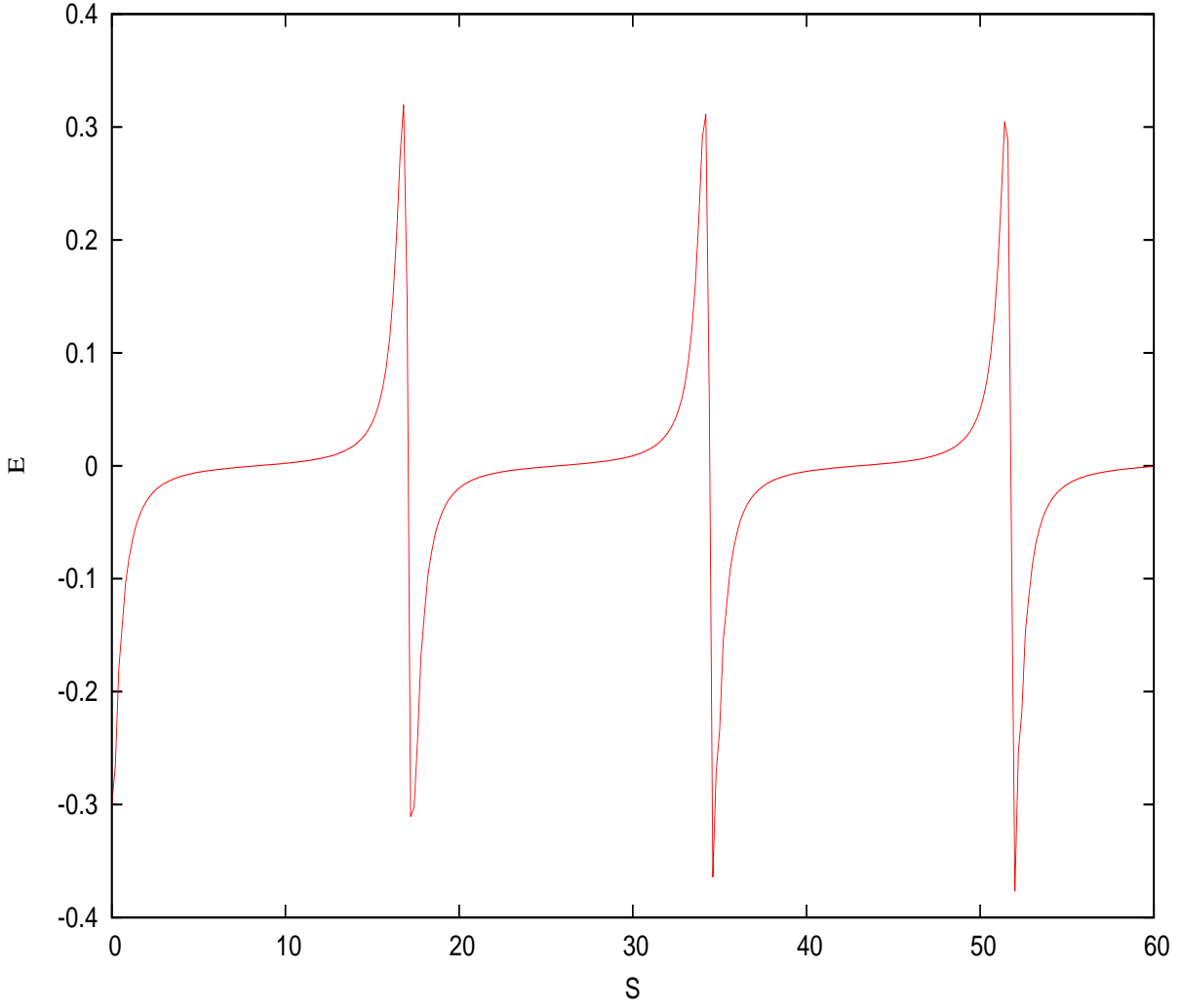


Figure 3.17: Numerical solution of normalized parallel electric field for the parameters $E_0 = 0.3$, $M = 2.5$, $R = 3.0$, $\theta = 2^\circ$, $T_i/T_h = 0.0$, $n_{i0}/n_{e0} = 0.5$ and $\delta_i = 0.20$. The period of the wave is $T_w = 2.81\tau_{ci}$ (frequency $f_w = 0.355f_{ci}$).

Effect of Propagation angle θ

Figures 3.18 - 3.21 illustrate the normalized electric field for different values of the angle of wave propagation θ for fixed parameters $M = 2.5$, $\delta_i = 0.0$, $n_{i0}/n_{e0} = 0.5$, $T_i/T_h = 0.0$, $R = 3.0$ and $E_0 = 0.3$. We vary θ from 2° to 80° and we observe that the period of oscillations decreases slightly from $3.45\tau_{ci}$ to $3.34\tau_{ci}$ i.e there is a slight increase in frequency [Maharaj et al., 2008; Reddy et al., 2006]. The variation of propagation angle has no effect on the wave structures. This confirms the assumption of [Reddy et al., 2002; Moolla et al., 2007, 2012], that the angle of wave propagation with the earth's magnetic field may be set to two degree ($\theta = 2^\circ$) for parallel propagation during investigation of electrostatic waves in Earth's magnetosphere.

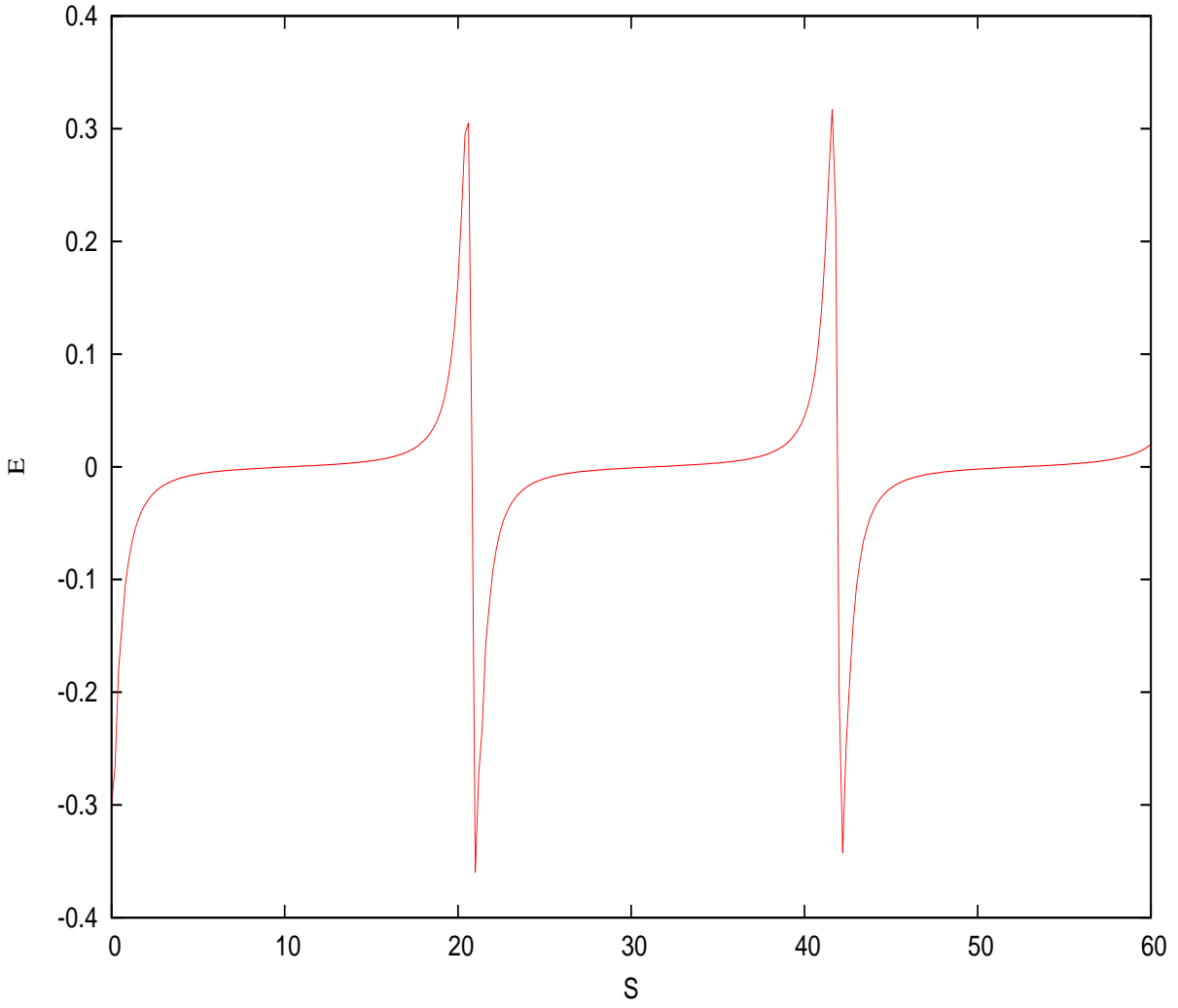


Figure 3.18: Numerical solution of normalized parallel electric field for the parameters $M = 2.5$, $\delta_i = 0.0$, $n_{i0}/n_{e0} = 0.5$, $T_i/T_h = 0.0$, $R = 3.0$, $E_0 = 0.3$ and $\theta = 2^\circ$.

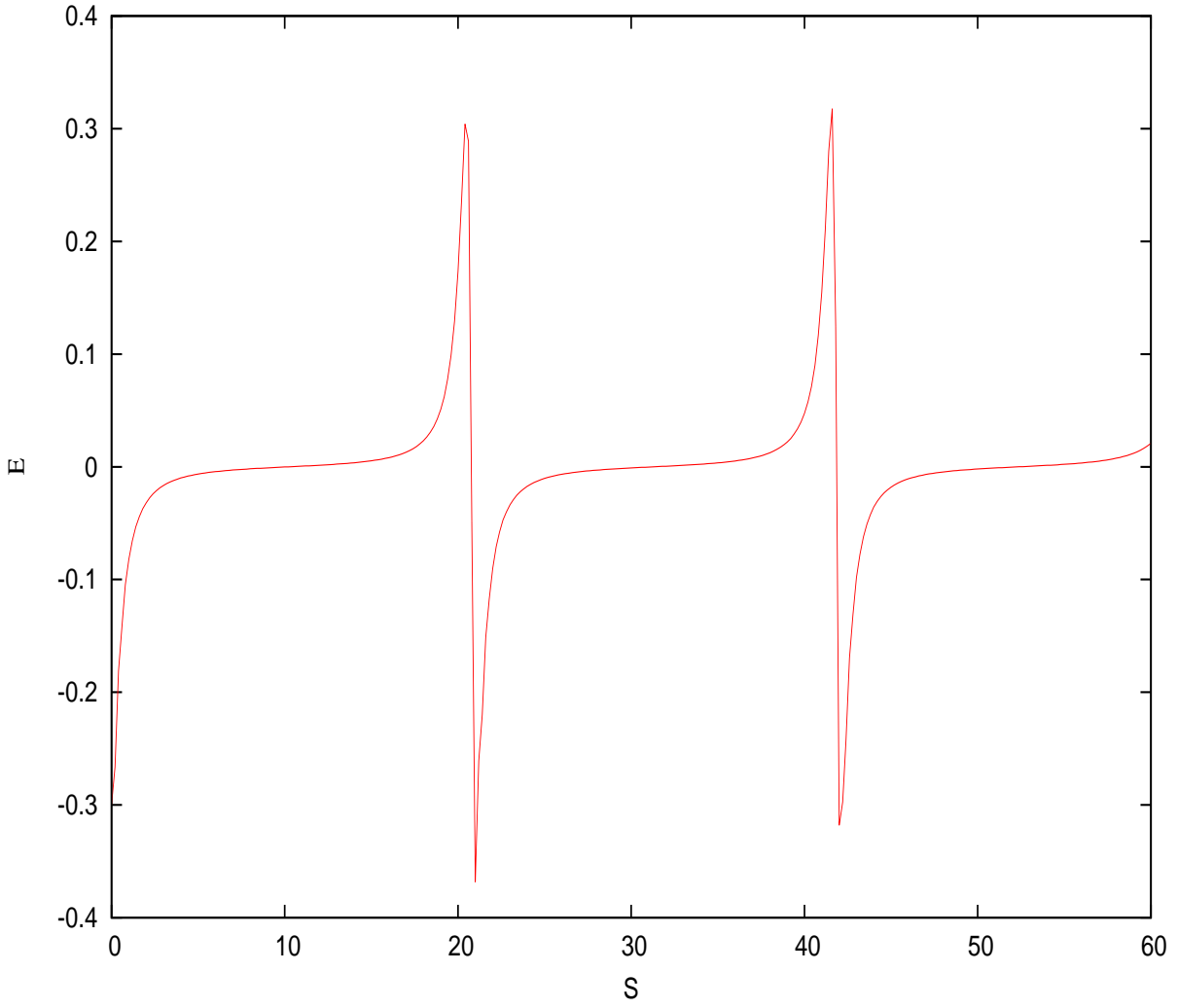


Figure 3.19: Numerical solution of normalized parallel electric field for the parameters $M = 2.5$, $\delta_i = 0.0$, $n_{i0}/n_{e0} = 0.5$, $T_i/T_h = 0.0$, $R = 3.0$, $E_0 = 0.3$ and $\theta = 25^\circ$.

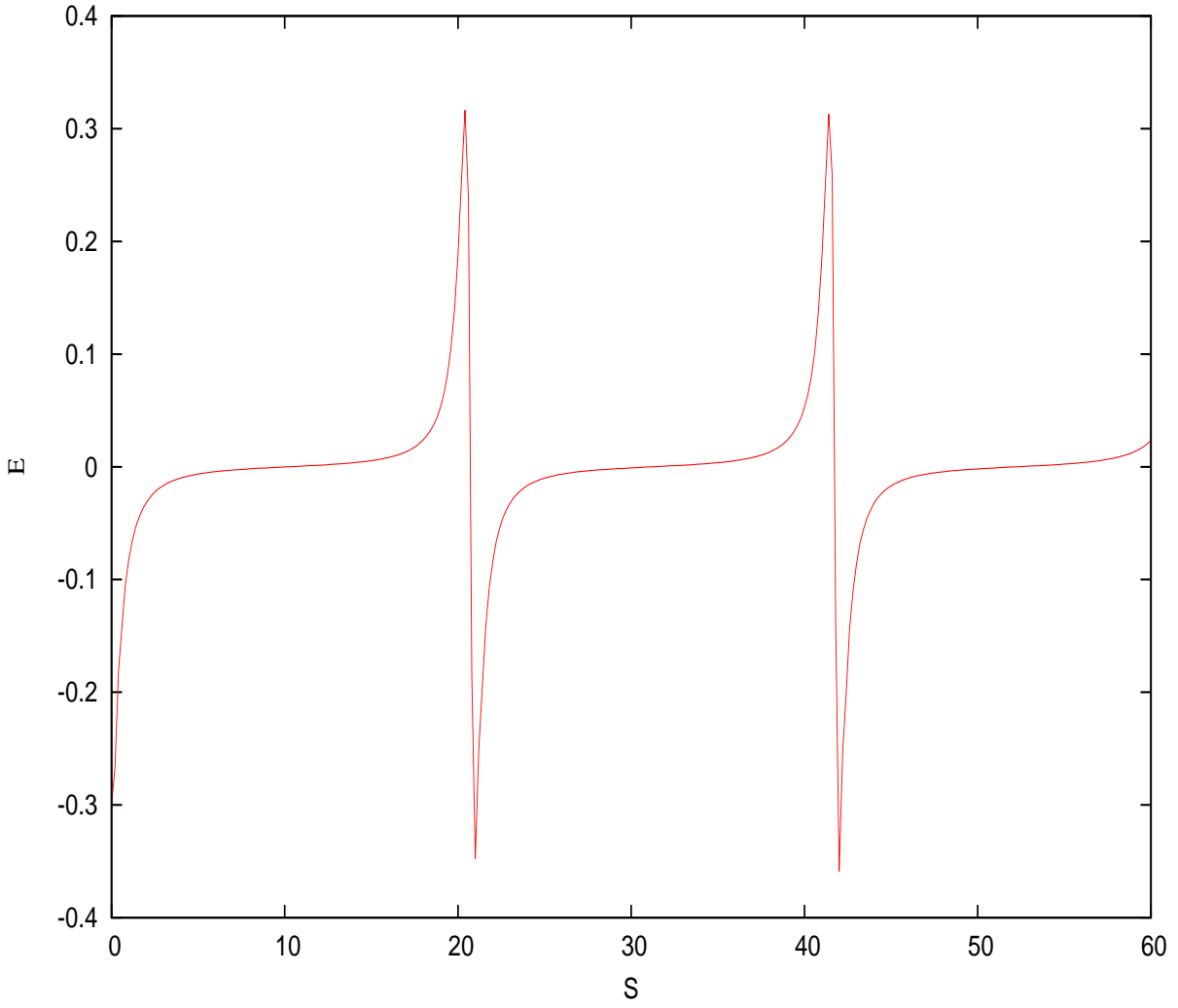


Figure 3.20: Numerical solution of normalized parallel electric field for the parameters $M = 2.5$, $\delta_i = 0.0$, $n_{i0}/n_{e0} = 0.5$, $T_i/T_h = 0.0$, $R = 3.0$, $E_0 = 0.3$ and $\theta = 50^\circ$.

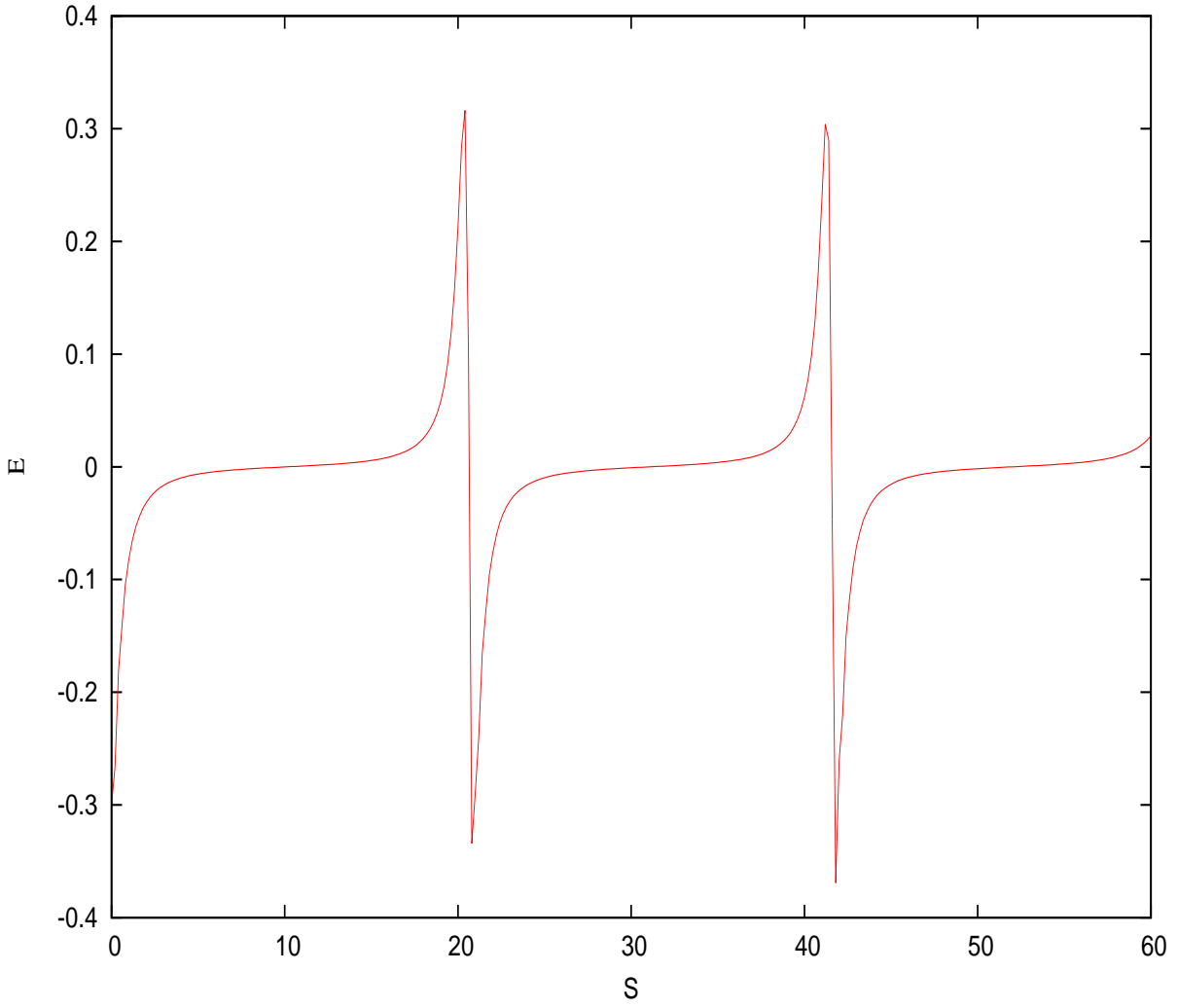


Figure 3.21: Numerical solution of normalized parallel electric field for the parameters $M = 2.5$, $\delta_i = 0.0$, $n_{i0}/n_{e0} = 0.5$, $T_i/T_h = 0.0$, $R = 3.0$, $E_0 = 0.3$ and $\theta = 80^\circ$.

Effect of *Mach* number M

Figures 3.22 -3.25 illustrate the effect of the *Mach* number on the parallel electric field. We have varied the *Mach* number M by keeping $E_0 = 0.3$, $R = 3.0$, $\delta_i = \delta_e = \delta_p = 0.0$, $\theta = 2^\circ$, $T_i/T_h = 0.0$, $n_{p0}/n_{e0} = n_{i0}/n_{e0} = 0.5$ constant. Our investigations show that the value of M needs to be in a narrow range for the electric field structures to exist. Varying M from 2.2 to 2.5, the period of oscillations decreases slightly from $3.45\tau_{ci}$ to $3.36\tau_{ci}$ with no change in nonlinearity. The findings are in agreement with the results found by Moolla et al. [2007].

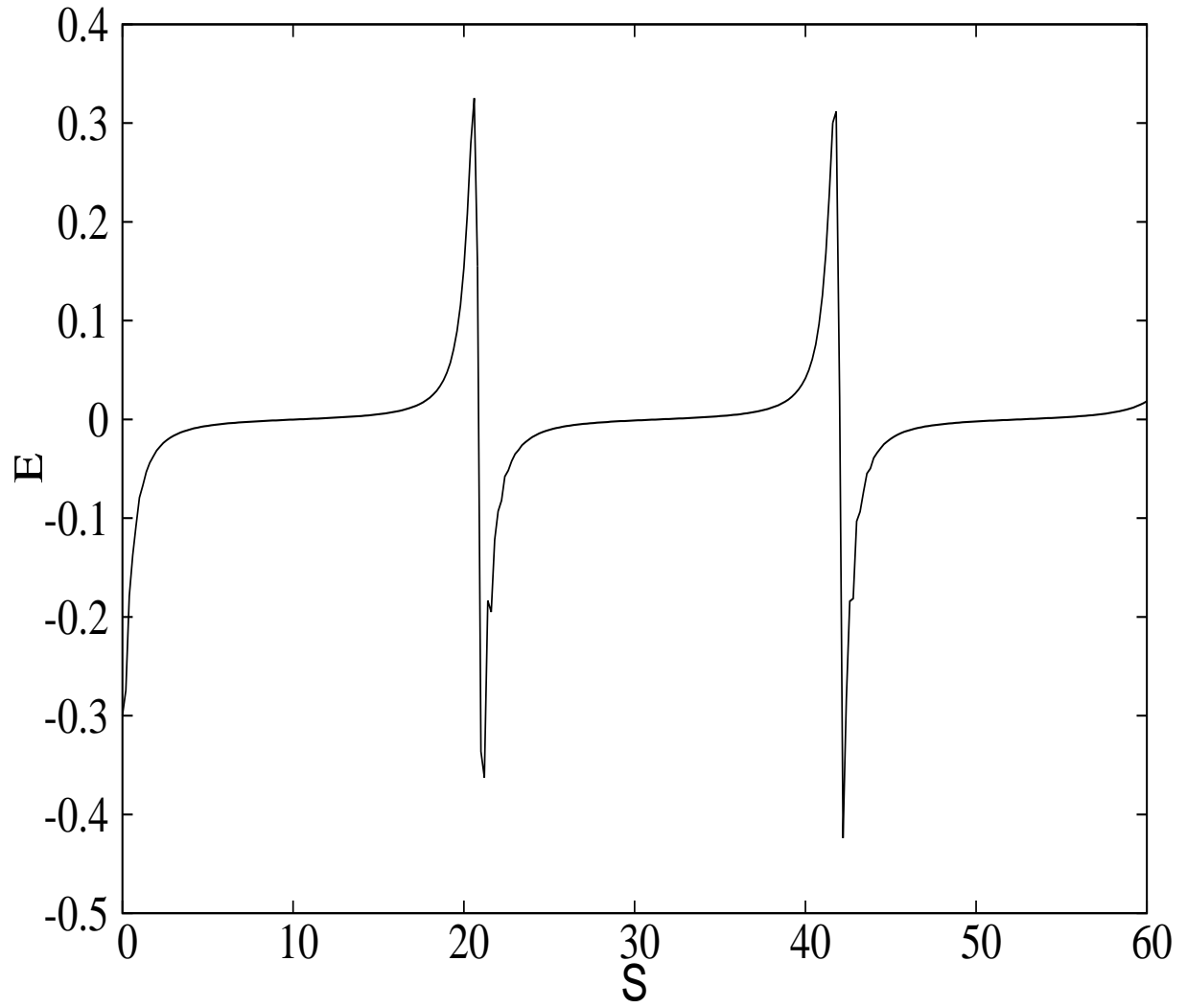


Figure 3.22: Numerical solution of normalized parallel electric field for the parameters $E_0 = 0.3$, $R = 3.0$, $\delta_i = \delta_e = \delta_p = 0.0$, $\theta = 2^\circ$, $T_i/T_h = 0.0$, $n_{p0}/n_{e0} = n_{i0}/n_{e0} = 0.5$ and $M = 2.2$.

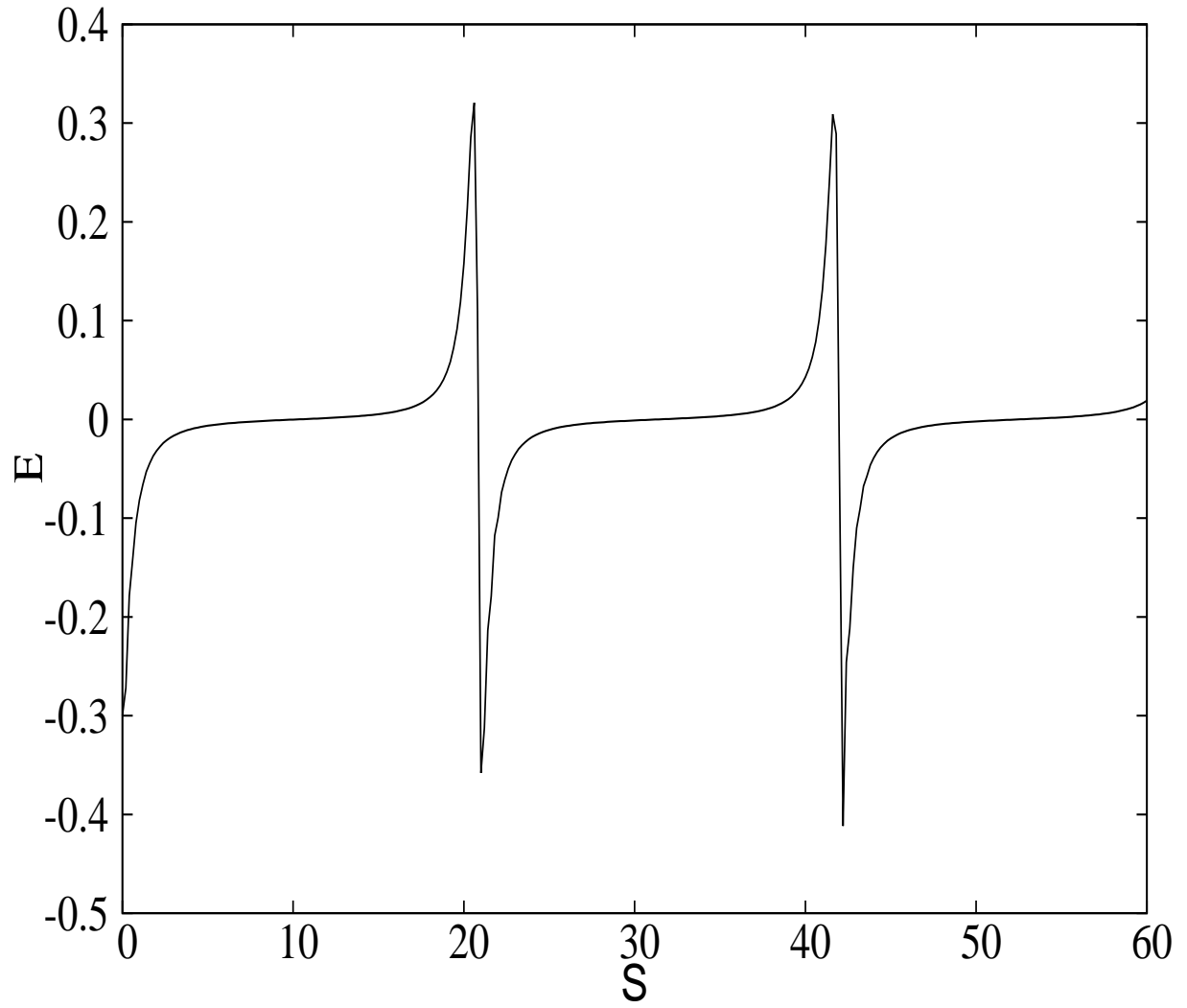


Figure 3.23: Numerical solution of normalized parallel electric field for the parameters $E_0 = 0.3$, $R = 3.0$, $\delta_i = \delta_e = \delta_p = 0.0$, $\theta = 2^\circ$, $T_i/T_h = 0.0$, $n_{p0}/n_{e0} = n_{i0}/n_{e0} = 0.5$ and $M = 2.3$.

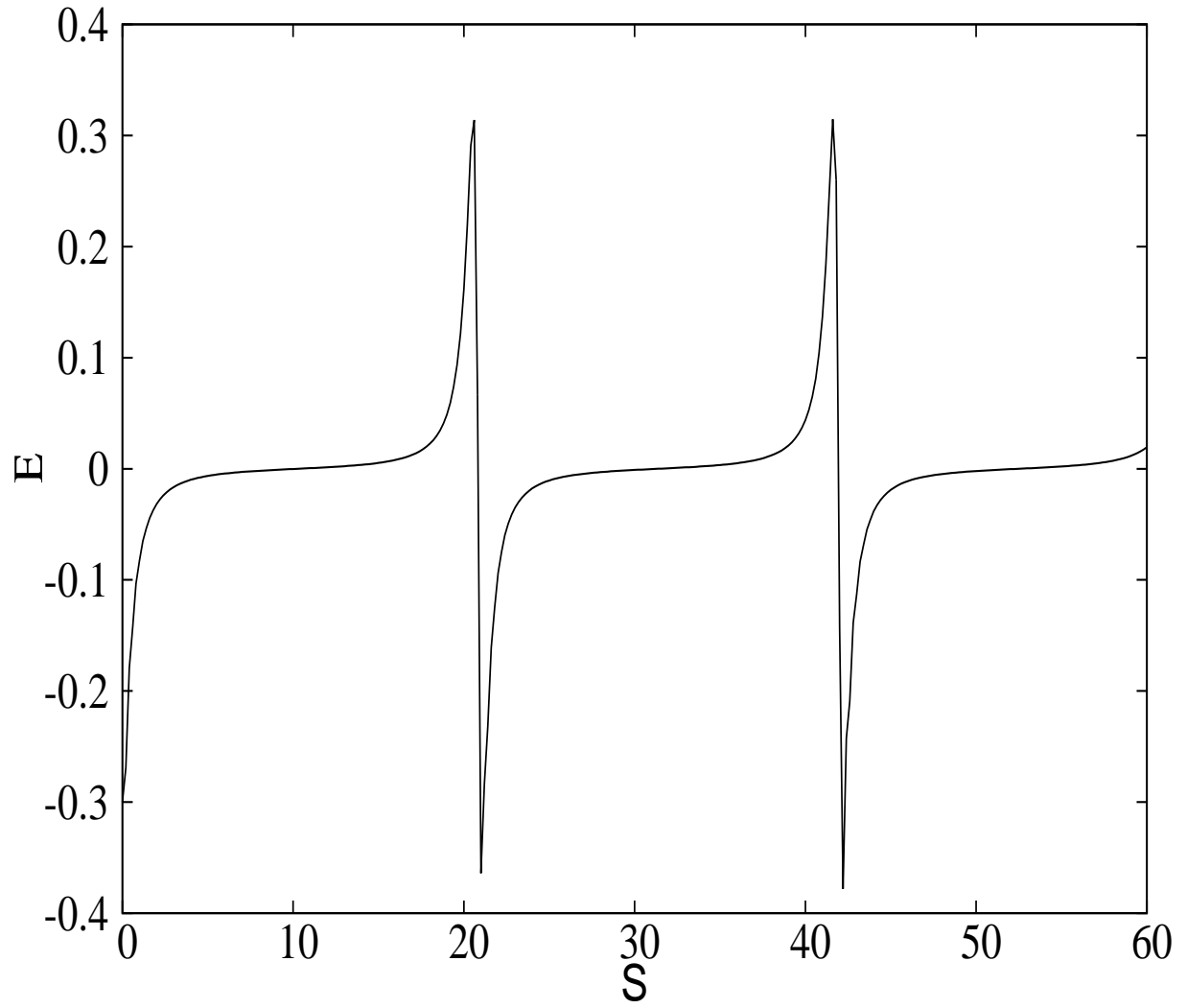


Figure 3.24: Numerical solution of normalized parallel electric field for the parameters $E_0 = 0.3$, $R = 3.0$, $\delta_i = \delta_e = \delta_p = 0.0$, $\theta = 2^\circ$, $T_i/T_h = 0.0$, $n_{p0}/n_{e0} = n_{i0}/n_{e0} = 0.5$ and $M = 2.4$.

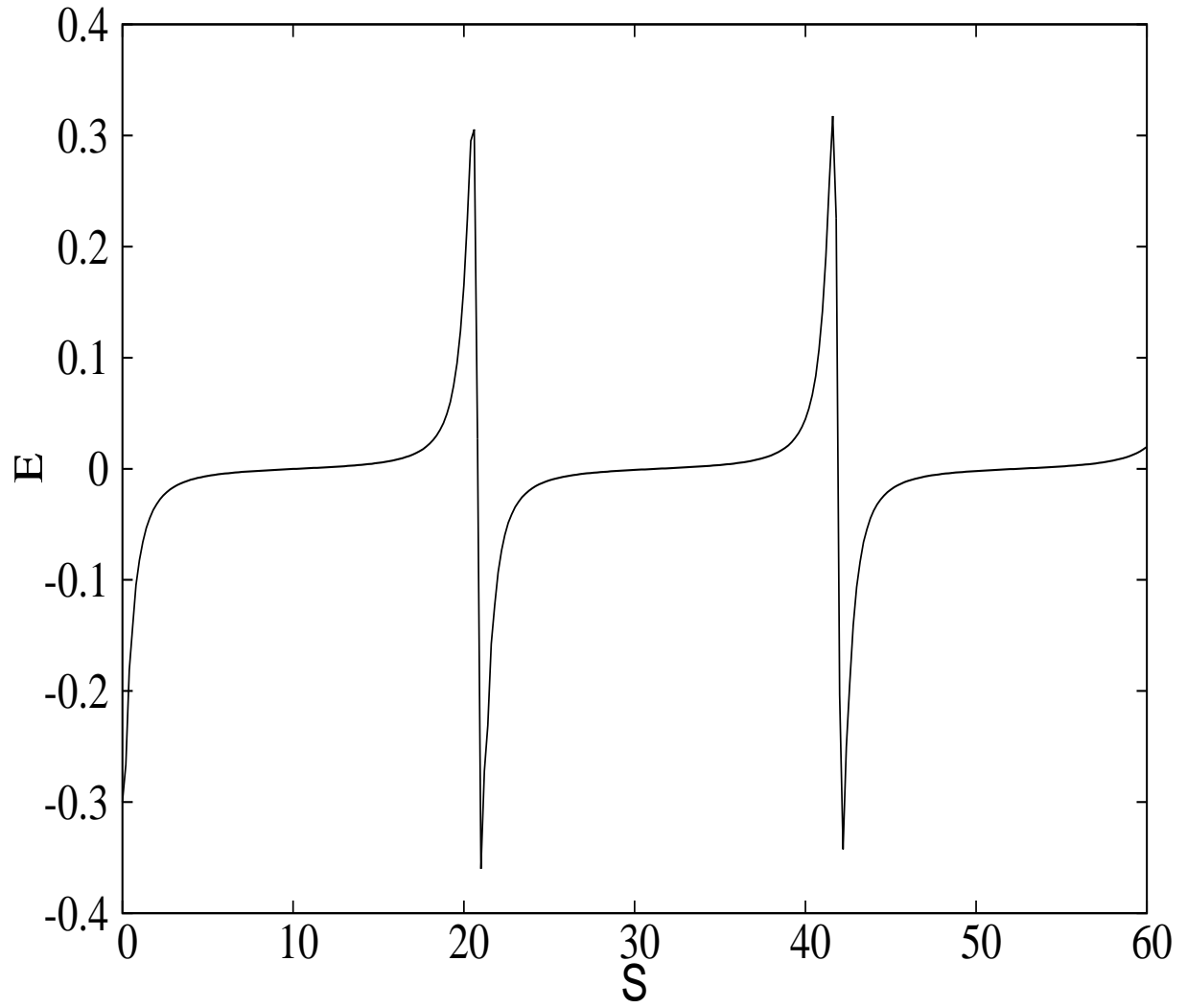


Figure 3.25: Numerical solution of normalized parallel electric field for the parameters $E_0 = 0.3$, $R = 3.0$, $\delta_i = \delta_e = \delta_p = 0.0$, $\theta = 2^\circ$, $T_i/T_h = 0.0$, $n_{p0}/n_{e0} = n_{i0}/n_{e0} = 0.5$ and $M = 2.5$.

Chapter 4

Nonlinear waves in electron - positron - ion plasmas including the full dynamics for all species

4.1 Literature Review

Observations made by different spacecrafts have established the presence of broadband electrostatic noise (BEN) in various regions of the earth's magnetosphere. Several theoretical models have been introduced in order to explain BEN detected in such environments. During these investigations, many authors [Reddy et al., 2002, 2006; Bharuthram et al., 2002; Moolla et al., 2003, 2007] considered a magnetized plasma consisting of hot and cold species. The hot species were governed by the Boltzmann density distribution function and the cold species were governed by the fluid equations. They either used the quasi-neutrality condition or the Poisson equation to close their system of equations. Their results pointed out that the nonlinear coupling oscillations generates spiky structures with the period varying from ion acoustic range to the ion cyclotron [Bharuthram et al., 2002; Reddy et al., 2002].

Moolla et al. [2003] extended the work of Reddy et al. [2002] by including the Poisson equation. Their model was a three component plasma consisting of cold electrons and cold

ions, and hot electrons, where all species were governed by the fluid equations. They found that the nonlinear coupling between the high frequency electron-cyclotron and electron-acoustic modes could explain the spiky structures in the high frequency region of BEN.

More recently, Moolla et al. [2007] extended their previous high frequency study by considering finite temperature effects. They investigated the pulse widths and periods of the waves and concluded that the ratio of the pulse widths to the periods of the electrostatic waves (ESW) is a constant. They also pointed out that with the inclusion of a finite cool electron temperature, the waves broadened and the nonlinearity was enhanced.

In this chapter, we explore the extension of Chapter 3, whereby all species are described by fluid equations.

4.2 Basic theory and Model of fluid equations governing the plasma dynamics

We consider a collisionless, magnetized three-component plasma consisting of warm ions (i) and hot positrons (p) and electrons (e) in the presence of an external magnetic field B_0 which assumed to be in the $x - z$ plane and making an angle θ with the x - axis. The basic equations, governing the dynamical system, are the equations of continuity and momentum which are written as

$$\frac{\partial n_j}{\partial t} + \frac{\partial n_j v_{jx}}{\partial x} = 0, \quad (4.1)$$

$$\frac{\partial v_{jx}}{\partial t} + v_{jx} \frac{\partial v_{jx}}{\partial x} + \frac{1}{n_j m_j} \frac{\partial p_j}{\partial x} = -\frac{\varepsilon_j e}{m_i} \frac{\partial \varphi}{\partial x} + \varepsilon_j \Omega_j v_{jy} \sin \theta, \quad (4.2)$$

$$\frac{\partial v_{jy}}{\partial t} + v_{jx} \frac{\partial v_{jy}}{\partial x} = \varepsilon_j \Omega_j v_{jz} \cos \theta - \varepsilon_j \Omega_j v_{jx} \sin \theta, \quad (4.3)$$

$$\frac{\partial v_{jz}}{\partial t} + v_{jx} \frac{\partial v_{jz}}{\partial x} = -\varepsilon_j \Omega_j v_{jy} \cos \theta, \quad (4.4)$$

$$\frac{\partial p_j}{\partial t} + v_{jx} \frac{\partial p_j}{\partial x} + 3p_j \frac{\partial v_{jx}}{\partial x} = 0. \quad (4.5)$$

Equations (4.1) - (4.5) are closed with the Poisson equation

$$\varepsilon_0 \frac{\partial^2 \varphi}{\partial x^2} = -e(n_p - n_e + n_i). \quad (4.6)$$

In equations (4.1)-(4.6), $\varepsilon_j = -1(1)$ for $j = e(i, p)$, $\Omega_j = eB_0/m_j$ is the ion (electron) cyclotron frequency for the $j = i(e, p)$, n_j is the density of the j th species, v_{jx}, v_{jy} and v_{jz} are the components of the velocity of the j species along the x, y and z directions.

4.2.1 Nonlinear Analysis

For the nonlinear analysis, the new physical stretch variable depending on s and v are introduced (see 3.2.2). We transform equations (4.1)-(4.6) to a stationary frame using $s = (x - vt)/(v/\Omega_i)$ and normalize velocities with respect to the ion thermal velocity $C_s = \sqrt{T_i/m_i}$, densities with respect to the total unperturbed electron density n_{e0} , pressures with respect to $n_{e0}T_h$ and potential with respect to T_h/e . We replace $\frac{\partial}{\partial t}$ by $-\Omega_i \frac{\partial}{\partial s}$ and $\frac{\partial}{\partial x}$ by $(\Omega_i/v) \frac{\partial}{\partial s}$ in equations (4.1)-(4.6) and define the normalized electric potential $\psi = e\varphi/T_h$ and electric field $E = -\frac{\partial \psi}{\partial s}$. We use the following initial conditions: $\psi = 0$, $\partial \psi / \partial s = E_0$, $\partial^2 \psi / \partial s^2 = 0$, $n_j = n_{j0}$ and $V_{jx} = v_{j0} \cos \theta$ at $s = 0$. In addition, we assume point quasineutrality, that is, $n_{i0} + n_{p0} = n_{e0}$ at equilibrium. The results obtained are expressed as a set of differential equations given below:

$$\frac{\partial \psi}{\partial s} = -E \quad (4.7)$$

$$\frac{\partial E}{\partial s} = M^2 R^2 \frac{n_{e0}}{n_{i0}} (\tilde{n}_p + \tilde{n}_i - \tilde{n}_e) \quad (4.8)$$

$$\frac{\partial \tilde{n}_e}{\partial s} = \frac{\tilde{n}_e^3 [E + \frac{m_i}{m} M \tilde{v}_{ey} \sin \theta]}{(M - \delta_e)^2 - 3\tilde{n}_e \tilde{P}_e} \quad (4.9)$$

$$\frac{\partial \tilde{P}_e}{\partial s} = \frac{3\tilde{P}_e \tilde{n}_e^2 [E + \frac{m_i}{m} M \tilde{v}_{ey} \sin \theta]}{(M - \delta_e)^2 - 3\tilde{n}_e \tilde{P}_e} \quad (4.10)$$

$$\frac{\partial \tilde{v}_{ey}}{\partial s} = \left(\frac{m_i}{m}\right) \frac{\tilde{n}_e M}{(M - \delta_e)} [\tilde{v}_{ez} \cos \theta - M \sin \theta] + \left(\frac{m_i}{m}\right) M \sin \theta \quad (4.11)$$

$$\frac{\partial \tilde{v}_{ez}}{\partial s} = - \left(\frac{m_i}{m}\right) \frac{n_{en} M \tilde{v}_{ey} \cos \theta}{(M - \delta_e)} \quad (4.12)$$

$$\frac{\partial \tilde{n}_p}{\partial s} = \frac{\tilde{n}_p^3 [-E - \frac{m_i}{m} M \tilde{v}_{py} \sin \theta]}{\left(\frac{n_{p0}}{n_{e0}}\right)^2 (M - \delta_p)^2 - 3 \left(\frac{n_{p0}}{n_{e0}}\right) \tilde{n}_p \tilde{P}_p} \quad (4.13)$$

$$\frac{\partial \tilde{P}_p}{\partial s} = \frac{3 \tilde{P}_p \tilde{n}_p^2 [-E - \frac{m_i}{m} M \tilde{v}_{py} \sin \theta]}{\left(\frac{n_{p0}}{n_{e0}}\right)^2 (M - \delta_p)^2 - 3 \left(\frac{n_{p0}}{n_{e0}}\right) \tilde{n}_p \tilde{P}_p} \quad (4.14)$$

$$\frac{\partial \tilde{v}_{py}}{\partial s} = \left(\frac{m_i}{m}\right) \left(\frac{n_{e0}}{n_{p0}}\right) \frac{\tilde{n}_p M}{(M - \delta_p)} [M \sin \theta - \tilde{v}_{pz} \cos \theta] - \left(\frac{m_i}{m}\right) M \sin \theta \quad (4.15)$$

$$\frac{\partial \tilde{v}_{pz}}{\partial s} = \left(\frac{m_i}{m}\right) \frac{\tilde{n}_p M \tilde{v}_{ey} \cos \theta}{(M - \delta_p)} \quad (4.16)$$

$$\frac{\partial \tilde{n}_i}{\partial s} = \frac{\tilde{n}_i^3 [-E - M \tilde{v}_{iy} \sin \theta]}{\left(\frac{n_{i0}}{n_{e0}}\right)^2 (M - \delta_i)^2 - 3 \tilde{n}_i \tilde{P}_i} \quad (4.17)$$

$$\frac{\partial \tilde{P}_i}{\partial s} = \frac{3 \tilde{P}_i \tilde{n}_i^2 [-E - M \tilde{v}_{iy} \sin \theta]}{\left(\frac{n_{i0}}{n_{e0}}\right)^2 (M - \delta_i)^2 - 3 \tilde{n}_i \tilde{P}_i} \quad (4.18)$$

$$\frac{\partial \tilde{v}_{iy}}{\partial s} = \frac{\tilde{n}_i M}{\left(\frac{n_{i0}}{n_{e0}}\right) (M - \delta_i)} [M - \tilde{v}_{iz} \cos \theta] - M \sin \theta \quad (4.19)$$

$$\frac{\partial \tilde{v}_{iz}}{\partial s} = \frac{\tilde{n}_i M \tilde{v}_{iy} \cos \theta}{\left(\frac{n_{i0}}{n_{e0}}\right) (M - \delta_i)} \quad (4.20)$$

where m is the mass of the electrons/positrons, $\delta_j = v_{j0}/C_s$ is the normalized flow velocity of the j th species, $M = v/C_s$ is the *Mach* number and $R = \omega_{pi}/\Omega_i$. The additional superscript ' \sim ' introduced in equations (4.8)-(4.20) indicates normalized quantities.

4.2.2 Calculation of Initial Conditions

For calculation of the initial plasma parameters, we apply the same technique as in the previous chapter. The values of \tilde{v}_{iy0} and \tilde{v}_{iz0} are calculated self consistently as follows:

At equilibrium, we recall the quasineutrality condition which is expressed below as

$$\tilde{n}_i = \tilde{n}_e - \tilde{n}_p. \quad (4.21)$$

Differentiating the above equation we get

$$\frac{\partial \tilde{n}_i}{\partial s} = \frac{\partial \tilde{n}_e}{\partial s} - \frac{\partial \tilde{n}_p}{\partial s}. \quad (4.22)$$

For convenience, the following definitions are introduced

$$F_1 = \tilde{n}_i^3 \quad (4.23)$$

$$F_2 = \left(\frac{n_{i0}}{n_{e0}} \right)^2 (M - \delta_i)^2 - 3\tilde{n}_i \tilde{P}_i \quad (4.24)$$

$$F_3 = \tilde{n}_p^3 \left[-E - \frac{m_i}{m} M \tilde{v}_{py} \sin \theta \right] \quad (4.25)$$

$$F_4 = \left(\frac{n_{p0}}{n_{e0}} \right)^2 (M - \delta_p)^2 - 3 \left(\frac{n_{p0}}{n_{e0}} \right) \tilde{n}_p \tilde{P}_p \quad (4.26)$$

$$F_5 = \tilde{n}_e^3 \left[E + \frac{m_i}{m} M \tilde{v}_{ey} \sin \theta \right] \quad (4.27)$$

$$F_6 = (M - \delta_e)^2 - 3\tilde{n}_e \tilde{P}_e. \quad (4.28)$$

Substituting equations (4.9),(4.13) and (4.17) into equation (4.22) and using the above def-

initions, we obtain the value of \tilde{v}_{iy0} as

$$\tilde{v}_{iy0} = \frac{E_0 + \left(\frac{F_3}{F_4} - \frac{F_5}{F_6}\right) \left(\frac{F_2}{F_1}\right)}{M \sin \theta}. \quad (4.29)$$

Now, the value of \tilde{v}_{iz0} is determined by twice differentiating the quasineutrality condition

$$\frac{\partial^2 \tilde{n}_i}{\partial s^2} = \frac{\partial^2 \tilde{n}_e}{\partial s^2} - \frac{\partial^2 \tilde{n}_p}{\partial s^2}. \quad (4.30)$$

Using the above definitions, equation (4.30) reduces to

$$\frac{\partial}{\partial s} \left(\frac{F_1}{F_2} [-E - M\tilde{v}_{iy} \sin \theta] \right) = \frac{\partial}{\partial s} \left(\frac{F_5}{F_6} \right) - \frac{\partial}{\partial s} \left(\frac{F_3}{F_4} \right). \quad (4.31)$$

Solving (4.31) and using equation (4.19), we get the value of \tilde{v}_{iz0}

$$\begin{aligned} \tilde{v}_{iz0} = \frac{\left(\frac{n_{i0}}{n_{e0}}\right) (M - \delta_i)}{M^2 \tilde{n}_i \sin \theta \cos \theta} \left\{ \frac{\partial}{\partial s} \left(\frac{F_5}{F_6} \right) - \frac{\partial}{\partial s} \left(\frac{F_3}{F_4} \right) - [-E_0 - M\tilde{v}_{iy0} \sin \theta] \frac{\partial}{\partial s} \left(\frac{F_1}{F_2} \right) \right\} \\ - \frac{\left(\frac{n_{i0}}{n_{e0}}\right) (M - \delta_i)}{\tilde{n}_i} - \frac{\sin \theta}{\cos \theta} + \frac{M}{\cos \theta}, \end{aligned} \quad (4.32)$$

where

$$\frac{\partial}{\partial s} (F_1) = \frac{3n_{in}^5 [-E - M\tilde{v}_{iy} \sin \theta]}{\left(\frac{n_{i0}}{n_{e0}}\right)^2 (M - \delta_i)^2 - 3\tilde{n}_i \tilde{P}_i}, \quad (4.33)$$

$$\frac{\partial}{\partial s} (F_2) = -12\tilde{P}_i \frac{\tilde{n}_i^3 [-E - M\tilde{v}_{iy} \sin \theta]}{\left(\frac{n_{i0}}{n_{e0}}\right)^2 (M - \delta_i)^2 - 3\tilde{n}_i \tilde{P}_i}, \quad (4.34)$$

$$\begin{aligned} \frac{\partial}{\partial s} (F_3) = \frac{3\tilde{n}_p^5 \left(-E - \frac{m_i}{m} M\tilde{v}_{py} \sin \theta\right)^2}{\left(\frac{n_{p0}}{n_{e0}}\right)^2 (M - \delta_p)^2 - 3\left(\frac{n_{p0}}{n_{e0}}\right) \tilde{n}_p \tilde{P}_p} - \tilde{n}_p^3 \left(\frac{m_i}{m}\right)^2 M \sin \theta \\ \left\{ \left(\frac{n_{e0}}{n_{p0}}\right) \frac{\tilde{n}_p M}{(M - \delta_p)} [M \sin \theta - \tilde{v}_{pz} \cos \theta] - M \sin \theta \right\} \end{aligned} \quad (4.35)$$

$$\frac{\partial}{\partial s}(F_4) = -\frac{12\tilde{P}_p\tilde{n}_p^3\left(\frac{n_{p0}}{n_{e0}}\right)\left[-E - \frac{m_i}{m}M\tilde{v}_{py}\sin\theta\right]}{\left(\frac{n_{p0}}{n_{e0}}\right)(M - \delta_p)^2 - 3\tilde{n}_p\tilde{P}_p}, \quad (4.36)$$

$$\frac{\partial}{\partial s}(F_5) = \frac{3\tilde{n}_e^5\left(E + \frac{m_i}{m}M\tilde{v}_{ey}\sin\theta\right)^2}{(M - \delta_e)^2 - 3\tilde{n}_e\tilde{P}_e} + \tilde{n}_e^3\left(\frac{m_i}{m}\right)^2 M \sin\theta \left\{ \frac{\tilde{n}_e M}{(M - \delta_e)} [\tilde{v}_{ez}\cos\theta - M \sin\theta] + M \sin\theta \right\} \quad (4.37)$$

and

$$\frac{\partial}{\partial s}(F_6) = -\frac{12\tilde{P}_e\tilde{n}_e^3\left(E + \frac{m_i}{m}M\tilde{v}_{ey}\sin\theta\right)^2}{(M - \delta_e)^2 - 3\tilde{n}_e\tilde{P}_e}. \quad (4.38)$$

4.3 Numerical Results and Discussion

The set of nonlinear differential equations (4.7)-(4.20) is solved numerically using the Runge-Kutta method. The initial values of \tilde{v}_{ey} , \tilde{v}_{ez} , \tilde{v}_{py} , \tilde{v}_{pz} are given but \tilde{v}_{iy0} and \tilde{v}_{iz0} are calculated self consistently. We shall investigate the effects of the driving amplitude, temperature, densities, *Mach* number, propagation angle and drift velocity of the different species on the nonlinear wave structures.

Effect of the driving amplitude, E_0 on the driving electric field

For fixed parameters $M = 3.5$, $\delta_e = \delta_p = \delta_i = 0.0$, $n_{i0}/n_{e0} = 0.5$, $T_i/T_h = 0.0$, $R = 5.0$ and $\theta = 2^0$, we vary the driving electric field E_0 from 0.35 to 2.5. The results are presented in Figures (4.1)-(4.4). These figures show that increasing E_0 , results in the increasing the period of oscillations from $1.12\tau_{ci}$ to $2.43\tau_{ci}$, where $\tau_{ci} = 2\pi/\Omega_i$ is the ion cyclotron period. We observe the transition from ion-cyclotron waves to ion-acoustic waves as the electric field structures evolve from a sinusoidal waveform to a sawtooth structure. The present plasma model can generate spiky structures for a minimum driving field $E_0 = 0.35$, while the plasma models investigated by Bharuthram et al. [2002] and Moolla et al. [2012] required a driving field strength 1.1 and 0.3 respectively for the onset of spikes. Comparing these results to those obtained in the previous Chapter, we observe the increase in the driving field for the onset of spikes from 0.01 for the Boltzmann density distribution to 0.35 for full dynamical system, while the value of R increases from 3 to 5.

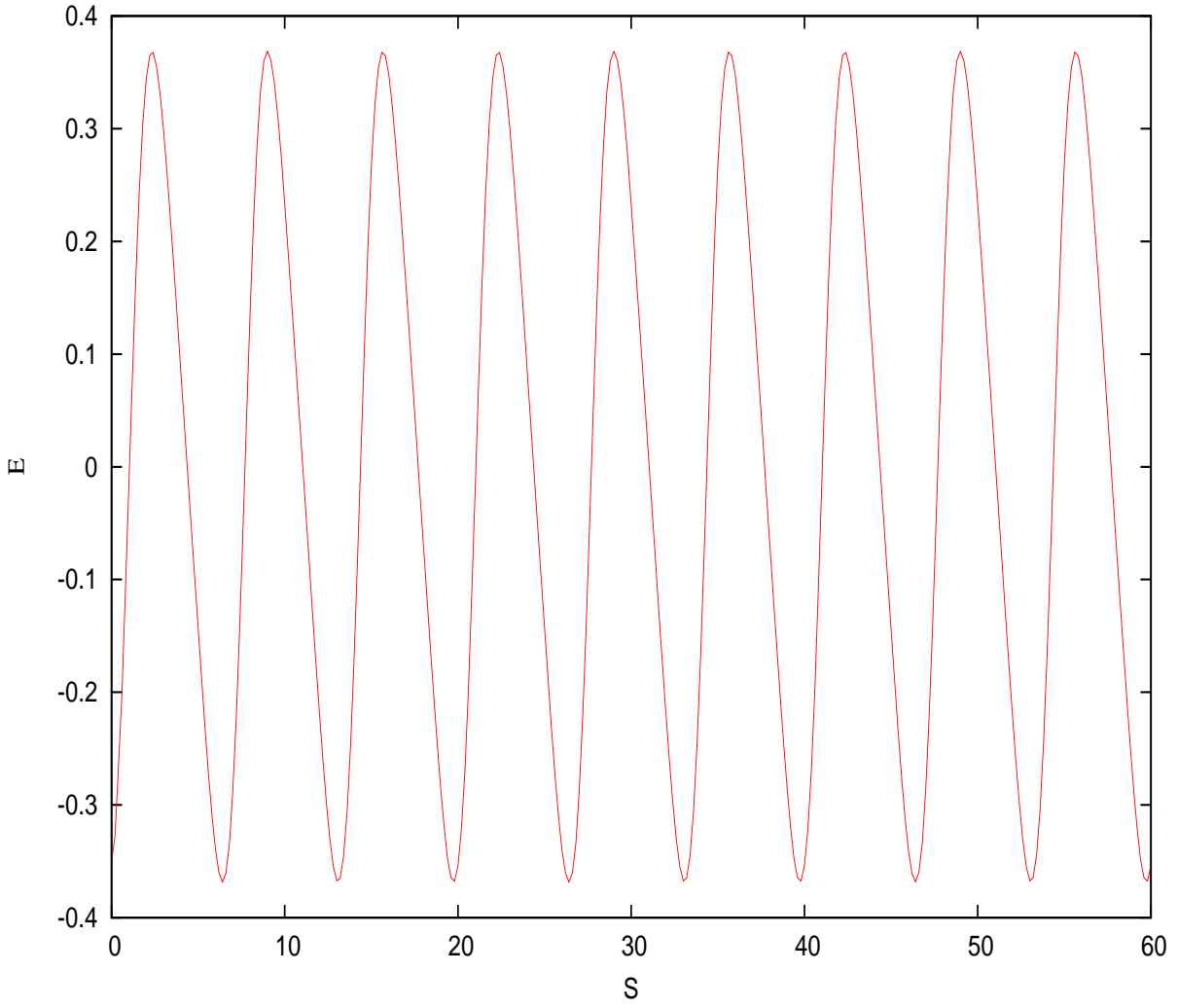


Figure 4.1: Numerical solution of normalized parallel electric field for the parameters $M = 3.5$, $R = 5.0$, $\delta_i = \delta_e = \delta_p = 0.0$, $n_{i0}/n_{e0} = 0.5$, $n_{p0}/n_{e0} = 0.5$, $T_i/T_h = 0.0$, $\theta = 2^\circ$ and $E_0 = 0.35$.

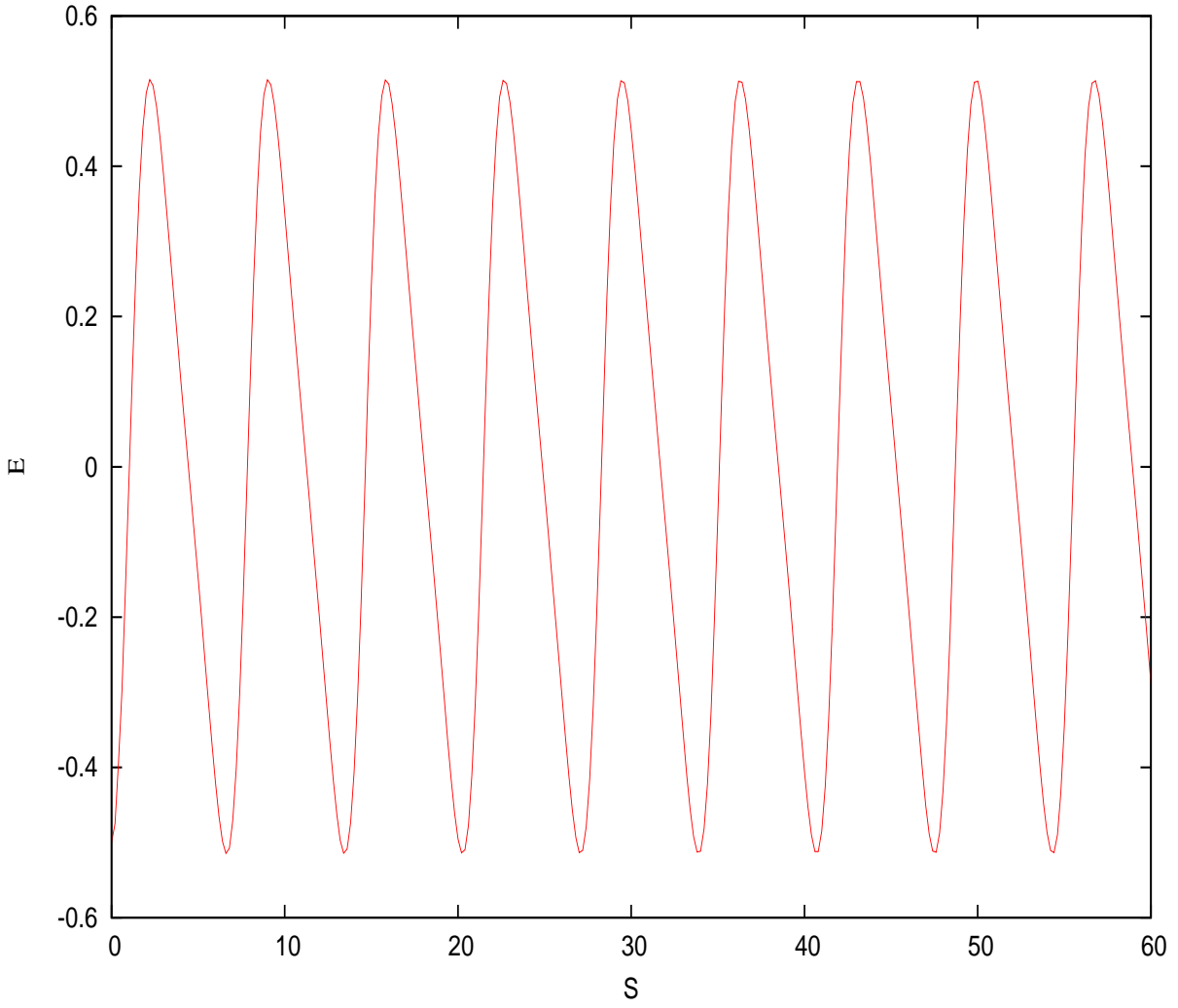


Figure 4.2: Numerical solution of normalized parallel electric field for the parameters $M = 3.5$, $R = 5.0$, $\delta_i = \delta_e = \delta_p = 0.0$, $n_{i0}/n_{e0} = 0.5$, $n_{p0}/n_{e0} = 0.5$, $T_i/T_h = 0.0$, $\theta = 2^0$ and $E_0 = 0.5$.

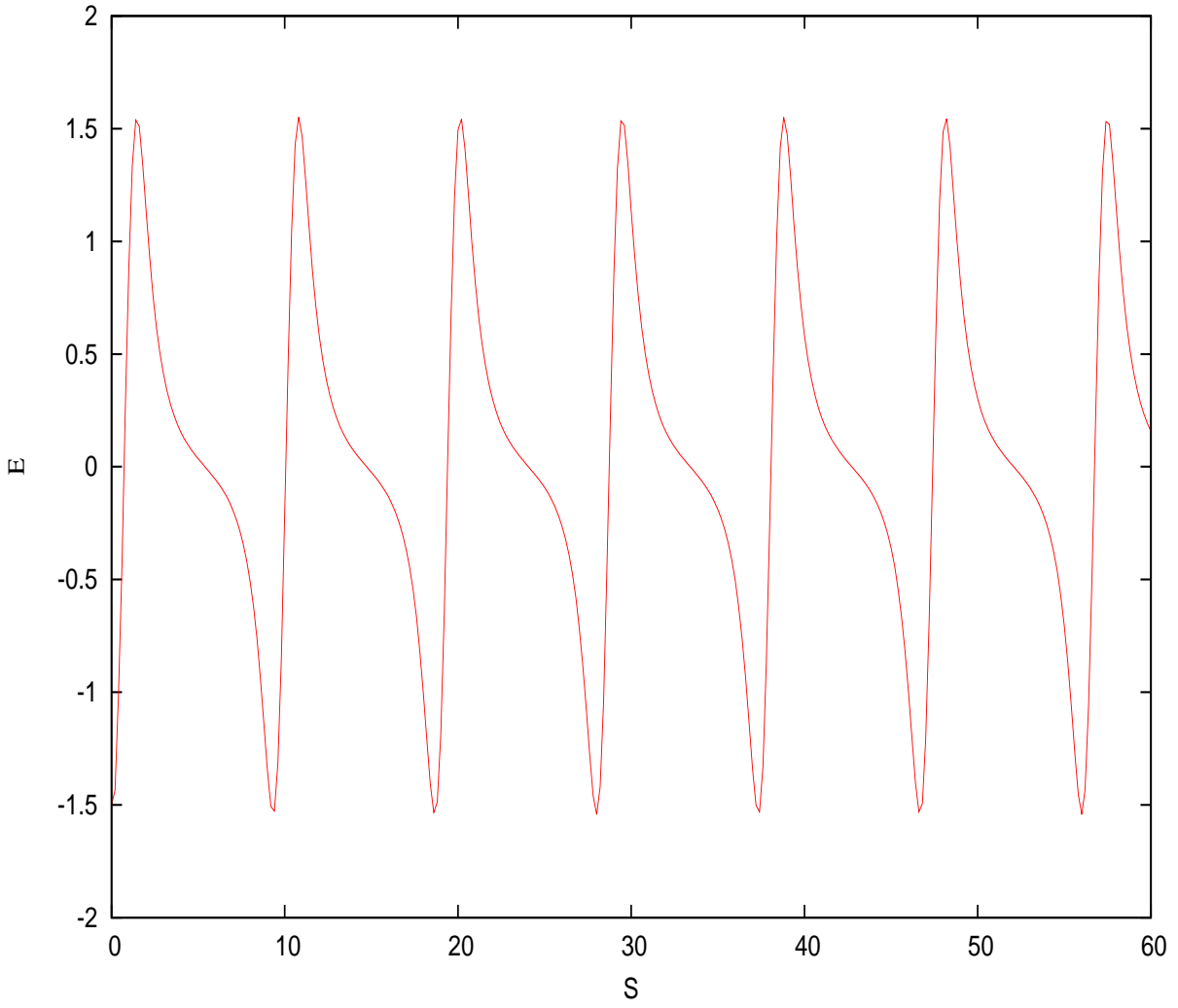


Figure 4.3: Numerical solution of normalized parallel electric field for the parameters $M = 3.5$, $R = 5.0$, $\delta_i = \delta_e = \delta_p = 0.0$, $n_{i0}/n_{e0} = 0.5$, $n_{p0}/n_{e0} = 0.5$, $T_i/T_h = 0.0$, $\theta = 2^0$ and $E_0 = 1.5$.

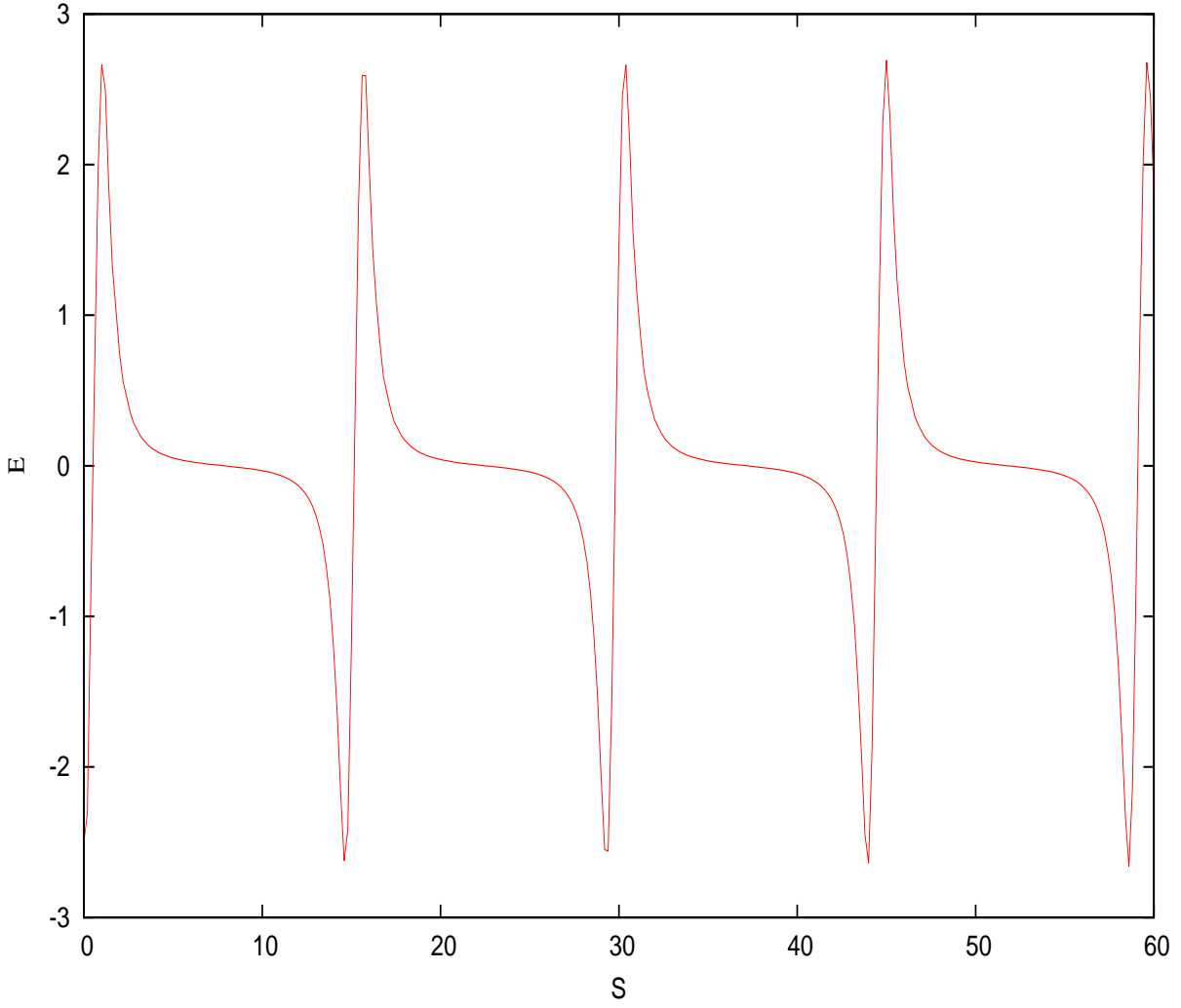


Figure 4.4: Numerical solution of normalized parallel electric field for the parameters $M = 3.5$, $R = 5.0$, $\delta_i = \delta_e = \delta_p = 0.0$, $n_{i0}/n_{e0} = 0.5$, $n_{p0}/n_{e0} = 0.5$, $T_i/T_h = 0.0$, $\theta = 2^\circ$ and $E_0 = 2.5$.

Effect of the temperature ratio T_i/T_h

Figures 4.5-4.8 show the effect of the ion-electron temperature ratio T_i/T_h on the parallel electric field structures for the following fixed parameters $M = 3.50$, $E_0 = 2.5$, $\delta_e = \delta_p = \delta_i = 0.0$, $n_{i0}/n_{e0} = 0.5$, $R = 5.0$ and $\theta = 2^0$. The variation of the ion-electron temperature ratio does not affect the nonlinearity of the waves (see Fig. 4.9) and the wave structures are spiky in nature [Moolla et al., 2012]. However, increasing this ratio from 0.0 to 0.2 results in the period of the waves increasing from $2.43\tau_{ci}$ to $2.57\tau_{ci}$. This due to the dispersive effect results in broadening of the waves.

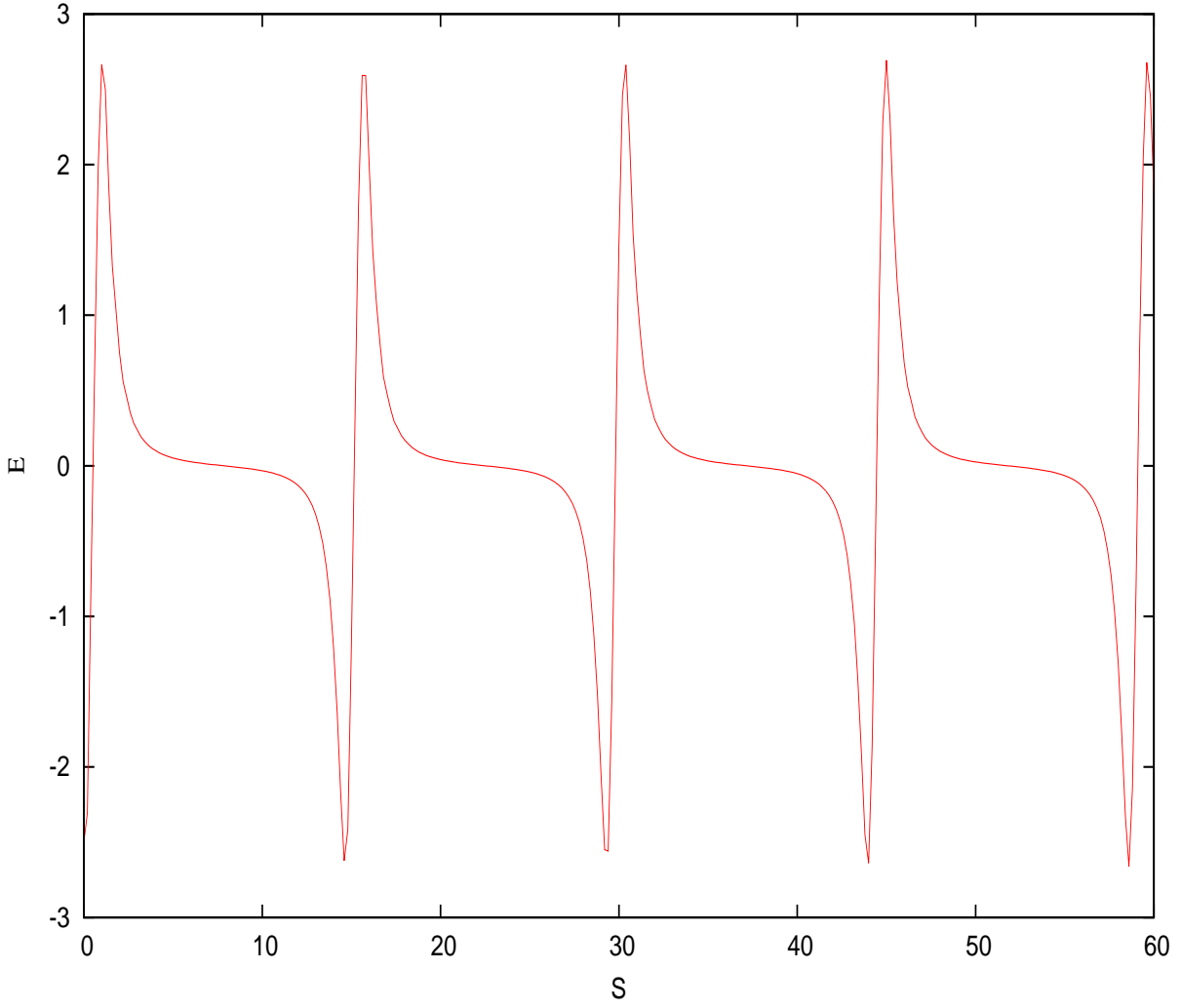


Figure 4.5: Numerical solution of normalized parallel electric field for the parameters $E_0 = 2.5$, $M = 3.5$, $R = 5.0$, $\delta_i = \delta_e = \delta_p = 0.0$, $n_{i0}/n_{e0} = 0.5$, $\theta = 2^0$ and $T_i/T_h = 0.0$.

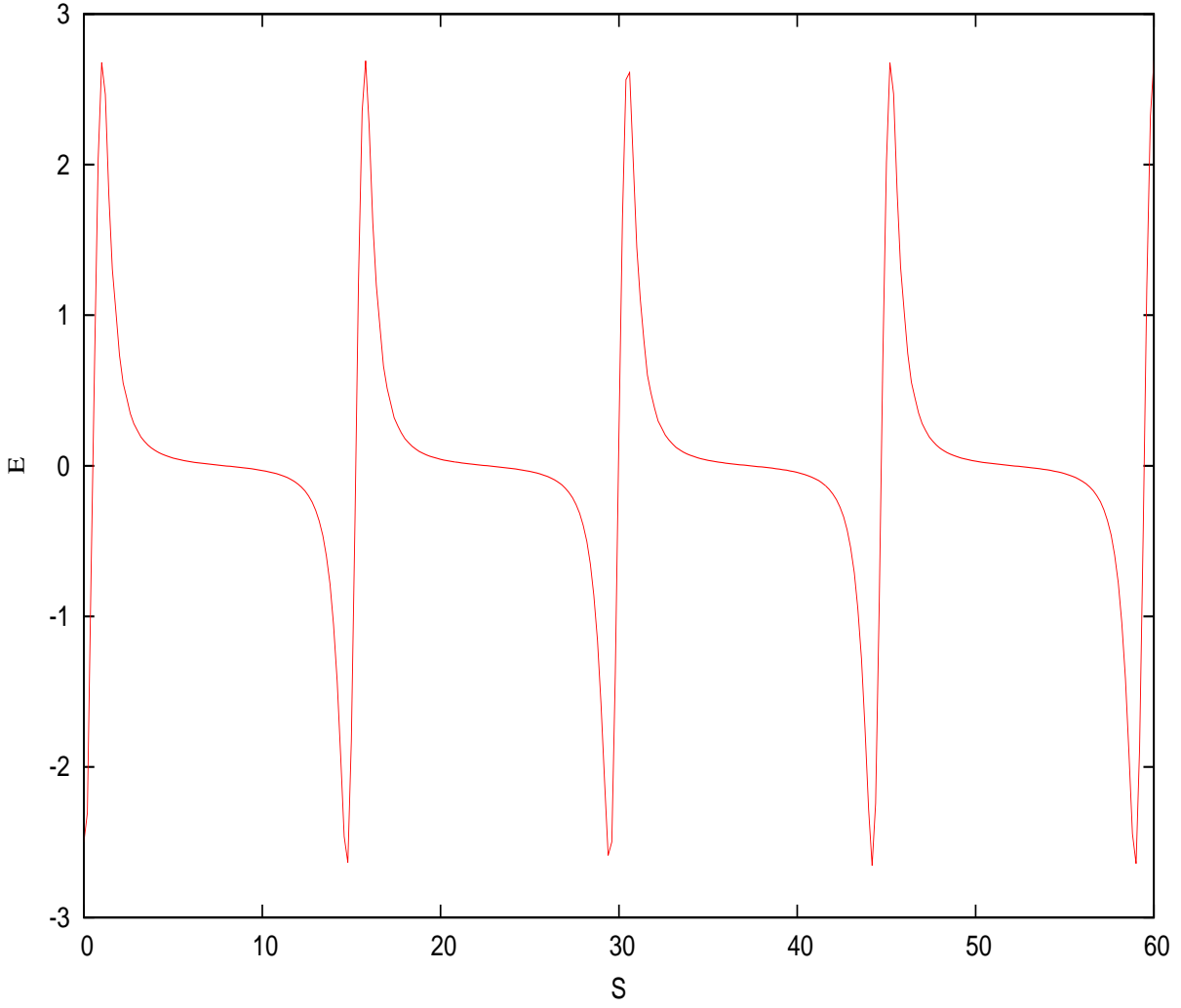


Figure 4.6: Numerical solution of normalized parallel electric field for the parameters $E_0 = 2.5$, $M = 3.5$, $R = 5.0$, $\delta_i = \delta_e = \delta_p = 0.0$, $n_{i0}/n_{e0} = 0.5$, $\theta = 2^0$ and $T_i/T_h = 0.05$.

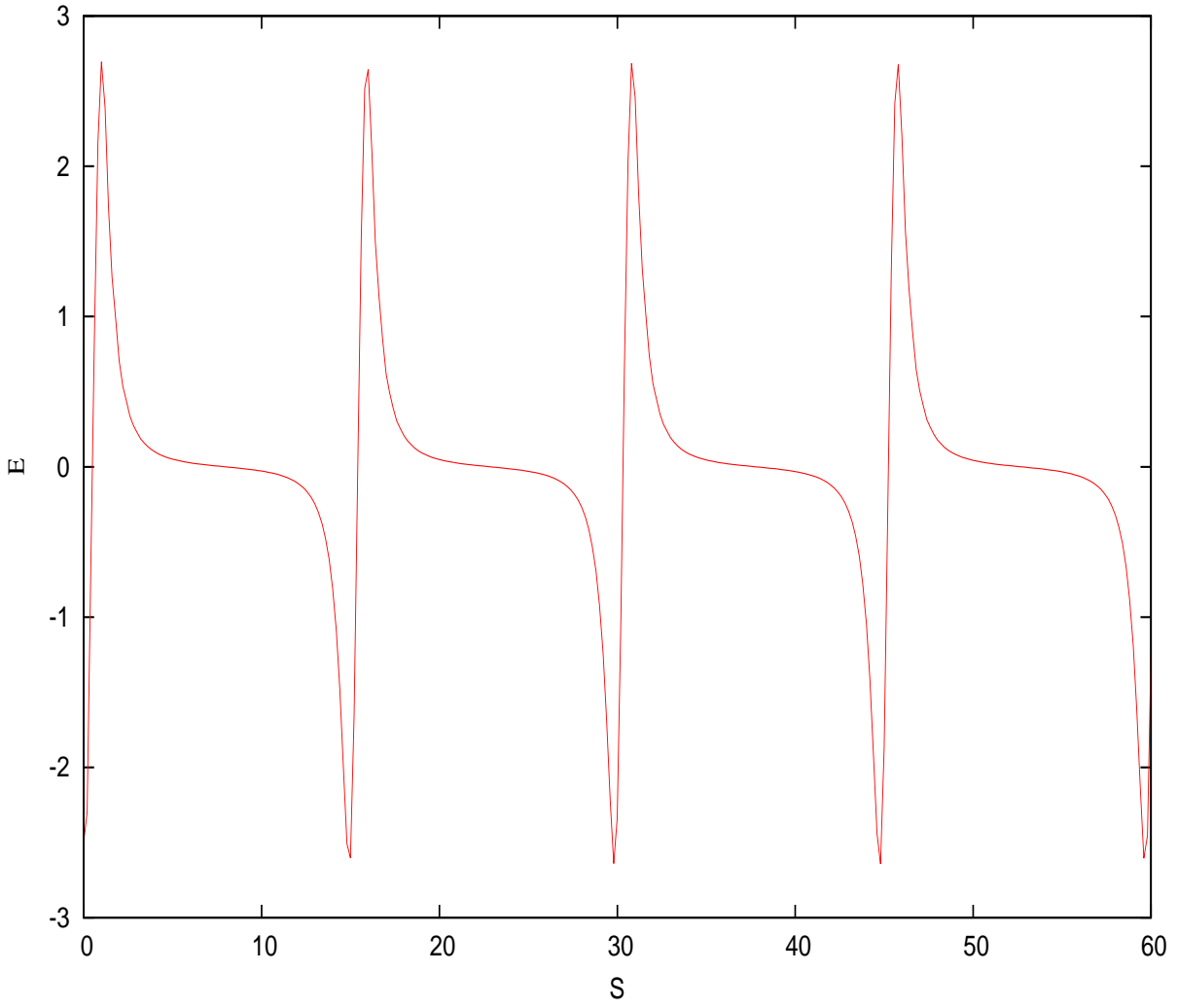


Figure 4.7: Numerical solution of normalized parallel electric field for the parameters $E_0 = 2.5$, $M = 3.5$, $R = 5.0$, $\delta_i = \delta_e = \delta_p = 0.0$, $n_{i0}/n_{e0} = 0.5$, $\theta = 2^0$ and $T_i/T_h = 0.15$.

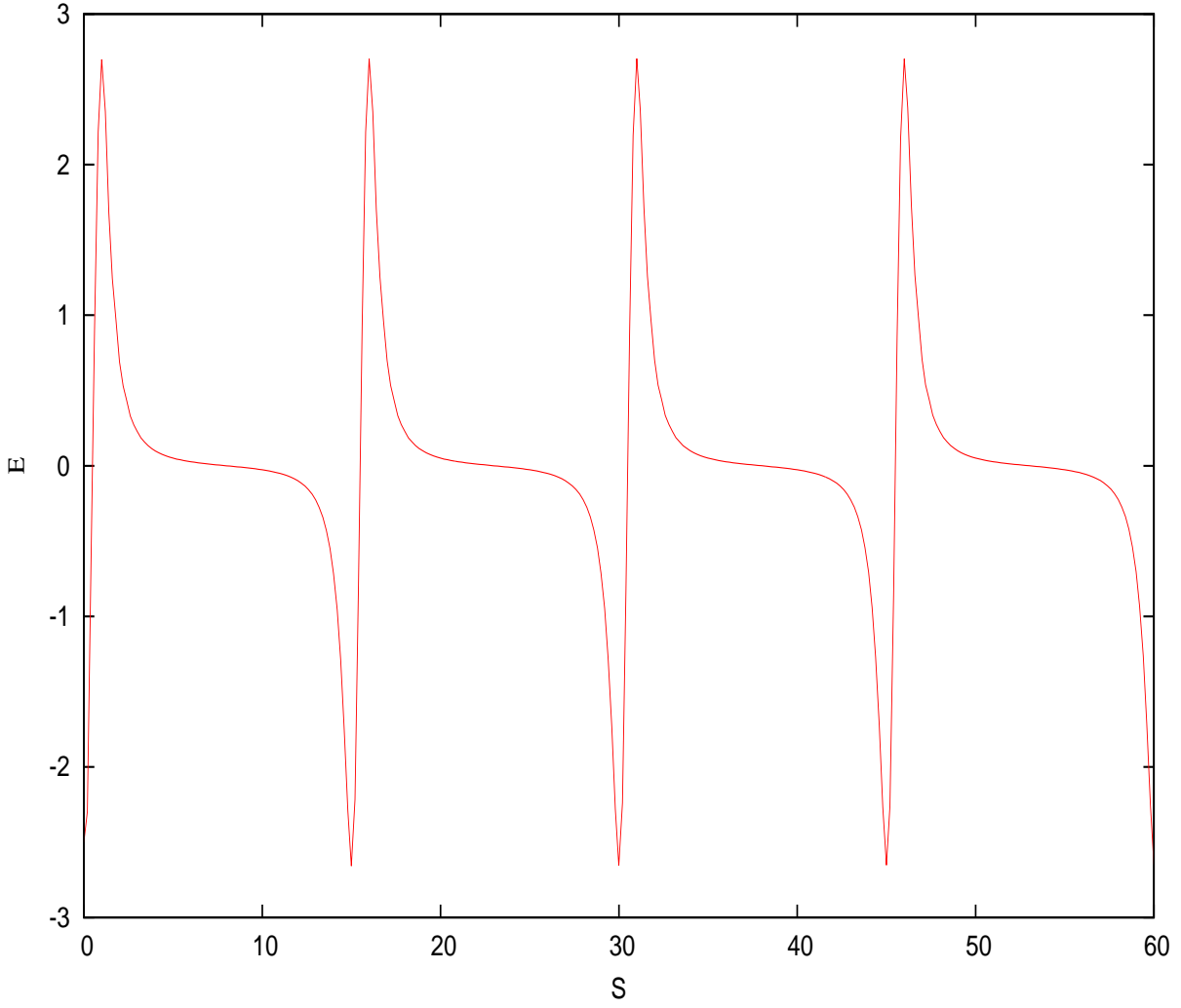


Figure 4.8: Numerical solution of normalized parallel electric field for the parameters $E_0 = 2.5$, $M = 3.5$, $R = 5.0$, $\delta_i = \delta_e = \delta_p = 0.0$, $n_{i0}/n_{e0} = 0.5$, $\theta = 2^\circ$ and $T_i/T_h = 0.2$.

For simplification we present the figures (4.5) - (4.8) on one system of axes.

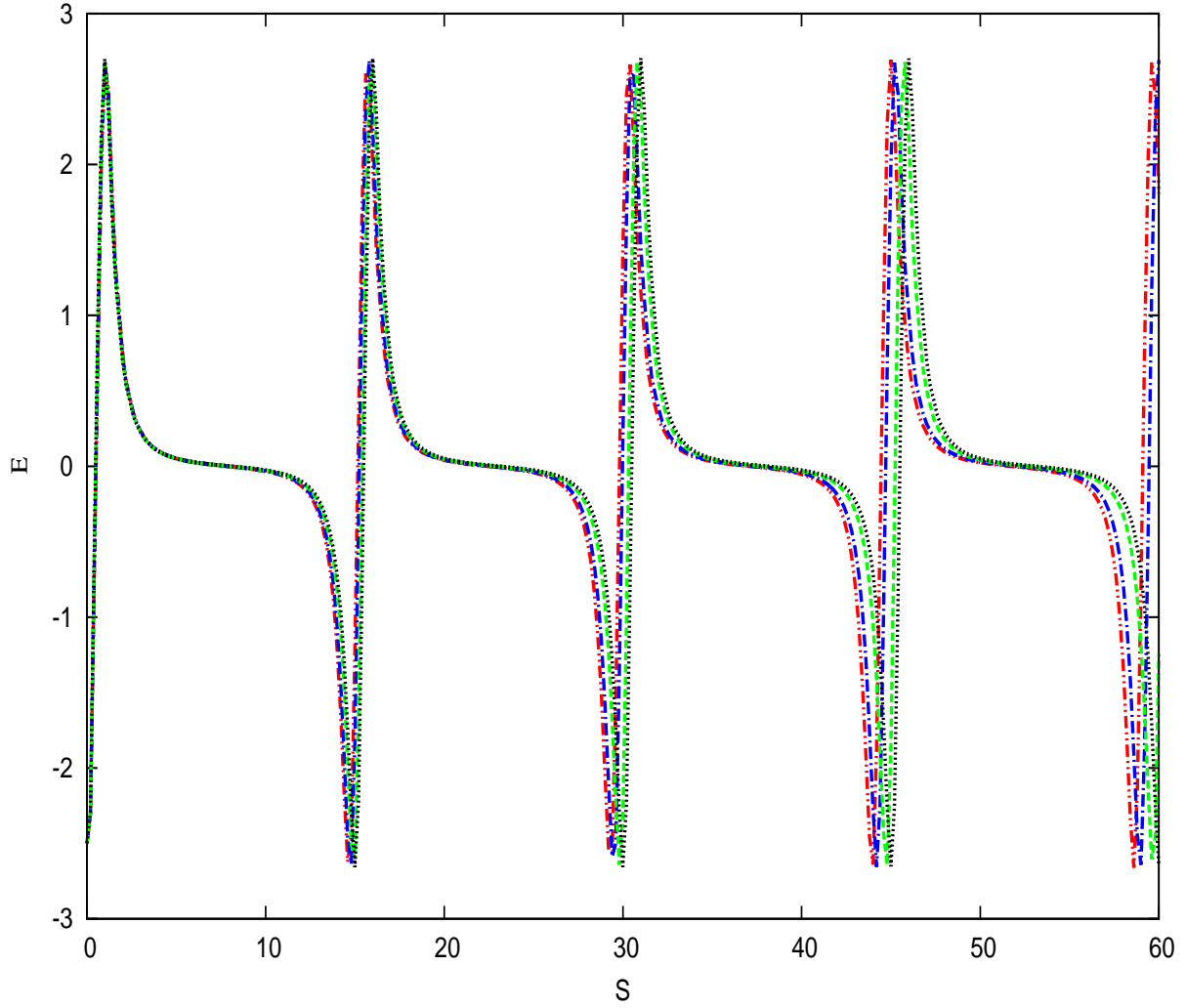


Figure 4.9: Numerical solution of normalized parallel electric field for the parameters $E_0 = 2.5$, $M = 3.5$, $R = 5.0$, $\delta_i = \delta_e = \delta_p = 0.0$, $n_{i0}/n_{e0} = 0.5$ and $\theta = 2^0$. The curves present the effects of the temperature for different values of ratio $T_i/T_h = 0.0$ (dashdot=red), 0.05 (dashdot=blue), 0.15 (broken=green), 0.2 (dotted=black).

Effect of the density ratio n_{p0}/n_{e0}

Figures 4.10 - 4.13 illustrate the effect of the positron density on the parallel electric field structures for the following fixed parameters $M = 3.5$, $E_0 = 2.5$, $\delta_e = \delta_p = \delta_i = 0.0$, $R = 5.0$ and $\theta = 2^0$. It is seen that as n_{p0}/n_{e0} increases from 0.3 to 0.5, the waveforms become more nonlinear and the period of these waveforms increases from $1.31\tau_{ci}$ to $2.43\tau_{ci}$ respectively. The increase in positron densities enhances nonlinearity, making spiky structures easier to generate. These results are similar to those of Moolla et al. [2012].

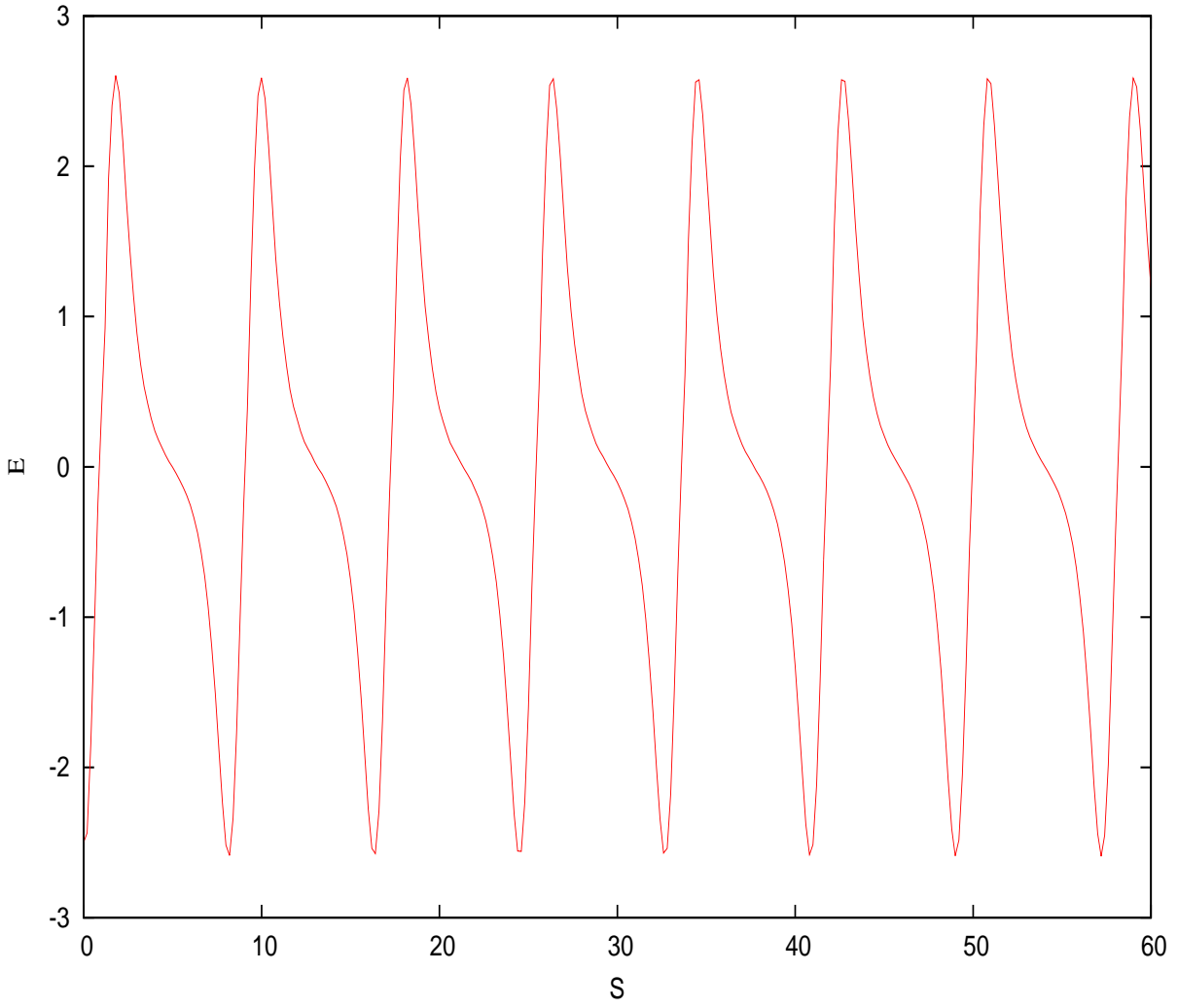


Figure 4.10: Numerical solution of normalized parallel electric field for the parameters $E_0 = 2.5$, $M = 3.5$, $R = 5.0$, $\delta_i = \delta_e = \delta_p = 0.0$, $\theta = 2^\circ$, $T_i/T_h = 0.0$ and $n_{i0}/n_{e0} = 0.7$.

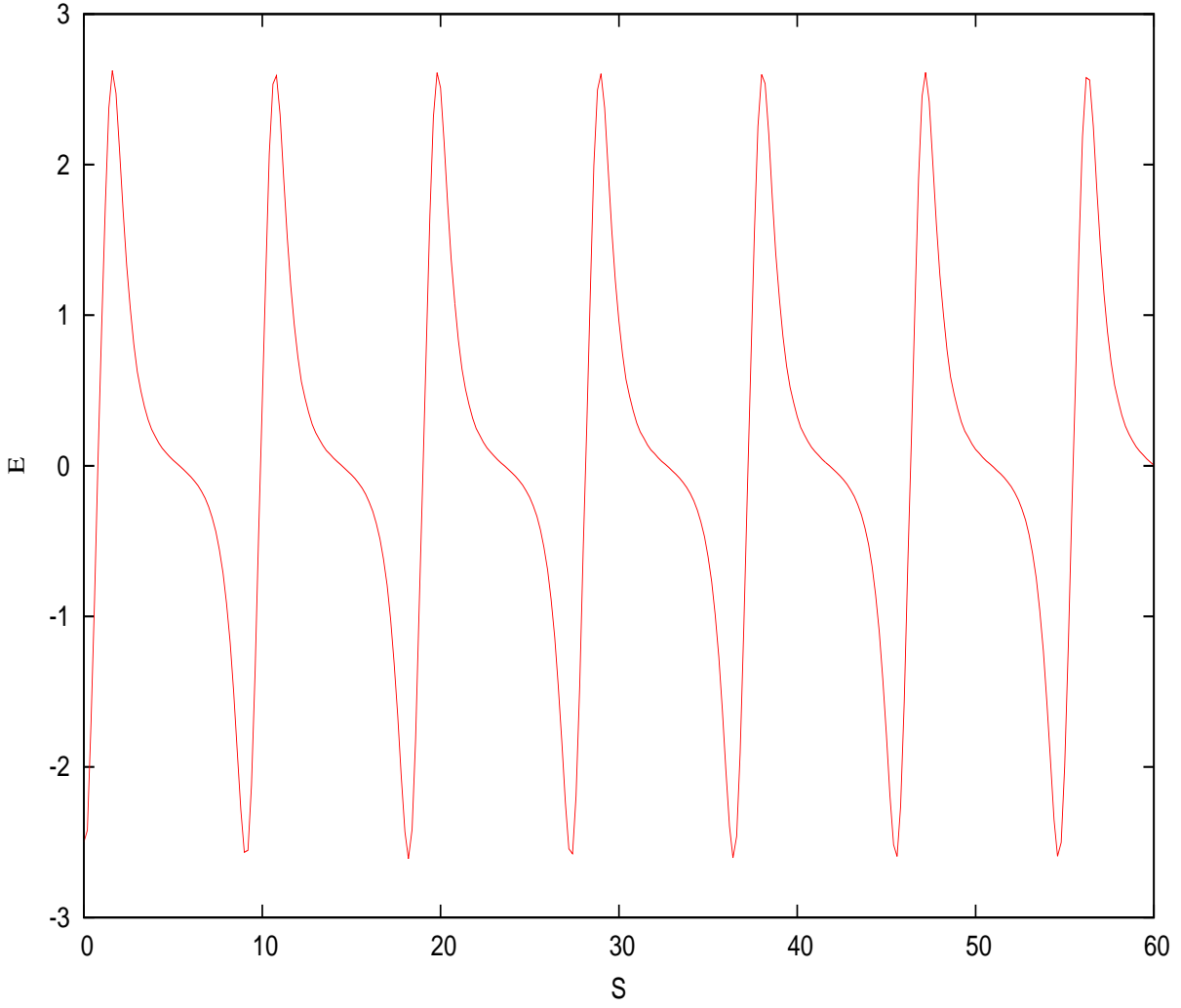


Figure 4.11: Numerical solution of normalized parallel electric field for the parameters $E_0 = 2.5$, $M = 3.5$, $R = 5.0$, $\delta_i = \delta_e = \delta_p = 0.0$, $\theta = 2^\circ$, $T_i/T_h = 0.0$ and $n_{i0}/n_{e0} = 0.65$.

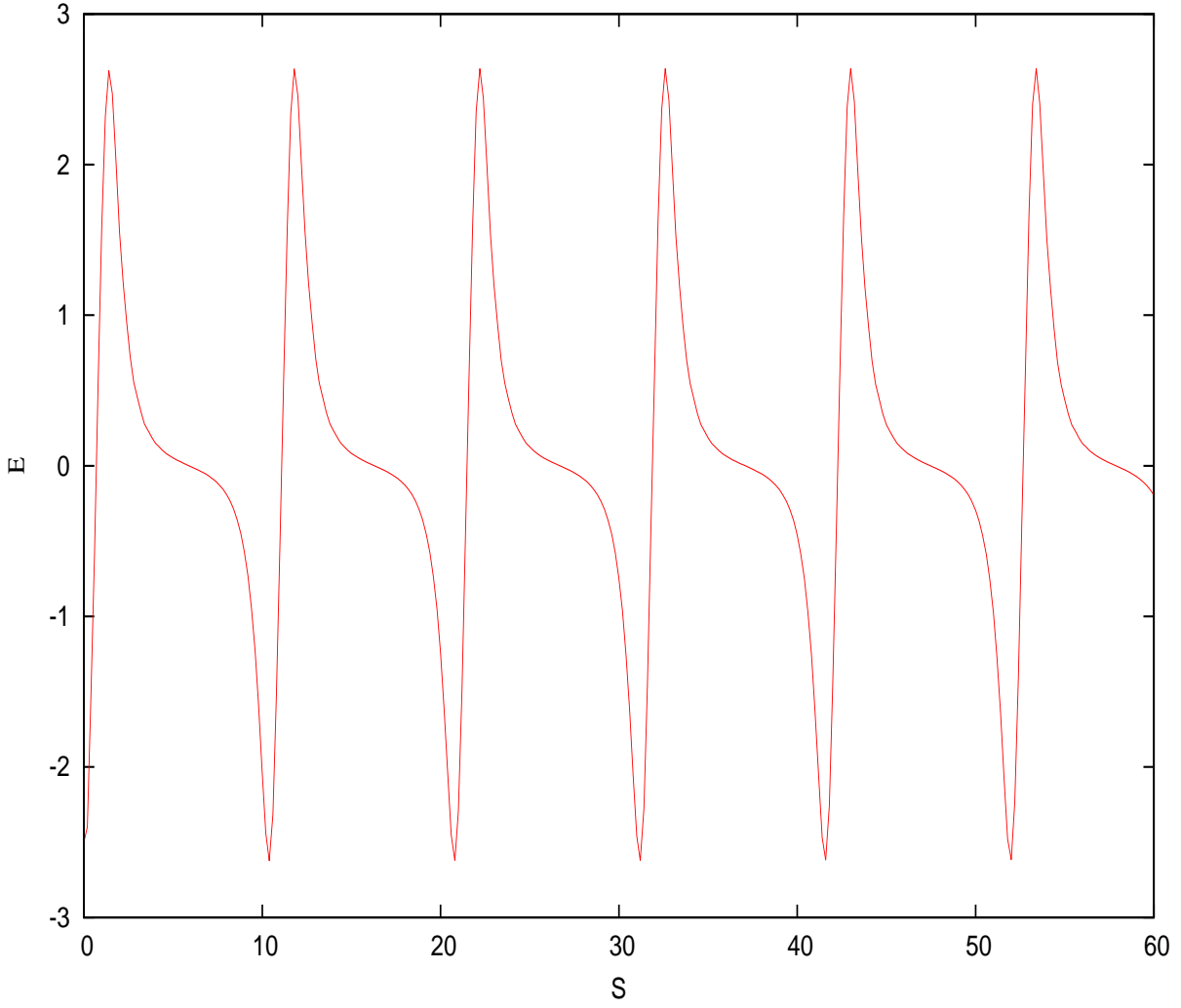


Figure 4.12: Numerical solution of normalized parallel electric field for the parameters $E_0 = 2.5$, $M = 3.5$, $R = 5.0$, $\delta_i = \delta_e = \delta_p = 0.0$, $\theta = 2^\circ$, $T_i/T_h = 0.0$ and $n_{i0}/n_{e0} = 0.6$.

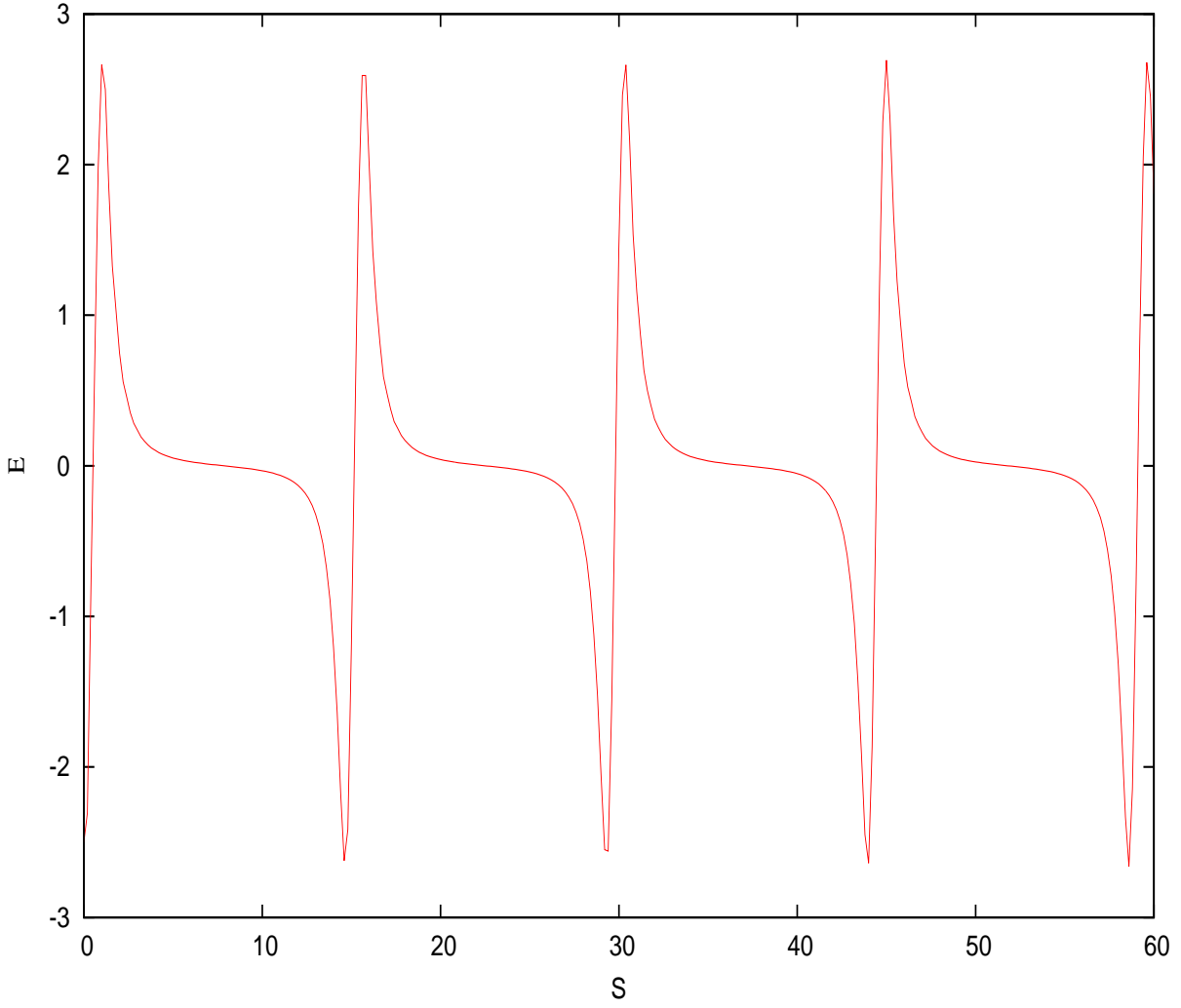


Figure 4.13: Numerical solution of normalized parallel electric field for the parameters $E_0 = 2.5$, $M = 3.5$, $R = 5.0$, $\delta_i = \delta_e = \delta_p = 0.0$, $\theta = 2^\circ$, $T_i/T_h = 0.0$ and $n_{i0}/n_{e0} = 0.5$.

Effect of *Mach* number M

Figures 4.14 - 4.17 illustrate the effect of the *Mach* number on the parallel electric field structures for the following fixed parameters $E_0 = 2.5$, $\delta_e = \delta_p = \delta_i = 0.0$, $n_{p0}/n_{e0} = n_{i0}/n_{e0} = 0.5$, $R = 5.0$ and $\theta = 2^0$. It is seen that as the *Mach* number increases from 3.5 to 4.0, the period of these waveforms decreases from $2.38\tau_{ci}$ to $2.43\tau_{ci}$. Our studies showed that the value of M needs to be in a narrow range for the electric field structures to exist. Hence, varying the values of M in this range shows little effect on the waves. These results are similar to those of Moolla et al. [2007].

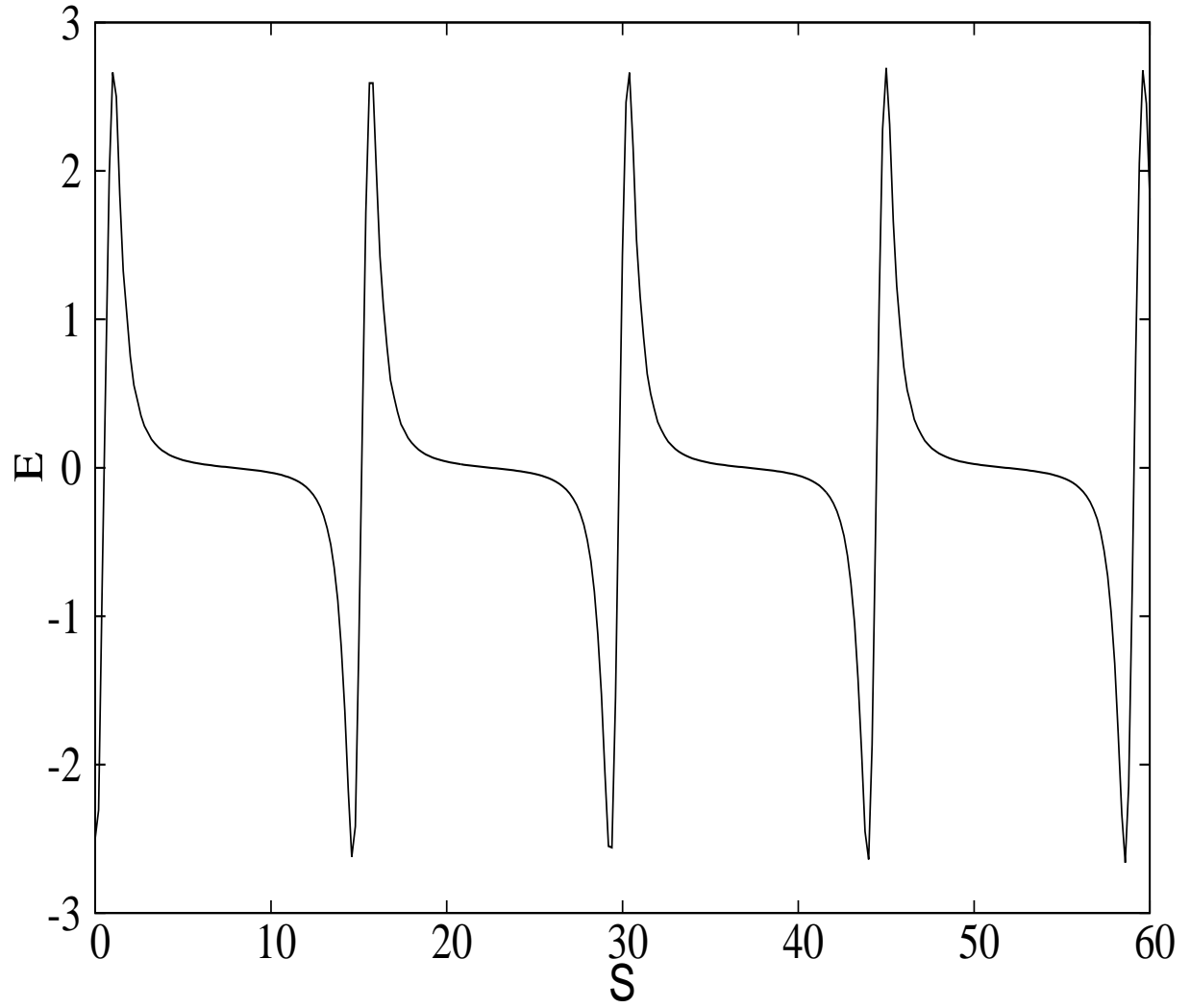


Figure 4.14: Numerical solution of normalized parallel electric field for the parameters $E_0 = 2.5$, $R = 5.0$, $\delta_i = \delta_e = \delta_p = 0.0$, $\theta = 2^\circ$, $T_i/T_h = 0.0$, $n_{p0}/n_{e0} = n_{i0}/n_{e0} = 0.5$ and $M = 3.5$.

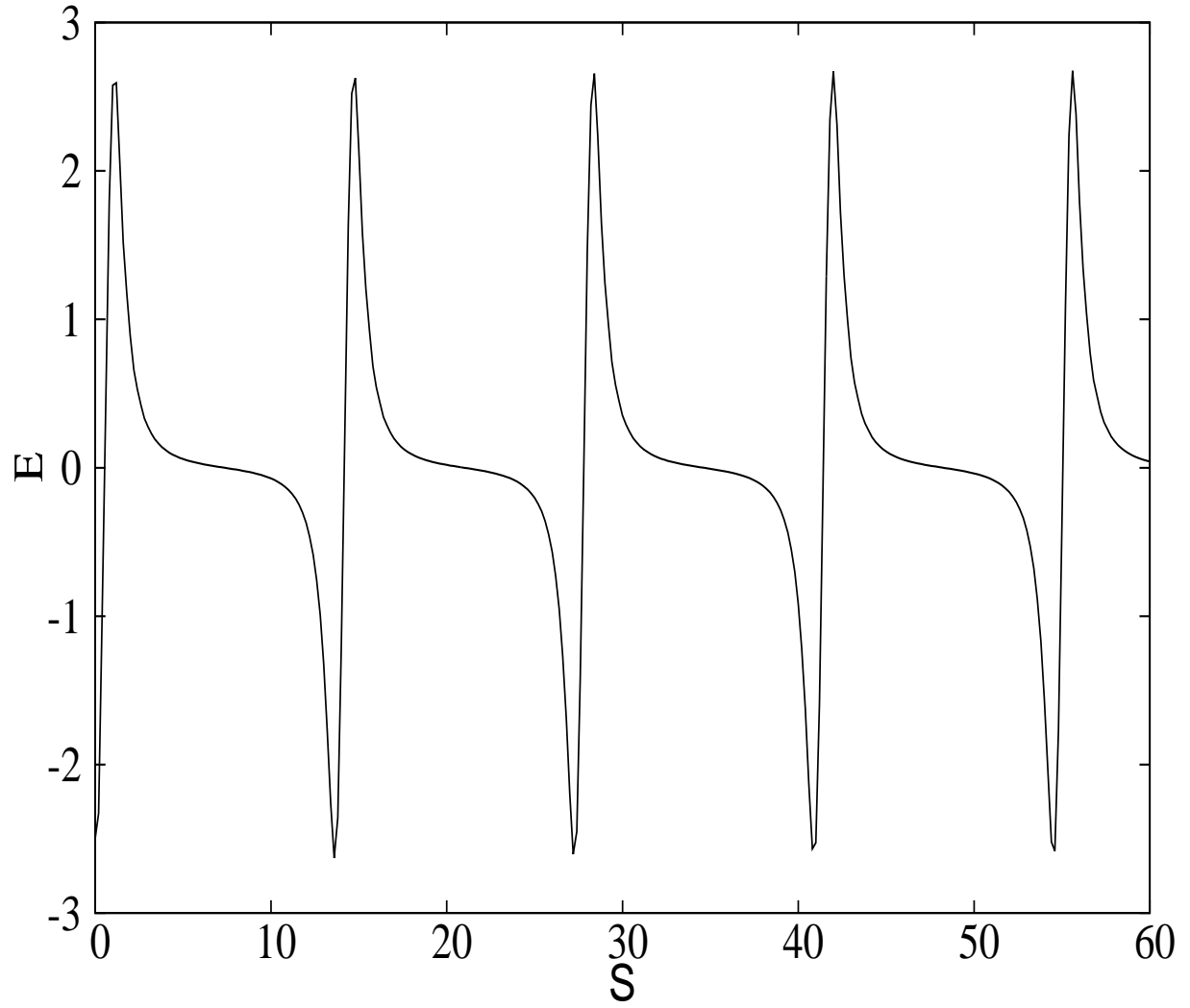


Figure 4.15: Numerical solution of normalized parallel electric field for the parameters $E_0 = 2.5$, $R = 5.0$, $\delta_i = \delta_e = \delta_p = 0.0$, $\theta = 2^\circ$, $T_i/T_h = 0.0$, $n_{p0}/n_{e0} = n_{i0}/n_{e0} = 0.5$ and $M = 3.7$.

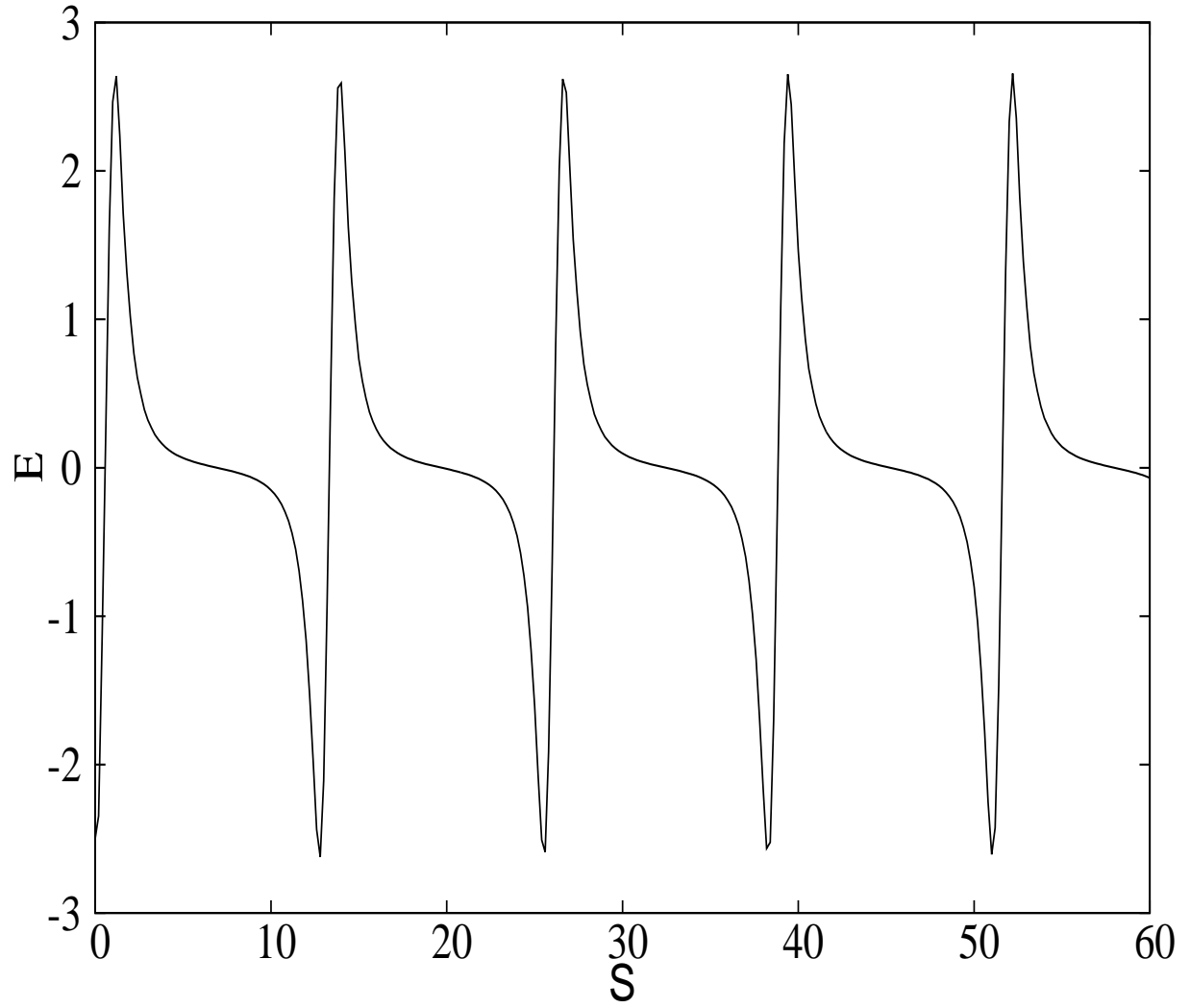


Figure 4.16: Numerical solution of normalized parallel electric field for the parameters $E_0 = 2.5$, $R = 5.0$, $\delta_i = \delta_e = \delta_p = 0.0$, $\theta = 2^\circ$, $T_i/T_h = 0.0$, $n_{p0}/n_{e0} = n_{i0}/n_{e0} = 0.5$ and $M = 3.8$.

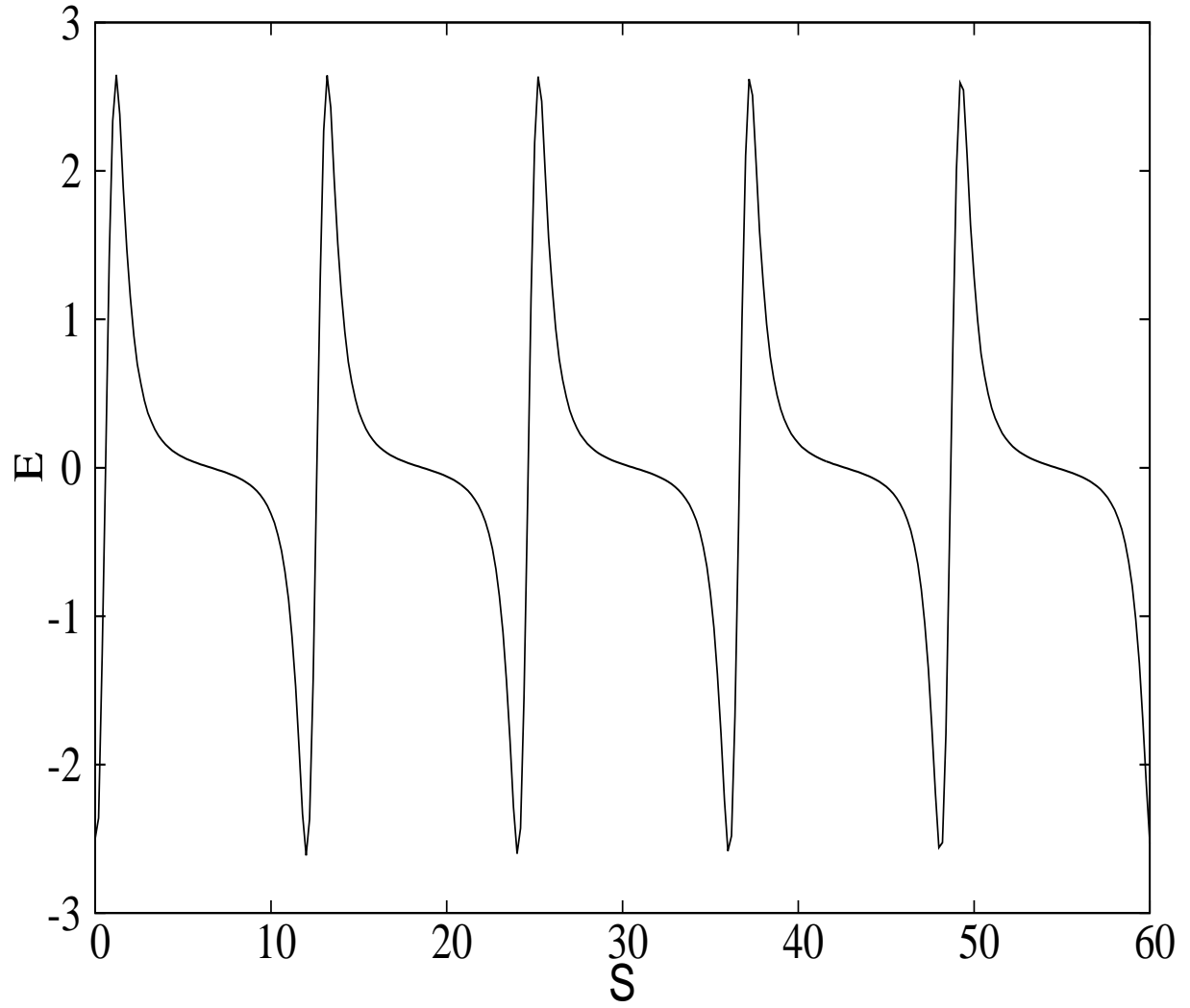


Figure 4.17: Numerical solution of normalized parallel electric field for the parameters $E_0 = 2.5$, $R = 5.0$, $\delta_i = \delta_e = \delta_p = 0.0$, $\theta = 2^\circ$, $T_i/T_h = 0.0$, $n_{p0}/n_{e0} = n_{i0}/n_{e0} = 0.5$ and $M = 4.0$.

Effect of the propagation angle θ

Figures 4.18 - 4.21 illustrate the effect of the propagation angle on the parallel electric field structures for the following fixed parameters: $E_0 = 2.5$, $\delta_e = \delta_p = \delta_i = 0.0$, $n_{p0}/n_{e0} = n_{i0}/n_{e0} = 0.5$, $R = 5.0$ and $M = 3.5$. We vary the propagation angle from $\theta = 0^\circ$ to $\theta = 15^\circ$. This results in increasing the period of oscillations from $2.38\tau_{ci}$ to $3.18\tau_{ci}$. It is seen that there is a decrease in frequency with no effect on nonlinearity. In this study, the maximum propagation angle is approx $\theta = 15^\circ$, beyond this value our model does not present the waveforms similar to those observed by Matsumoto et al. [1994]. The assumption of Reddy et al. [2002] and Moolla et al. [2007] showing that the angle of wave propagation with the earth's magnetic field may be set to two degree ($\theta = 2^\circ$) during investigation of electrostatic waves in Earth's magnetosphere remains reasonable.

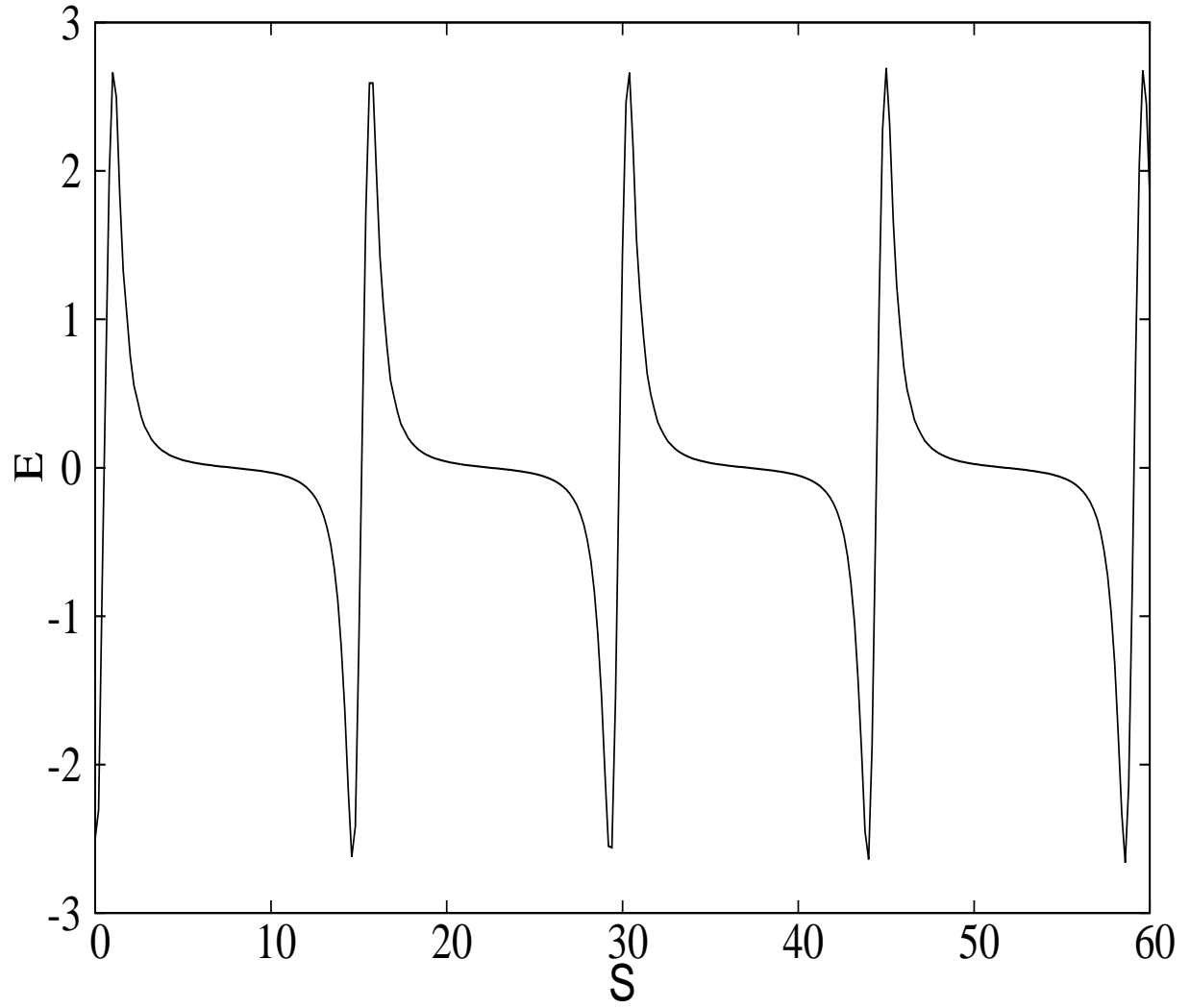


Figure 4.18: Numerical solution of normalized parallel electric field for the parameters $E_0 = 2.5$, $M = 3.5$, $R = 5.0$, $\delta_i = \delta_e = \delta_p = 0.0$, $T_i/T_h = 0.0$, $n_{p0}/n_{e0} = n_{i0}/n_{e0} = 0.5$ and $\theta = 2^\circ$.

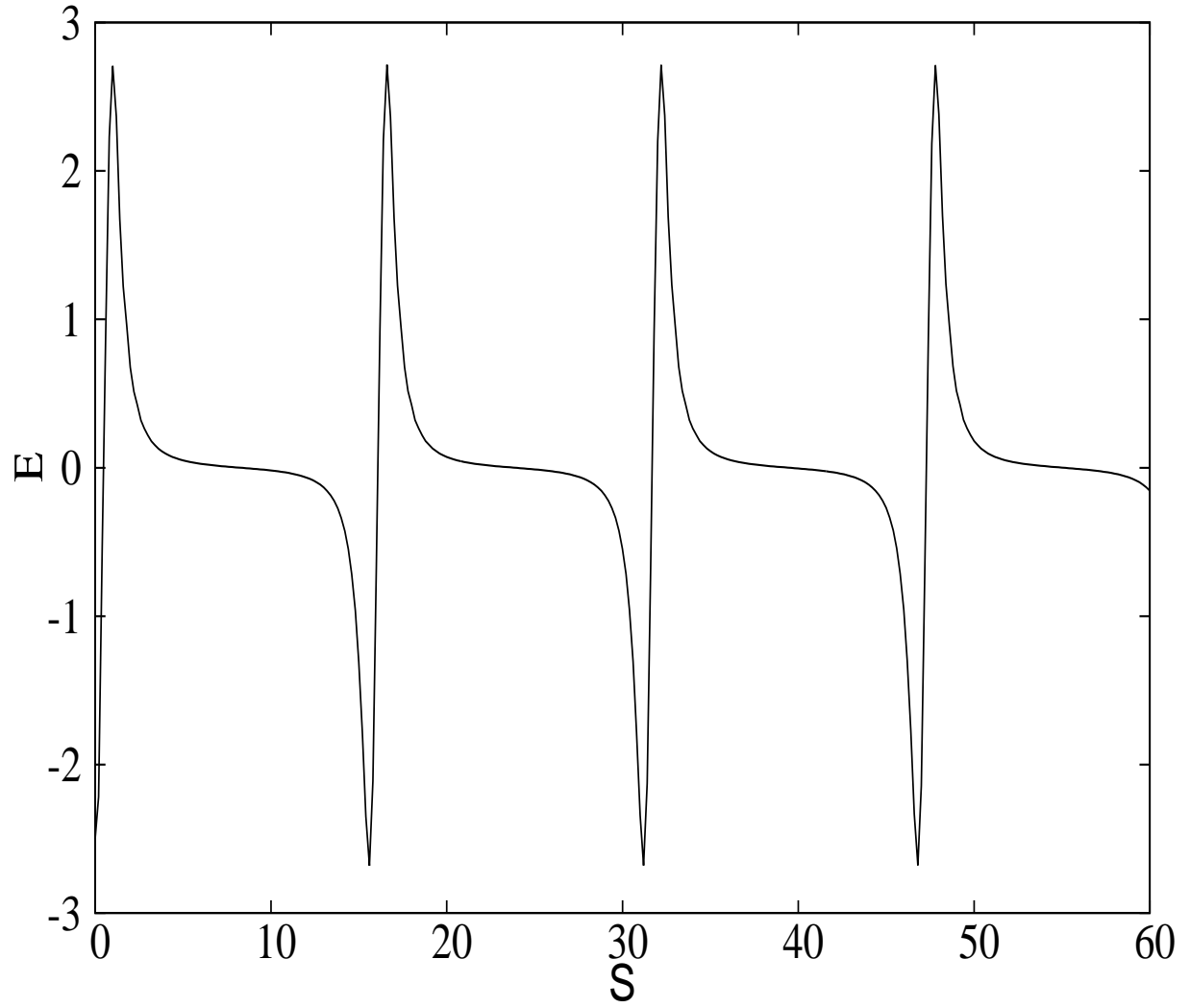


Figure 4.19: Numerical solution of normalized parallel electric field for the parameters $E_0 = 2.5$, $M = 3.5$, $R = 5.0$, $\delta_i = \delta_e = \delta_p = 0.0$, $T_i/T_h = 0.0$, $n_{p0}/n_{e0} = n_{i0}/n_{e0} = 0.5$ and $\theta = 6^\circ$.

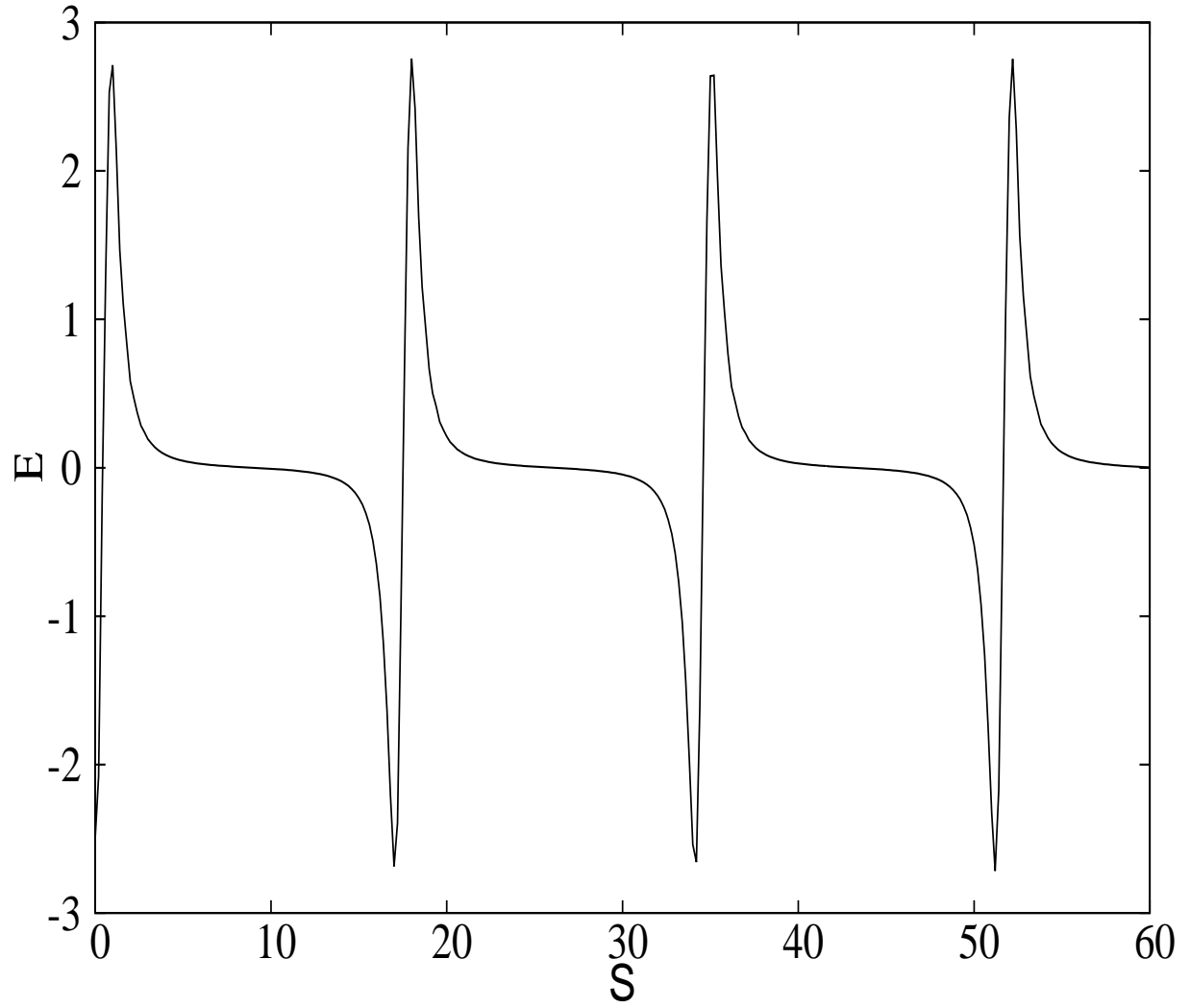


Figure 4.20: Numerical solution of normalized parallel electric field for the parameters $E_0 = 2.5$, $M = 3.5$, $R = 5.0$, $\delta_i = \delta_e = \delta_p = 0.0$, $T_i/T_h = 0.0$, $n_{p0}/n_{e0} = n_{i0}/n_{e0} = 0.5$ and $\theta = 10^0$.

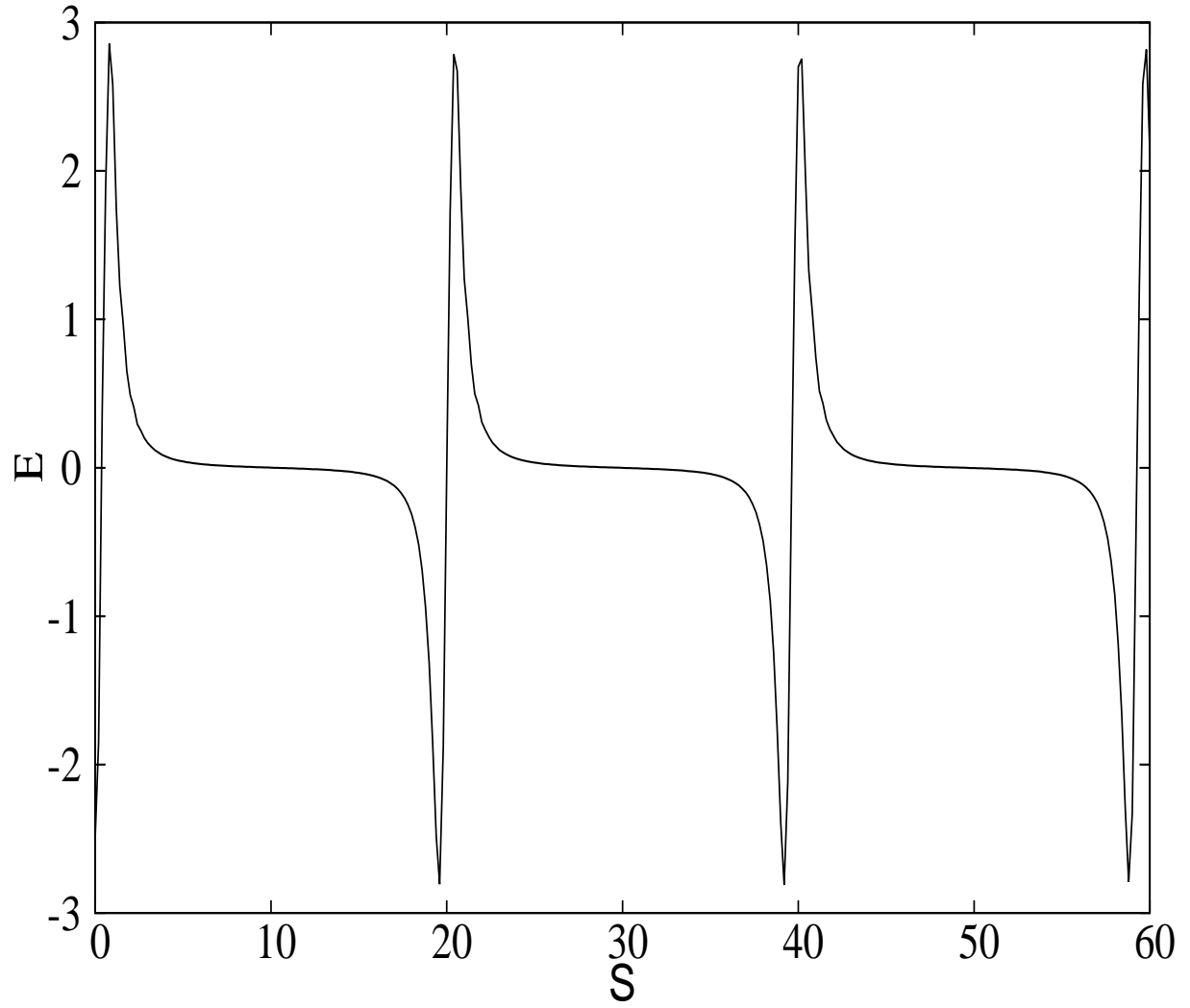


Figure 4.21: Numerical solution of normalized parallel electric field for the parameters $E_0 = 2.5$, $M = 3.5$, $R = 5.0$, $\delta_i = \delta_e = \delta_p = 0.0$, $T_i/T_h = 0.0$, $n_{p0}/n_{e0} = n_{i0}/n_{e0} = 0.5$ and $\theta = 15^\circ$.

Effect of the electron drift

The effect of the electron drift velocity on the electric field structures for the fixed the parameters: $E_0 = 2.5$, $M = 3.5$, $R = 5.0$, $\theta = 2^0$, $T_i/T_h = 0.0$, $\delta_i = \delta_p = 0.0$ and $n_{p0}/n_{e0} = n_{i0}/n_{e0} = 0.5$ are depicted in Figures 4.22 - 4.24. It is seen that for antiparallel electron drifts ($\delta_e < 0$), the periods of the waves are significantly lower compared to parallel drifts ($\delta_e > 0$). Consequently, the period of the waves increases from $2.25\tau_{ci}$ for $\delta_e = -0.10$ to $2.45\tau_{ci}$ for $\delta_e = 0.10$. However, the nonlinearity is unaffected and all waveforms are spiky in nature. Similar results have been reported by Moolla et al. [2007] during an investigation of the effect of the cool electron drift.

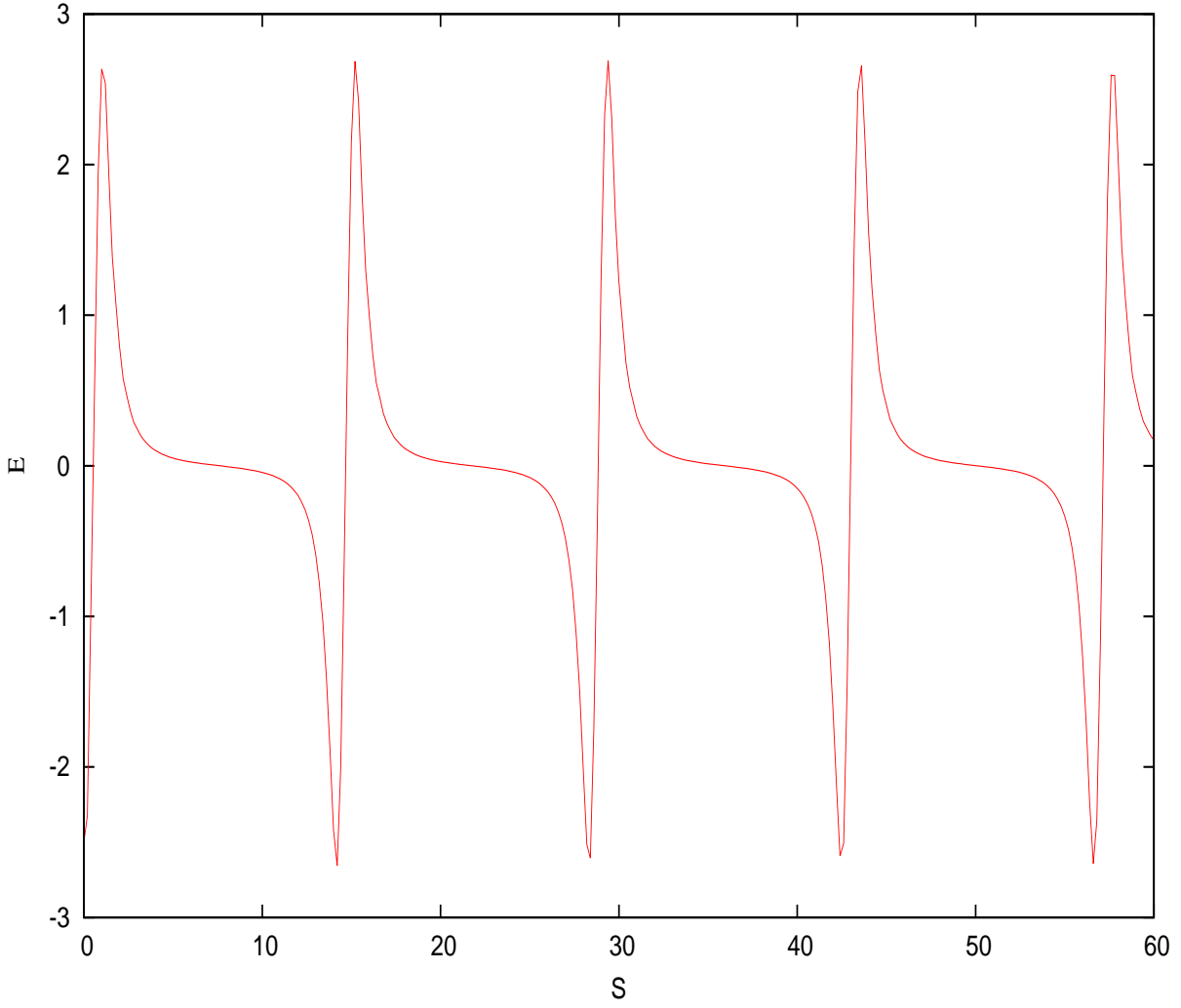


Figure 4.22: Numerical solution of normalized parallel electric field for the parameters $E_0 = 2.5$, $M = 3.5$, $R = 5.0$, $\delta_i = \delta_p = 0.0$, $\theta = 2^\circ$, $T_i/T_h = 0.5$, $n_{p0}/n_{e0} = n_{i0}/n_{e0} = 0.5$ and $\delta_e = -0.10$.

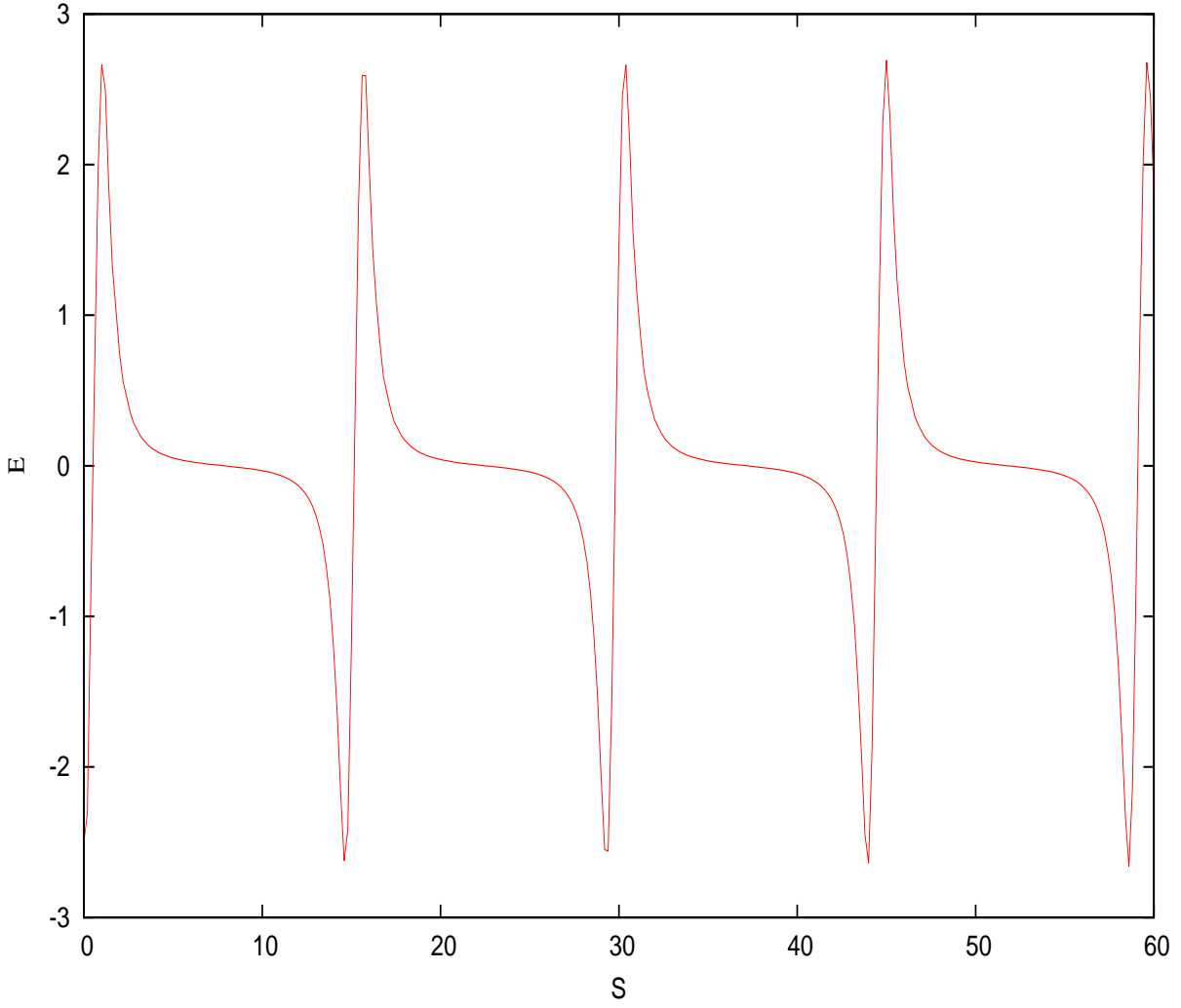


Figure 4.23: Numerical solution of normalized parallel electric field for the parameters $E_0 = 2.5$, $M = 3.5$, $R = 5.0$, $\delta_i = \delta_p = 0.0$, $\theta = 2^\circ$, $T_i/T_h = 0.5$, $n_{p0}/n_{e0} = n_{i0}/n_{e0} = 0.5$ and $\delta_e = 0.0$.

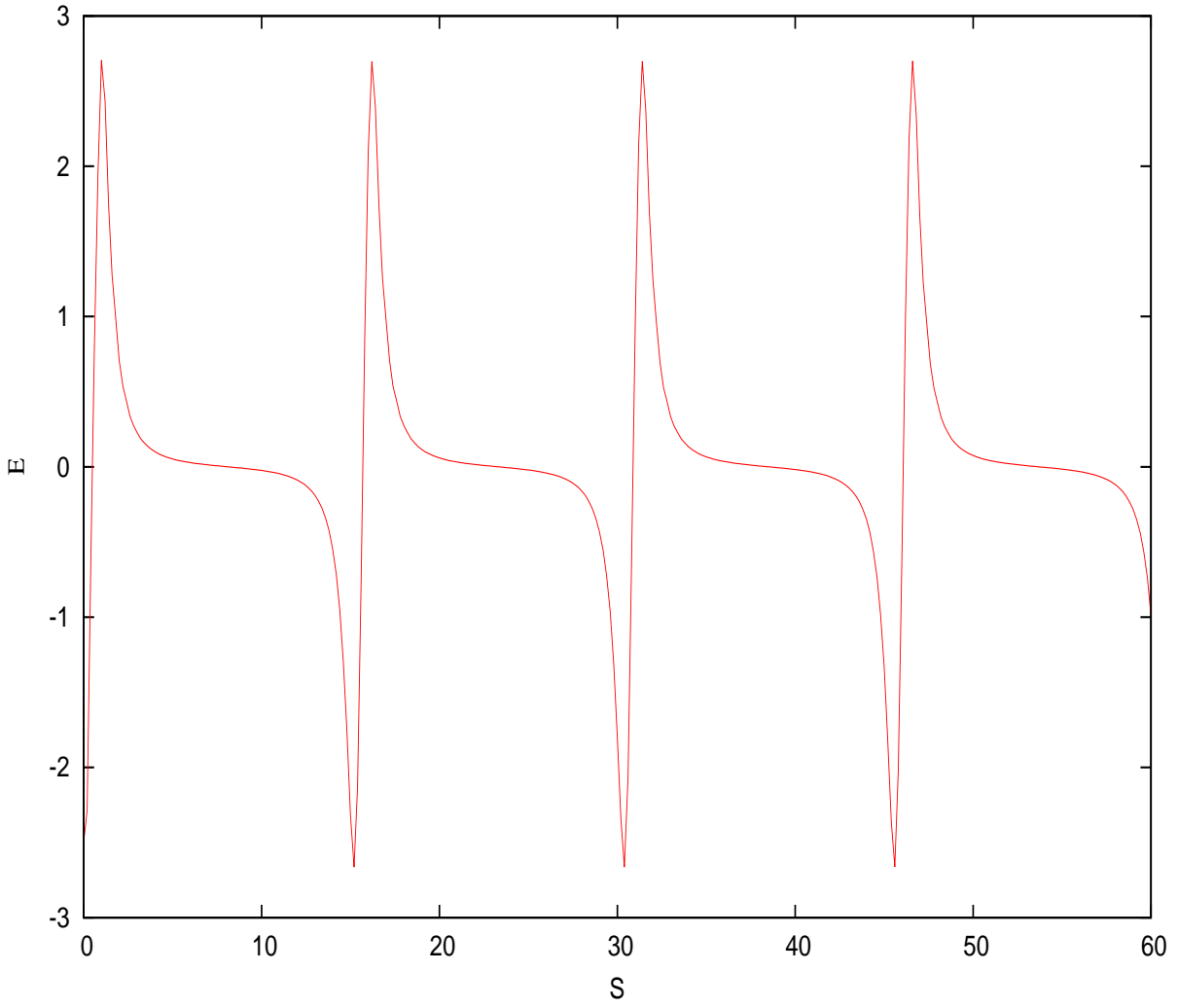


Figure 4.24: Numerical solution of normalized parallel electric field for the parameters $E_0 = 2.5$, $M = 3.5$, $R = 5.0$, $\delta_i = \delta_p = 0.0$, $\theta = 2^\circ$, $T_i/T_h = 0.5$, $n_{p0}/n_{e0} = n_{i0}/n_{e0} = 0.5$ and $\delta_e = 0.10$.

Effect of the ion drift

The effect of the ion drift velocity on the electric field structures is presented in Figures 4.25 - 4.27 for the fixed the parameters $E_0 = 2.5$, $M = 3.5$, $R = 5.0$, $\theta = 2^0$, $T_i/T_h = 0.0$, $\delta_e = \delta_p = 0.0$ and $n_{p0}/n_{e0} = n_{i0}/n_{e0} = 0.5$. It is seen that for antiparallel ion drift ($\delta_i < 0$), the periods of the waves are significantly higher compared to parallel drift ($\delta_i > 0$). From anti-parallel to parallel drifts the period of spikes decreases from $2.52\tau_{ci}$ for $\delta_i = -0.10$ to $2.19\tau_{ci}$ for $\delta_i = 0.10$. However, the nonlinearity is unaffected and all waveforms are spiky in nature. These results are similar to those of Moolla et al. [2012] and are in agreement with the satellite observations showing that the period of the spiky structures vary rapidly due to the drifting particles being accelerated in bursts [Moolla et al., 2003].

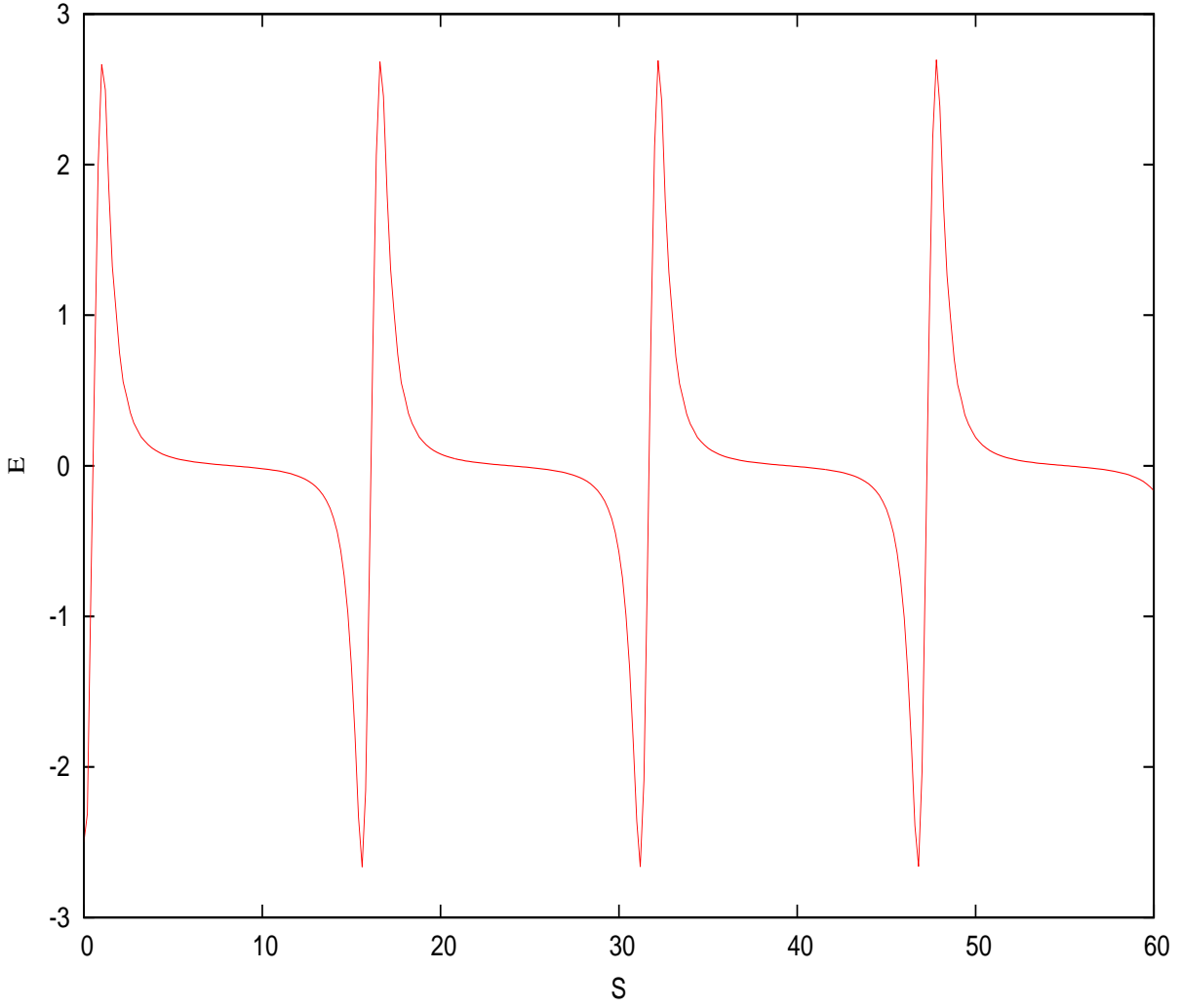


Figure 4.25: Numerical solution of normalized parallel electric field for the parameters $E_0 = 2.5$, $M = 3.5$, $R = 5.0$, $\delta_e = \delta_p = 0.0$, $\theta = 2^0$, $T_i/T_h = 0.5$, $n_{p0}/n_{e0} = n_{i0}/n_{e0} = 0.5$ and $\delta_i = -0.10$.

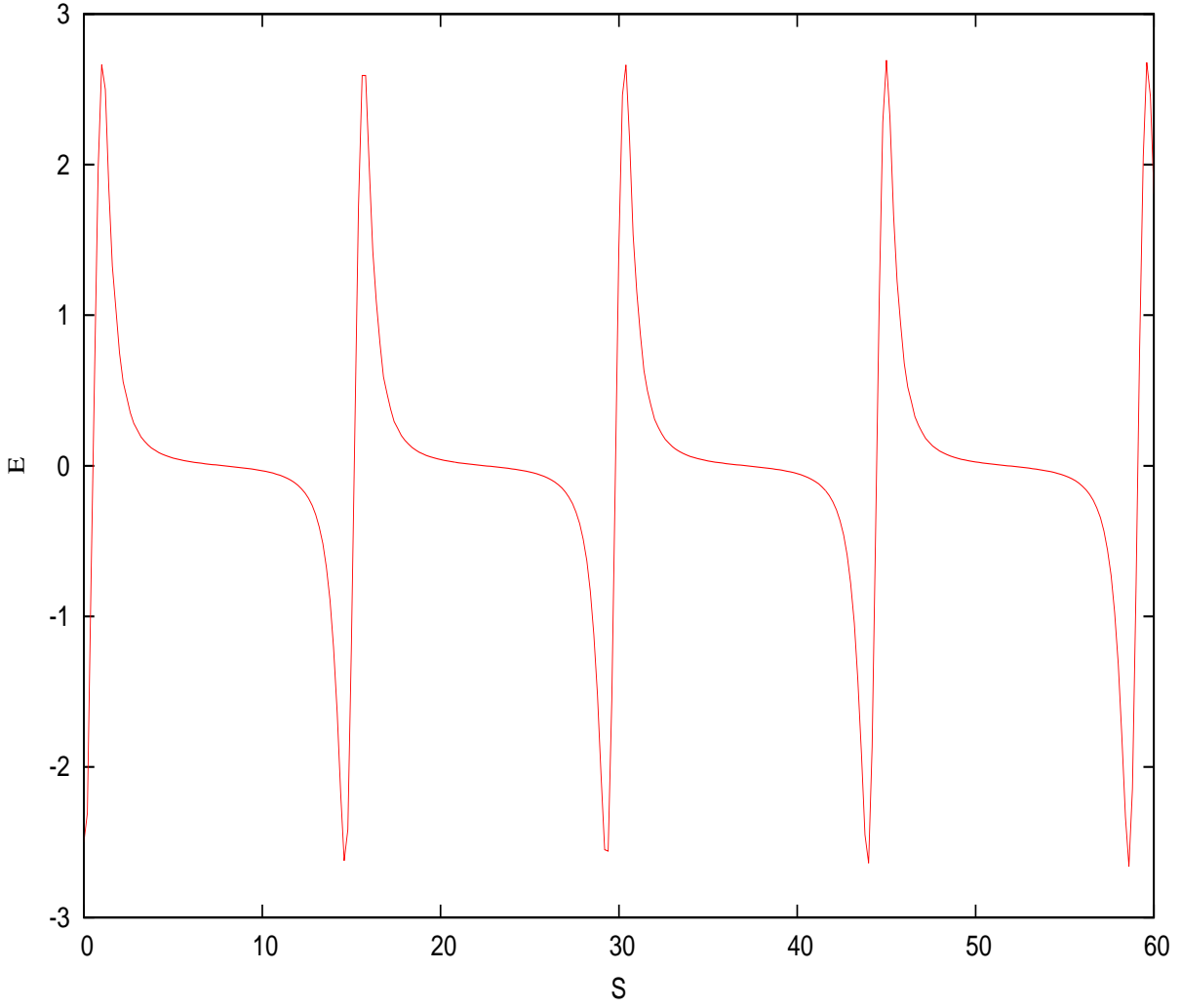


Figure 4.26: Numerical solution of normalized parallel electric field for the parameters $E_0 = 2.5$, $M = 3.5$, $R = 5.0$, $\delta_e = \delta_p = 0.0$, $\theta = 2^\circ$, $T_i/T_h = 0.5$, $n_{p0}/n_{e0} = n_{i0}/n_{e0} = 0.5$ and $\delta_i = 0.0$.

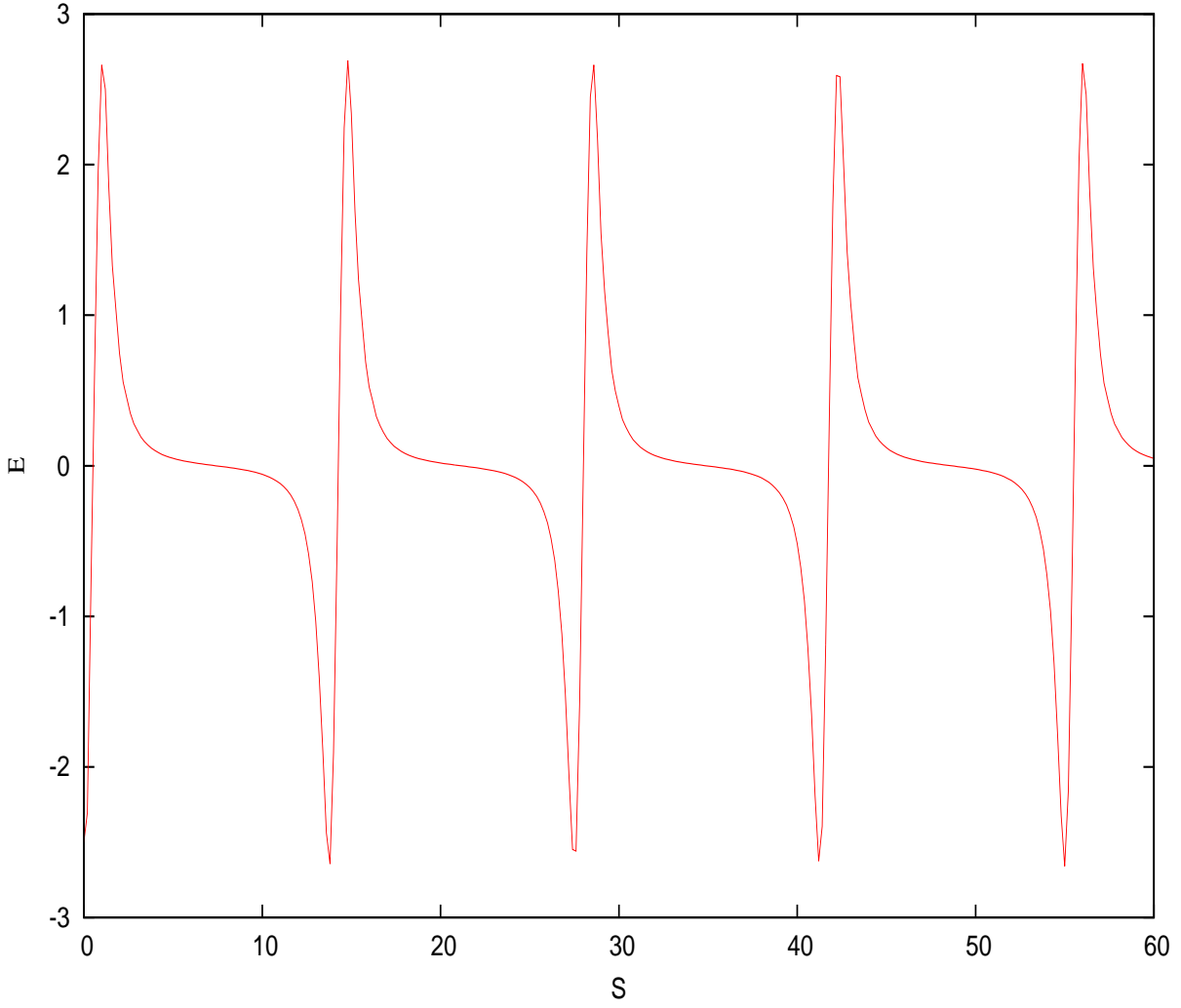


Figure 4.27: Numerical solution of normalized parallel electric field for the parameters $E_0 = 2.5$, $M = 3.5$, $R = 5.0$, $\delta_e = \delta_p = 0.0$, $\theta = 2^\circ$, $T_i/T_h = 0.5$, $n_{p0}/n_{e0} = n_{i0}/n_{e0} = 0.5$ and $\delta_i = 0.1$.

Effect of the positron drift

We investigate the effect of the positron drift velocity on the electric field structures as shown in Figures 4.28-4.30 for the fixed the parameters: $E_0 = 2.5$, $M = 3.5$, $R = 5.0$, $\theta = 2^0$, $T_i/T_h = 0.0$, $\delta_i = \delta_e = 0.0$ and $n_{p0}/n_{e0} = n_{i0}/n_{e0} = 0.5$. It is seen that for antiparallel positron drift ($\delta_p < 0$), the period of the waves is significantly lower compared to parallel drift ($\delta_p > 0$). From anti-parallel to parallel drift the frequency of electrostatic waves decreases, i.e the period of spikes increases from $2.25\tau_{ci}$ for $\delta_p = -0.10$ to $2.45\tau_{ci}$ for $\delta_p = 0.10$. However, the nonlinearity is unaffected and all waveforms are spiky in nature. The behavior of the spiky electric field is similar to that of electron drift. We note that the period of the spiky structures for positrons and electrons drift increases from antiparallel to parallel drifts, while, for the case of the ion drift velocity δ_i , the opposite trend occurs.

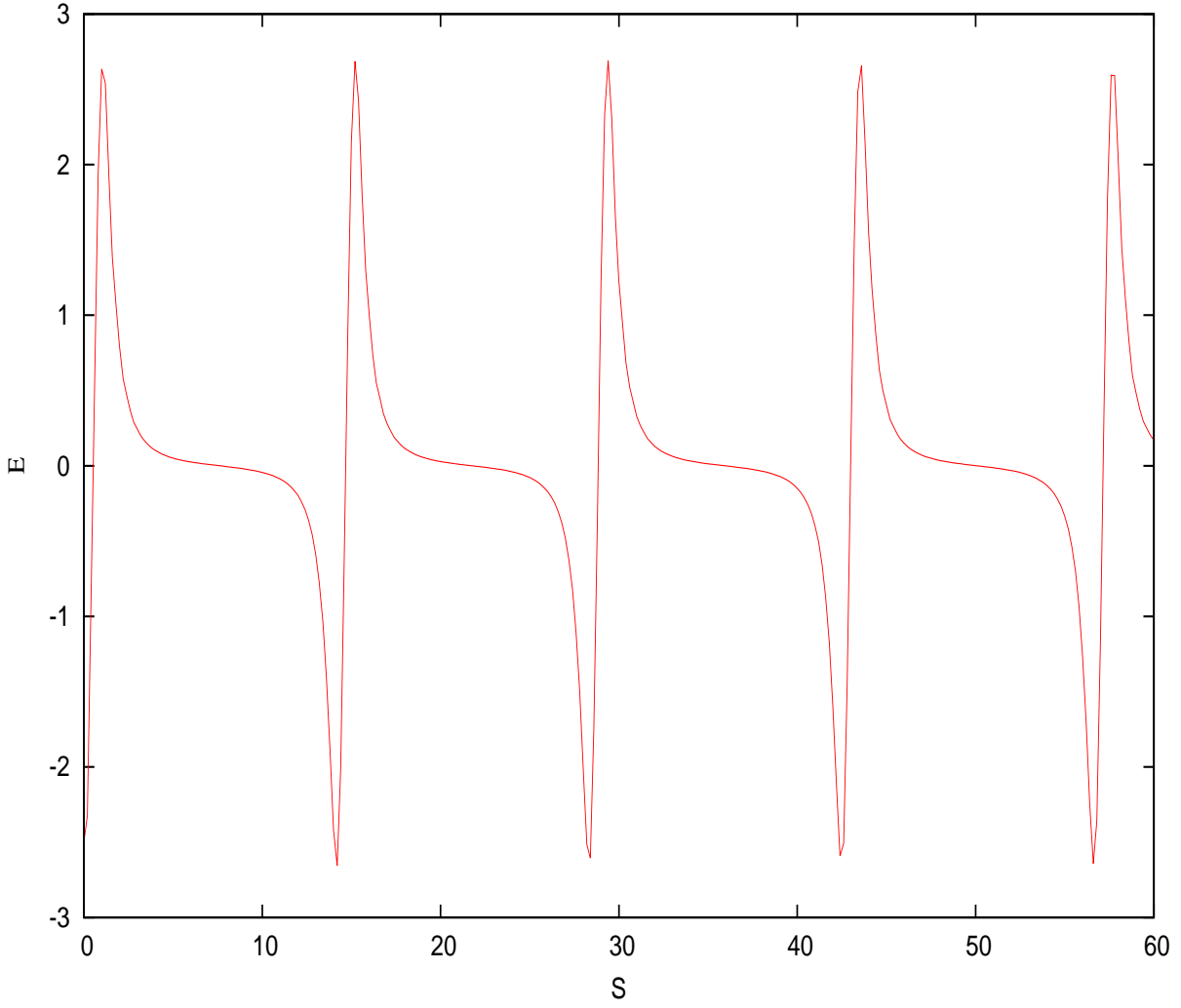


Figure 4.28: Numerical solution of normalized parallel electric field for the parameters $E_0 = 2.5$, $M = 3.5$, $R = 5.0$, $\delta_i = \delta_e = 0.0$, $\theta = 2^\circ$, $T_i/T_h = 0.5$, $n_{p0}/n_{e0} = n_{i0}/n_{e0} = 0.5$ and $\delta_p = -0.10$.

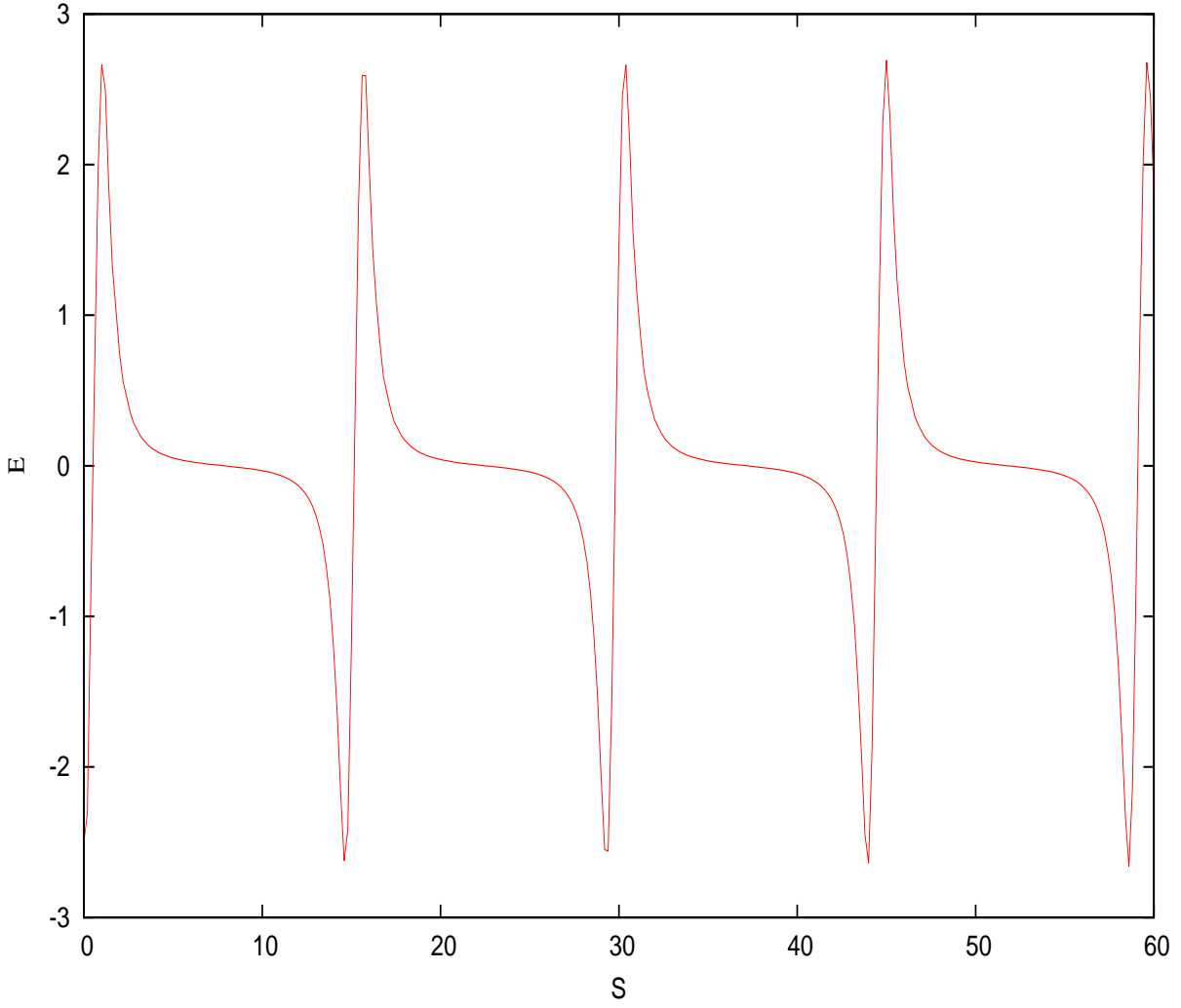


Figure 4.29: Numerical solution of normalized parallel electric field for the parameters $E_0 = 2.5$, $M = 3.5$, $R = 5.0$, $\delta_i = \delta_e = 0.0$, $\theta = 2^\circ$, $T_i/T_h = 0.5$, $n_{p0}/n_{e0} = n_{i0}/n_{e0} = 0.5$ and $\delta_p = 0.0$.

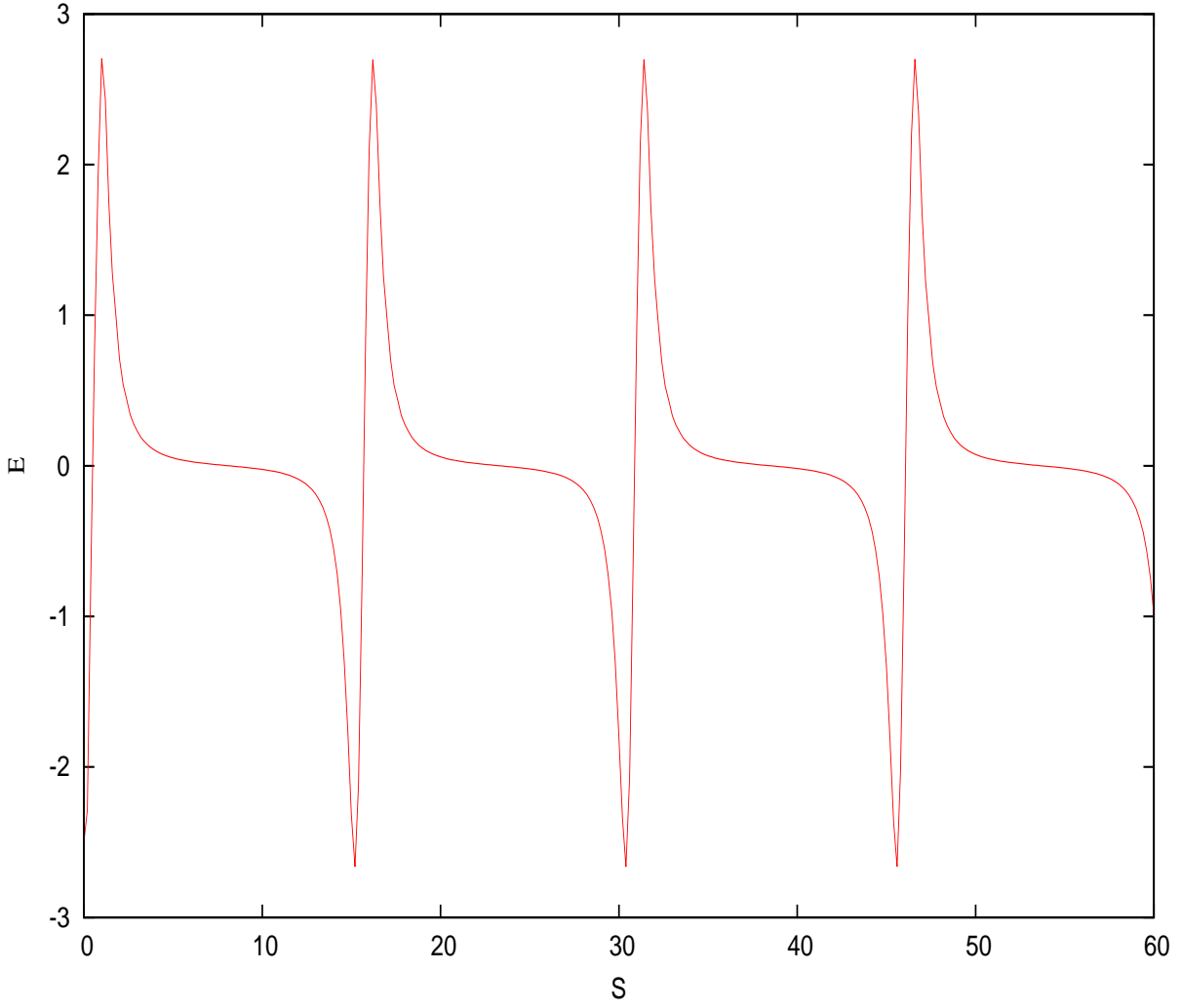


Figure 4.30: Numerical solution of normalized parallel electric field for the parameters $E_0 = 2.5$, $M = 3.5$, $R = 5.0$, $\delta_i = \delta_e = 0.0$, $\theta = 2^\circ$, $T_i/T_h = 0.5$, $n_{p0}/n_{e0} = n_{i0}/n_{e0} = 0.5$ and $\delta_p = 0.1$.

Chapter 5

Solitary waves in three-component electron - positron - dust plasmas

5.1 Literature Review

Dust particles are an extremely massive species compared to ions. These dust particles, together with electrons-positrons and ions are present in astrophysical environments [Horanyi and Mendis, 1986; Havnes et al., 1996; Verheest, 1999; Samarian et al., 2001; Shukla and Mamun, 2002; Mamun and Shukla, 2005]. The dust grains are characterized by their heavy mass ($10^9 - 10^{12}$ proton mass), their sizes vary from nanometers to millimeters and they may be either negatively or positively charged, depending on the plasma environment, with charges varying from hundred to ten thousand times the charge on the electron. It is now well known that the dust particles are ubiquitous in various space plasmas including the Earth's magnetosphere [Goertz, 1989].

Dusty plasmas can also be observed in the flame of a humble candle, in the zodiacal light, in volcanic eruptions and in ball lightning [Abrahamson and Dinniss, 2000; Abrahamson, 2002]. The same dust grains with size distributions have also been detected in fusion plasmas [Winter, 1998]. Moreover, the coexistence of positively and negatively charged dust can be found in laboratory plasmas [Mendis and Rosenberg, 1994; Ma and Liu, 1997].

The presence of heavy dust particles can significantly modify the parameter regime of electrostatic structures and this plasma modification generates new modes such as dust-ion acoustic mode, dust cyclotron mode and dust drift mode [Rao et al., 1990; Shukla and Silin, 1992].

The applicability of dusty plasmas is encountered in industries [Selwyn et al., 1989], in such technologies as microelectronics [Vladimirov and Ostrikov, 2004], in plasma spraying and in electrostatic painting. Recently, the novel applications of dusty plasmas in microbiology has been suggested [Laroussi et al., 2003], as well as in medicine [Stoffels et al., 2003].

The presence of dust grains in a plasma resulting in two interesting effects, viz the reduction of the number of free mobile electrons, as some of them are absorbed on the grains [Moolla et al., 2005] and the introduction of a new time scale [Mamun and Hassan, 2000]. These two effects are of interest in understanding the behavior of solitary waves in dusty plasmas. One necessarily is restricted to the study of only one solitary wave, sometimes called a soliton.

Solitons are a particular type of nonlinear waves (solitary) with finite energy and necessary conditions for its existence. These waves conserve their shape along their propagation. They are a fundamental phenomenon in nonlinear dynamics and continue to attract the attention of researchers from the physical and mathematical sciences, due to their wide range of applications. Solitons were found in water waves, solid-state physics, plasma physics, particle physics, biological systems and nonlinear optics.

Several studies on the existence and behaviors of nonlinear low frequency soliton and double layer structures propagating in different plasmas have been performed experimentally [Ikezi et al., 1970; Ikezi, 1973], as well as theoretically [Tagare, 1973; Abrol and Tagare, 1980; Gell and Roth, 1981]. Therefore, understanding soliton dynamics is vital for understanding the dynamics of different non-solitonic waves.

The study of solitary structures with negative potentials was motivated by the Viking satellite observations. Many authors developed different theoretical models to investigate nonlinear ion acoustic waves in multi-component plasmas [Yadav and Sharma, 1990; Reddy

and Lakhina, 1991; Ghosh et al., 1996; Lakhina, 2004]. Baboolal [1988] studied solitons and classified them into two categories, namely: small and large amplitude.

In plasmas, the existence of the ion acoustic solitary waves of small but finite amplitudes was first theoretically predicted by Washimi and Taniuti [1966] and it was shown that the linear study can mostly be applied to small amplitude solitary waves.

Large amplitude solitary waves can only be studied analytically if they are assumed to be stationary from the onset, using pseudopotential methods, such as the Sagdeev analysis [Sagdeev, 1966]. It has been shown that a pair plasma, consisting of electrons and positrons, is highly symmetric. Particularly interesting in our investigation, is to conduct a study in such plasmas contaminated with charged dust particles, usually treated as an extremely heavy, negative ion component. These plasmas can occur in supernovae and pulsar environments, as well as in cluster explosions by intense laser beams in laboratory experiments [Shukla and Marklund, 2004; Saberian et al., 2015] .

In this chapter, we study the conditions under which electrostatic solitons may exist in a plasma consisting of electrons, positrons and positive dust grains, and establish the existence domains for solitons in an appropriate parameter space. Such existence diagrams are fruitful both in interpretation of electrostatic spikes or other persistent wavelike structures observed in magnetospheric environments and the findings obtained in laboratory experiments. Our model is limited to recombination (annihilation) times for the electrons and positrons that are sufficiently large to work on the dust time scale.

5.2 Basic theory and Model of fluid equations governing the plasma dynamics

We consider a collisionless, one-dimensional unmagnetized three component electron-positron-dust (e-p-d) plasma consisting of a hot species of electrons (eh) and positrons (ph), and cool dust (dc). The cool dust grains carry a positive charge and are governed by the fluid equations while the hot electron and positron densities are assumed to be Boltzmann distributed.

At equilibrium the densities and temperatures of the electrons and positron are different.

To describe the processes occurring in e-p-d plasmas, we will employ the continuity and momentum equations for positive dust particles:

$$\frac{\partial n_d}{\partial t} + \frac{\partial n_d v_{dx}}{\partial x} = 0 \quad (5.1)$$

$$\frac{\partial v_{dx}}{\partial t} + v_{dx} \frac{\partial v_{dx}}{\partial x} + \frac{1}{n_d m_d} \frac{\partial p_d}{\partial x} = -\frac{q_d}{m_d} \frac{\partial \varphi}{\partial x}. \quad (5.2)$$

In this model, the Boltzmann density distribution for hot species is given by

$$n_{ph} = n_{p0} \exp\left(-\frac{e\varphi}{T_p}\right) \quad (5.3)$$

$$n_{eh} = n_{e0} \exp\left(\frac{e\varphi}{T_e}\right) \quad (5.4)$$

Equations (5.1) -(5.4) are closed with the Poisson equation

$$\varepsilon_0 \frac{\partial^2 \varphi}{\partial x^2} = -e(n_{ph} - n_{eh} + n_d Z_d) \quad (5.5)$$

where $q_d = eZ_d$ is the dust charge, n_d is the dust density, v_{dx} is the dust velocity along the x direction, p_d is the dust pressure, φ is the electrostatic potential and m_d is the dust mass.

To obtain the linear dispersion relation, we assume that equations (5.1) - (5.5) have harmonic solutions, i.e. all variables are of the form $\exp(i(kx - \omega t))$. We introduce the following definitions: $\partial/\partial x \rightarrow ik$ and $\partial/\partial t \rightarrow -i\omega$. For linearization, we have neglected the '1' for the first order in the continuity equation and all terms which are second and

higher order in the momentum equation. The continuity equation becomes:

$$-n_{dc}i\omega + ikv_{dx}n_{d0} = 0 \quad (5.6)$$

for which

$$n_{dc} = \frac{kn_{d0}}{\omega}v_{dx}. \quad (5.7)$$

Linearizing equation (5.2), we can express the velocity for cool dust grains as:

$$v_{dx} = \frac{kq_d\varphi}{\omega m_d}. \quad (5.8)$$

Combining equations (5.7) and (5.8), we obtain the expression for the dust density as:

$$n_d = \frac{k^2 n_{d0} q_d \varphi}{\omega^2 m_d}. \quad (5.9)$$

Linearizing equations (5.3) and (5.4), we have dropped the second and higher order terms in the Taylor series expansion of the exponential so that the perturbed densities of hot species become:

$$n_{eh} = n_{e0} \frac{e\varphi}{T_e} \quad (5.10)$$

$$n_{ph} = -n_{p0} \frac{e\varphi}{T_p} \quad (5.11)$$

Substituting equations (5.9), (5.10) and (5.11) into the Poisson equation (5.5), we get

$$1 + \frac{e^2}{\varepsilon_0 k^2} \frac{n_{p0} T_e + n_{e0} T_p}{T_p T_e} = \frac{\omega_{pd}^2}{\omega^2}. \quad (5.12)$$

The general dispersion relation for a multicomponent plasma consisting of hot electrons, positrons and cold dust is obtained to be:

$$\omega^2 = \frac{k^2 \lambda_{De}^2 \omega_{pd}^2}{k^2 \lambda_{De}^2 + \left(\frac{n_{p0}}{n_{e0}} \sigma + 1\right)}, \quad (5.13)$$

where $\sigma = \frac{T_e}{T_p}$ and $\omega_{pd} = \sqrt{\frac{n_{d0} Z_d^2 e^2}{\epsilon_0 m_d}}$.

Introducing the definitions $V_D = \omega_{pd} \lambda_D$ and $\lambda_D = \epsilon_0 T_p T_e / e^2 (n_{p0} T_e + n_{e0} T_p)$, equation (5.13) reduces to

$$\omega = \frac{k V_D}{\sqrt{k^2 \lambda_D^2 + \left(\frac{n_{p0}}{n_{e0}} \sigma + 1\right)}}, \quad (5.14)$$

where, V_D is the dust acoustic speed.

For $T_e \ll T_p$, equation (5.14) can be rewritten as

$$\omega = \frac{k V_D}{\sqrt{k^2 \lambda_D^2 + 1}}. \quad (5.15)$$

The above equation is known as the dispersion relation for dust acoustic waves which is similar to the results obtained by [Moolla et al., 2005; Shukla and Eliasson, 2009].

5.3 Arbitrary Amplitude solitary waves in an electron-positron-dust plasma

We consider wave propagating in the x direction with a constant speed and transform from the laboratory frame of reference to a new reference frame related to the wave motion where all the fluid equations (5.1), (5.2) and (5.5), are assumed to depend on a single variable $s = x - Mt$, where M is the dimensionless normalized solitary wave velocity (*Mach* number).

With this transformation $\frac{\partial}{\partial t} \rightarrow -M \frac{\partial}{\partial s}$, $\frac{\partial}{\partial x} \rightarrow \frac{\partial}{\partial s}$, the continuity, momentum and Poisson equations become

$$-M \frac{\partial n_d}{\partial s} + \frac{\partial n_d v_{dx}}{\partial s} = 0, \quad (5.16)$$

$$-M \frac{\partial v_{dx}}{\partial s} + v_{dx} \frac{\partial v_{dx}}{\partial s} + \frac{1}{n_d m_d} \frac{\partial p_d}{\partial s} = -\frac{q_d}{m_d} \frac{\partial \varphi}{\partial s}, \quad (5.17)$$

$$\varepsilon_0 \frac{\partial^2 \varphi}{\partial s^2} = -e(n_{ph} - n_{eh} + n_d Z_d). \quad (5.18)$$

Normalizing and integrating equations (5.16) and (5.17) by using the boundary conditions, e.g., densities and pressure tend to their undisturbed values and potential tends to zero at $s \rightarrow \infty$: $n_d \rightarrow \alpha$, $v_d \rightarrow 0$, $\psi \rightarrow 0$, $\frac{\partial \psi}{\partial s} \rightarrow 0$, we get respectively

$$n_d = \frac{M\alpha}{M - v_{dx}} \quad (5.19)$$

$$\frac{v_d^2}{2} - Mv_d + Z_d \frac{m}{m_d} \psi = 0, \quad (5.20)$$

where $\psi = \frac{e\varphi}{T_e}$.

Substituting (5.19) into (5.20), we obtain the following quadratic equation

$$(M\alpha)^2 - [M^2 - 2Z_d(m/m_d)\psi]n_d^2 = 0, \quad (5.21)$$

where n_d is the dust density normalized to n_{e0} .

The above equation can be rewritten as

$$n_d^2 = \frac{(M\alpha)^2}{M^2 - 2Z_d(m/m_d)\psi} \quad (5.22)$$

or

$$n_d = \frac{M\alpha}{\sqrt{M^2 - 2Z_d(m/m_d)\psi}} \quad (5.23)$$

which satisfies our boundary conditions at $\psi = 0$. This is the expression for the density of the positively charged dust grains.

Equations similar to (5.23) have been obtained by various authors [Rao et al., 1990; Mamun, 1999; Moolla et al., 2005] and several methods have been used to obtain the corresponding pseudopotential. However, in order to obtain an integrable form of n_d in deriving the corresponding Sagdeev potential analytically, we have followed the approach of Shukla and Mamun [2002].

5.3.1 Sagdeev pseudopotential Approach

The full nonlinear solution for an acoustic soliton are obtained by using Sagdeev pseudopotential method [Sagdeev, 1966]. First, we normalize equations (5.3), (5.4) and (5.18) and get

$$n_{phn} = \frac{n_{p0}}{n_{e0}} \exp(-\sigma_{ep}\psi), \quad (5.24)$$

$$n_{ehn} = \exp(\psi), \quad (5.25)$$

$$\frac{\partial^2 \psi}{\partial s^2} = n_{ehn} - n_{phn} - Z_d n_d, \quad (5.26)$$

where $\sigma_{ep} = \frac{T_e}{T_p}$ is the temperature ratio between electrons and positrons.

Substituting equations (5.23), (5.24) and (5.25) into (5.26), one obtains the Poisson equation in dimensionless form

$$\frac{\partial^2 \psi}{\partial s^2} = e^\psi - \frac{n_{p0}}{n_{e0}} e^{-\sigma_{ep}\psi} - \frac{M\alpha}{\sqrt{M^2 - 2Z_d(m/m_d)\psi}}. \quad (5.27)$$

Multiplying the above equation by $d\psi/ds$, we integrate with respect to s and get an 'energy integral' for moving particle of unit mass with velocity $d\psi/ds$ at the position $d\psi$ in a nonlinear potential $V(\psi)$.

$$\frac{1}{2} \left(\frac{d\psi}{ds} \right)^2 + V(\psi, M) = 0, \quad (5.28)$$

which can be expressed as [Popel et al., 1995]

$$\frac{d^2 \psi}{ds^2} = -V'(\psi), \quad (5.29)$$

where, the prime denotes the derivative with respect to ψ . Equation (5.28) is known as the Sagdeev equation.

We recall the boundary conditions at $s \rightarrow \infty$: $n_d \rightarrow \alpha$, $v_d \rightarrow 0$, $\psi \rightarrow 0$, $\frac{\partial \psi}{\partial s} \rightarrow 0$.

Under these conditions, equation (5.27) can be reduced to equation (5.28) and the Sagdeev potential $V(\psi, M)$ is given by

$$V(\psi, M) = \int_0^\psi \frac{M\alpha}{\sqrt{M^2 - 2Z_d(m/m_d)\psi}} - \int_0^\psi e^\psi d\psi + \int_0^\psi \frac{n_{p0}}{n_{e0}} e^{-\sigma_{ep}\psi} d\psi. \quad (5.30)$$

After integration, the Sagdeev potential (5.30) becomes

$$V(\psi, M) = 1 - e^\psi + \frac{n_{p0}}{n_{e0}\sigma_{ep}} (1 - e^{-\sigma_{ep}\psi}) + \frac{M^2\alpha}{Z_d(m/m_d)} \left[1 - \left(1 - \frac{2Z_d(m/m_d)\psi}{M^2} \right)^{1/2} \right]. \quad (5.31)$$

Equation (5.31) is similar to the equations obtained by [Rao et al., 1990; Mamun, 1999; Moolla et al., 2005; Gogoi et al., 2012] and satisfies our boundary conditions for $\psi = 0$. We note that in our study, the condition for the Sagdeev potential to be real is $M^2 \geq 2Z_d(m/m_d)\psi$. This condition reveals the maximum value (ψ_m) of ψ for which the dust number density n_d is real and expressed as

$$\psi_m = \frac{M^2}{2Z_d(m/m_d)}. \quad (5.32)$$

where ψ_m is the amplitude of the solitary wave. The above equation is used to determine the maximum speed (upper limit) of solitary wave structures.

The solutions of the Sagdeev pseudoenergy conservation law (5.30) can predict the existence of the solitary structures. These solutions must satisfy the following conditions, which give the minimum and maximum values of the *Mach* number for the formation and stability of solitary structures. The following conditions can easily be verified for the existence of solitary waves:

- (a) There exists a minimum ($\psi = 0$) and maximum (ψ_m) at which equation (5.28) approaches zero ($V(0) = V(\psi_m) = 0$).
- (b) $V'(\psi = 0) = 0$ and $V''(\psi = 0) < 0$, where the primes indicate differentiation with respect to ψ . This condition satisfies also the existence of double layers.
- (c) To have the real soliton solution in (5.28), one requires $V(\psi) < 0$ for ψ lying between 0

and ψ_m .

Using these soliton conditions, we can obtain the values of the *Mach* number M for which the existence of solitary waves and double layers can exist.

Solving equation (5.28), we get

$$S = \int \frac{d\psi}{\sqrt{-2V(\psi, M)}}. \quad (5.33)$$

This equation can yield the solution in the form of solitary pulses. By solving equation (5.33) numerically, we obtain the arbitrary amplitude solitary wave solutions which will be discussed below.

5.4 Numerical results and Discussion

Equation (5.33) was numerically solved with the appropriate boundary conditions. The investigation of solitons in an e-p-d plasma included a parametric study of the effect of *Mach* number M , temperature σ_{ep} and the density α on the existence of solitary waves by analyzing the Sagdeev pseudopotential for arbitrary amplitude dust-acoustic waves. The values used are physically meaningful and correspond to magnetospheric plasma region [Bharuthram and Shukla, 1992; Moolla et al., 2005; Berbri and Tribeche, 2009; Bret and Dieckmann, 2010; Chang-Mo and Helen, 2010; Jinhy et al., 2012]. In our study, we have analysed the Sagdeev potential $V(\psi)$, for the following fixed parameters $\sigma_{ep} = 0.5$ and $\alpha = 0.5$, and we found that the solitary waves can exist for M lying between 0.008 (lower limit) and 0.011 (upper limit). The maximum electrostatic potential $\psi_m = 0.6$, the point where $V(\psi)$ crosses the horizontal axis corresponding to the maximum amplitude of the soliton. The results show that the present plasma model permits only compressive solitons. The Sagdeev potential curves and the corresponding solitary wave profiles for different values of M are plotted in Fig.5.1 - 5.6, respectively. It can be seen from Fig.5.1 that as we increase the value of M , the depth of the Sagdeev potential increases on the positive ψ -axis. This is a consequence of the compressive solitary waves with larger amplitude. Noting that for our model the solitary wave profiles

exist for a narrow range of M and it is observed in Fig.5.4 that an increase in *Mach* number M enhances the amplitude. These results are similar to those found during the investigation of solitary waves in a three component plasma consisting of Boltzmann electrons and ions, and negative dust grains, although the wave profiles were rarefactive solitons [Moolla et al., 2005].

The graphs illustrating the effect of dust density on the characteristics of solitary waves and the corresponding soliton profiles are represented in Fig.5.2 and Fig.5.5. From Fig.5.2, we can note the values of α for which the Sagdeev potential can exist. It is obvious that when the dust concentration increases (decrease of positron concentration), both the depth of the Sagdeev potential curves and the amplitude of soliton profiles slightly decrease [Alinejad, 2010; Saini et al., 2013]. The Fig.5.2 shows the value of dust density (α) for which our model is satisfied. We have numerically analyzed the dependence of the Sagdeev potential on α and our investigations show that the value of dust density needs to be in a narrow range for solitary waves structures to exist.

We have also studied the effect of the electron-positron temperature ratio ($\sigma = T_e/T_p$) on the characteristics of solitary waves. From Fig.5.3, we observe that an increase in the electron temperature (i.e an increase of σ) leads to an increase in the potential depth when the *Mach* number and the dust density are fixed [Alinejad, 2010]. The corresponding soliton profiles for different values of σ are depicted in Fig.5.6 and shows that with an increase in electron temperature, the amplitude of the compressive solitons slightly increases.

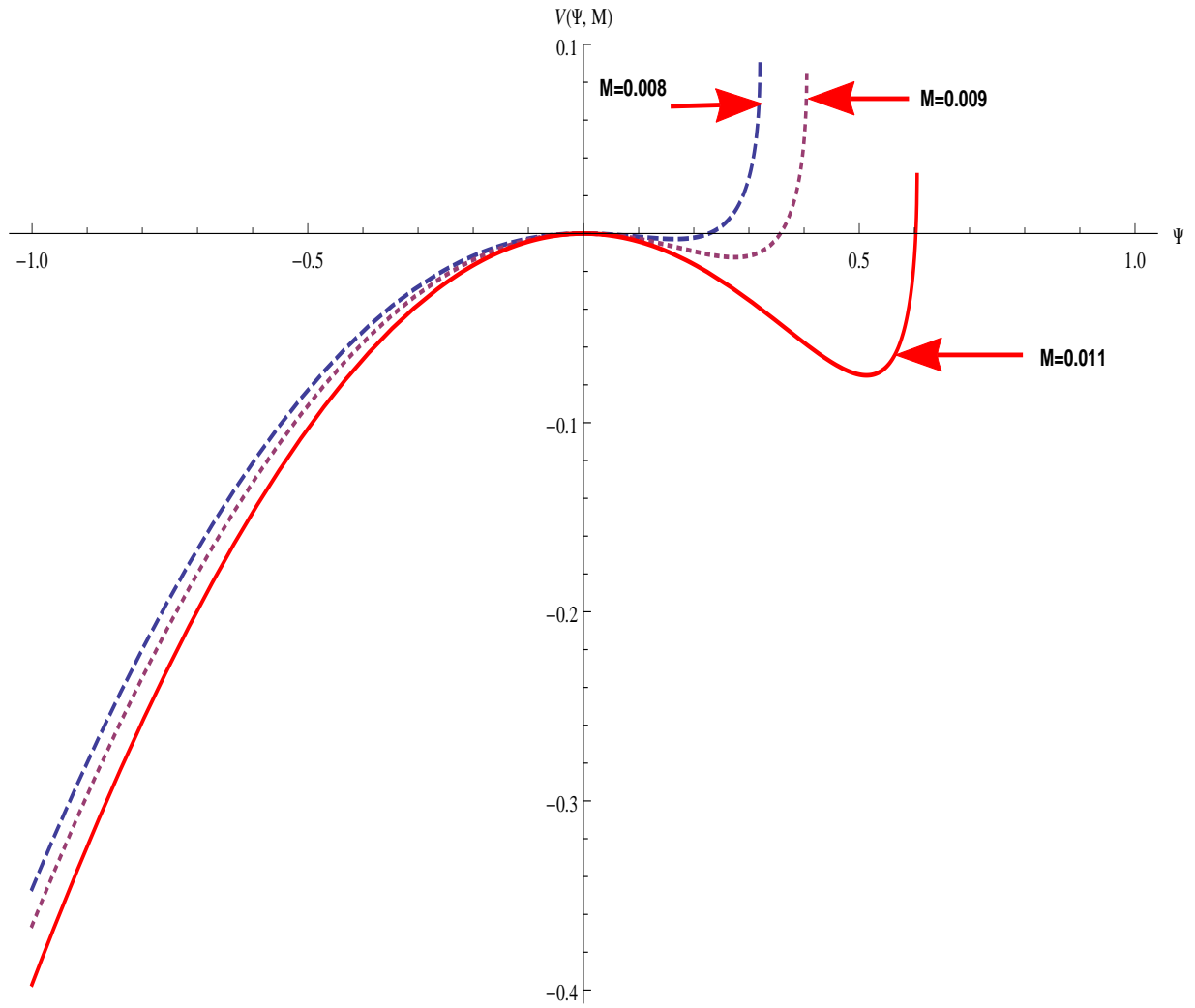


Figure 5.1: Plot of the Sagdeev potential $V(\psi)$ against the potential ψ for the the fixed parameters $Z_d = 1000$, $m/m_d = 10^{-7}$, $\sigma_{ep} = 0.5$ and $\alpha = 0.5$.

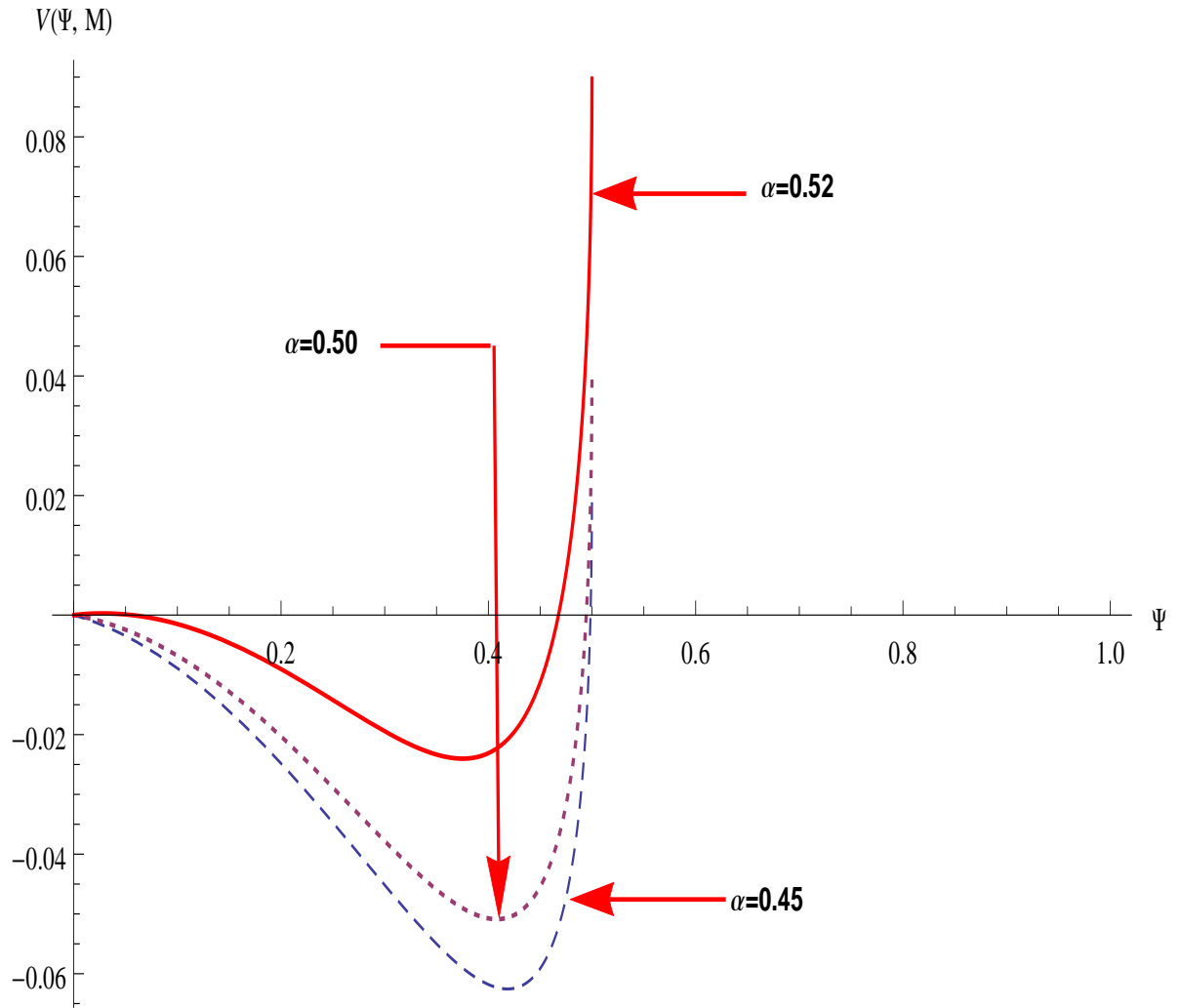


Figure 5.2: Plot of the Sagdeev potential $V(\psi)$ for the parameters $Z_d = 1000$, $m/m_d = 10^{-7}$, $\sigma_{ep} = 0.5$ and $M = 0.01$.

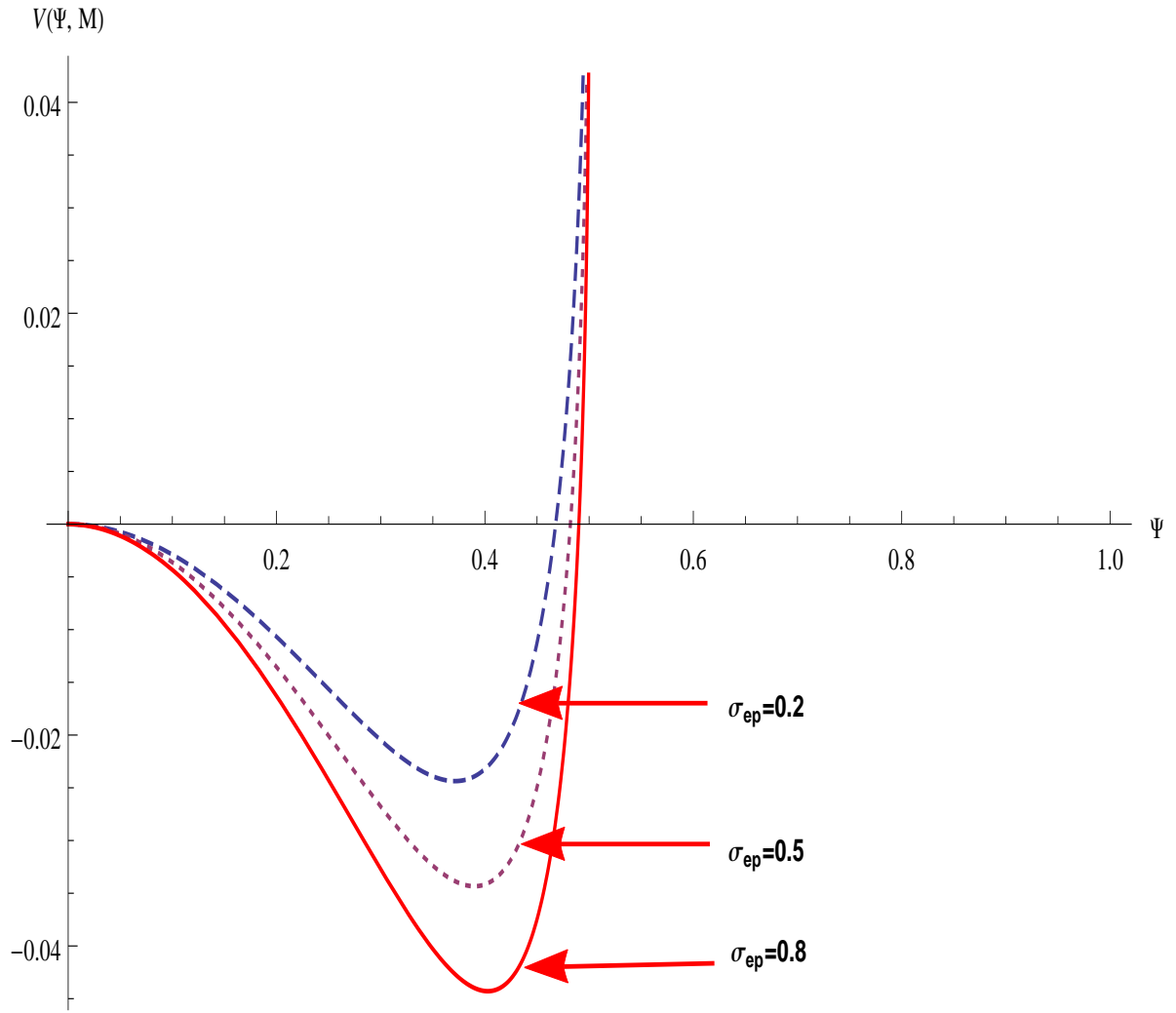


Figure 5.3: Plot of the Sagdeev potential $V(\psi)$ for the parameters $Z_d = 1000$, $m/m_d = 10^{-7}$, $\alpha = 0.5$, and $M = 0.01$.

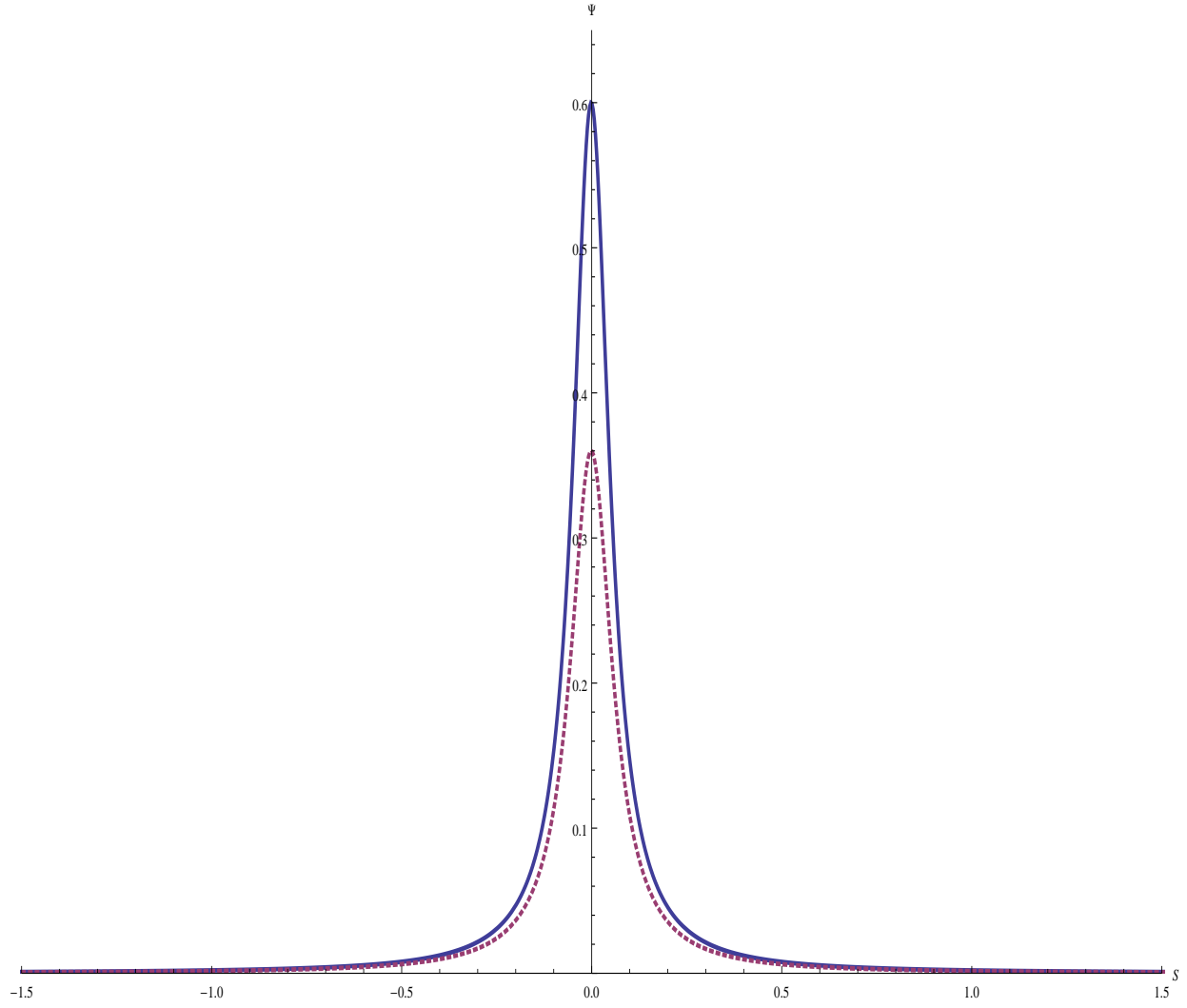


Figure 5.4: Soliton profile $\psi(S)$ for selected curves from Fig. 5.1 with the dotted(solid) curves corresponding to $M = 0.009$ (0.011) for the fixed parameters $Z_d = 1000$, $m/m_d = 10^{-7}$, $\sigma_{ep} = 0.5$ and $\alpha = 0.5$.

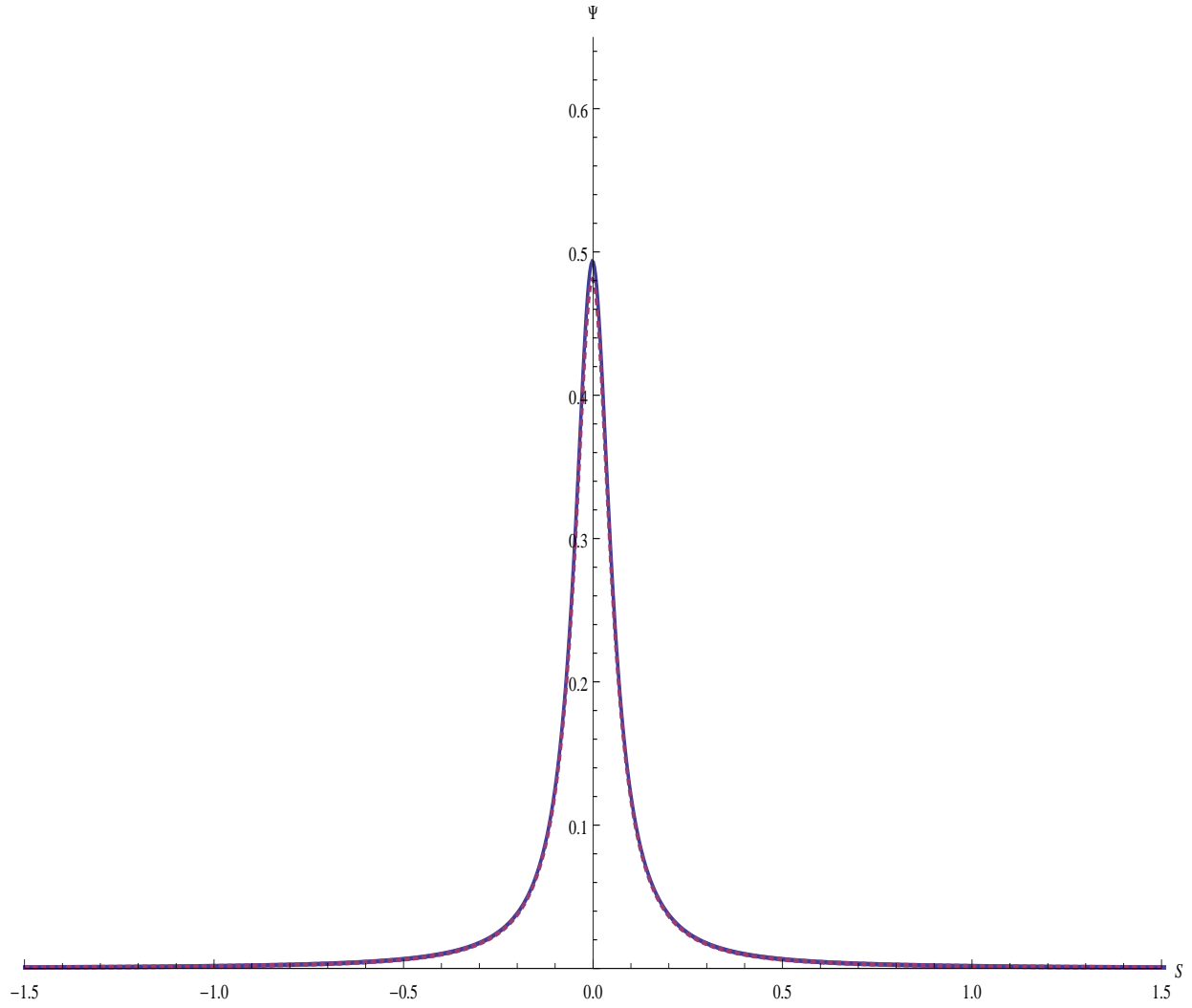


Figure 5.5: Soliton profile $\psi(S)$ for selected curves from Fig.5.2 with the solid (dotted) curves corresponding to $\alpha = 0.45$ (0.5) for the fixed parameters $M = 0.011$, $Z_d = 1000$, $m/m_d = 10^{-7}$ and $\sigma_{ep} = 0.5$.

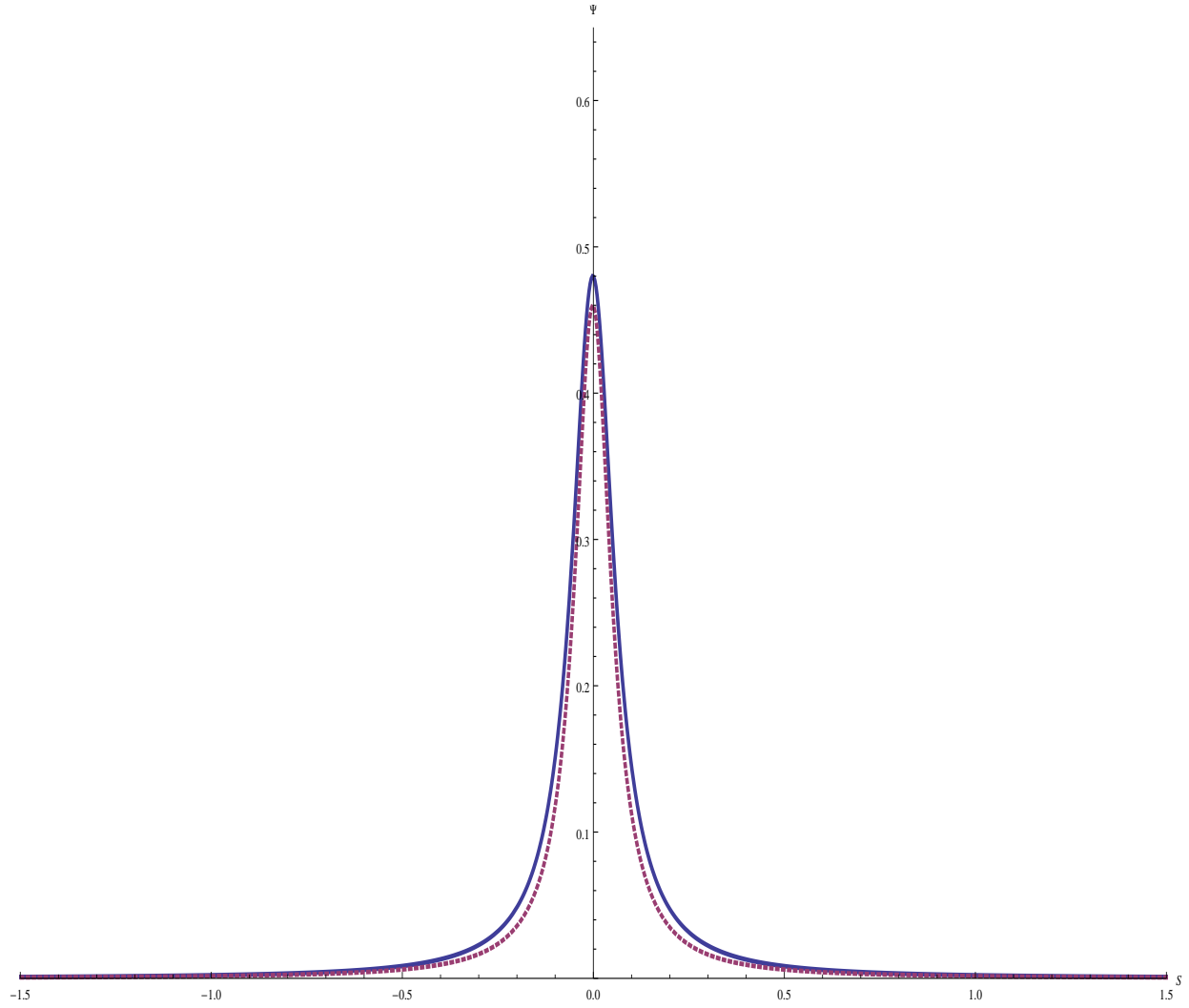


Figure 5.6: Soliton profile $\psi(S)$ for selected curves from Fig. 5.3, with the dotted (solid) curves corresponding to $\sigma_{ep} = 0.2$ (0.8) for the fixed parameters $M = 0.011$, $Z_d = 1000$, $m/m_d = 10^{-7}$, $T_e/T_p = 0.5$ and $\alpha = 0.5$.

Chapter 6

Summary

In this thesis, studies on linear and nonlinear waves in multicomponent plasmas have been carried out in an attempt to explain recent observations in space environments. These investigations revealed the behaviour of electrostatic waves in electron-positron-ion plasmas and showed the conditions for which solitons can occur in electron-positron-dust plasmas. In this chapter, we summarize the important results obtained in preceding chapters.

In chapter 2, we have studied linear electrostatic waves in a three component electron-positron-ion plasma in the low-frequency regime. Using the continuity and momentum equations along with Poisson's equation, the dispersion relation for the electron-positron-ion plasma consisting of cool ions and hot Boltzmann electrons and positrons was derived. We also studied the effects of the density and temperature on the electrostatic wave structures for two interesting limiting cases, viz, parallel and perpendicular propagation. Parallel wave propagation identified the existence of the ion-acoustic wave mode and the analysis revealed that the frequency of the ion-acoustic mode increased as the ion density ratio of the cool and hot species increased. On the other hand, for perpendicular propagation, it showed the existence of a cyclotron mode due to both cooler and hotter species. The density of the cool species played a significantly role in the modification of the wave properties. Comparing our results to those presented in Ref. Lazarus et al. [2012], we note that the introduction of the ions species to the e-p plasma resulted in a substantial lowering of the frequency range.

In the absence of a hot species, the cyclotron mode approaches the upper hybrid frequency. These findings have been published in Physics of Plasmas [Mugemana et al., 2014]. The present investigation yields an improved understanding of nonlinear waves propagating in a magnetized e-p-i plasma.

In chapter 3, we have studied nonlinear low frequency waves in an e-p-i plasma including charge separation. Using the fluid equations along with Poisson's equation, nonlinear electrostatic waves have been investigated in a plasma consisting of Boltzmann electrons and positrons and cool ions. We discussed the existence of nonlinear electric field structures in the form of solitary waves in different regions of the Earth's magnetosphere. The effects of driving electric field, ion temperature, positron density, *Mach* number, propagation angle and ion drift velocity were studied. The increase of the driving electric field (E_0), the nonlinear structures progressed from a sinusoidal, through a sawtooth, to spiky waveform. It was found that the period of oscillations depended on the electric field. An increase in ion-electron temperature (T_i/T_h) resulted in an increase in the period of waves. We also discussed the effect of the density ratio (n_{p0}/n_{e0}) on the parallel electric field structures and it has been shown that the increase in positron densities enhanced nonlinearity of wave structures. The electric fields of the nonlinear waves were investigated and we have shown that for high positron density, the spiky structures are easier to generate. Our model showed that the *Mach* number and the angle of propagation do not affect the nonlinearity of wave structures. This study has been conducted in a magnetized plasma in order to explain in detail the nonlinear electrostatic waves observed in the Broadband Electrostatic Noise (BEN).

In chapter 4, we have extended the problem discussed in the previous chapter, in the sense that the plasma model is treated using full dynamics for all three species. The effects of driving electric field, ion temperature, positron density, *Mach* number, propagation angle and drift velocity for each component were studied. Comparing these results to those obtained in chapter 3, where the hot species was described by the Boltzmann density distribution, we can highlight the following:

- The driving electric fields (E_0) for the onset of spiky structures for chapter 3 and chapter

4 were found to be 0.01 and 0.35, respectively. Hence it is easier to generate spikes when the hot species follows a Boltzmann distribution.

- The *Mach* number to support the electrostatic waves of chapter 3 and chapter 4 were found to be 2.5 and 3.5, respectively.
- The electrostatic waves were possible for R values of 3 and 5, respectively.

We note that the electric field structures found for both models varied from sinusoidal to sawtooth to spiky waveforms, confirming the results of Bharuthram et al. [2014] who showed that the nonlinear waves evolve in a consistent fashion irrespective of the plasma composition. The results of our analysis can be applied to similar environments generally found around other solar and extra-solar planetary bodies.

In chapter 5, electrostatic dust acoustic solitary structures were investigated in a collisionless unmagnetized plasma consisting of hot electrons and positrons, and positive dust grains of constant charge. The electrons and positrons were assumed to be Boltzmann distributed, while the dust grains were described by the fluid equations. An expression for the Sagdeev potential was derived without any approximations and assuming constant dust charge. The large amplitude dust ion acoustic solitons was studied for different plasma parameters M , α and σ . The analytical studies revealed that the plasma model could support only solitary waves of positive potential and the corresponding soliton profiles were compressive in nature. The minimum and maximum *Mach* numbers between which the solitary waves existed were computed. The results obtained showed that the Sagdeev pseudopotential $V(\psi)$ and the characteristics of the solitons depended on the positron concentration, dust concentration, electron temperature and *Mach* number. These results could play a pivotal role in understanding nonlinear wave structures in astrophysical environments.

Appendix A

CODES

```
! ROOTFINDER PROGRAM
! LINEAR ELECTROSTATIC WAVES IN A THREE COMPONENT E-P-I PLASMA
! FOR VARIOUS PARAMETERS - ANGLES,DENSITIES, TEMPERATURE RATIO THTC,
! MASS RATIO MEMI. R=W/WP, KLAMDA=K*LAMDA, TCTH=TC/TH,Z=ME/MI
! N0C=N0C/N0, N0H=N0H/N0 (N0=N0C+N0H UNNORMALIZED DENSITY)
! W NORMALIZED BY :  $LAMDA_D2 = Th/4PIN0E2$ 
PROGRAM ROOTFINDER
IMPLICIT NONE
INTEGER I
REAL*8 A,B,C,P1,P2,ROOT1,ROOT2,N0I,N0H,TITH,Z
REAL*8 R,R2,THETA,KLAMDA,KLAMDA2
REAL*8 NUM,DEN,PI
!*****
! INITIAL VALUES
!*****
PI=3.1415927D0
N0I=0.1D0
N0H=1.0D0-N0I
```



```

TITH=0.01d0
R=0.3333D0
Z=1.0d0/1836.0d0 THETA=(0.0d0/180.0d0)*PI
R2=R**2
KLAMDA=0.0D0
OPEN(25,FILE='root1.dat')
OPEN(26,FILE='root2.dat')
|*****
DO I=1,201
KLAMDA2=KLAMDA*KLAMDA
NUM=Z*KLAMDA2*N0I/N0H
DEN=2.0D0+KLAMDA2/N0H
A=1.0D0
B=-((1.0D0/R2+3.0D0*Z*KLAMDA2*TITH+NUM/DEN)
C=((COS(THETA)**2)/R2)*(3.0D0*Z*KLAMDA2*TITH+NUM/DEN)
P1=(-B+SQRT(B**2-4.0D0*A*C))/(2.0D0*A)
P2=(-B-SQRT(B**2-4.0D0*A*C))/(2.0D0*A)
ROOT1=SQRT(P1)
ROOT2=SQRT(P2)
write(6,*) KLAMDA,ROOT2
write(25,*) KLAMDA,ROOT1
write(26,*) KLAMDA,ROOT2
KLAMDA=KLAMDA+0.1D0 ENDDO
END

```

```

! PROGRAM EPI
! Nonlinear waves in electron-positron-ion plasmas
! Cool ions and Hot Boltzmann electrons and positrons.  $d(\psi)/d(s)=-E$ .
IMPLICIT NONE
external derivs
external rk4
INTEGER i,n,NMAX
REAL*8 h,x,dydx(6),y(6),yout(6),M,M2,theta,E0,TITH
REAL*8 deltaI,deltaH,MST,MCT,R,NONI
REAL*8 pi,ST,CT,MMDI,NONI2
REAL*8 NINO2,MMDI2,MMDH2,NIN
REAL*8 NONI3,NONI4,INVMMDI,INVMMDH,F22,F23
REAL*8 INVMMDI2,INVMMDH2,TERMZ1,TERMZ2,TERMZ21,TERMZ22,TERMZ23
REAL*8 DF1F2,DF3F4,DF5F6,DF7F8,DF1,DF2,DF3,DF4,DF5,DF6
REAL*8 DF7,DF8,DF11,DF121,DF122,DF71,DF721,DF722,DF51
REAL*8 DF521,DF522,nphno,nehno,nino,npcco
REAL*8 F1,F2,F3,F4,F5,F6,F7,F8
common /pl/M,theta,R,deltaI,deltaH,nino,npcco,nehno,nphno,TITH
pi=3.1415927d0
h=0.2d0
n=6
x=0.0d0
! *****PARAMETERS*****
M=2.50d0
deltaI=0.0d0
TITH=0.0d0
theta=(2.0d0/180.0d0)*pi
E0=0.3d0

```

```

R=3.0d0
nphno=0.5d0
nehno=1.0d0
nino=nehno-nphno
! *****
! psi=y(1)
! E=-y(2)
! nin=y(3)
! pin=y(4)
! viyn=y(5)
! vizn=y(6)
!*****
MMDI=(M-deltaI)
MMDI2=MMDI**2
INVMMDI=1.0d0/MMDI
INVMMDI2=1.0d0/MMDI2
NONI=1.0d0/NINO
NONI2=NONI**2
NONI3=NONI*NONI2
NONI4=NONI2*NONI2
NINO2=NINO**2
M2=M*M
ST=dsin(theta)
CT=dcos(theta)
MST=M*ST
MCT=M*CT
!
y(1)=0.0d0

```

```

y(2)=E0
y(3)=nino
y(4)=nino*TITH
!
F1=y(3)**3
F2=NINO2*MMDI2-3.0d0*y(3)*y(4)
F3=F2*(NPHNO+NEHNO)/F1
!
y(5)=(-y(2)+(F3*y(2)))/MST
! y(5)=0.01d0
! F22=F2*F2
! F23=F2**3
TERMZ1=(M-(MMDI*NINO)/y(3))*(ST/CT)
TERMZ21=((F2)*MMDI*NINO)/(F1*M2*ST*CT*y(3))
TERMZ22=(-y(2)-MST*y(5))
DF1=3.0d0*(y(3)**5)*(TERMZ22)/F2
DF2=(-12.0d0*y(4)*F1*(TERMZ22 ))/F2
DF1F2=(F2*DF1-F1*DF2)/(F2**2)
! DF1F2=DF1+DF2
y(6)=TERMZ1-TERMZ21*((nphno-nehno)*(y(2)**2)+TERMZ22*DF1F2)
! y(6)=0.01d0
! Let's loop here
open(25,file="good4.dat",status="unknown")
! open(25,file="epi.dat",status="unknown")
write(25,*) x,-y(2)
write(6,*) x,-y(2),y(5),y(6)
do i=1,800
call derivs(x,y,dydx)

```

```

call rk4(y,dydx,n,x,h,yout,derivs)
y(1)=yout(1)
y(2)=yout(2)
y(3)=yout(3)
y(4)=yout(4)
y(5)=yout(5)
y(6)=yout(6)
x=x+h write(25,*) x,-yout(2)
write(6,*) x,-y(2)
enddo
endfile(25)
close(25)
end
!*****
SUBROUTINE derivs(x,y,dydx)
! Subroutine expressing the differential equations for Model 2 with -E
IMPLICIT NONE
REAL*8 x,dydx(6),y(6),theta,M,R,R2,M2,A1,A2
REAL*8 ST,CT,MST,MCT,NONI,NONPC,NONEH,NONPH
REAL*8 NONI2,NONPC2,NINO2,NPCNO2,NEHNO2,NPHNO2
REAL*8 NONEH2,NONPH2,MMDI,MMDH,MMDI2,MMDH2
REAL*8 INVMMDI,INVMMDH,INVMMDI2,INVMMDH2
REAL*8 TERM1,TERM2,TERM3,TERM4
REAL*8 deltaI,deltaH,nin3,npcn3,nphno,nehno,nino,npcno
REAL*8 N1,N2,N3,N4,N5,N6,N7,N8,F1,F2,F3,F4,F5,F6,F7,F8,TITH
common /pl/M,theta,R,deltaI,deltaH,nino,npcno,nehno,nphno,TITH
! x=x
!*****

```

```

! psi=y(1)
! E=y(2)
! nin=y(3)
! pin=y(4)
! viyn=y(5)
! vizn=y(6)
!*****
A1=nphno*(cosh(y(1))-sinh(y(1)))
A2=nehno*(cosh(y(1))+sinh(y(1)))
R2=R**2
M2=M**2
ST=dsin(theta)
CT=dcos(theta)
MST=M*ST
MCT=M*CT
MMDI=M-deltaI
MMDI2=MMDI**2
NONI=1.0d0/NINO
NONI2=NONI**2
NINO2=NINO**2
INVMMDI=(1.0d0/MMDI)
INVMMDI2=INVMMDI**2
TERM1=M-((MMDI*NINO)/(y(3)))
N1=INVMMDI*M*NONI*y(3)
N2=INVMMDI*MCT*NONI
N3=NINO2*MMDI2-3.0d0*y(3)*y(4)
! ***** Runge-Kutte form *****
dydx(1)=-1.0d0*y(2)

```

dydx(2)=-1.0d0*R2*M2*NONI*(y(3)+A1-A2)

! Cold Ions (nin,viyn,vizn,pin)

dydx(3)=(y(3)**3)*(-y(2)-MST*y(5))/N3

dydx(4)=(3.0d0*y(4)*(y(3)**2))*(-y(2)-MST*y(5))/N3

dydx(5)=N1*(MST-CT*y(6))-MST

dydx(6)=y(3)*N2*y(5)

END

!*****

SUBROUTINE rk4(y,dydx,n,x,h,yout,derivs)

IMPLICIT NONE

INTEGER n,NMAX

REAL*8 h,x,dydx(n),y(n),yout(n)

EXTERNAL derivs

PARAMETER (NMAX=50)

INTEGER i

REAL*8 h6,hh,xh,dym(NMAX),yt(NMAX),dym(NMAX)

hh=h*0.5d0

h6=h/6.0d0

xh=x+hh

do i=1,n

yt(i)=y(i)+hh*dydx(i)

enddo

call derivs(xh,yt,dym)

do i=1,n

yt(i)=y(i)+hh*dym(i)

enddo

call derivs(xh,yt,dym)

do i=1,n

```
yt(i)=y(i)+h*dym(i)
dym(i)=dyt(i)+dym(i)
enddo
call derivs(x+h,yt,dyt)
do i=1,n
yout(i)=y(i)+h6*(dydx(i)+dyt(i)+2.0d0*dym(i))
enddo
return
END
```


! PROGRAM EPI3COMP

! Cool ions, warm electrons and warm positrons - All Fluid. $d(\psi)/d(s)=-E$.

IMPLICIT NONE

external derivs

external rk4

INTEGER i,n,NMAX

REAL*8 h,x,dydx(14),y(14),yout(14),M,M2,theta,E0,TITE

REAL*8 deltaE,deltaP,deltaI,MST,MCT,R,NPONEO,NIONE0

REAL*8 pi,ST,CT,MMDE,MMDP,MMDI,MIME,NEONIO,NE0NPO

REAL*8

NPONEO2,NIONE02,MMDE2,MMDP2,MMDI2,NEONPO,INVNIONE0,AARON6

REAL*8 NPO-

NEO3,NIONE03,INVMMDE2,INVMMDP2,INVMMDI2,INVNPONEO2,INVNIONE02

REAL*8 NPO-

NEO5,NIONE04,AARON1,AARON2,AARON3,AARON4,AARON5,INVMMDP,INVMMDI

REAL*8 DF1,DF2,DF3 ,DF4,DF5,DF6,DF12,DF34,DF56,INVMMDE,F42,F43

REAL*8 F1,F2,F3,F4,F5,F6,T1,A1,A2,A3,A4,F22,F23,F32,F33,F62,F63

common /pl/M,theta,R,deltaE,deltaP,deltaI,nponeo,nioneo

pi=3.1415927d0

h=0.2d0

n=14

x=0.0d0

! *****PARAMETERS*****

M=3.50d0

deltaE=0.0d0

deltaP=0.0d0

deltaI=0.0d0

TITE=0.0d0

```

theta=(2.0d0/180.0d0)*pi
E0=2.5d0
R=5.0d0
nioneo=0.5d0
nponeo=1.0d0-nioneo
MIME=2.0d0
! *****
! psi=y(1)
! E=-y(2)
! WARM ELECTRONS
! nen=y(3)
! pecn=y(4)
! veyn=y(5)
! vezn=y(6)
! WARM POSITRONS
! npn=y(7)
! ppn=y(8)
! vpyn=y(9)
! vpzn=y(10)
! COOL IONS
! nin=y(11)
! pin=y(12)
! viyn=y(13)
! vizn=y(14)
!*****
MMDE=(M-deltaE)
MMDP=(M-deltaP)
MMDI=(M-deltaI)

```

$MMDE2=MMDE^{**2}$
 $MMDP2=MMDP^{**2}$
 $MMDI2=MMDI^{**2}$
 $INVMMDE=1.0d0/MMDE$
 $INVMMDP=1.0d0/MMDP$
 $INVMMDI=1.0d0/MMDI$
 $INVMMDI2=1.0d0/MMDI2$
 $NEONPO=1.0d0/NPONEO$
 $NEONIO=1.0d0/NIONEIO$
 $NPONEO2=NPONEO^{**2}$
 $NIONEIO2=NIONEIO^{**2}$
 $NPONEO3=NPONEO*NPONEO^{**2}$
 $NIONEIO3=NIONEIO*NIONEIO^{**2}$
 $NIONEIO4=NIONEIO^{**2}*NIONEIO^{**2}$
 $NPONEO5=NPONEO3*NPONEO^{**2}$
 $M2=M*M$
 $ST=dsin(theta)$
 $CT=dcos(theta)$
 $MST=M*ST$
 $MCT=M*CT$
 !
 $y(1)=0.0d0$
 $y(2)=E0$
 $y(3)=1.0d0$
 $y(4)=1.0d0$
 $y(5)=0.001d0$
 $y(6)=0.001d0$
 $y(7)=nponeo$

$$y(8)=nponeo$$

$$y(9)=0.001d0$$

$$y(10)=0.001d0$$

$$y(11)=1.0d0-nponeo$$

$$y(12)=nioneo*TITE$$

!

$$F1=y(11)**3$$

$$F2=NIONEO2*MMDI2-3.0d0*y(11)*y(12)$$

$$F3=(y(7)**3)*(-y(2)-MIME*y(9)*MST)$$

$$5 F4=NPONEO2*MMDP2-3.0d0*NPONEO*y(7)*y(8)$$

$$F5=(y(3)**3)*(y(2)+MIME*y(5)*MST)$$

$$F6=MMDE2-3.0d0*y(3)*y(4)$$

$$A1=-y(2)/MST$$

$$A2=F3/F4$$

$$A3=F5/F6$$

$$A4=F2/F1$$

!

$$y(13)=(-y(2)+(A2-A3)*A4)/MST$$

$$F22=(3.0d0*(y(7)**5)*(-y(2)-MIME*y(9)*MST)**2)/F4$$

$$F23=(y(7)**4)*MIME**2*M2*ST*NEONPO*INVMMDP$$

$$F32=(M-MMDP*(NPONEO/y(7)))*ST$$

$$F33=3.0d0*((y(3)**5)*(y(2)+MIME*y(5)*MST)**2)/F6$$

$$F42=(y(3)**4)*(MIME**2)*M2*ST*INVMMDE$$

$$F43=(M-(INVMMDE/y(3)))*ST$$

$$F62=F6*F6$$

$$F63=F6**3$$

!

$$DF1=3.0d0*(y(11)**5)*(-y(2)-MST*y(13))/F2$$

```

DF2=-12.0d0*y(12)*(y(11)**3)*(-y(2)-y(13)*MST)/F2
DF3= F22-F23*(F32-y(10)*MCT
DF4=-12.0d0*y(8)*(y(7)**3)*NPONEO*(-y(2)-MIME*y(9)*MST)/F4
DF5=F33+F42*(y(6)*CT-F43)
DF6=-12.0d0*y(4)*(F5/F6)
DF12=(F2*DF1-F1*DF2)/(F2**2)
DF34=(F4*DF3-F3*DF4)/(F4**2)
DF56=(F6*DF5-F5*DF6)/(F6**2)
T1=MST*MCT*F1*y(11)
AARON1=NIONEO*MMDI*(F2/T1)
AARON2=DF56-DF34
AARON3=(-y(2)-y(13)*MST)*DF12
AARON4=(M-(MMDI*NIONEO/y(11)))*ST/CT
! AARON5=NEONIO*INVMMDI*M2*y(11)
y(14)=AARON1*(AARON2-AARON3)+AARON4
! Let's loop here
open(25,file="good1.dat",status="unknown")
! open(25,file="C:/IAN/GRAPHS/E/E1.5.dat",status="unknown")
write(25,* ) x,-y(2)
write(6,* ) x,-y(2)
do i=1,400
call derivs(x,y,dydx)
call rk4(y,dydx,n,x,h,yout,derivs)
y(1)=yout(1)
y(2)=yout(2)
y(3)=yout(3)
y(4)=yout(4)
y(5)=yout(5)

```

```

y(6)=yout(6)
y(7)=yout(7)
y(8)=yout(8)
y(9)=yout(9)
y(10)=yout(10)
y(11)=yout(11)
y(12)=yout(12)
y(13)=yout(13)
y(14)=yout(14)
x=x+h
write(25,*) x,-yout(2)
write(6,*) x,-y(2)
enddo
endfile(25)
close(25)
end
!*****
SUBROUTINE derivs(x,y,dydx)
! Subroutine expressing the differential equations for Model 2 with +E
IMPLICIT NONE
REAL*8 x,dydx(14),y(14),theta,M,R,R2,M2
REAL*8 ST,CT,MST,MCT,NIONEO
REAL*8 NPONEO2,NIONEO2,MIME,NEONIO,NPONEO
REAL*8 MMDE,MMDP,MMDI,MMDE2,MMDP2,MMDI2
REAL*8 INVMMDE,INVMMDP,INVMMDI,INVMMDE2,INVMMDP2,INVMMDI2
REAL*8 TERM1,TERM2,TERM3,NEONPO
REAL*8 deltaE,deltaP,necn3,nIn3,nphno,nehno,necno,nIno
REAL*8 N1,N2,N3,F1,F2,F3,F4,F5,F6,deltaI,G1,G2,G3,G4,G5,G6

```

```

common /pl/M,theta,R,deltaE,deltaP,deltaI,nponeo,nioneo
! x=x
!*****
! psi=y(1)
! E=y(2)
! WARM ELECTRONS
! nen=y(3)
! pecn=y(4)
! veyn=y(5)
! vezn=y(6)
! WARM POSITRONS
! npn=y(7)
! ppn=y(8)
! vpyn=y(9)
! vpzn=y(10)
! COOL IONS
! nin=y(11)
! pin=y(12)
! viyn=y(13)
! vizn=y(14)
!*****
R2=R**2
M2=M**2
ST=dsin(theta)
CT=dcos(theta)
MST=M*ST
MCT=M*CT
MMDE=M-deltaE

```

$MMDP = M - \text{delta}P$
 $MMDI = M - \text{delta}I$
 $MMDE2 = MMDE^{**2}$
 $MMDP2 = MMDP^{**2}$
 $MMDI2 = MMDI^{**2}$
 $NEONPO = 1.0d0 / NPONEO$
 $NEONIO = 1.0d0 / NIONEIO$
 $NPONEO2 = NPONEO^{**2}$
 $NIONEIO2 = NIONEIO^{**2}$
 $INVMMDE = (1.0d0 / MMDE)$
 $INVMMDE2 = INVMMDE^{**2}$
 $INVMMDP = (1.0d0 / MMDP)$
 $INVMMDI = (1.0d0 / MMDI)$
 $INVMMDP2 = INVMMDP * INVMMDP$
 $INVMMDI2 = INVMMDI^{**2}$
 $TERM1 = MIME * INVMMDE * y(3) * M$
 $TERM2 = MIME * NEONPO * INVMMDP * M * y(7)$
 $TERM3 = INVMMDI * M * y(11) * NEONIO$
 $F1 = y(11)^{**3}$
 $F2 = NIONEIO2 * MMDI2 - 3.0d0 * y(11) * y(12)$
 $F3 = (y(7)^{**3}) * (-y(2) - MIME * y(9) * MST)$
 $F4 = NPONEO2 * MMDP2 - 3.0d0 * NPONEO * y(7) * y(8)$
 $F5 = (y(3)^{**3}) * (y(2) + MIME * y(5) * MST)$
 $F6 = MMDE2 - 3.0d0 * y(3) * y(4)$
 $! G1 = y(11)^{**3}$
 $! G2 = NIONEIO2 * MMDI2 - 3.0d0 * y(11) * y(12)$
 $! G3 = (y(7)^{**3}) * (-y(2) - MIME * y(9) * MST)$
 $! G4 = NPONEO2 * MMDP2 - 3.0d0 * NPONEO * y(7) * y(8)$


```

! G5=(y(3)**3)*(y(2)+MIME*y(5)*MST)
! G6=MMDE2-3.0d0*y(3)*y(4)
N1=-y(2)-MIME*y(9)*MST
! N2= -y(2)-y(13)*MST
! ***** Runge-Kutte form *****
dydx(1)=-y(2)
dx(2)=1.0d0*R2*M2*NEONIO*(y(7)+y(11)-y(3))
! Warm Electrons (necn,pecn,vecyn,veczn)
dydx(3)=(F5/F6)
dydx(4)=3.0d0*y(4)*(y(3)**2)*(y(2)+MIME*y(5)*MST)/F6
dydx(5)=TERM1*(y(6)*CT-(M-(MMDE/y(3)))*ST)
dydx(6)=(-MIME*INVMMDP*y(3)*y(5)*MCT )
! Warm Positrons (npn,ppn,vpyn,vpzn)
dydx(7)=(F3/F4)
dydx(8)=(3.0d0*(y(7)**2)*y(8)*N1)/F4
dydx(9)=TERM2*((M-NPONEO*(INVMMDP/y(7)))*ST-y(10)*CT)
dydx(10)=NEONPO*MIME*INVMMDP*y(7)*y(9)*MCT
! Cold Ions (nin, pin,viyn,vizn)
dydx(11)=(y(11)**3)*(-y(2)-y(13)*MST)/F2
dydx(12)=3.0d0*y(12)*(y(11)**2)*(-y(2)-y(13)*MST)/F2
dydx(13)= TERM3*(M-CT*y(14))-MST
dydx(14)=TERM3*y(13)*CT
END
!*****
SUBROUTINE rk4(y,dydx,n,x,h,yout,derivs)
IMPLICIT NONE
INTEGER n,NMAX
REAL*8 h,x,dydx(n),y(n),yout(n)

```

```

EXTERNAL derivs
PARAMETER (NMAX=50)
INTEGER i
REAL*8 h6,hh,xh,dym(NMAX),yt(NMAX),dym(NMAX)
hh=h*0.5d0
h6=h/6.0d0
xh=x+hh
do i=1,n
yt(i)=y(i)+hh*dydx(i)
enddo
call derivs(xh,yt,dym)
do i=1,n
yt(i)=y(i)+hh*dym(i)
enddo
call derivs(xh,yt,dym)
do i=1,n
yt(i)=y(i)+h*dym(i)
dym(i)=dym(i)+dym(i)
enddo
call derivs(x+h,yt,dym)
do i=1,n
yout(i)=y(i)+h6*(dydx(i)+dym(i)+2.0d0*dym(i))
enddo
return
END

```

SAGDEEV POTENTIAL

```

Clear[M2, α2, μ2, σ2, δ2];
M2 = 0.01;
α2 = 0.5;
μ2 = 0.0000001;
σ2 = 0.5;
δ2 = 0.5;
Zd2 = 1000;
x1 = ((M2^2) * α2) / (Zd2 * μ2);
x2 = (Sqrt[1 - (2 * Zd2 * μ2 * Ψ) / M2^2]);
x3 = (1 - E^Ψ);
x4 = ((δ2 * (1 - E^- (σ2 * Ψ))) / σ2);
x5 = (x1 * (1 - x2));
b = x3 + x4 + x5;

Clear[M3, α3, μ3, σ3, δ3];
M3 = 0.01;
α3 = 0.5;
μ3 = 0.0000001;
σ3 = 0.5;
δ3 = 0.5;
Zd3 = 1000;
h1 = ((M3^2) * α3) / (Zd3 * μ3);
h2 = (Sqrt[1 - (2 * Zd3 * μ3 * Ψ) / M3^2]);
h3 = (1 - E^Ψ);
h4 = ((δ3 * (1 - E^- (σ3 * Ψ))) / σ3);
h5 = (h1 * (1 - h2));
c = h3 + h4 + h5;

Clear[M4, α4, μ4, σ4, δ4];
M4 = 0.01;
α4 = 0.5;
μ4 = 0.0000001;
σ4 = 0.5;
δ4 = 0.5;
Zd4 = 1000;
g1 = ((M4^2) * α4) / (Zd4 * μ4);
g2 = (Sqrt[1 - (2 * Zd4 * μ4 * Ψ) / M4^2]);
g3 = (1 - E^Ψ);
g4 = ((δ4 * (1 - E^- (σ4 * Ψ))) / σ4);
g5 = (g1 * (1 - g2));
d = g3 + g4 + g5;

Plot[{b, c, d}, {Ψ, -1.0, 1.0},
PlotStyle → {{Dashed, Thickness[0.005]}, {Dotted, Thickness[0.005]}},
{Red, Thickness[0.003]}, {Blue, Thickness[0.003]}}, AxesLabel → {Ψ, V[Ψ, ("M")]}]

```

```

! PROGRAM TEST
! DETERMINE SOLITON PROFILE IN ELECTRON-POSITRON-DUST
IMPLICIT NONE
external derivs
INTEGER i,n,NMAX
REAL*8 h,x,dydx(1),y(1),yout(1)
REAL*8 M,NPONEO,TETP,ALPHA,Zd,MEMD,M2
! common /plasma /M,NPONEO,TETP,ALPHA,Zd,MEMD,M2
h=0.005d0
n=1
x=0.0d0
! *****PARAMETERS*****
M=0.010d0
MEMD=0.0000001d0
NPONEO=0.50d0
Zd=1000.0d0
TETP=0.35d0
ALPHA=(1.0d0-NPONEO)/Zd
! *****
! psi=y(1)
M2=M*M
!NEHN=dexp(PSI)
!NPHN=NPONEO*dexp(-TETP*PSI)
!NDN= (M*A)/(SQRT(M2-2.0*ZD*MEMD*PSI))
y(1)=0.45d0
!F1=1.0d0-dEXP(PSI)
!F6=(-TETP*PSI)
!F5=1.0d0-dEXP(F6)

```

```

!F2= NPONEO*F5/TETP
!F3= M2*A/(ZD*MEMD)
! F4=2.0d0*ZD*MEMD*PSI/M2
!V=F1+F2+F3*(1.0d0-SQRT(1.0d0-F4))
! Let's loop here
open(25,file="good1.dat")
open(26,file="good2.dat")
write(6,*) x, y(1)
write(25,*) x, y(1)
write(26,*) -1.0d0*x, y(1)
do i=1,280
call derivs(x,y,dydx)
call rk4(y,dydx,n,x,h,yout,derivs)
y(1)=yout(1)
x=x+h
write(6,*) x, yout(1)
write(25,*) x, yout(1)
write(26,*) -1.0d0*x, yout(1)
enddo
endfile(25)
endfile(26)
close(25)
close(26)
end
!*****
SUBROUTINE derivs(x,y,dydx)
IMPLICIT NONE
REAL*8 x,dydx(1),y(1)

```

```

REAL*8 M, NPONEO,TETP,ALPHA,Zd,MEMD,AARON
REAL*8 TERM1,TERM2,TERM3,TERM4,TERM5,TERM6,M2
! common /plasma / M,NPONEO,TETP,ALPHA,Zd,MEMD,M2
M=0.010d0
MEMD=0.0000001d0
NPONEO=0.75d0
Zd=1000.0d0
TETP=0.35d0
ALPHA=(1.0d0-NPONEO)/Zd
!
M2=M*M
TERM1=(M2*ALPHA)/(MEMD*Zd)
TERM2=1.0d0-(2.0d0*MEMD*Zd*y(1)/M2)
TERM5=dsqrt(TERM2)
TERM3=dexp(y(1))
TERM4=dexp(-1.0d0*TETP*y(1))
TERM6=NPONEO*(1.0d0-TERM4)/TETP
write(6,*) TERM2
! psi=y(1)
! ***** Runge-Kutte form *****
AARON=2.0d0*(TERM3-1.0d0)-2.0d0*TERM6-2.0d0*TERM1*(1.0d0-TERM5)
! AARON=2.0d0*TERM1*(TERM5-1.0d0)+2.0d0*delta*(TERM3-1.0d0)+TERM6
! write(6,*) AARON
dydx(1)=-dsqrt(AARON)
END
!*****
SUBROUTINE rk4(y,dydx,n,x,h,yout,derivs)
IMPLICIT NONE

```

```

INTEGER n,NMAX
REAL*8 h,x,dydx(n),y(n),yout(n)
EXTERNAL derivs
PARAMETER (NMAX=50)
INTEGER i
REAL*8 h6,hh,xh,dym(NMAX),yt(NMAX),dym(NMAX)
hh=h*0.5d0
h6=h/6.0d0
xh=x+hh
do i=1,n
yt(i)=y(i)+hh*dydx(i)
enddo
call derivs(xh,yt,dym)
do i=1,n
yt(i)=y(i)+hh*dym(i)
enddo
call derivs(xh,yt,dym)
do i=1,n
yt(i)=y(i)+h*dym(i)
dym(i)=dym(i)+dym(i)
enddo
call derivs(x+h,yt,dym)
do i=1,n
yout(i)=y(i)+h6*(dydx(i)+dym(i)+2.0d0*dym(i))
enddo
return
END

```

References

- Abdelsalam, U., Moslem, W., Shukla, P., 2008. Ion-acoustic solitary waves in a dense pair-ion plasma containing degenerate electrons and positrons. *Phys. Lett. A* 372, 4057–4061.
- Abrahamson, J., 2002. Ball lightning from atmospheric discharges via metal nanosphere oxidation: from soils, wood or metals. *Roy. Soc. of London Phil Tr. A* 360, 61–88.
- Abrahamson, J., Dinniss, J., 2000. Ball lightning caused by oxidation of nanoparticle networks from normal lightning strikes on soil. *Nature* 403, 519–521.
- Abrol, P.S., Tagare, S.G., 1980. Ion-beam generated ion acoustic solitons in beam plasma system with non-isothermal electrons. *J. Plasma Phys.* 22, 831–841.
- Akimoto, K., Omidi, N., 1986. The generation of BEN by an ion beam in the magnetotail. *Geophys. Res. Lett.* 13, 97.
- Alinejad, H., 2010. Non-linear localized ion-acoustic waves in electron–positron–ion plasmas with trapped and non-thermal electrons. *Astrophys Space Sci.* 325, 209–215.
- Alinejad, H., Mamun, A., 2011. Oblique propagation of electrostatic waves in a magnetized electron-positron-ion plasma with superthermal electrons. *Phys. Plasmas* 18, 112103.
- Anderson, R., Harvey, C., Hoppe, M., Tsurutani, B., Eastman, T., Etcheto, J., 1982. Plasma waves near the magnetopause. *J. Geophys. Res.* 87, 2087.
- Baboolal, S., 1988. On small amplitude theories of double layers in negative ion plasma and auroral double layers. *Physical Society of Japan* 57, 750, 751.

- Begelman, M., Blandford, R., Rees, M., 1984. Theory of extragalactic radio sources. *Rev. Mod. Phys.* 56, 255.
- Berbri, A., Tribeche, M., 2009. Weakly nonlinear dust ion-acoustic shock waves in a dusty plasma with nonthermal electrons. *Phys. Plasmas* 16, 053701.
- Berezhiani, V.I., Mahajan, S.M., 1994. Large Amplitude Localized Structures in a relativistic Electron-Positron- ion Plasma. *Phys.Rev.Lett.* 73, 1110–1113.
- Bharuthram, R., 1991. Electron-acoustic instability driven by a field-aligned hot electron beam *journal of Plasma Physics.* *J.Plasma Physics* 46, 1–10.
- Bharuthram, R., Reddy, R.V., Lakhina, G., Singh, N., 2002. Low frequency nonlinear waves in the auroral plasma. *Physica Scripta* 98, 137.
- Bharuthram, R., Shukla, P.K., 1992. Large amplitude ion-acoustic solitons in a dusty plasma. *Planet. Space Sci.* 40, 973–977.
- Bharuthram, R., Singh, S.V., Maharaj, S.K., Moolla, S., Lazarus, I.J., Reddy, R.V., Lakhina, G.S., 2014. Do nonlinear waves evolve in a universal manner in dust and other plasma environments? *J. Plasma Physics* 80, 825–832.
- Boström, R., Gustafsson, B., Holback, G., Holmgren, H., Koskinen, P., 1988. Characteristics of solitary waves and weak double layers in the magnetospheric plasma. *Phys. Rev. Lett.* 61, 82–85.
- Bret, A., Dieckmann, E., 2010. How large can the electron to proton mass ratio be in particle- in- cell simulations of unstable systems? *Phys. Plasmas* 17, 032109.
- Bulanov, S., 2004. Pair production by a circularly polarized electromagnetic wave in a plasma. *Phys. Rev.* 69, 036408.
- Cattell, C.A., Dombeck, J., Wygant, J.R., Hudson, M.K., Mozer, F.S., Temerin, M., Peterson, W.K., Russell, C.T., Kletzing, C.A., Pfaff, R.F., 1999. Comparisons of Polar

- Satellite Observations of Solitary Wave Velocities in the Plasma Sheet Boundary and the High-altitude cusp to those in the Auroral Zone. *Geophys. Res. Lett.* 26, 425.
- Chang-Mo, R., Helen, H.K., 2010. Effects of the ion mass ratio on the relativistic Weibel instability. . *J. Plasma Fusion Res. SERIES* Vol.9.
- Dombeck, J., Cattell, C., Crumley, J., Peterson, W.K., Collin, H.L., Kletzing, C., 2001. Observed trends in auroral zone ion mode solitary wave structure characteristics using data from Polar. *Geophys. Res. Lett.* 106, 19013–19021.
- Dubinov, A., Sazonkin, M., 2009. Nonlinear Theory of Ion-Acoustic Waves in an Electron–Positron–Ion Plasma. *Plasma Phys. Rep.* 35, 14–24.
- Dubouloz, N., Pottelette, R., Holmgren, G., Lindqvist, P.A., 1991. Detailed Analysis of Broadband Electrostatic Noise in the Dayside Auroral Zone. *J. Geophys. Res.* 96, 3565–3579.
- Dusenbery, P.B., Lyons, L., 1985. The generation of electrostatic noise in the plasma sheet boundary layer. *J. Geophys. Res.* 90, 10935.
- Ergun, R.E., Carlson, C., McFadden, J., Mozer, F., Delroy, G., Peria, W., Chaston, C., Temerin, M., Elphic, R., Strangeway, R., Pfaff, R.C., Cattell, A., Cattell, A., 1998. FAST satellite observations of electric field structures in the auroral zone. *Geophys. Res. Lett.* 25, 2025.
- Frank, L., 1971. Plasma in the Earth’s Polar Magnetosphere. *J. Geophys. Res.* 76, 5202.
- Gary, P.S., Tokar, L.R., 1985. A Region of Intense Plasma Wave Turbulence on Auroral Field Lines. *Phys. Fluids* 28, 2439.
- Gell, Y., Roth, I., 1981. The effects of an ion beam on the motion of solitons in an ion beam-plasma system. *J. Plasma Physics* 23, 651–656.
- Ghosh, S., Bharuthram, R., 2008. Ion acoustic solitons and double layers in electron–positron–ion plasmas with dust particulates. *Astrophys. Space Sci.* 314, 121–127.

- Ghosh, S., Ghosh, K., Sekar Iyengar, A.N., 1996. Large Mach number ion acoustic rarefactive solitary waves for a two electron temperature warm ion plasma. *Phys. Plasmas* 3, 3939.
- Goertz, C.K., 1989. Dusty plasmas in the solar system. *Rev.Geophys.* 27, 271–292.
- Gogoi, R., Roychoudhury, R., Khan, M., 2012. Arbitrary amplitude dust ion acoustic solitary waves and double layers in a plasma with non-thermal electrons. *Indian Journal of Pure & Applied Physics* 50, 110–116.
- Goldreich, P., Julian, W., 1969. Pulsar electrodynamics . *ApJ* 157, 869.
- Grabbe, C.L., Eastman, T., 1984. Generation of broadband electrostatic waves in the magnetotail. *J. Geophys. Res.* 89, 3865.
- Greaves, R., Tinkle, M., Surko, C., 1994. Creation and Uses of Positron Plasmas. *Phys. Plasmas* 1, 1439.
- Gurnett, D., Frank, L., Lepping, R., 1976. Plasma waves in the distant magnetotail. *Journal of Geophysical Research. J. Geophys. Res.* 81, 6059–6071.
- Hamid, R.P., 2009. Ion acoustic solitary waves in plasma with nonthermal electron and positron. *Phys. Lett. A* 373, 847–850.
- Haque, Q., Saleem, H., Vranjic, 2002. Electromagnetic vortices in electron-positron-ion plasmas with shear flow. *Phys. Plasmas* 9, 474.
- Hasegawa, H., Irie, S., Usami, S., Ohsawa, Y., 2002. Perpendicular nonlinear waves in an electron–positron–ion plasma. *Phys.Plasmas* 9, 2549.
- Havnes, O., Troim, J., Blix, T., Mortensen, W., Naesheim, L., Thrane, I.E., Tonnesen, T., 1996. First detection of charged dust particles in the Earth’s mesosphere. *J. Geophys. Res* 101, 10839–10847.
- Horanyi, M., Mendis, D.A., 1986. The dynamics of charged dust in the tail of comet Giacobini-Zinner. *J. Geophys. Res* 91, 355–361.

- Hoshino, M., Arons, J., 1991. Preferential Positron Heating and Acceleration by Synchrotron Maser Instabilities in Relativistic Positron-Electron-Proton Plasmas. *Phys. Fluids, B* 3, 818–833.
- Ikezi, H., 1973. Experiments on ion-acoustic solitary waves. *Phys. Fluids* 16, 1668.
- Ikezi, H., Taylor, R.J., Baker, D.R., 1970. Formation and Interaction of Ion-Acoustic Solitons. *Phys.Rev.Lett.* 25, 11–14.
- Jammalamadaka, S., Shukla, P.K., Stenflo, L., 1996. Vortices in strongly magnetized nonuniform electron-positron-ion plasmas. *Astrophys. Space Sci.* 240, 39–43.
- Jilani, K., Mirza, A., Khan, T., 2013. Electrostatic electron acoustic solitons in electron-positron-ion plasma with superthermal electrons and positrons. *Astrophys. Space Sci.* 13, 1637.
- Jinhy, H., Ensang, L., Kyoungwook, M., George, K.P., 2012. Effect of ion-to electron mass ratio on the evolution of ion beam driven instability in particle –in-cell simulations. *Phys.Plasmas* 196, 092111.
- Kakati, H., Goswami, K., 1998. Solitary Alfvén wave in an electron positron ion plasma. *Phys. Plasmas* 5, 4229.
- Kakati, H., Goswami, K., 2000. On the existence of small amplitude double layers in an electron-positron-ion plasma. *Phys. Plasmas* 7, 808.
- Kluger, Y., Eisenberg, J., Svetitsky, B., Cooper, F., Mottola, E., 1991. Pair production in a strong electric field. *Phys.Rev.Lett.* 67, 2427.
- Kojima, H., Matsumoto, H., Miyatake, T., Nagano, I., Fujita, A., Frank, L.A., Mukai, T., Paterson, W.R., Saito, Y., Machida, S., R., A.R., 1994. Relation Between Electrostatic Solitary Waves and Hot Plasma Flow in the Plasma Sheet Boundary Layer: Geotail Observations. *Geophys.Res. Lett.* 21, 2919–2922.

- Kourakis, I., Moslem, W.M., Abdelsalam, U.S., Sabry, M.R., Shukla, P.K., 2009. Nonlinear Dynamics of Rotating Multi-Component Pair Plasmas and e-p-i Plasmas. *Plasma and Fusion Research* 4, 1–11.
- Kourakis, I., Verheest, F., Cramer, N., 2007. Nonlinear perpendicular propagation of ordinary mode electromagnetic wave packets in pair plasmas and electron-positron-ion plasmas. *Phys. Plasmas* 14, 1–10.
- Kozlovsky, B., Murphy, R., Share, G., 2004. Positron-emitter production in solar ares from ^3He -reactions. *ApJ* 604, 892–899.
- Lakhina, G.S., 2004. Anomalous width variation of rarefactive ion acoustic solitary waves in the context of auroral plasmas. *Nonlinear Proc. Geophys.* 11, 219–228.
- Laroussi, M., Mendis, D.A., Rosenberg, M., 2003. Plasma interaction with microbes. *New J. Phys.* 5, 419.
- Lazarus, I., Bharuthram, R., Singh, S., Pillay, S., Lakhina, G., 2012. Linear electrostatic waves in two-temperature electron–positron plasmas. *J. Plasma Physics* 78, 621.
- Lee, W., Ruiz, E., 2005. Dynamical evolution of neutrino-cooled accretion disks: detailed mircophysics, lepton-driven convection and global energetics. *Astrophys. J.* 632, 421.
- Ma, J.X., Liu, J., 1997. Dust-acoustic soliton in a dusty plasma. *Phys. Plasmas* 4, 253–255.
- Maharaj, S.K., Bharuthram, R., Singh, S.V., Pillay, S.R., Pillay, S., Lakhina, G.S., 2008. Electrostatic solitary waves in a magnetized dusty plasma. *Phys. Plasmas* 15, 113701.
- Mahmood, S., Akhtar, N., 2008. Ion acoustic solitary waves with adiabatic ions in magnetized electron-positron-ion plasmas. *Eur. Phys. J. D* 49, 217–222.
- Mahmood, S., Mushtaq, H., Saleem, H., 2003. Ion acoustic solitary wave in homogeneous magnetized electron-positron-ion plasmas. *New. J. Phys.* 5, 289–298.

- Mamun, A., Hassan, M.H.A., 2000. Effects of dust grain charge fluctuation on an obliquely propagating dust acoustic solitary potential in a magnetized dusty plasma. *J. Plasma Physics* 632, 191–200.
- Mamun, A., Shukla, P.K., 2005. Nonlinear waves and structures in dusty plasmas. *Plasma Phys. Control. Fusion* 47, 1–9.
- Mamun, A.A., 1999. Arbitrary Amplitude Dust-acoustic Solitary Structures in a Three-component Dusty Plasma. *Astrophys. Space Sci.* 268, 443–454.
- Matsumoto, H.H., Kojima, T., Miyatake, Y., Omura, M., Okada, I., Nagano, Tsutsui, M., 1994. Electrostatic Solitary Waves (ESW) in the Magnetotail : BEN Wave forms observed by GEOTAIL. *Geophys. Res. Lett.* 21, 2915–2918.
- Mendis, D.A., Rosenberg, M., 1994. Cosmic Dusty Plasmas. *An.Rev. Astronomy and Astrophysics* 323, 419–463.
- Meuris, P., Verheest, F., 1996. Korteweg-de Vries equation for magnetosonic modes in dusty plasmas . *Phys. Lett. A* 219, 299–302.
- Michel, F., 1982. Theory of pulsar magnetospheres. *Rev. Mod. Phys.* 54, 1–66.
- Miller, H., Witta, P., 1987. *Active Galactic Nuclei*. Springer- Verlag, Berlin.
- Moola, S., Bharuthram, R., Baboolal, S., 2005. Reduction of dust acoustic soliton amplitude due to dust charge variation. *Phys. Plasmas* 12, 042310.
- Moola, S., Bharuthram, R., Singh, S., Lakhina, G., 2003. Non-linear high-frequency waves in the magnetosphere. *Pramana J.Phys.* 61, 1209–1214.
- Moola, S., Bharuthram, R., Singh, S., Lakhina, G., Reddy, R.V., 2010. Nonlinear low-frequency structures in the auroral plasma in the presence of an oxygen beam including charge separation. *Phys.Plasmas* 17, 022903.

- Moolla, S., Bharuthram, R., Singh, S.V., Lakhina, G.S., Reddy, R.V., 2007. An Explanation for high-frequency broadband electrostatic noise in the Earth's magnetosphere . J. Geophys. Res 112, A07214.
- Moolla, S., Lazarus, I., Bharuthram, R., 2012. Nonlinear low-frequency structures in an electron-positron-ion plasma. J. Plasma Phys. 78, 545–551.
- Mozer, F., Ergun, R., Temerin, M., Cattell, C., Dombeck, J., Wygant, J., 1997. New features of time domain electric-field structures in the auroral acceleration region. Phys. Rev. Lett. 79, 1281.
- Mugemana, A., Lazarus, I.J., Moolla, S., 2014. Linear electrostatic waves in a three-component electron-positron-ion plasma. Phys. Plasmas 21, 122119.
- Nejoh, Y., 1996. The effect of the ion temperature on large amplitude ionacoustic waves in an electron-positron-ion plasma. Phys. Plasmas 3, 1447.
- Nejoh, Y.N., 1997. Effects of Positron Density and Temperature on Large Amplitude Ionacoustic Waves in an Electron-Positron-Ion Plasma. Austral. J. Phys. 50, 309.
- Nishida, A., Hada, T., Anderson, K.A., Anderson, R.R., Bame, S.J., Hones, E.W.J., 1985. Broadband electrostatic noise in the magnetotail: Its relation to plasma sheet dynamics. J. Geophys. Res. 90, 4453.
- Omidi, N., 1985. Broadband electrostatic noise produced by ion beams in the earth's magnetotail. J. Geophys. Res. 90, 12330.
- Pakzad, H., 2009. Ion acoustic solitary waves in plasma with nonthermal electron, positron and warm ion. Astrophys. Space Sci. 323, 345–350.
- Pickett, J., Chen, L., Kahler, S.W., Santolík, O., Gurnett, D.A., Tsurutani, B.T., Balogh, A., 2004. Isolated electrostatic structures observed throughout the Cluster orbit: relationship to magnetic field strength . Ann. Geophys. 22, 2515–2523.

- Pickett, J., Chen, L., R.L., M., Christopher, I., Santol'k, O., Lakhina, G.S., Singh, S.V., Reddy, R.V., Gurnett, D.A., Tsurutani, B., Lucek, E., Lavraud, B., 2008. Furthering our understanding of electrostatic solitary waves through Cluster multispacecraft observations and theory. *Adv. Space Res.* 41, 1666–1676.
- Pickett, S., Menietti, J.D., Gurnett, D.A., Tsurutani, B.T., Kintner, P., Klatt, E., Balogh, A., 2003. Solitary potential structures observed in the magnetosheath by the Cluster spacecraft. *Nonlinear Proc.Geophys.* 10, 3–11.
- Popel, S., Vladimirov, S., Shukla, P., 1995. Ionacoustic solitons in electron–positron–ion plasmas. *Phys.Plasmas* 2, 716.
- Rao, N.N., Shukla, P., Yu, M.Y., 1990. Dust acoustic waves in dust plasmas. *Planet. Space Sci.* 38, 543–546.
- Rasheed, A., Murtaza, G., Tsintsadze, N., 2010. Nonlinear structure of ion acoustic waves in complete degenerate electron-positron and ion plasma. *Phys. Rev. Lett.* 82, 016403.
- Reddy, R.V., Lakhina, G.S., 1991. Ion acoustic double layers and solitons in auroral plasma. *Planet. Space Sci.* 39, 1343–1350.
- Reddy, R.V., Lakhina, G.S., Singh, N., Bharuthram, R., 2002. Spiky parallel electrostatic ion cyclotron and ion acoustic waves. *Nonlinear Proc. Geophys.* 9, 25–29.
- Reddy, R.V., Singh, S.V., Lakhina, G.S., Bharuthram, R., 2006. Parallel electric field structures associated with the low-frequency oscillations in the auroral plasma. *Earth Planets Space* 58, 1227–1232.
- Rizzato, F., 1988. Weak nonlinear electromagnetic waves and low-frequency magnetic-field generation in electron-positron-ion plasmas . *J. Plasma Phys.* 40, 289–298.
- Ruderman, M., Sutherland, P., 1975. Theory of pulsars-Polar caps, sparks, and coherent microwave radiation . *ApJ* 196, 519–521.

- Saberian, E., Esfandyari-Kalejahi, A., Afsari-Ghazi, M., 2015. Large Amplitude Dust-acoustic Solitons in a Plasma Consisting of Super-thermal Electron-positron Pairs and Dust Particulates. *The Open Plasma Physics Journal* 80, 8–22.
- Sagdeev, R.Z., 1966. Cooperative Phenomena and Shock Waves in Collisionless Plasmas. *Rev. Plasma Physics* 4, 23.
- Saini, N.S., Chahal, B.S., Bains, A.S., 2013. Large amplitude dust ion-acoustic solitary waves in a plasma in the presence of positrons. *Astrophys Space Sci.* 347, 129–138.
- Salahuddin, M., Saleem, H., Saddiq, M., 2002. Ion-acoustic envelope solitons in electron-positron-ion plasmas. *Phys. Rev. E* 66, 036407.
- Samaritan, A.A., Vaulina, O.S., Nefedov, A.P., Fortov, V., James, B.W., Petrov, O.F., 2001. Positively charged particles in dusty plasmas. *Phys. Rev. E* 64, 055407.
- Schrifer, D., Ashour-Abdalla, M., 1987. Generation of High-Frequency Broadband Electrostatic Noise: The Role of Cold Electrons. *J. Geophys. Res.* 92, 5807–5819.
- Selwyn, G.S., Singh, J., Bennett, R.S., 1989. In situ laser diagnostic studies of plasma-generated particulate contamination. *Journal of Vacuum Science & Technology A* 7, 2758–2765.
- Shukla, P., Mamun, A., 2002. *Introduction to Dust Plasma Physics*. IoP Publishing Ltd. Bristol .
- Shukla, P.K., Eliasson, B., 2009. Colloquium: Fundamentals of dust-plasma interactions. *Rev. Mod. Phys.* 81, 25.
- Shukla, P.K., Marklund, M., 2004. Dust acoustic wave in a strongly magnetized pair-dust plasma. *Physica Scripta* 36.
- Shukla, P.K., Rao, N.N., Yu, M.Y., Tsintsadze, N., 1986. Relativistic nonlinear effects in plasmas. *Phys. Rep.* 135, 1.
- Shukla, P.K., Silin, V.P., 1992. Dust ion-acoustic wave. *Physica Scripta* 45, 508.

- Stoffels, E., Kieft, I.E., Sladek, R.E., 2003. Superficial treatment of mammalian cells using plasma needle . *J.Phy.D* 36, 2908–2913.
- Surko, C.M., Murphy, T.J., 1990. Use of the Positron as a Plasma Particle. *Phys. Fluids* 2, 1372.
- Tagare, S.G., 1973. Effect of ion temperature on propagation of ion-acoustic solitary waves of small amplitudes in collisionless plasma. *J. Plasma Physics* 15, 1247–1252.
- Tarsem, S., Amandeep, S., Harvinder, K., Nareshpal, S.S., Parveen, B., 2007. Ion-acoustic solitons in weakly relativistic plasma containing electron–positron and ion. *Phys. Lett. A* 361, 364–367.
- Temerin, M., Cerny, K., Lotko, W., 1982. observations of double layers and solitary waves in the auroral plasma. *Phys.Rev.Lett.* 48, 1175–1179.
- Tiwari, R., 2008. Ion-acoustic dressed solitons in electron–positron–ion plasmas. *Phys. Lett. A* 372, 3461–3466.
- Tiwari, R., Kaushik, A., Mishra, M., 2007. Effects of positron density and temperature on ion acoustic dressed solitons in an electron–positron–ion plasma. *Phys. Lett. A* 365, 335–340.
- Tokar, R.L., Gary, S., 1984. Electrostatic hiss and the beam driven electron acoustic instability in the dayside polar cusp. *Geophys. Res. Lett.* 11, 1180–1984.
- Verheest, F., 1999. Dusty plasmas in application to astrophysics. *Plasma Phys. Control. Fusion* 41, 445–451.
- Vladimirov, S.V., Ostrikov, K., 2004. Dynamic self-organization phenomena in complex ionized gas systems: new paradigms and technological aspects. *Phys. Rep.* 393, 175.
- Washimi, H., Taniuti, T., 1966. Propagation of Ion-Acoustic Solitary Waves of Small Amplitude. *Phys. Rev. Lett.* 17, 996.

- Winter, J., 1998. Dust in fusion devices - experimental evidence, possible sources and consequences. *Plasma Phys. Controlled Fusion* 40, 1201.
- Wu, D.J., Huang, D.Y., Fälthammar, C.G., 1996. Solitary kinetic Alfvén waves in the twofluid model. *Phys. Plasmas* 3, 2879.
- Yadav, L., Sharma, S., 1990. Obliquely propagating ion-acoustic solitons in a warm-ion magnetized plasma. *Phys. Lett. A* 150, 397.
- Zank, G., Greaves, R., 1995. Linear and nonlinear modes in nonrelativistic electron-positron plasmas. *Phys. Rev. E* 51, 6079.
- Zeba, I., Moslem, W.M., Shukla, P.K., 2012. Ion solitary pulses in warm plasmas with ultrarelativistic degenerate electrons and positrons. *ApJ* 750, 72.